Mechanistic Transport Analysis to Predict *In Vivo* Oral
Bioperformance

by

Deanna M. Mudie

A dissertation submitted in partial fulfillment
of the requirements for the degree of
Doctor of Philosophy
(Pharmaceutical Sciences)
in the University of Michigan
2014

Doctoral Committee:

      Research Professor Gregory E. Amidon, Co-Chair
      Professor Gordon L. Amidon, Co-Chair
      Professor Ronald G. Larson
      Professor Steven P. Schwendeman

Dedication

To my mother Bernice, my husband David, and my sons Ian and Luke

Acknowledgments

I would like to thank my primary advisor, Dr. Gregory Amidon, for his support, guidance, understanding and friendship throughout my graduate studies, and for encouraging me to pursue a graduate degree in the first place. He was always available to set aside time to listen and provide advice, as well as to assist with technical issues in the laboratory, and always provided prompt and thorough reviews of my work. I am forever grateful for the inspiration he instilled in me through his enthusiasm for science and pharmaceutical research.

I would also like to thank my secondary advisor, Dr. Gordon Amidon, for encouraging me to maintain focus on the big picture, to carefully phrase my observations and ideas and to present my research as a meaningful and compelling story. I would like to thank my cognate committee member from the Chemical Engineering Department, Dr. Ronald Larson, for accepting the invitation to be on my committee and for his excellent technical input and suggestions. I am also grateful to Dr. Steven Schwendeman for serving on my committee, and for his enthusiasm at my committee meetings, technical input and valuable feedback regarding the written and oral presentation of my research.

I would like to recognize Dr. Ping Gao and Dr. Yi Shi (AbbVie Inc., North Chicago, IL) for their collaboration on the work presented in Chapters 2 and 4, as well as for meaningful technical discussions and input as part of our research collaboration on the two-phase dissolution apparatus. I would also like to recognize Dr. Haili Ping and Nicholas Waltz for conducting some of the two-phase partitioning experiments, and Yeo Jung Park and Dr. Kerby Shedden for performing and designing the non-linear regression analysis of the *in vitro*

Table of Contents

List of Tables

List of Figures

Abstract

Oral delivery of solid dosage forms is the most frequently used route of administration for pharmaceutical drug products. Despite their ubiquity, development of robust oral dosage forms can be challenging due to the complex nature of dissolution and absorption in the gastrointestinal tract. The goal of this research was to set a basis for development of practical *in vitro* physiological dissolution methodologies that could be used to design drug product formulations and scientifically justify reduced regulatory requirements for product approval (e.g. introduction of generic products). While existing methodologies can be used as benchmarks for development of new dosage forms, no single *in vitro* apparatus captures the range of key physiological conditions that can impact *in vivo* bioperformance of a diverse range of drug products.

In this work we provide a comprehensive and up-to-date summary of the critical physiological parameters affecting dissolution and absorption of oral dosage forms in humans and dogs, including average values and ranges for each parameter from the literature. Next, we developed a mechanistic transport model that successfully described the kinetics of partitioning of weak acids in solution from aqueous to organic medium, and proposed scaling factors for establishing physiological relevance of the *in vitro* two-phase dissolution apparatus. In contrast to previous kinetically derived mathematical models, our model uses physical input parameters that are known or can be estimated *a priori*. Next, we developed a mechanistic transport model for predicting the rate and extent of dissolution of solid drug particles under physiological conditions (e.g. low buffer capacity and moderate drug saturation), extending previously published models by taking into account the impact of dissolved drug concentration on pH change and dissolution performance as a function of time.

Finally, we developed an *in vivo* transport analysis to identify practical *in vitro* dissolution methodologies that could be used to predict *in vivo* performance of oral formulations of the BCS II weak acid, Ibuprofen, in dogs. Taken as a whole, this work sets a basis for determination of the key, rate-determining factors driving *in vivo* oral drug product bioperformance, and selection of appropriate *in vitro* predictive dissolution methodologies.

Chapter 1

Physiological Parameters for Oral Delivery and *In vitro* Testing

Abstract

Pharmaceutical solid oral dosage forms must undergo dissolution in the intestinal fluids of the gastrointestinal tract before they can be absorbed and reach the systemic circulation. Therefore, dissolution is a critical part of the drug-delivery process. The rate and extent of drug dissolution and absorption depend on the characteristics of the active ingredient as well as properties of the dosage form. Just as importantly, characteristics of the physiological environment such as buffer species, pH, bile salts, gastric emptying rate, intestinal motility, and hydrodynamics can significantly impact dissolution and absorption. While significant progress has been made since 1970 when the first compendial dissolution test was introduced (USP Apparatus 1), current dissolution testing does not take full advantage of the extensive physiologic information that is available. For quality control purposes, where the question is one of lot-to-lot consistency in performance, using nonphysiologic test conditions that match drug and dosage form properties with practical dissolution media and apparatus may be appropriate. However, where *in vitro* – *in vivo* correlations are desired, it is logical to consider and utilize knowledge of the *in vivo* condition. This publication critically reviews the literature that is relevant to oral human drug delivery. Physiologically relevant information must serve as a basis for the design of dissolution test methods and systems that are more representative of the human condition. As *in vitro* methods advance in their physiological relevance, better *in vitro* - *in vivo* correlations will be possible. This will, in turn,

will lead to *in vitro* systems that can be utilized to more effectively design dosage forms that have improved and more consistent oral bioperformance.

Introduction

Pharmaceutical solid oral dosage forms directed to the systemic circulation must dissolve in the intestinal fluids of the gastrointestinal (GI) tract prior to absorption, making dissolution vital to drug delivery. Pharmaceutical scientists must understand dissolution to efficiently develop robust dosage forms and ensure that drug products consistently meet critical performance criteria. The rate and extent of drug dissolution and absorption depend on characteristics of the active ingredient such as pK_a, crystal form, and solubility, as well as properties of the dosage form [1]. Just as importantly, characteristics of the physiological environment such as buffer species, pH, bile salts, gastric emptying rate, intestinal motility, hydrodynamics, and shear rates significantly impact dissolution and absorption [2].

To understand the complicated process of *in vivo* drug dissolution, scientists have attempted to replicate it using a variety of *in vitro* test methods. Numerous methodologies have been developed that are routinely used for quality control purposes (e.g., USP tests) and as tools to understand the effects of formulation and processing changes [3]. While these methodologies have existed for many years and have been used extensively, none accurately reflect *in vivo* conditions. Conventional USP testing methods employ simple, non-physiologic buffers (e.g., phosphate, acetate, maleate) and hydrodynamic conditions (e.g., single-chambered glass vessels) that do not accurately reflect dynamic *in vivo* conditions. To bridge the gap between *in vitro* and *in vivo* dissolution and absorption, the Biopharmaceutics Classification System (BCS) provides some guidance for predicting *in vivo* performance based on a drug's solubility, permeability, and *in vitro* testing results [4]. The BCS has had a significant effect on the regulatory environment as the FDA and WHO consider biowaivers for some drugs, particularly those considered to be BCS Class 1 (high

solubility, high permeability) and BCS Class III (high solubility, low permeability) [5].

While significant progress has been made since 1970, when the first compendial dissolution test was introduced (USP Apparatus 1), current dissolution testing does not take full advantage of the extensive physiologic information that is available. For quality control purposes, where the question is one of lot-to-lot consistency in performance, utilizing nonphysiologic test conditions that match drug and dosage form properties with practical dissolution media and apparatus may be appropriate. However, where *in vitro – in vivo* correlations (IVIVCs) are desired, it is logical to consider and utilize our knowledge of the *in vivo* condition. Strides have been made in making dissolution testing methods more biologically based. Dressman et al. developed several biorelevant dissolution media designed to better reflect compositions and physicochemical characteristics of the fasted and fed states in the stomach and small intestine [6]. In addition, several authors have developed dissolution apparatuses that better capture aspects of the physiological environment compared to USP tests [7]-[9].

Several good reviews of human GI physiology are available [2], [10]-[11] but none provide a comprehensive review of the physiological parameters that influence oral absorption in the context of dosage form performance and drug dissolution. The focus of this publication is to critically review the literature that is relevant to oral human drug delivery. This physiologically relevant information should serve as a basis for the design of dissolution test methods and systems that are more representative of the human gastrointestinal tract. As *in vitro* methods advance in their physiological relevance, better *in vitro - in vivo* correlations will be possible, leading to improved oral bioperformance of dosage forms.

Factors Affecting Dissolution and Absorption

Absorption is what ultimately carries orally administered drugs into the intestinal membrane to be transferred to the blood stream. However, the drug must dissolve before absorption can occur or the drug can act locally in the GI tract. Therefore, it is important to have a fundamental understanding of the key drug properties affecting both dissolution and absorption. These principles have taken a variety of mathematical forms over the years. According to Amidon et al., for example, the fraction of drug absorbed is a function of drug solubility, dose, and GI permeability [4]. According to **Equation 1.1**, the flux of drug across the intestinal wall, J_w, is dependent on the intestinal wall permeability, P_w (an effective permeability), and the concentration of drug at the wall, C_w. The equation applies to each point along the membrane, assumes that each parameter is dependent upon time and position, and assumes the concentration of drug in the epithelial cell to essentially equal to zero. Assuming no luminal reactions, the absorption rate is given by **Equation 1.2**, where A is the area available for absorption (i.e., membrane surface in contact with the drug) and m is mass.

(1.1) $\quad J_w = P_w C_w$

(1. 2) $\quad \dfrac{dM}{dt} = \iint_A P_w C_w \, dA$

Factors that affect dissolution can be understood by examining the simple Noyes-Whitney equation, which describes the mass of drug dissolving as a function of time. The equation, for dissolution from a planar surface, is given in **Equation 1.3**, where M is mass, D is drug diffusion coefficient, A is drug surface area available for dissolution, h is empirical thickness of the hydrodynamic boundary layer, C_s is the solubility at the solid liquid interface, and C_b is the bulk drug concentration [12].

(1.3) $Dissolution\ rate = \dfrac{dM}{dt} = -\dfrac{DA}{h}(C_s - C_b)$

Each of the parameters in **Equation 1.2**, describing absorption, and **Equation 1.3**, describing dissolution, is influenced by properties of the drug substance, drug product, and GI tract.

From the above description it is clear that *in vivo* dissolution and absorption are dependent on properties of the physiological environment and properties of the drug itself. Key physiological parameters include the dimensions of the GI tract, the volume and composition of fluid, the fluid hydrodynamics (i.e., flow rate, gastric-emptying rate, shear rate), and the properties of the intestinal membrane. Important drug properties include dose, solubility, pK_a, diffusion coefficient, permeability, and particle size. A more complete list of drug properties and physiologic properties that influence oral drug dissolution and absorption is provided in **Table 1.1**.

Composition of the Gastrointestinal Fluid

Gastrointestinal fluid is a complex, dynamic mixture of components from a number of different sources within the gastrointestinal tract. Gastric fluid is made up of saliva, gastric secretions, dietary food and liquid, and refluxed liquid from the duodenum. The gastric fluid composition changes as the fluid is mixed and delivered to the duodenum. Some major components of gastric fluid important for drug disposition include hydrogen ion concentration, bile salts, lipase, and the protein-digesting enzyme pepsin (Refer to **Tables 1.2 & 1.3** for a summary of components and concentrations.). The concentration of hydrogen ions affects the pH and thus the dissolution of some ionizable drugs. Pepsin may interfere with the stability of proteins and peptides, while lipase may affect drug release from lipid-based dosage forms [2]. Bile salts can combine with lipids to form mixed micelles, enhancing the solubility of some drugs and may also decrease surface tension and thus enhance wetting [13].

Kalantzi et al. found median pepsin levels in the fasted state to range from 0.11-0.22mg/mL [14], while other researchers have found them to be between 0.1 and 1.3 mg/mL [15]-[16]. Pepsin in the fed state is typically higher and has been shown to range from 0.26 to 1.72 mg/mL [14], [16]. The concentration of hydrogen ions, which are secreted by the stomach in the form of hydrochloric acid is reflected in the pH, which is typically 1-2 in the fasted state (0.01-0.1 M) and ranges from about 3-7 in the fed state (10^{-3} – 10^{-7} M). Vertzoni and co-workers state that gastric lipase is probably not important in the fasted state since it is active in the pH range of 3-6 and is thought to be present at concentrations of 0.1mg/mL [17]. Lipase activity in the fed stomach has been shown to range from 11.4-43.9 U/mL [18]. Bile salt levels have been found to be about 0.08 to 0.275 mM in the fasted stomach [17], [19] and 0.06 mM in the fed stomach [20]. Vertzoni and co-workers recently measured the relative amounts of individual bile salts in the fasted stomach and found glycochenodeoxycholate and glycocholate to predominate [19]. Bicarbonate concentrations in the fasted stomach have been shown to range from 7 to 20 mEq/L [21]-[22].

The composition of the fluid in the upper small intestine is made up of chyme from the stomach, as well as secretions from the liver, the pancreas, and the wall of the small intestine. Composition is affected by fluid compartmentalization, mixing patterns, absorption of fluid into the intestinal wall, and transit down the intestinal tract. Secretions from the pancreas include bicarbonate as well as proteases (the major ones are trypsin and chymotrypsin), amylases, and lipases [23]. The liver secretes bile, which contains bile salts, phospholipids, bicarbonate, cholesterol, bile pigments, and organic wastes. The wall of the small intestine secretes mineral ions such as bicarbonate, sodium, and chloride, as well as water. Bicarbonate is secreted to neutralize gastric secretion in the GI lumen and by the duodenal epithelial cells to protect the duodenal epithelium from acid-related damage [24]. The buffer species in the gastrointestinal media can significantly affect the dissolution rates of ionizable drugs [25].

As food intake triggers many of the secretions in the small intestine, the composition of fed state intestinal fluid can vary greatly from fasted state intestinal fluid. This difference in composition can be partially responsible for differences in bioavailability seen when drug is administered in the fed versus the fasted state. For some lipophilic drugs, coadministration with a meal has been shown to increase bioavailability compared to the fasted state. Sunesen et al. showed that the oral bioavailability of the poorly soluble drug danazol was three-fold higher when taken with a high-lipid meal compared with 200 mL of water [26]. However, in some cases the oral bioavailability can be negatively affected due to chelation of a drug with food components [27].

The increased bioavailability seen for some drugs in the fed state can be attributed to the enhanced solubilizing capacity of intestinal fluids due to bile and pancreatic secretions and the presence of exogenous lipid products [28]. For instance, dietary triglycerides are hydrolyzed into free fatty acids and monoglycerides in the duodenum mainly due to pancreatic lipase, and the free fatty acids combine with bile salts to form mixed micelles, which can be transported to the intestinal membrane [29]. Many instances of enhanced solubility and dissolution due to mixed micelles formed by bile secretions, and lipolysis products formed in the fed state exist in the literature [30]-[32].

Concentrations of lipolytic products, bile salts, and phospholipids in the upper small intestine tend to show high variability with time and between study subjects [14], [33]. Lipolytic product concentrations have ranged from 0-1.8 mg/mL in the fasted and 0.5-100 mg/mL in the fed upper small intestine [18], [33]. After administration of Ensure Plus® (fed), and Scandishake Mix® (fat-enriched fed) Clarysse et al. found the dominant lipolytic products in the duodenum to be monoglycerides, which accounted for 5-88% of total lipids, followed by free fatty acids [33]. Phospholipid concentrations have ranged from 0.03-0.6 mM in the fasted [33]-[34] and 0.8-3 mM in the fed state [33], [35]. Bile salt concentrations have ranged from 0.6-17 mM [2], [33] and 1.6-40 mM [36]-[37] in the fasted and fed states, respectively. Clarysse et al. found duodenal bile salts to be made up of cholate and chenodeoxycholate (which comprised about

65%) as well as deoxycholate and ursodeoxycholate [33], while Vertzoni found the major bile salts in the duodenum to be glycodeoxycholate, glycochenodeoxycholate, and glycocholate in the fed state [19]. Concentrations of lipolytic products and phospholipids in the ileum are unavailable, but bile salt concentrations have ranged from 2-10 mM and 0.2-30 mM in the fasted and fed states, respectively [36], [38].

The concentration of bicarbonate in the small intestine is dynamic and depends on location and prandial state. The bicarbonate concentration in the fasted state has ranged from about 2 to 30 mM in the duodenum and jejunum and 30-75 mM in the ileum [39]-[43]. Values in the fed state are less abundant. Rune and co-workers reported a value of 10 mEq L^{-1} in the fed duodenum [44].

Properties of the Gastrointestinal Fluid

pH

The pH of the GI fluids in the local region of the intestine will influence a drug's dissolution rate and possibly its permeability[4]. The pH strongly influences the solubility of weak electrolytes by determining their ionization state. When the pH is such that a drug is in its ionic form, the drug behaves like a strong electrolyte and solubility is usually high compared to its nonionized form[45]. The pH thus has a strong effect on the dissolution of drug products, especially those with pK_a values within the physiological range. This phenomenon has been demonstrated for different types of dosage forms such as immediate- and modified-release [46]-[48].

The pH in the gastrointestinal tract is a function of many variables including prandial condition, time, meal volume and content, and volume of secretions, and it varies along the length of the GI tract (Refer to **Table 1.3** for a summary of pH values in the stomach, duodenum, jejunum and ileum.). The gastric pH in the fasted state has been recorded between 1 and 8 for individuals [49]-[50], with typical median values falling between about 1 and 2 [14], [51]. Dressman et al. found gastric pH to remain below pH 2 68% of the time and

8

below pH 3 90% of the time [51]. Shortly after ingestion of a meal, the pH has been shown to rise to about 6.0-7.0, and decreases back to fasting levels after approximately one to four hours, depending on factors such as meal composition, amount, and pH [14]. Gastric pH values in the fed state have ranged from 2.7-6.4 [14], [51]. An approximation of a typical gastric pH profile as measured by Dressman et al. [51] is shown in **Figure 1.1**.

Average pH values in the fasted upper small intestine have been reported to range from about 4 to 8 [52], [50], with typical values around 6.5 [52]-[54]. Clarysse et al. found duodenal pH in the fasted state to display considerable intra- and inter-subject variability as shown in **Figure 1.2** [33]. In the ileum pH has be reported as 6.5-8 in the fasted state [55]-[56].

The pH in the upper small intestine tends to be lower in the fed compared to the fasted state. As is found in the fed stomach, the pH in the upper small intestine tends to rise after meal intake and slowly decreases over time. Average values have been shown to vary from about 3 to 7 [14], [51], with typical median values around 5 during the later post-prandial stage [56]-[57]. Kalantzi et al. found the pH in the distal duodenum to decrease from 6.6 to 5.2 over the first 210 min following administration of Ensure Plus® [14]. Fed pH values in the ileum have been reported in the range of 6.8-8 [58]. Clarysse et al. found the pH of the administered meal to have a strong impact on local pH, leading to decreased intersubject variability compared to the fasted state during the first 3 hours after meal intake [33]. They found the pH to decrease with time, with minimum individual values of 3.9-4.9, returning to fasting values after about 300 min after meal ingestion. Plots of individual and median pH versus time for the five healthy volunteers in the fasted and fed states as measured by Clarysse et al. are given in **Figure 1.2.**

Buffer capacity

The buffer capacity of the gastrointestinal fluid can affect the dissolution rate, particularly for ionizable drugs. The higher the buffer capacity, the more the buffer will influence pH changes at the drug-liquid interface (i.e., the surface pH)

[25]. The buffer capacity depends on the pH of the fluid, the pK_a of the buffer, and the buffer concentration.

Kalantzi et al. found the median buffer capacity in the stomach to be 7 mmol L^{-1} ΔpH^{-1} 20 min after administration of water and 18 mmol L^{-1} ΔpH^{-1} at later time points (fasted-state conditions) [14]. In the fed state (after ingesting 500 mL Ensure plus), they found median values of gastric buffer capacity to increase from 14 to 28 mmolL^{-1} ΔpH^{-1} over a 30- to 210-min sampling period. They also found intersubject variability to increase with time after meal administration. Values for buffer capacity in the small intestine have ranged from 2-13 mmol/L/pH in the fasted state [35], [53], and 13-30 mmol/L/pH in the fed state [14], [35]. While buffer capacity in the fed ileum is not available, Fadda and co-workers reported buffer capacity in the fasted state to be 6.4 mmol/L/pH [59]. Buffer capacity values found in the literature are summarized in **Table 1.3**.

Osmolality

Osmolality can affect drug release and excipient performance [6]. Delayed dissolution of 5-aminosalicylic acid from Eudragit L coated tablets was shown at higher osmolality [60]. Gastric osmolality in the fasted state has been shown to range from 29-276 mOsm/kg [61]-[62]. Kalantzi et al. found gastric contents in the fasted state to be hypoosmotic, with lower values of 98 mOsm/kg at early time points, plateauing to 140 mOsm/kg at later times. After a meal, Kalantzi et al. found the median value in the stomach to be 559 mOsm/kg after 30 min and 217 mOsm/kg after 210 min, with variability decreasing with time after the meal [14].

In the upper small intestine, osmolality values range from 124-278 mOsm/kg in the fasted state [33], [63], and 250-367 in the fed state [33]. Clarysse et al. found variability in osmolality to be higher in the fed compared to the fasted state, with high fed state fluctuations until 240 min after food intake [33]. They found fasted state values to be hypoosmotic or close to isoosmotic, with an overall median value of 224 mOsm/kg. In the fed- and fat-enriched-fed states they found values to be hyperosmotic during the first three hours post-

prandially, with isoosmotic overall median values of 285 and 278 mOsm/kg, respectively. Jantratid and co-workers also state that osmolality in the distal duodenum increases slightly during the first 120 min after meal intake, and then gradually equilibrates to isosmotic [6]. Osmolality values in the stomach and upper small intestine are provided in **Table 1.3**. Literature values of osmolality in the ileum could not be found.

Surface tension

Surface tension can affect dissolution by influencing wetting of the dosage form [13], with a higher surface tension leading to decreased wetting. Gastric surface tension values in the fasted and fed states range from about 41-46 and 30-31 mN/m, respectively [14]. In the upper small intestine, surface tension values range from 28-46 mN/m in the fasted state, and 27-37 mN/m in the fed state [33], [35]. Surface tension values in the ileum are not available.

Viscosity

Measurement of the viscosity of fluids can be complex. Simple fluids such as water, tea, coffee, simple syrups and edible oils behave as Newtonian fluids where viscosity is constant (i.e., shear rate is proportional to shear stress) [64]. However, many liquefied foods and biological fluids demonstrate non-Newtonian flow behavior meaning that viscosity is dependent upon shear rate, often exhibiting decreased viscosity with increased shear rate (i.e., shear thinning) [64]. For non-Newtonian fluids it is therefore important to know the shear rate at which the viscosity is measured. In part for these reasons, measured values of GI fluid viscosity for humans in the fed and fasted states are very limited. The viscosity of water at 37°C is 0.691 cP (1cP = 1 mPa-s), while the viscosity of various test meals consisting of dietary fibers (e.g., methylcellulose, bran, psyllium, and guar gum) are often administered in solutions with viscosities that range from 10 to >10,000 cP [64]-[66]. Typical meals have therefore been characterized to have viscosities in the range of 10 to 2000 cP [65], [67]. Marciani and coworkers utilized echo-planar Magnetic Resonance Imaging (MRI) in humans to monitor

changes in viscosity of viscous meals and demonstrated significant and rapid reductions in viscosity with time due to dilution by gastric fluids [64]. Viscosity is also influenced by pH in addition to soluble meal content and concentration. Increased viscosity has been shown to generally decrease stomach emptying and prolong GI transit and has been shown to influence blood glucose and cholesterol levels [65], [68].

Temperature

The temperature of GI fluids also affects dissolution and absorption. It can affect the diffusion coefficients of the drug and buffer species, the drug solubility, and the bulk drug concentration. The average GI temperature is generally considered to be 37°C. Several researchers have found 37°C to be an accurate resting temperature, but temperature can increase slightly after exercise. Chin Leong Lim and co-workers used an ingestible telemetric temperature sensor to measure GI temperature during rest and exercise and found the average GI temperature of nine healthy male runners to increase from 37.6°C at rest to 39.3°C after running outside for 45 minutes [69].

Volume

The volume of liquid in the gastrointestinal tract affects the amount and potentially the concentration of dissolved drug. If the volume of liquid is such that the potential bulk concentration of drug exceeds the solubility of the drug, then only a small fraction of the original dose may go into solution. Like other GI parameters, the volume of liquid in the various compartments can vary within and between individuals as well as with time and prandial state. It is affected by the amount of liquid ingested, the volume of gastric and pancreatic secretions, gastric-emptying rate, intestinal transit time, as well as uptake and efflux of liquids along the GI membrane.

Volume of liquid in the stomach depends on the amount of liquid ingested, the rate and amount of secretions, and the rate at which it empties into the small

intestine. Using MRI, Steingoetter and co-workers measured liquid volumes in the fasted stomach before and after ingesting 300 mL of water and found them to be 28 (18-54) mL before water and 296 (279-323) mL after water [70]. However, in another study when Kwiatek et al. examined the ratio of the initial postprandial liquid volume in the stomach to the volume of the infused meal (nutrient drink), they found it to decrease as a function of infused meal volume (ratios of 1.25, 0.95, 0.92, and 0.83 for 200-, 400-, 600-, and 800-mL meal volumes, respectively) [71]. They attributed this progressive decrease in initial gastric volume as a function of meal volume to a larger proportion of liquid nutrient passing into the small intestine during a rapid, early emptying phase. After their measurements of initial volume, they also found the gastric volumes to increase further (due to gastric secretions) before volumes started to decline. They found this increase to be independent of caloric load and greater for the smaller rather than the larger infused meal volumes, demonstrating a slower rate of emptying compared to rate of secretion for the smaller volumes, but a faster rate of emptying compared to rate of secretion for larger volumes. For study participants in a seated position, Steingoetter and co-workers found the contents to be distributed throughout the proximal and distal portions of the stomach, with a distal-to-proximal ratio of 0.23 upon ingestion of the water and 0.58 after 30 min.

Liquid volume in the small intestine depends on the amount of liquid emptying from the stomach, absorption of fluid through the intestinal wall, and intestinal transit time. Volume in the fasted small intestine has been shown to range from 30-420 mL [72], with average values tending to fall near 100 mL in several studies [73]-[75]. It seems that fasting volumes in the small intestine are less dependent on the amount of liquid ingested than fasting volumes in the stomach. Volume in the fed small intestine has been recorded in the range of about 18 to 660 mL [73]-[74], and is more highly dependent on the amount and contents of the meal. Sutton recently modeled the mean plasma concentration profiles of four solubility-limited compounds using literature values of small and large intestinal liquid volumes [76]. On average a small intestinal liquid volume of about 130 mL (range of 10-150 mL) provided the best fits to the data, which is in

agreement with the average small intestinal liquid volumes reported in the literature. Measured human gastric and intestinal liquid volumes from the literature are provided in **Table 1.4**.

Schiller et al. used MRI to show that the GI lumen does not represent a continuous watery compartment [72]. Instead, they found the free water content to exist as fluid pockets. In the fasted small intestine they found the mean number of fluid pockets to be equal to 4, with a median volume of 12 mL per fluid pocket (Refer to **Table 1.5**.). In the fed small intestine the mean number of fluid pockets was 6, with a 4-mL median volume per pocket. In addition, they found the volume of free liquid to be lower in the fed than in the fasted state. Schiller et al. also showed that non-disintegrating capsules ingested prior to MRI acquisition were not completely surrounded by fluid in both the stomach and small intestine in the fasted and fed states. In the fasted small intestine only fifty-percent of ingested capsules (14 out of 28 capsules across multiple subjects) were completely surrounded by fluid. In the fed small intestine 1 out of 5 capsules were completely surrounded by fluid.

Based on these results, it is possible that the volume of water a dosage form is in contact with is less than the volumes shown in **Table 1.4**. In addition, a dosage form may not be exposed to fluid during the entire time it spends in the GI tract. Both scenarios could decrease the solubility and dissolution rate and could lead to an inhomogeneous concentration of drug in the GI lumen. Consequently, the absorption rate of the drug into the GI membrane may not be adequately predicted, as the drug concentration at the intestinal wall may not be similar to the bulk drug concentration.

Hydrodynamics

GI hydrodynamics are partially dependent on contractions in the stomach and small intestine, as well as the amount of liquid and solids present. Layers of smooth muscle contract in a coordinated, rhythmic motion. The contractions cause motility that propels food through the GI tract in a peristaltic motion, mixes

chyme within the GI lumen, and juxtaposes chyme with the brush border of the enterocytes. Smooth muscle also causes intestinal villi to undulate, agitating the unstirred layer of fluid associated with the brush border of the enterocytes [11]. Contractile activity typically initiates in the antrum and migrates distally through the duodenum of the small intestine. The autonomic nervous system and various digestive system hormones control the contractions.

Contractility in the fasted state is characterized by cyclical fluctuations. The cycle comprises three well-defined phases, including a quiescent phase (phase I), a phase of intermittent and irregular contractions that gradually increase in strength (phase II), and a short period of intense contractions (phase III) [77]. This cyclical contractility pattern is called the Migrating Motility Complex (MMC). The MMC can initiate not only in the stomach, but also at various points along the esophagus and small intestine, with the incidences varying in the different segments [10]. The total cycle typically lasts approximately 90-120 min, but has been shown to range from 15-180 min [78].

In the fed state, the MMC is replaced by regular, tonic contractions that propel food toward the antrum and mix it with gastric secretions [79]. During these contractions fine particles and liquids pass from the stomach to the duodenum, while larger particles are retro-pulsed back into the body of the stomach. Once the meal has been emptied from the stomach, the MMC resumes. Gastrointestinal motility influences the gastric emptying rate, intestinal transit time, and mixing patterns of solids and liquids in the stomach and intestine [80]-[83].

Gastric-emptying rate and forces

The gastric emptying rate defines the rate at which liquids and solids empty from the stomach into the upper small intestine. It determines the residence time of a drug in the stomach as well as the rate at which the drug is introduced into the small intestine. As most drugs are absorbed primarily in the small intestine, the rate and extent to which dissolved drug is presented to this segment influences drug absorption, and thus onset of the desired therapeutic

response. Gastric emptying can be the rate-limiting step in absorption for rapidly dissolving, immediate-release BCS I drugs [84].

In the fasted state, the MMC greatly regulates gastric emptying rate, while in the fed state gastric emptying is influenced by low-amplitude contractions as well as pyloric resistance and duodenal feedback mechanisms[77]. In both the fasted and fed states, emptying rate also depends on the amount of liquid or solid ingested, the size/nature of the liquid or solid ingested, and the phase of contraction during which the liquid or solid was ingested (Refer to **Table 1.6** for a summary of gastric residence times from the literature).

Non-nutrient liquids do not normally interrupt the MMC and are typically emptied in an exponential pattern [70], [79]. Granger and co-workers showed that the half-time for saline emptying from the human stomach is 12 min [85], and Steingoetter and co-workers found the half-time for emptying 300 mL of water to be 15.8 min [70].

Gastric emptying postprandially is largely dependent on meal size and composition [79]. When nutrient liquids or solid meals are ingested, the MMC can be interrupted due to feedback mechanisms in the duodenum. A 25% glucose solution has been shown to empty in 75 min in humans [79]. Kwiatek and co-workers found gastric emptying half time to decrease with increasing nutrient liquid volume and increase with increasing calorie load [71] as shown in **Table 1.7**. Dressman et al. summarized typical solid-meal half-emptying rates in humans from the literature and found them to range from 70-130 min [79].

It is thought by many researchers that beyond a size of 2-7 mm, gastric emptying of solid dosage forms or solid particulates differs from that of liquids and occurs mainly during phase II and III of the MMC [84]. Bass showed that single tablets ranging in diameter from about 5-13 mm typically left the stomach between 5 and 120 min (the average MMC cycle time), although times ranged from 5 to over 200 min, with high intrasubject and intersubject variability [77]. Rhie et al. demonstrated that gastric emptying of 0.7 mm caffeine pellets happened during the fed state, while 3.6 mm acetaminophen pellets emptied following the onset of phase II contractions in the fasted state [86]. Using

modeling, Higaki et al. found gastric emptying of 0.7 mm caffeine pellets in the fed state to be regulated by gastric motor activity, with absorption kinetics closely related to the gastric-emptying profiles. Podczeck et al. showed that 3-mm- and 10-mm-diameter tablets emptied after food (dextrose solution, beef solution, or shepherd's pie) had left the stomach, and that the influence of tablet diameter on median emptying time was significantly less than the influence of administering solid food (shepherd's pie) compared to liquid meals (dextrose or beef solutions) [87].

The forces to which tablets are exposed in the stomach were evaluated in both the fed and fasted states by Kamba and coworkers [88]. They utilized specially designed Teflon tablets with predetermined crushing strengths to evaluate these forces. They found that tablets with a crushing strength of 1.5 N were crushed in all four subjects under fed conditions and two of five subjects under fasting conditions. Tablets with a higher crushing strength of 1.89 N were crushed in two of six subjects under fed conditions and zero of five subjects under fasting conditions. The authors reasoned that the lower crushing forces in the fasted state occurred because of the open pylorus, resulting in lower overall forces being applied to the stomach contents. Laulicht and coworkers also investigated gastric forces using a magnetic tracking system [89]. The average human gastric emptying force was 414±194 dyn in the fasted state, which was statistically insignificantly lower than the 657±84 dyn measured in the fed state. Corresponding area normalized gastric emptying pressures were approximately 600 dyn/cm^2 in the fasted state and 960 dyn/cm^2 in the fed state.

Intestinal transit time and flow rate

The transit time (i.e., residence time) of a drug in the intestinal tract is a strong determinant of dissolution and absorption. It affects the amount of time a drug has to dissolve and absorb in the GI tract. The transit time of a dosage form in different segments of the GI tract is dependent upon factors such as gastric emptying rate and flow rate, and can vary significantly for even a single individual. Weitschies et al. performed a study on one individual in which they

17

administered a non-disintegrating capsule to a volunteer on several separate occasions and monitored it using magnetic marker monitoring [90]. As shown in **Figure 1.3**, the variability in residence times in different segments of the GI tract was high even for a single individual. Refer to **Table 1.6** for a summary of intestinal residence times from the literature.

Transit time in the small intestine is often quoted to be 3-4 h. McConnell and co-workers found times to range from 0.5-5.4 h with a mean of 3.2 h for a single individual given a 1-1.4-mm ethylcellulose –coated pellet on eight separate occasions[10]. Based on a review of the literature they stated that food has generally not been associated with changes in transit time in the small intestine.

Davis et al. completed a meta-analysis of transit data and found no difference in the intestinal transit times of tablets, pellets, and liquids [91]. Coupe et al. found transit times in the small intestine to range from 2.2 to 5.9 h for pellets and 0.9-6.2 h for 11.5-mm tablets [92].

The mean intestinal flow rate during fasting for all three phases of the MMC was shown to be 0.73 mL/min in the jejunum and 0.33 mL/min in the ileum (the flow rate in the duodenum was too fast to measure) [93]. The flow rates were shown to increase postprandially, with a value of 3.0 mL/min in the jejunum and 2.35 mL/min in the ileum [93]. Granger and co-workers stated that chyme traverses the small intestine in humans at a rate of 1-4 cm/min, with the velocity being faster in the duodenum and proximal jejunum compared to the ileum [85]. **Table 1.6** includes a summary of intestinal transit times and flowrates from the literature.

Intestinal transit time is especially important for dosage forms that are not fully absorbed, as a change in contact time with the absorption area will result in a change in the fraction absorbed. While in general an increase in transit time will lead to an increase in the absorption of poorly or incompletely absorbed drugs, absorption can be decreased in cases where transit time is slowed because of an inhibition of smooth muscle motility due to a decrease in agitation of the unstirred layer [11].

18

Geometry & Composition of Intestinal Membrane

Surface area

Absorption rate is a function of the gastrointestinal surface area over which the drug is exposed. Generally speaking, a larger surface area would lead to a greater absorption rate. Drugs are rarely absorbed in the stomach due to its small surface area and short residence times [94]. The small intestine is the major site of drug absorption due to its large surface area and longer residence times. The mucosal surface of the small intestinal lumen is convoluted. Finger-like projections called villi extend from the luminal surface, and each villus is covered with smaller microvilli. Together, the convoluted mucosa along with the villi and microvilli increase the surface area of the small intestine approximately 600-fold above that of a flat tube of the same overall length and diameter [23]. These anatomical modifications increase the surface area of the duodenum and upper jejunum to a greater extent than the ileum, with the majority of surface area in the small intestine found in the jejunum [11].

While the absolute surface area in the small intestine is quite large as described above, the geometric surface area (calculated solely based on the overall length and diameter of the intestine) may be a better estimate of the area of exposure for a dosage form, as it more accurately reflects the surface area of the unstirred layer which is a barrier to drug absorption. Absolute and geometric surface areas, as well as geometries are included in **Table 1.4**.

Nature of intestinal membrane and absorption mechanisms

Absorption of drugs in the GI tract occurs mainly in the intestine. Several positive factors help drive absorption, including a concentration gradient, electrochemical potential difference, and hydrostatic pressure gradient between the intestinal lumen and the membrane [95]. In addition, several other factors deter drug absorption, including the physical barrier of the intestinal mucosa as a result of tight junctions and the lipid composition of the membrane, as well as

biochemical barriers such as the presence of metabolizing enzymes and efflux transporters [95].

The pathways for drug absorption include carrier-mediated transcellular transport, vesicular transport, passive paracellular transport, and passive transcellular transport. In carrier-mediated transcellular transport, influx transporters expressed on the mucosa actively carry drugs across the membrane. The vesicular transport route includes fluid-phase endocytosis, receptor-mediated endocytosis, and transcytosis. In the passive paracellular route, drug absorption occurs through an extracellular route across the epithelium. Diffusion is regulated by electrochemical potential gradients derived from concentration differences and by electrical and hydrostatic pressure gradients between the two sides of the epithelium [95]. Tight junctions are the main barriers to this type of absorption. Finally, passive transcellular transport occurs when drugs move across the apical membrane, through the cytoplasm, and across the basolateral membrane. The surface area available for this type of transport makes up 99.9% versus 0.01% for the passive paracellular pathway [95].

As mentioned above, enzymes expressed on enterocytes can metabolize some drugs, causing a decrease in absorption. In addition, drugs can be metabolized or degraded in the GI lumen. In addition, efflux transporters mediate the transfer of some compounds from the cytoplasm back into the intestinal lumen. These factors all decrease the net absorption of drugs in the intestinal membrane and thus lower the potential bioavailability.

Physiological dissolution methodologies

Simulated gastric and intestinal fluids are media designed to mimic the major characteristics of *in vivo* fluids. Simulated gastric fluid (SGF) and simulated intestinal fluid (SIF) were described in the USP as early as 1955 [96]. As our knowledge of GI physiology has increased over the years, these fluids have been updated to more closely mimic *in vivo* characteristics. The most recent update

by Jantratid and co-workers presents the most up-to-date fluids (Refer to **Tables 1.8** and **1.9.)** and summarizes some of the changes made over the years [6]**.** Jantratid and co-workers have proposed the use of "snapshot media" to simulate both gastric and intestinal fluids during different stages after meal consumption. Despite some potential drawbacks, simulated gastric and intestinal fluids make dissolution testing more physiological compared to using simple buffers and a number of successful IVIVCs have been generated using these fluids [97]-[98].

While existing *in vitro* systems partially address some of the major fluid components by utilizing simulated fluids, existing dissolution and dosage form testing methodologies generally fail to adequately address physiologically relevant hydrodynamics of fluid flow, shear and viscosity [2], [6], [67]. New, innovative dissolution methodologies that are more reflective of *in vivo* hydrodynamics and fluid content in the human intestinal tract are needed. Current dissolution methodologies produce variable and generally extremely high fluid velocities and thus "unrealistic" fluid flow (e.g., 5000<Re<10000) [99]-[102], while current information on fluid flow in the human stomach and intestine indicate Re in the range of 1 to 30 [67], [82]-[83], [103]-[104]. Novel dissolution methodologies that characterize dissolution under low Re and fluid shear are required to better simulate dissolution *in vivo*.

Conclusions

Pharmaceutical solid oral dosage forms must undergo dissolution in the intestinal fluids of the gastrointestinal tract before they can be absorbed and reach the systemic circulation. Therefore, dissolution is a critical part of the drug-delivery process. The characteristics of the physiological environment such as buffer species, pH, bile salts, gastric emptying rate, intestinal motility, and hydrodynamics will significantly impact dissolution and absorption. While significant progress has been made since 1970, when the first compendial dissolution test was introduced, current dissolution testing does not take full advantage of the extensive physiologic information that is available. For quality

control purposes, where the question is one of lot-to-lot consistency in performance, utilizing nonphysiological test conditions that match drug and dosage form properties with practical dissolution media and apparatus may be appropriate. However, where IVIVCs are desired, it is logical to consider and utilize knowledge of the *in vivo* situation. Physiologically relevant information must serve as a basis for the design of dissolution test methods and systems that are more representative of the human condition. As *in vitro* methods advance in their physiological relevance, better IVIVCs will be possible. *In vitro* systems can then be more effectively utilized to design dosage forms that have improved and consistent oral bioperformance.

Tables and Figures

Table 1.1. Drug properties and physiological properties that influence oral drug dissolution and absorption

Parameter	Drug properties	Physiological parameters
Drug diffusion coefficient, D	Radius, mass, volume	Solute concentration, temperature, fluid viscosity
Drug surface area, A	Particle size, size distribution, shape, state of particle aggregation	Fluid hydrodynamics
Length of hydrodynamic boundary layer (stagnant diffusion layer), h	Particle size, diffusion coefficient	Fluid velocity, viscosity, diffusion coefficients of diffusing species
Saturated solubility, C_s	Intrinsic solubility (molecular size, crystal properties, chemical groups), pK_a	Buffer species, buffer concentration, buffer capacity, pH, presence of lipolytic products, bile salts, and phospholipids, temperature
Bulk concentration, C_b	Dose, intrinsic solubility (molecular size, crystal properties, chemical groups), pK_a, intestinal permeability	Fluid volume (fluid ingested, gastric-emptying rate, transit time), absorption in GI membrane, buffer species, buffer concentration, buffer capacity, pH, presence of lipolytic products, bile salts, and phospholipids, temperature
Intestinal wall permeability, P_w	Absorption mechanism (Simple diffusion: lipophilicity, charge, polarity. Facilitated diffusion or active transport: affinity for membrane channels or pumps)	Intestinal segment, Composition of intestinal wall, number of channels or transporters, apparent permeability to mass transport (turbulence due to intestinal wall contractions)
Concentration at the intestinal wall, C_w	Dose, intrinsic solubility (molecular size, crystal properties, chemical groups), pK_a, permeability, diffusion coefficient	Hydrodynamics, viscosity, shear, transit time

Table 1.2. Literature values for concentrations of some major components of fluid in the fasted and fed stomach and small intestine

The designation (e) indicates a value that was measured early in the post-prandial phase (between 0 and 60 minutes), (m) denotes a value measured in the mid post-prandial phase, and (l) denotes a value that was measured late in the post-prandial phase (greater than 100 minutes). Unless indicated next to the value, units are noted next to the name of the component.

			Stomach	Duodenum	Jejunum	Ileum
Bicarbonate (mEq L^{-1})	Fasted	Mean	7.3^a	2.7[105], 6.7[106], 15^b	17[105], 30^b, 30^c, 8.2±5 mM^d	40^d, 50[107], 70^b, 74[108], 75^c, 30±11mM^d
		Range	9-20^g		2-20^e, 5-10[109], 6-20^f	
	Fed	Mean		10^h		
Bile salts (mM)	Fasted	Median	0.100^j	2.7^k, 2.6^l		
		Mean	0.08±0.03^l, 0.275[110], 0.081^m	6.4±1.3^n, 4.3±1.2^n, 5.90±1.8^o	2±0.2^p	
		Range		1-5.3^q, 0.6-5.1^r, 0.3-9.6^j	0.8-5.5^r, 0.1-13.3^j, 5-6^n, 0-17^n	2-10^s
	Fed	Median		3.6^j, 5.2^j, 8.3 (e)^j, 11.9 (e)^j, 11.2(e)^k, 5.2(l)^k		1.0^t, 0.5^t
		Mean	0.06[20]	14.5(e)^u, 5.2(m)^u, 16.2±1.5[111], 9.7±1[111], 9.1^m	8[112], 15[112], 8±0.1^p, 6.5±0.9[111]	
		Range		1.6-6.2^j, 3.2-6.8^j, 6.7-13.4^o	0.5-40^t(graph), 3-34[112]	0.5-30^t, 0.2-1.3^t

^{a} From reference 21. ^{b} From reference 40. ^{c} From reference 42. ^{d} From reference 43. ^{e} From reference 39. ^{f} From reference 41. ^{g} From reference 22. ^{h} From reference 44. ^{i} From reference 50. ^{j} From reference 33. ^{k} From reference 14. ^{l} From reference 20. ^{m} From reference 19. ^{n} From reference 2. ^{o} From reference 18. ^{p} From reference 35. ^{q} From reference 34. ^{r} From reference 53. ^{s} From reference 38. ^{t} From reference 36. ^{u} From reference 37. ^{v} From reference 15. ^{w} From reference 16. ^{x} From reference 17.

Table 1.2 (Cont'd)

			Stomach	Duodenum	Jejunum	Ileum
Lipids (mg/mL)	Fasted	Median	0.56[o]	0.5[j]	0.1±0.01mM[p]	
		Mean		0.6[o]		
		Range		0-1.8[j]		
	Fed	Median		1.8[j], 2.6[j]	22±1mM[p]	
		Mean				
		Range	50 (l)[o], 150(e)[o]	0.5-4.6[j], 1.1-3.6[j], 55-100[o]		
Phospholipids (mM)	Fasted	Median		0.6[j]	0.2±0.07[p]	
		Mean				
		Range		0.1-1.5[j], 0.03-0.06[q]		
	Fed	Median		1.8[j], 1.2[j]	3±0.3[p]	
		Mean				
		Range		1.3-2.4[j], 0.8-1.6[j]		
Pepsin (mg/mL)	Fasted	Median	0.11 (e)[k], 0.22 (m)[k]			
		Mean	0.87[v]			
		Range	0.83-1.27[w]			
	Fed	Median				
		Mean	1.25[v], 1.68[v]			
		Range	0.26-0.58[w], 0.56-1.72[w]			
Lipase	Fasted	Mean	~0.1mg/mL[x]			
		Range				
	Fed	Range	11.4-43.9 U/mL[o]			
Potassium (mM)	Fasted	Mean	13.4±3.0[i]		5.4±2.1[i], 4.8±0.5[43]	4.9±1.5[43]
Sodium (mM)	Fasted	Mean	68±29[i]		142±13[i], 142±7[43]	140±6[43]
	Fed	Mean			106±15[t], 101±17[t]	139±11[t], 133±8[t]
Chloride (mM)	Fasted	Mean	102±28[i]		126±19[i], 135±8[43]	125±12[43]
Calcium (mM)	Fasted	Mean	0.6±0.2[i]		0.5±0.3[i]	

[a] From reference 21. [b] From reference 40. [c] From reference 42. [d] From reference 43. [e] From reference 39. [f] From reference 41. [g] From reference 22. [h] From reference 44. [i] From reference 50. [j] From reference 33. [k] From reference 14. [l] From reference 20. [m] From reference 19. [n] From reference 2. [o] From reference 18. [p] From reference 35. [q] From reference 34. [r] From reference 53. [s] From reference 38. [t] From reference 36. [u] From reference 37. [v] From reference 15. [w] From reference 16. [x] From reference 17.

Table 1.3. Literature values for properties of fluids in the fasted and fed stomach and small intestine

The designation (e) indicates a value that was measured early in the post-prandial phase (between 0 and 60 minutes), (m) denotes a value measured in the mid post-prandial phase, and (l) denotes a value that was measured late in the post-prandial phase (greater than 100 minutes). Unless indicated nest to the value, units are noted next to the name of the component.

			Stomach	Duodenum	Jejunum	Ileum
Buffer capacity (mmol L^{-1} pH^{-1}	Fasted	Median	7 (e)[a], 18[a]	5.6[a]		
		Mean			3.23[59]	6.4[b]
		Range		4-13[c]	2.4-2.8[d]	
	Fed	Range	14-28[a]	18-30[a]	13.2-14.6[d]	
Osmolality (mOsm kg^{-1})	Fasted	Median	98 (e)[a], 140 (l)[a]	178[a], 224[e]		
		Mean	29[t], 191±36[g], 33.6±5.9[h] 221±15[h]	142[t], 137±54[c]	271±15[g], 200±68[c], 278±16[h]	
		Range	171-276[l]	124-266[e]		
	Fed	Median	559 (e)[a], 217 (l)[a]	287[e], 276[e], >287 (e)[a], 287 (l)[a]		
		Range		250-367[e], 268-304[e]		
Surface tension (mN m^{-1})	Fasted	Median		32.3[a], 41.2[e]		
		Mean			28±1[d], 33.7±2.8[h]	
		Range	41.9-45.7[a]	33.3-46.0[e]		
	Fed	Median		34.2[e], 35.4[e]		
		Mean			27±1[d]	
		Range	30-31[a]	32.2-36.7[e], 33.7-36.0[e]		

[a] From reference 14. [b] From reference 59. [c] From reference 53. [d] From reference 35. [e] From reference 33. [f] From reference 61. [g] From reference 50. [h] From reference 63. [i] From reference 62. [j] From reference 67. [k] From reference 51. [l] From reference 52. [m] From reference 57. [n] From reference 54. [o] From reference 55. [p] From reference 49. [q] From reference 56. [r] From reference 58. [s] From reference 58.

Table 1.3. (cont'd)

			Stomach	Duodenum	Jejunum	Ileum
Viscosity (cP)	Fasted	Range				
	Fed	Range	10-2000[l]			
pH	Fasted	Median	1.7[k], 2.4 (e)[a], 1.7 (l)[a], 1.8[143]	6.1, 6.2[a], 6.6[e], 5.63[113]	7.2[k]	
		Mean	2.9 ± 1.97[g]	6.71±0.44[l], 7.0±0.4[c], 4.9[m], 6.4±0.6[n]	6.8±0.4[c], 7.5[d], 7.1± 0.60[g]	6.5±0.2[o]
		Range	1-2.5[p], 1.4-2.1[k], 1.23-7.36[a], 1.4-7.5[g]	5.8-6.5[k], 4.00-5.39[m], 5.17-6.10[n]	4.4-6.5[114], 5.3-8.1[k], 5.3-8.1[g]	6.8-8.0[q]
	Fed	Median	5.0[k], 6.4 (e)[a], 2.7 (l)[a]	5.4[k], 6.6 (e)[a], 5.2 (l)[a], 5.9[e], 6.1[e], 5.35[r]		
		Mean		5.2 (e)[m], 4.2 (l)[m]	6.2±0.2 (e)[115], 5.4 ± 0.2 (l)[115], 6.1[d]	7.5[116]
		Range	4.3-5.4[k]	3.1-6.7[k], 4.5-5.5 (e)[m], 3.9-4.8 (l)[m], 5.1-5.7 (e)[117], 5.3-6.1 (l)[117], 4.6-6.3[58]	5.2-6.0 (e)[m]	6.8-7.8[118], 6.8-8.0[s]

[a] From reference 14. [b] From reference 59. [c] From reference 53. [d] From reference 35. [e] From reference 33. [f] From reference 61. [g] From reference 50. [h] From reference 63. [i] From reference 62. [j] From reference 67. [k] From reference 51. [l] From reference 52. [m] From reference 57. [n] From reference 54. [o] From reference 55. [p] From reference 49. [q] From reference 56. [r] From reference 58. [s] From reference 58.

27
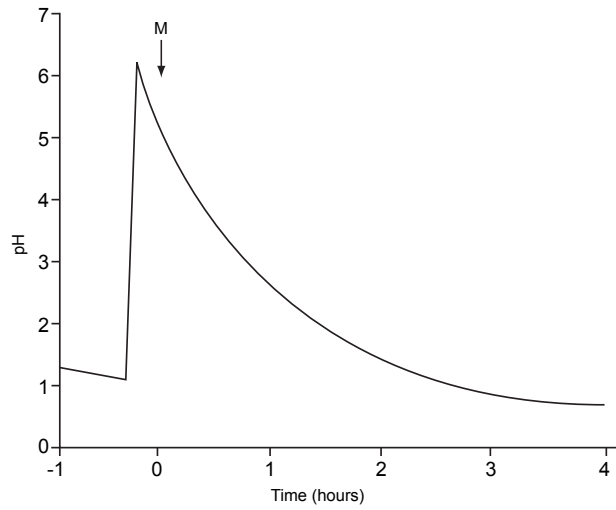
Figure 1.1. Approximation of a typical pH profile in the stomach

The letter "M" denotes food intake (Redrawn from reference 51).
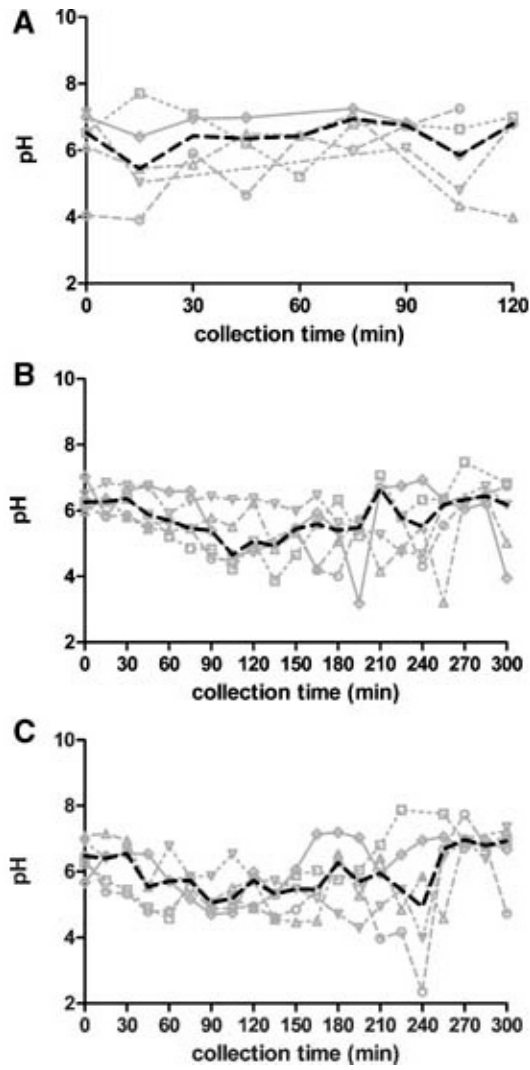
Figure 1.2. Individual and median pH versus time in fasted (A), fed (B), and fat-enriched fed (C) state human duodenal fluid for five healthy subjects
Darkened lines represent median values[33]. (Reprinted from reference 33 with permission.)

Table 1.4. Literature values for liquid volumes and geometry in the fasted and fed stomach and small intestine
Values for the small intestine are for the entire small intestine unless the value is contained in an individual column.

			Stomach	Small Intestine		
				Duodenum	Jejunum	Ileum
Volume (mL)	Fasted	Mean	28[a] 296 (300mL water)[a] 27[119]	86[b], 81[b], 112±27[c], 109 ± 36[c], 165±22[d], 105±72[e]		
		Range	18-54[a] 279-323(300mL water)[a] 21-33[119]	34-46[b] 37-130[b] 45-319[e]		
	Fed	Mean	250±23 (200mL)[f], 380±25 (400mL)[f], 555±30 (600mL)[f], 664±34(800mL)[f]	47[b] 381[b] 590±73[c] 54±41[e]		
		Range		18-78[b], 343-491[b], 20-156[e]		
Surface area (cm²)	Absorbing[120]	Mean	525.58 ± 24.143[g], 1100[h]	10^4-1.2 X 10^4 (considering valves of keckring), 10^5 (considering villi), 2 X 10^6 (considering microvilli)		
				900[h]	600000[h]	600000[h]
	Geometric	Mean	942[i]	393[i], 197-490[j] 3300[120]	4712[i], 825-1319j	4712[i], 980-1862j

[a] From reference 70. [b] From reference 73. [c] From reference 74. [d] From reference 75. [e] From reference 72. [f] From reference 71. [g] Surface area of gastric mucosa. [h] From reference 95. [i] Calculated using length and diameter from reference 95 assuming cylindrical geometry. [j] Calculated using absolute diameter and physiological length from reference 120 assuming cylindrical geometry. [k] Anatomical lengths measured at autopsy or from material recovered from surgery and physiological lengths measured from living persons.

Table 1.4 (Cont'd)

			Stomach	Small Intestine		
				Duodenum	Jejunum	Ileum
Length (cm)[120, k]	Anatomical	Mean			680	
		Range			255-1128	
		Mean			260	395
		Range		25-30		
	Physiological	Mean			282	
		Range			229-337	
		Mean		21	105	156
		Range		18-26		
Diameter (cm)	Absolute	Mean	15[h]	5[h], 4[120]	5[h]	5[h]
		Range		3.5-6[120]	2.5-4[120]	2-3.8[120]
	Cranial to caudal [120]	Mean	37			
		Range	29.5-49.5			
	Greatest diameter[120]	Mean	15			
		Range	6.5-21.5			
	Body[120]	Mean	11			
		Range	4-19			
	Pyloric antrum[120]	Range	4-5			

[a] From reference 70. [b] From reference 73. [c] From reference 74. [d] From reference 75. [e] From reference 72. [f] From reference 71. [g] Surface area of gastric mucosa. [h] From reference 95. [i] Calculated using length and diameter from reference 95 assuming cylindrical geometry. [j] Calculated using absolute diameter and physiological length from reference 120 assuming cylindrical geometry. [k] Anatomical lengths measured at autopsy or from material recovered from surgery and physiological lengths measured from living persons.

31

Table 1.5. Total volume, number and volume of liquid pockets, and proximity of capsules to liquid-filled regions in the fasted and fed small intestine
(Reproduced from reference [72].). Fasting conditions and 1 hour after a meal (n=12)[72].

Condition		Fasted	Fed
Total volume of liquid (mL)	Mean± s.d	105±72[a]	54±41[a]
	Range	45-319	20-156
	Median	83	39
	Individual (approx.)[b]	45, 48, 69, 73, 77, 81, 85, 94, 113, 115, 130, 319	20, 22, 26, 28, 30, 38, 44, 50, 70, 75, 101, 156
Number of liquid pockets	Mean	4[c]	6[c]
	Individual (approx.)[b]	2, 3, 4, 5, 8	2, 5, 6, 7, 11
Volume of liquid pocket (mL)	Median	12[d]	4[d]
Number of capsules surrounded by liquid	No./Total	14/28	1/5
Number of capsules partially surrounded by liquid	No./Total	6/28	1/5
Number of capsules not in contact with liquid	No./Total	8/28	3/5

[a] $P<0.01$. [b] Approximate values read from graph. [c] $P<0.05$. [d]$P<0.001$
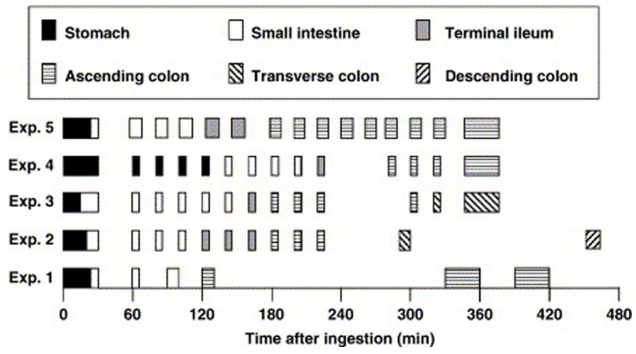
Figure 1.3. Gastrointestinal transit of magnetically marked non-disintegrating capsules in a single volunteer after ingestion with 150 mL of water
Capsule taken after 8 h of fasting. Lunch served 240 min after ingestion of the capsule in experiments 1-4[90] (Reprinted from reference 90, with permission.).

Table 1.6. Literature values for residence time in the stomach, residence time in the small intestine and small intestinal flow rates

Time for half-emptying - stomach (min)	Fasted	Mean	15.8 (300mL water) [a], 12 (saline) [b], 75 (glucose) [c]
		Range	11.5-17.0 (300mL water) [a]
	Fed	Mean	44±15 (liquids) [121], 105±21 (solids) [121], 40±13 [121], 32±7 (liquids) [122], 46±9 (liquids) [122], 67±9 (liquids) [122], 76±6 (liquids) [122], 72 [d], 69 [d]
		Range	69-93 [d], 50-76 [d]
Time for complete emptying - stomach (min)	Fasted	Mean	25 [a]
	Fed	Mean	40 [d]
Transit time - entire small intestine (min)	Fasted	Mean	192 (coated pellets) [e]
		Range	90-324 (coated pellets) [e], 132-354 (pellets) [f], 54-372 (tablets) [f]
	Fed	Mean	276±99 h (liquids) [121], 342±120 h [g]
		Range	
Transit time - duodenum to jejunum (min) [123],	Fed	Mean	32±3 (40kcal/h) 30±1 (90kcal/h), 32±2 (160kcal/h)
Transit time - duodenum to ileum (min) [123]	Fed	Mean	59±2 (160kcal/h), 47±3 (40kcal/h), 47±2 (90kcal/h)
Flow rate - jejunum (mL/min) [h]	Fasted	Mean	0.73
	Fed	Mean	3.0
Flow rate – ileum (mL/min) [h]	Fasted	Mean	0.33
	Fed	Mean	2.35

[a] From reference 70. [b] From reference 85. [c] From reference 79. [d] From reference 73. [e] From reference 10. [f] From reference 92. [g] From reference 49. [h] From reference 93.

Table 1.7. Effects of meal volume and caloric load on the half-emptying time of gastric contents

(Reproduced from reference 71.) Data and standard error between any 2 volumes (in parenthesis) were estimated from mixed-effects model. The standard errors for differences between 2 volumes are given in parenthesis[71].

Caloric load (kcal)	Meal Volume (mL)			
	200	400	600	800
200	56 (7)	41 (8)	42 (8)	38 (8)^a
300	74 (7)$^+$	59 (8)^b	60 (8)^b	56 (8)^{a,b}
400	92 (7)$^+$	77 (8)^b	78 (8)	74 (8)^{a,b}

^{a}P ≤ 0.05 vs. 200 mL ^{b}P < 0.01 vs. 200 kcal[71].

Table 1.8. Evolution of fasted and fed simulated gastric fluids

Fluid name	USP SGF, TS[96]	FaSSGF[a]	N/A[b]	FeSSGF[b]	N/A[b]
Prandial state	Fasted	Fasted	Fed (early)	Fed (middle)	Fed (late)
Year	1955	2005	2008	2008	2008
Buffer type	-	-	-	Acetate	Phosphate
Buffer concentration (mM)	-	-	-	46.9	37.5
pH	~1.2	1.6	6.4	5.0	3
Buffer capacity (mmol/L/pH)	-	-	21.33	25	25
Osmolality (mOsm/kg)	Not available	120.7 ± 2.5	559	400	300
Surface tension (mN/m)	50.81[124]	42.6	49.7 ± 0.3	52.3 ± 0.3	58.1 ± 0.2
Composition	Hydrochloric acid, 70 mM Pepsin, 3.2 g/L Sodium chloride, 34.2 mM	Sodium taurocholate, 80 µM Lecithin, 20 µM Pepsin, 0.1 mg/mL Sodium Chloride, 34.2 mM Hydrochloric acid, q.s.	Sodium chloride, 148 mM Milk:buffer, 1:0 Hydrochloric acid/Sodium hydroxide, q.s.	Sodium chloride, 237.02 mM Acetic acid, 17.12 mM Sodium acetate, 29.75 mM Milk:buffer, 1:1 Hydrochloric acid/Sodium hydroxide, q.s.	Sodium chloride, 122.6 mM Ortho-phosphoric acid, 5.5 mM Sodium dihydrogen phosphate, 32 mM Milk:buffer, 1:3 Hydrochloric acid/Sodium hydroxide, q.s.

[a] From reference 17. [b] From reference 6.

Table 1.9. Evolution of fasted and fed simulated intestinal fluids

Fluid name	USP SIF, TS[a]	USP SIF, TS[b]	FaSSIF[125]	FaSSIFm[126]	FaSSIF-V2[c]	FeSSIF[125]	FeSSIFc[126]	FeSSIF-V2[c]
Prandial state	N/A	Fasted	Fasted	Fasted	Fasted	Fed	Fed	Fed (early, middle, late)
Year	1960[d]	1996	1998	2004	2008	1998	2004	2008
Buffer type	Phosphate	Phosphate	Phosphate	Maleate	Maleate	Acetate	Citrate	Maleate
Buffer concentration (mM)	50.0[d]	50.0	28.7	25.0	19.1	144	84	55.0
pH	7.5	6.8	6.5	6.5	6.5	5.0	5.0	5.8
Buffer capacity (mmol/L/pH)	N/A	18.4 ± 0.2 (w/o pancreatin)	12	12	10	76	76	25
Osmolality (mOsm/kg)	N/A	113	270±10	270±10	180±10	635 ± 10	635 ± 10	390 ± 10
Surface tension (mN/m)	N/A	N/A	N/A	N/A	54.3	N/A	N/A	40.5 ± 2
Composition (mM unless otherwise specified)	Monobasic K phosphate, 50.0[d] NaOH, ~15.4[d] Pancreatin, 10.0g/L HCl/NaOH, q.s.	Monobasic K phosphate, 50.0 NaOH, ~15.4 Pancreatin, 10.0g/L HCl/NaOH, q.s.	Sodium taurocholate, 3 Egg phosphatidylcholine, 0.75 Na dihydrogen phosphate, 28.66 NaOH, ~13.8 NaCl, 106	Na taurocholate, 3 Egg phosphatidylcholine, 0.75 Maleic anhydride, 25.01 NaOH, ~45 NaCl, 109	Na taurocholate, 3 Lecithin, 0.2 Maleic acid, 19.12 NaOH, 34.8 NaCl, 68.62	Na taurocholate, 15 Egg phosphatidylcholine, 3.75 Acetic acid, 144 NaOH, ~101 NaCl, 173	Na taurocholate, 15 Egg phosphatidylcholine, 3.75 Citric acid, 84 NaOH, ~200 NaCl, 206	Na taurocholate, 10 Lecithin, 2 Glyceryl monooleate, 5 Maleic acid, 55.02 Na oleate, 0.8 NaOH, 81.65 NaCl, 125.5

[a] From reference 127. [b] From reference 128. [c] From reference 6. [d] USP SIF, TS was first introduced in 1955 with a buffer concentration of 6.4 mM and a sodium hydroxide concentration of about 38 mM [96].

References

1.   Abdou, H. M., Effect of the Physicochemical Properties of the Drug on Dissolution Rate. In *Dissolution, Bioavailability and Bioequivalence*, 1st ed.; Gennaro, A.;Migdalof, B.;Hassert, G. L.;Medwick, T., Eds. Mack Publishing: Easton, PA, 1989; pp 56-72.

2.   Dressman, J. B., Amidon, G. L., Reppas, C. and Shah, V. P., Dissolution Testing as a Prognostic Tool for Oral Drug Absorption: Immediate Release Dosage Forms. *Pharm. Res.* **1998**, *15*, 11-22.

3.   USP, The United States Pharmacopeia USP 31, the National Formulary NF 26. The United States Pharmacopeial Convention, Inc.: Rockville, 2008.

4.   Amidon, G. L., Lennernas, H., Shah, V. P. and Crison, J. R., A Theoretical Basis for a Biopharmaceutic Drug Classification: The Correlation of in Vitro Drug Product Dissolution and in Vivo Bioavailability. *Pharm. Res.* **1995**, *12*, 413-420.

5.   FDA, Guidance for Industry. Waiver of the in Vivo Bioavailability and Bioequivalence Studies for Immediate-Release Solid Oral Dosage Forms Based on a Biopharmaceutics Classification System. U.S. Department of Health and Human, Food and Drug Administration (FDA), Center for Drug Evaluation and Research: Washington, DC, 2000; pp 1-13.

6.   Jantratid, E., Janssen, N., Reppas, C. and Dressman, J., Dissolution Media Simulating Conditions in the Proximal Human Gastrointestinal Tract: An Update. *Pharm. Res.* **2008**, *25*, 1663-1676.

7.   Carino, S. R., Sperry, D. C. and Hawley, M., Relative Bioavailability Estimation of Carbamazepine Crystal Forms Using an Artificial Stomach-Duodenum Model. *J. Pharm. Sci.* **2006**, *95*, 116-125.

8.   Grassi, M., Grassi, G., Lapasin, R. and Colombo, I., Drug Dissolution and Partitioning. In *Understanding Drug Release and Absorption Mechanisms, a Physical and Mathematical Approach*, CRC Press: Boca Raton, 2007; pp 249-327.

9.   Vangani, S., Li, X., Zhou, P., M., D.-B., Chiu, R., Cauchon, N., Gao, P., Medina, C. and Jasti, B., Dissolution of Poorly Water-Soluble Drugs in Biphasic Media Using Usp 4 and Fiber Optic System. *Clinical Research and Regulatory Affairs* **2009**, *26*, 8-19.

10. McConnell, E. L., Fadda, H. M. and Basit, A. W., Gut Instincts: Explorations in Intestinal Physiology and Drug Delivery. *Int. J. Pharm.* **2008**, *364*, 213-226.

11. DeSesso, J. M. and Jacobson, C. F., Anatomical and Physiological Parameters Affecting Gastrointestinal Absorption in Humans and Rats. *Food Chem. Toxicol.* **2001**, *39*, 209-228.

12. Florence, A. T. and Attwood, D., Properties of the Solid State. In *Physicochemical Principles of Pharmacy*, 2nd ed.; Chapman and Hall: New York, 1988; pp 21-46.

13. Dahan, A. S. and Amidon, G. L., Gastrointestinal Dissolution and Absorption of Class II Drugs. In *Drug Bioavailability, Estimation of Solubility, Permeability, Absorption, and Bioavailability*, 2 ed.; van de Waterbeemd, H.;Testa, B., Eds. Wiley-VCH: Weinheim, 2009; pp 33-51.

14. Kalantzi, L., Goumas, K., Kalioras, V., Abrahamsson, B. and Reppas, C., Characterization of the Human Upper Gastrointestinal Contents under Conditions Simulating Bioavailability/Bioequivalence Studies. *Pharm. Res.* **2006**, *23*, 165-176.

15. Schmidt, H. A., Fritzlar, G., Dolle, W. and Goebell, H., Comparative Studies on the Histamine and Insulin Stimulated Acid Pepsin Secretion in Patients Suffering from Ulcus Duodeni and Control Persons. *Dtsch. Med. Wochenschr.* **1970**, *95*, 2011-2006.

16. Lambert, R., Martin, F. and Vagne, M., Relationship between Hydrogen Ion and Pepsin Concentration in Human Gastric Secretion. *Digestion* **1968**, *1*, 65-77.

17. Vertzoni, M., Dressman, J., Butler, J., Hempenstall, J. and Reppas, C., Simulation of Fasting Gastric Conditions and Its Importance for the in Vivo Dissolution of Lipophilic Compounds. *Eur. J. Pharm. Biopharm.* **2005**, *60*, 413-417.

18. Armand, M., Borel, P., Pasquier, B., Dubois, C., Senft, M., Andre, M., Peyrot, J., Salducci, J. and Lairon, D., Physicochemical Characteristics of Emulsions During Fat Digestion in Human Stomach and Duodenum. *American Journal of Physiology-Gastrointestinal and Liver Physiology* **1996**, *34*, G172-G183.

19. Vertzoni, M., Archontaki, H. and Reppas, C., Determination of Intralumenal Individual Bile Acids by HPLC with Charged Aerosol Detection. *J. Lipid Res.* **2008**, *49*, 2690-2695.

20. Rhodes, J., Barnardo, D. E., Phillips, S. F., Rovelsta.Ra and Hofmann, A. F., Increased Reflux of Bile into Stomach in Patients with Gastric Ulcer. *Gastroenterology* **1969**, *57*, 241-252.

21. Kristensen, M., Titration Curves for Gastric-Secretion - Study on Duodenal-Ulcer and Gastric-Ulcer with Particular Reference to Effect of Glycopyrronium. *Scand. J. Gastroenterol.* **1975**, *10*, 1-148.

22. Rees, W. D., Botham, D. and Turnberg, L. A., A Demonstration of Bicarbonate Production by the Normal Human Stomach in Vivo. *Dig. Dis. Sci.* **1982**, *27*, 961-966.

23. Widmaier, E. P., Raff, H. and Strang, K. T., The Digestion and Absorption of Food. In *Vander's Human Physiology: The Mechanisms of Body Function*, 10th ed.; McGraw-Hill: New York, 2006; pp 575-614.

24. Konturek, P. C., Konturek, S. J. and Hahn, E. G., Duodenal Alkaline Secretion: Its Mechanisms and Role in Mucosal Protection against Gastri Acid. *Dig. Liver Dis.* **2004**, *36*, 505-512.

25. Sheng, J. J., McNanara, D. P. and Amidon, G. L., Toward an in Vivo Dissolution Methodology: A Comparison of Phosphate and Bicarbonate Buffers. *Mol. Pharmaceutics* **2009**, *6*, 29-39.

26. Sunesen, V. H., Vedelsdal, R., Kristensen, H. G., Christrup, L. and Mullertz, A., Effect of Liquid Volume and Food Intake on the Absolute Bioavailability of Danazol, a Poorly Soluble Drug. *Eur. J. Pharm. Sci.* **2005**, *24*, 297-303.

27. Leyden, J. J., Absorption of Minocycline Hydrochloride and Tetracycline Hydrochloride - Effect of Food, Milk, and Iron. *J. Am. Acad. Dermatol.* **1985**, *12*, 308-312.

28. Clarysse, S., Psachoulias, D., Brouwers, J., Tack, J., Annaert, P., Duchateau, G., Reppas, C. and Augustijns, P., Postprandial Changes in Solubilizing Capacity of Human Intestinal Fluids for Bcs Class II Drugs. *Pharm. Res.* **2009**, *26*, 1456-1466.

29. Evans, D. F. and H., W., Micellar Solutions Play a Key Role in Many Industrial and Biological Processes. In *The Colloidal Domain: Where Physics, Chemistry, Biology, and Technology Meet*, 2nd ed.; VCH Publishers Inc.: New York, 1999; pp 198-216.

30. Rosoff, M. and Serajuddin, A. T. M., Solubilization of Diazepam in Bile-Salts and in Sodium Cholate-Lecithin-Water Phases. *Int. J. Pharm.* **1980**, *6*, 137-146.

31. Mithani, S. D., Bakatselou, V., TenHoor, C. N. and Dressman, J. B., Estimation of the Increase in Solubility of Drugs as a Function of Bile Salt Concentration. *Pharm. Res.* **1996**, *13*, 163-167.

32. Cai, X. H., Grant, D. J. W. and Wiedmann, T. S., Analysis of the Solubilization of Steroids by Bile Salt Micelles. *J. Pharm. Sci.* **1997**, *86*, 372-377.

33. Clarysse, S., Tack, J., Lammert, F., Duchateau, G., Reppas, C. and Augustijns, P., Postprandial Evolution in Composition and Characteristics of Human Duodenal Fluids in Different Nutritional States. *J. Pharm. Sci.* **2009**, *98*, 1177-1192.

34. Brouwers, J., Tack, J., Lammert, F. and Augustijns, P., Intraluminal Drug and Formulation Behavior and Integration in in Vitro Permeability Estimation: A Case Study with Amprenavir. *J. Pharm. Sci.* **2006**, *95*, 372-383.

35. Persson, E. M., Gustafsson, A. S., Carlsson, A. S., Nilsson, R. G., Knutson, L., Forsell, P., Hanisch, G., Lennernas, H. and Abrahamsson, B., The Effects of Food on the Dissolution of Poorly Soluble Drugs in Human and in Model Small Intestinal Fluids. *Pharm. Res.* **2005**, *22*, 2141-2151.

36. Ladas, S. D., Isaacs, P. E., Murphy, G. M. and Sladen, G. E., Comparison of the Effects of Medium and Long Chain Triglyceride Containing Liquid Meals on Gall Bladder and Small Intestinal Function in Normal Man. *Gut* **1984**, *25*, 405-411.

37. Fausa, O., Duodenal Bile Acids after a Test Meal. *Scand. J. Gastroenterol.* **1974**, *9*, 567-570.

38. Northfield, T. C. and McColl, I., Postprandial Concentrations of Free and Conjugated Bile Acids Down the Length of the Normal Human Small Intestine. *Gut* **1973**, *14*, 513-518.

39. McGee, L. C. and Hastings, A. B., The Carbon Dioxide Tension and Acid-Base Balance of Jejunal Secretions in Man. *J. Biol. Chem.* **1942**, *142*, 893-904.

40. Hardman, J. G., *Goodman & Gilman's the Pharmacological Basis of Therapeutics*. 10th ed.; McGraw-Hill: New York, 2001.

41. Davenport, H. W., Digestion and Absorption. In *Physiology of the Digestive Tract*, Year Book Medical Publishers, Inc.: Chicago, 1982; pp 179-235.

42. White, A., Handler, P. and Smith, E. L., Specialized Extracellular Fluids. In *Principles of Biochemistry*, 4 ed.; McGraw-Hill: New York, 1968; pp 806-827.

43. Banwell, J. G., Gorbach, S. L., Pierce, N. F., Mitra, R. and Mondal, A., Acute Undifferentiated Human Diarrhea in Tropics 2. Alterations in Intestinal Fluid and Electrolyte Movements. *J. Clin. Invest.* **1971**, *50*, 890-900.

44. Rune, S. J., Acid-Base Parameters of Duodenal Contents in Man. *Gastroenterology* **1972**, *62*, 533-539.

45. Sinko, P. J., Solubility and Distribution Phenomena. In *Martin's Physical Pharmacy*, 5th ed.; Troy, D., Ed. Lippincott Williams & Wilkins: 2006; pp 231-266.

46. Sheng, J. J., Kasim, N. A., Chandrasekharan, R. and Amidon, G. L., Solubilization and Dissolution of Insoluble Weak Acid, Ketoprofen: Effects of pH Combined with Surfactant. *Eur. J. Pharm. Sci.* **2006**, *29*, 306-314.

47. Li, S. F., Wong, S. M., Sethia, S., Almoazen, H., Joshi, Y. M. and Serajuddin, A. T. M., Investigation of Solubility and Dissolution of a Free Base and Two Different Salt Forms as a Function of pH. *Pharm. Res.* **2005**, *22*, 628-635.

48. Phaechamud, T. and Ritthidej, G. C., Sustained-Release from Layered Matrix System Comprising Chitosan and Xanthan Gum. *Drug Dev. Ind. Pharm.* **2007**, *33*, 595-605.

49. Evans, D. F., Pye, G., Bramley, R., Clark, A. G., Dyson, T. J. and Hardcastle, J. D., Measurement of Gastrointestinal pH Profiles in Normal Ambulant Human Subjects. *Gut* **1988**, *29*, 1035-1041.

50. Lindahl, A., Ungell, A. L., Knutson, L. and Lennernas, H., Characterization of Fluids from the Stomach and Proximal Jejunum in Men and Women. *Pharm. Res.* **1997**, *14*, 497-502.

51. Dressman, J. B., Berardi, R. R., Dermentzoglou, L. C., Russell, T. L. and Jarvenpaa, K. M., Upper Gastrointestinal (GI) pH in Young, Healthy Men and Women. *Pharm. Res.* **1990**, *7*, 756-761.

52. Annaert, P., Brouwers, J., Bijnens, A., Lammert, F., Tack, J. and Augustijns, P., Ex Vivo Permeability Experiments in Excised Rat Intestinal Tissue and in Vitro Solubility Measurements in Aspirated Human Intestinal Fluids Support Age-Dependent Oral Drug Absorption. *Eur. J. Pharm. Sci.* **2010**, *39*, 15-22.

53. Perez de la Cruz Moreno, M., Oth, M., Deferme, S., Lammert, F., Tack, J., Dressman, J. and Augustijns, P., Characterization of Fasted-State Human Intestinal Fluids Collected from Duodenum and Jejunum. *J. Pharm. Pharmacol.* **2006**, *58*, 1079-1089.

54. Benn, A. and Cooke, W. T., Intraluminal pH of Duodenum and Jejunum in Fasting Subjects with Normal and Abnormal Gastric or Pancreatic Function. *Scand. J. Gastroenterol.* **1971**, *6*, 313-317.

55. Youngberg, C. A., Berardi, R. R., Howatt, W. F., Hyneck, M. L., Amidon, G. L., Meyer, J. H. and Dressman, J. B., Comparison of Gastrointestinal pH in Cystic-Fibrosis and Healthy Subjects. *Dig. Dis. Sci.* **1987**, *32*, 472-480.

56. Watson, B. W., Meldrum, S. J., Riddle, H. C., Brown, R. L. and Sladen, G. E., pH Profile of Gut as Measured by Radiotelemetry Capsule. *Br. Med. J.* **1972**, *2*, 104-106.

57. Ovesen, L., Bendtsen, F., Tage-Jensen, U., Pedersen, N. T., Gram, B. R. and Rune, S. J., Intraluminal Ph in the Stomach, Duodenum, and Proximal Jejunum in Normal Subjects and Patients with Exocrine Pancreatic Insufficiency. *Gastroenterology* **1986**, *90*, 958-962.

58. Bown, R. L., Sladen, G. E., Clark, M. L. and Dawson, A. M., The Production and Transport of Ammonia in the Human Colon. *Gut* **1971**, *12*, 863.

59. Fadda, H. M., Sousa, T., Carlsson, A., Abrahamsson, B., Kumar, D. and Basit, A. W. In *Drug Solubility in Luminal Fluids from Different Regions of the Small and Large Intestine of Humans*, AAPS Annual Meeting and Exposition, Los Angeles, Los Angeles, 2009; pp AAPS2009-003733.

60. Rudolph, M. W., Klein, S., Beckert, T. E., Petereit, H. and Dressman, J. B., A New 5-Aminosalicylic Acid Multi-Unit Dosage Form for the Therapy of Ulcerative Colitis. *Eur. J. Pharm. Biopharm.* **2001**, *51*, 183-190.

61. Gisolfi, C. V., Summers, R. W., Lambert, G. P. and Xia, T., Effect of Beverage Osmolality on Intestinal Fluid Absorption During Exercise. *J. Appl. Physiol.* **1998**, *85*, 1941-8.

62. Davenport, H. W., Secretion. In *Physiology of the Digestive Tract*, Year Book Medical Publishers, Inc.: Chicago, 1982; pp 101-178.

63. Pedersen, B. L., Mullertz, A., Brondsted, H. and Kristensen, H. G., A Comparison of the Solubility of Danazol in Human and Simulated Gastrointestinal Fluids. *Pharm. Res.* **2000**, *17*, 891-894.

64. Dikeman, C. L. and Fahey, G. C., Viscosity as Related to Dietary Fiber: A Review. *Crit. Rev. Food Sci. Nutr.* **2006**, *46*, 649-663.

65. Marciani, L., Gowland, P. A., Spiller, R. C., Manoj, P., Moore, R. J., Young, P., Al-Sahab, S., Bush, D., Wright, J. and Fillery-Travis, A. J., Gastric Response to Increased Meal Viscosity Assessed by Echo-Planar Magnetic Resonance Imaging in Humans. *J. Nutr.* **2000**, *130*, 122-127.

66. Dikeman, C. L., Murphy, M. R. and Fahey, G. C., Dietary Fibers Affect Viscosity of Solutions and Simulated Human Gastric and Small Intestinal Digesta. *J. Nutr.* **2006**, *136*, 913-919.

67. Abrahamsson, B., Pal, A., Sjoberg, M., Carlsson, M., Laurell, E. and Brasseur, J. G., A Novel in Vitro and Numerical Analysis of Shear-Induced Drug Release from Extended-Release Tablets in the Fed Stomach. *Pharm. Res.* **2005**, *22*, 1215-1226.

68. Malkki, Y., Physical Properties of Dietary Fiber as Keys to Physiological Functions. *Cereal Foods World* **2001**, *46*, 196-199.

69. Lim, C. L., Byrne, C. and Lee, J. K. W., Human Thermoregulation and Measurement of Body Temperature in Exercise and Clinical Settings. *Annals Academy of Medicine Singapore* **2008**, *37*, 347-353.

70. Steingoetter, A., Fox, M., Treier, R., Weishaupt, D., Marincek, B., Boesiger, P., Fried, M. and Schwizer, W., Effects of Posture on the Physiology of Gastric Emptying: A Magnetic Resonance Imaging Study. *Scand. J. Gastroenterol.* **2006**, *41*, 1155-1164.

71. Kwiatek, M. A., Menne, D., Steingoetter, A., Goetze, O., Forras-Kaufman, Z., Kaufman, E., Fruehauf, H., Boesiger, P., Fried, M., Schwizer, W. and Fox, M. R., Effect of Meal Volume and Calorie Load on Postprandial Gastric Function and Emptying: Studies under Physiological Conditions by Combined Fiber-Optic Pressure Measurement and Mri. *American Journal of Physiology-Gastrointestinal and Liver Physiology* **2009**, *297*, G894-G901.

72. Schiller, C., Frohlich, C. P., Giessmann, T., Siegmund, W., Monnikes, H., Hosten, N. and Weitschies, W., Intestinal Fluid Volumes and Transit of Dosage Forms as Assessed by Magnetic Resonance Imaging. *Aliment. Pharmacol. Ther.* **2005**, *22*, 971-979.

73. Marciani, L., Cox, E. F., Hoad, C. L., Pritchard, S., Totman, J. J., Foley, S., Mistry, A., Evans, S., Gowland, P. A. and Spiller, R. C., Postprandial Changes in Small Bowel Water Content in Healthy Subjects and Patients with Irritable Bowel Syndrome. *Gastroenterology* **2010**, *138*, 469-U90.

74. Placidi, E., Hoad, C. L., Marciani, L., Gowland, P. A. and Spiller, R. C. In *Effects of an Osmotic Laxative on the Distribution of Water between the Small and Large Intestine in Humans*, British Society of Gastroenterology Annual Scientific Meeting, 2010.

75. Marciani, L., Foley, S., Hoad, C., Campbell, E., Totman, J., Armstrong, A., Manby, P., Gowland, P. A. and Spiller, R. In *Effects of Ondansetron on Small Bowel Water Content: A Magnetic Resonance Imaging Study*, United European Gastroenterology Week (UEGW), Paris, Paris, 2007.

76. Sutton, S. C., Role of Physiological Intestinal Water in Oral Absorption. *AAPS J.* **2009**, *11*, 277-285.

77. Bass, P., Gastric Emptying; Differences among Liquid, Fiber, Polymer and Solid Dosage Forms of Medications. In Capsugel Symposium Series, 1993; pp 21-33.

78. Oberle, R. L., Chen, T. S., Lloyd, C., Barnett, J. L., Owyang, C., Meyer, J. and Amidon, G. L., The Influence of the Interdigestive Migrating Myoelectric Complex on the Gastric Emptying of Liquids. *Gastroenterology* **1990**, *99*, 1275-1282.

79. Dressman, J. B., Comparison of Canine and Human Gastrointestinal Physiology. *Pharm. Res.* **1986**, *3*, 123-131.

80. Pal, A., Indireshkumar, K., Schwizer, W., Abrahamsson, B., Fried, M. and Brasseur, J. G., Gastric Flow and Mixing Studied Using Computer Simulation. *Proceedings of the Royal Society of London Series B-Biological Sciences* **2004**, *271*, 2587-2594.

81. Indireshkumar, K., Brasseur, J. G., Faas, H., Hebbard, G. S., Kunz, P., Dent, J., Feinle, C., Li, M. J., Boesiger, P., Fried, M. and Schwizer, W., Relative Contributions Of "Pressure Pump" And "Peristaltic Pump" To Gastric Emptying. *American Journal of Physiology-Gastrointestinal and Liver Physiology* **2000**, *278*, G604-G616.

82. Pal, A., Williams, R. B., Cook, I. J. and Brasseur, J. G., Intrabolus Pressure Gradient Identifies Pathological Constriction in the Upper Esophageal Sphincter During Flow. *American Journal of Physiology-Gastrointestinal and Liver Physiology* **2003**, *285*, G1037-G1048.

83. Pal, A., Brasseur, J. G. and Abrahamsson, B., A Stomach Road Or "Magenstrasse" For Gastric Emptying. *Journal of Biomechanics* **2007**, *40*, 1202-1210.

84. Higaki, K., Choe, S. Y., Lobenberg, R., Welage, L. S. and Amidon, G. L., Mechanistic Understanding of Time-Dependent Oral Absorption Based on Gastric Motor Activity in Humans. *Eur. J. Pharm. Biopharm.* **2008**, *70*, 313-325.

85. Granger, D. N., Barrowman, J. A. and Kvietys, P. R., *Clinical Gastrointestinal Physiology*. W. B. Saunders: Philadelphia, 1985.

86. Rhie, J. K., Hayashi, Y., Welage, L. S., Frens, J., Wald, R. J., Barnett, J. L., Amidon, G. E., Putcha, L. and Amidon, G. L., Drug Marker Absorption in Relation to Pellet Size, Gastric Motility and Viscous Meals in Humans. *Pharm. Res.* **1998**, *15*, 233-238.

87. Podczeck, F., Mitchell, C. L., Newton, J. M., Evans, D. and Short, M. B., The Gastric Emptying of Food as Measured by Gamma-Scintigraphy and Electrical Impedance Tomography (EIT) and Its Influence on the Gastric Emptying of Tablets of Different Dimensions. *J. Pharm. Pharmacol.* **2007**, *59*, 1527-1536.

88. Kamba, M., Seta, Y., Kusai, A., Ikeda, M. and Nishimura, K., A Unique Dosage Form to Evaluate the Mechanical Destructive Force in the Gastrointestinal Tract. *Int. J. Pharm.* **2000**, *208*, 61-70.

89. Laulicht, B., Tripathi, A., Schlageter, V., Kucera, P. and Mathiowitz, E., Understanding Gastric Forces Calculated from High-Resolution Pill Tracking. *Proc. Natl. Acad. Sci. U. S. A.* **2010**, *107*, 8201-8206.

90.	Weitschies, W., Kosch, O., Monnikes, H. and Trahms, L., Magnetic Marker Monitoring: An Application of Biomagnetic Measurement Instrumentation and Principles for the Determination of the Gastrointestinal Behavior of Magnetically Marked Solid Dosage Forms. *Adv. Drug Delivery Rev.* **2005**, *57*, 1210-1222.

91.	Davis, S. S., Hardy, J. G. and Fara, J. W., Transit of Pharmaceutical Dosage Forms through the Small-Intestine. *Gut* **1986**, *27*, 886-892.

92.	Coupe, A. J., Davis, S. S. and Wilding, I. R., Variation in Gastrointestinal Transit of Pharmaceutical Dosage Forms in Healthy-Subjects. *Pharm. Res.* **1991**, *8*, 360-364.

93.	Kerlin, P., Zinsmeister, A. and Phillips, S., Relationship of Motility to Flow of Contents in the Human Small-Intestine. *Gastroenterology* **1982**, *82*, 701-706.

94.	Mayersohn, M., Principles of Drug Absorption. In *Modern Pharmaceutics*, Marcel Dekker: New York, 1996; pp 21-71.

95.	Grassi, M., Grassi, G., Lapasin, R. and Colombo, I., Part 1: Gastrointestinal Tract. In *Understanding Drug Release and Absorption Mechanisms, a Physical and Mathematical Approach*, 1st ed.; CRC Press: Boca Raton, 2007; pp 29-68.

96.	USP, *The Pharmacopeia of the United States of America Xv*. Mack Publishing Company: Easton, 1955.

97.	Jantratid, E., De Maio, V., Ronda, E., Mattavelli, V., Dressman, J. B. and et al., Application of Biorelevant Dissolution Tests to the Prediction of in Vivo Performance of Diclofenac Sodium from an Oral Modified-Release Pellet Dosage Form. *Eur. J. Pharm. Sci.* **2009**, *37*, 434-441.

98.	Jung, H., Milan, R. C., Girard, M. E., Leon, F. and Montoya, M. A., Bioequivalence Study of Carbamazepine Tablets: In Vitro in Vivo Correlation. *Int. J. Pharm.* **1997**, *152*, 37-44.

99.	Baxter, J. L., Kukura, J. and Muzzio, F. J., Hydrodynamics-Induced Variability in the USP Apparatus II Dissolution Test. *Int. J. Pharm.* **2005**, *292*, 17-28.

100.	Baxter, J. L., Kukura, J. and Muzzio, F. J., Shear-Induced Variability in the United States Pharmacopeia Apparatus 2: Modifications to the Existing System. *AAPS J.* **2005**, *7*, E857-E864.

101.	Kukura, J., Arratia, P. E., Szalai, E. S. and Muzzio, F. J., Engineering Tools for Understanding the Hydrodynamics of Dissolution Tests. *Drug Dev. Ind. Pharm.* **2003**, *29*, 231-+.

102.	Kukura, J., Baxter, J. L. and Muzzio, F. J., Shear Distribution and Variability in the USP Apparatus 2 under Turbulent Conditions. *Int. J. Pharm.* **2004**, *279*, 9-17.

103. Sjoberg, M., Laurell, E., Carlsson, M., Abrahamsson, B., Pal, A. and Brasseur, J. G., A New in Vitro Dissolution Method Providing in Vivo Relevant Gastric Shear Stress. *Eur. J. Pharm. Sci.* **2004**, *23*, S45-S45.

104. Sheng, J. J., Sirois, P. J., Dressman, J. B. and Amidon, G. L., Particle Diffusional Layer Thickness in a Usp Dissolution Apparatus II: A Combined Function of Particle Size and Paddle Speed. *J. Pharm. Sci.* **2008**, *97*, 4815-4829.

105. Bucher, G. R., Flynn, J. C. and Robinson, C. S., The Action of the Human Small Intestine in Altering the Composition of Physiological Saline. *J. Biol. Chem.* **1944**, *155*, 305-313.

106. Repishti, M., Hogan, D. L., Pratha, V., Davydova, L., Donowitz, M., Tse, C. M. and Isenberg, J. I., Human Duodenal Mucosal Brush Border Na+/H+ Exchangers Nhe2 and Nhe3 Alter Net Bicarbonate Movement. *American Journal of Physiology-Gastrointestinal and Liver Physiology* **2001**, *281*, G159-G163.

107. West, J. B., Absorption. In *Best and Taylor's Physiological Basis of Medical Practice*, 11 ed.; Williams & Wilkins: Baltimore, 1985; pp 751-790.

108. Johnson, L. R., Fluid and Electrolyte Absorption. In *Gastrointestinal Physiology*, 6th ed.; Johnson, L. R., Ed. Mosby: St. Louis, 2001; pp 143-154.

109. Rune, S. J. and Henriksen, F. W., Carbon Dioxide Tensions in the Proximal Part of the Canine Gastrointestinal Tract. *Gastroenterology* **1969**, *56*, 758-762.

110. Efentakis, M. and Dressman, J. B., Gastric Juice as a Dissolution Medium: Surface Tension and pH. *Eur. J. Drug Metab. Pharmacokinet.* **1998**, *23*, 97-102.

111. Rautureau, M., Bisalli, A. and Rambaud, J. C., Bile Salts and Lipids in Aqueous Intraluminal Phase During the Digestion of a Standard Meal in Normal Man. *Gastroenterol. Clin. Biol.* **1981**, *5*, 417-425.

112. Tangerman, A., van Schaik, A. and van der Hoek, E. W., Analysis of Conjugated and Unconjugated Bile Acids in Serum and Jejunal Fluid of Normal Subjects. *Clin. Chim. Acta* **1986**, *159*, 123-132.

113. Bratten, J. and Jones, M. P., Prolonged Recording of Duodenal Acid Exposure in Patients with Functional Dyspepsia and Controls Using a Radiotelemetry pH Monitoring System. *J. Clin. Gastroenterol.* **2009**, *43*, 527-533.

114. Maxwell, J. D., Ferguson, A. and Watson, W. C., The Effect of Gastric Secretory Status on Jejunal pH Measured by Radiotelemetering. *Digestion* **1971**, *4*, 345-352.

115. Zentler-Munro, P. L., Fine, D. R., F., F. W. J. and Northfield, T. C., Effect of Intrajejunal Acidity on Lipid Digestion and Aqueous Solbilisation of Bile Acids and Lipids in Health, Using a New Simple Method of Lipase Inactivation. *Gut* **1984**, *25*, 491-499.

116. Borgstrom, B., Dahlqvist, A., Lundh, G. and Sjovall, J., Studies of Intestinal Digestion and Absorption in the Human. *J. Clin. Invest.* **1957**, *36*, 1521-1536.

117. Malagelada, J. R., Longstreth, G. F., Summerskill, W. H. J. and Go, V. L. W., Measurement of Gastric Functions During Digestion of Ordinary Solid Meals in Man. *Gastroenterology* **1976**, *70*, 203-210.

118. Fordtran, J. S. and Locklear, T. W., Ionic Constituents and Osmolality of Gastric and Small-Intestinal Fluids after Eating. *Am. J. Dig. Dis.* **1966**, *11*, 503-521.

119. Lobo, D. N., Hendry, P. O., Rodrigues, G., Marciani, L., Totman, J. J., Wright, J. W., Preston, T., Gowland, P., Spiller, R. C. and Fearon, K. C. H., Gastric Emptying of Three Liquid Oral Preoperative Metabolic Preconditioning Regimens Measured by Magnetic Resonance Imaging in Healthy Adult Volunteers: A Randomised Double-Blind, Crossover Study. *Clin. Nutr.* **2009**, *28*, 636-641.

120. Snyder, W. S., Cook, M. J., Nasset, E. S., Karhausen, L. R., Howells, G. P. and Tipton, I. H., Anatomical Values for Reference Man. In *Report of the Task Group on Reference Man*, Pergamon Press: New York, 1975; pp 8-46.

121. Coleman, N. S., Marciani, L., Blackshaw, E., Wright, J., Parker, M., Yano, T., Yamazaki, S., Chan, P. Q., Wilde, K., Gowland, P. A., Perkins, A. C. and Spiller, R. C., Effect of a Novel 5-Ht3 Receptor Agonist Mkc-733 on Upper Gastrointestinal Motility in Humans. *Aliment. Pharmacol. Ther.* **2003**, *18*, 1039-1048.

122. Marciani, L., Gowland, P. A., Spiller, R. C., Manoj, P., Moore, R. J., Young, P. and Fillery-Travis, A. J., Effect of Meal Viscosity and Nutrients on Satiety, Intragastric Dilution, and Emptying Assessed by MRI. *American Journal of Physiology-Gastrointestinal and Liver Physiology* **2001**, *280*, G1227-G1233.

123. Holtmann, G., Kelly, D. G., Sternby, B. and DiMagno, E. P., Survival of Human Pancreatic Enzymes During Small Bowel Transit: Effect of Nutrients, Bile Acids, and Enzymes. *Am. J. Physiol.* **1997**, *273*, G553-G558.

124. Anwar, S., Fell, J. T. and Dickinson, P. A., An Investigation of the Disintegration of Tablets in Biorelevant Media. *Int. J. Pharm.* **2005**, *290*, 121-127.

125. Galia, E., Nicolaides, E., Horter, D., Lobenberg, R. and Dressman, J. B., Evaluation of Various Dissolution Media for Predicting in Vivo Performance of Class I and II Drugs. *Pharm. Res.* **1998**, *15*, 698-705.

126. Vertzoni, M., Fotaki, N., Kostewicz, E., Stippler, E., Leuner, C., Nicolaides, E., Dressman, J. and Reppas, C., Dissolution Media Simulating the Intralumenal Composition of the Small Intestine: Physiological Issues and Practical Aspects. *J. Pharm. Pharmacol.* **2004**, *56*, 453-462.

127. USP, *The Pharmacopeia of the United States of America XVI*. Mack Publishing Company: Easton, 1960.

128. Gray, V. A. and Dressman, J. B., Change of Ph Requirements for Standard Intestinal Fluid Ts. *Pharmacopeial Forum* **1996**, *22*, 1943-1945.

Chapter 2

Mechanistic analysis of solute transport in an *in vitro* physiological two-phase dissolution apparatus

Abstract

In vitro dissolution methodologies that adequately capture oral bioperformance of solid dosage forms are critical tools needed to aid formulation development. Such methodologies must encompass important physiological parameters and be designed with drug properties in mind. Two-phase dissolution apparatuses, which contain an aqueous phase in which the drug dissolves (representing the dissolution/solubility component) and an organic phase into which the drug partitions (representing the absorption component), have the potential to provide meaningful predictions of *in vivo* oral bioperformance for some BCS II, and possibly some BCS IV drug products. Before such an apparatus can be properly evaluated, it is important to understand the kinetics of drug substance partitioning from the aqueous to the organic medium.

We performed a mechanistic, drug-transport analysis of the partitioning of solutes in solution in an *in vitro* two-phase dissolution apparatus, and demonstrated the ability of our model to successfully describe the *in vitro* partitioning profiles of three BCS II weak acids in four different experimental set-ups. In contrast to previous kinetically derived mathematical models, our model uses physical input parameters that are known or can be estimated *a priori*. To establish the physiological relevance of the test for the drug product of interest, we proposed scaling factors (A_I/V_a, M_T/V_a, and $V_a/(K_{ap} V_o)$), the values of which can be determined based on molecular descriptors. When these scaling

50

parameters are maintained at physiologically relevant values and a physiological aqueous buffer is used, the saturation conditions in the aqueous medium of the two-phase system are expected to be similar to saturation conditions *in vivo*, and the *in vitro* partitioning rate is expected to be similar to the *in vivo* absorption rate. Potential IVIVCs between the *in vitro* partitioning and *in vivo* absorption profiles may result for some drug products that have relatively high fraction absorbed values and low extents of hepatic first-pass metabolism and gut degradation/metabolism. While this manuscript focuses on an analysis of drugs in solution, these scaling factors can be applied to dissolution of solid dosage forms in two-phase dissolution apparatuses, which will be the focus of future work.

Introduction

Pharmaceutical solid oral dosage forms must dissolve in the gastrointestinal lumen and absorb into the intestinal membrane before reaching systemic circulation. The rate and extent of drug dissolution and absorption depend on the characteristics of the active ingredient such as pK_a, crystal form, and solubility, as well as properties of the dosage form[1]. Just as importantly, characteristics of the physiological environment such as buffer species, pH, bile salts, gastric emptying rate, intestinal liquid volume, intestinal motility, and shear rates significantly impact dissolution and absorption[2]. While scientists have used *in vitro* test methods for many years, no single test or apparatus accurately captures the range of key *in vivo* conditions that have the potential to affect the relative rates and extents of *in vivo* dissolution and absorption for the range of diverse drug products. Due to the difficulty in developing a "one size fits all" physiological dissolution apparatus, it is helpful to use the physicochemical characteristics of the drug and dosage form to design a dissolution test that captures the key physiological conditions that have the potential to affect the oral bioperformance. For example, capturing the pH profile encountered when a drug travels from the acidic stomach to the less acidic small intestine is important for

low-solubility weak acids and bases with pK_as in the physiological range, whereas the type and concentration of bile salts in the dissolution medium rather than the pH profile is important for low-solubility neutral compounds.

The Biopharmaceutics Classification System (BCS) attempts to categorize *in vivo* oral bioperformance based on a drug's solubility, extent of permeation, and *in vitro* testing results [3]. It has had a significant effect on the regulatory environment as the Food and Drug Administration (FDA) and World Health Organization (WHO) consider biowaivers for some drugs [4]. The BCS classification of a drug can be used as a general guideline to predict whether solubility, dissolution rate, or permeation rate will be the rate-limiting step in reaching systemic circulation. However, even drugs within a single BCS class have a range of solubilities, effective human intestinal permeation rates, particle sizes, doses, and dosage forms, all of which may contribute to differences in dissolution and absorption characteristics *in vivo*. Therefore, for drugs that fall within BCS II, III, or IV, using its BCS classification alone to design the appropriate dissolution test has some limitations. For instance, performing a USP dissolution test in a non-physiological volume of buffer (i.e. 900 ml) to predict *in vivo* performance for certain BCS Class II (low solubility, high permeation) drugs may lead to poor *in vitro-in vivo* correlations (IVIVCs) due to an unrealistic degree of drug saturation in the dissolution medium, leading to *in vitro* dissolution rates that do not reflect the *in vivo* situation.

Two-phase dissolution apparatuses can simultaneously evaluate the kinetics of both drug dissolution and partitioning, and can simulate drug absorption while using a physiological volume of aqueous fluid (~100 ml in fasted humans [5]). These systems contain a volume of aqueous medium in which the drug dissolves and a second volume of an immiscible organic medium (e.g. 1-octanol) that allows drug partitioning from the aqueous medium. If designed properly, the rate of appearance of drug in the organic phase is expected to be similar to the rate of absorption *in vivo*. Assuming that an appropriate interfacial surface-area-to-volume ratio between the aqueous and organic phases is used, the organic phase can help to maintain physiologically relevant saturation

conditions in the aqueous phase and physiologically relevant partitioning kinetics for some potential drug candidates.

Researchers have been exploring the utility of two-phase systems for novel dosage forms such as lipid-filled capsules and controlled-release dosage forms, as well as immediate-release dosage forms since the 1960s. Pillay & Fassihi employed a two-phase method to study the dissolution of poorly-soluble nifedipine from a lipid-based capsule formulation [6]. Their purpose was to circumvent possible precipitation of the drug as well as analytical difficulties associated with lipid-based capsule formulations. Hoa and Kinget as well as Gabriels & Plaizier-Vercammen developed two-phase methods to overcome difficulties in maintaining sink conditions for poorly-soluble anti-malarial drugs such as arteminsinin, dihydroartemisinin, and artemether, that occurred using single-phase dissolution methods [7], [8]. Grundy et al. developed a two-phase system to measure release from the nifedipine gastrointestinal therapeutic system (GITS), a push-pull osmotic system, to maintain sink conditions and to develop an *in vitro-in vivo* correlation that could not be achieved with other dissolution methods such as the flow-through and differential (ALZA) method [9]. More recently, Heigoldt, et al. performed dissolution testing of modified release formulations of two weakly-basic BCS II drugs in a two-phase ("biphasic") dissolution test with a pH gradient in the aqueous medium [10]. They found the test to be "qualitatively predictive" of *in vivo* performance and found it to be superior to single-phase dissolution testing at a single pH. Shi et al. used a two-phase dissolution apparatus that incorporated both a USP II vessel and a USP IV flow-through cell to successfully differentiate between three formulations of celeboxib and generate a rank-order relationship between the amount of drug in the organic phase at two hours and the *in vivo* area under the plasma concentration-time curve (AUC) or maximum plasma concentration (C(max)) [11].

While two-phase systems have shown improvement over conventional methods in some cases, limited work has been undertaken to elucidate the mechanism by which they may facilitate improved IVIVCs over single phase

systems and determine for which types of drugs and drug products they could be most useful. The purpose of this work is to perform a mass transport analysis of the kinetics of partitioning of drugs in solution from the aqueous to the organic phase of a two-phase dissolution apparatus. While other researchers have provided mathematical analyses, we use a mechanistic approach to understand the drug transport phenomenon within the system [12], [13]. In this paper we present the theory and derivation of our model and compare it to an existing kinetic model. We demonstrate the effectiveness of our analysis in predicting experimental results in four different *in vitro* two-phase dissolution apparatuses using the BCS II weak acids Ibuprofen, Nimesulide, and Piroxicam. More importantly, we outline how a two-phase dissolution apparatus can be scaled to be physiologically relevant and reflect *in vivo* absorption kinetics, and discuss for which types of drug substances a two-phase system may be most useful.

Material and Methods

Description of the apparatus

Figure 2.1 is a schematic of a two-phase dissolution apparatus. It consists of a flat- or round-bottom glass vessel that is maintained at constant temperature. It contains both aqueous and organic media that are present in two distinct layers, and are agitated by a single shaft fitted with two impellers. At the beginning of the experiment, dissolved drug is added directly to the aqueous medium. Partitioning of drug from the aqueous to the organic medium is monitored as a function of time until the equilibrium concentration of drug in each phase is reached.

Derivation of the model

The kinetics of partitioning of drug from the aqueous to the organic phase of a two-phase system is described based on a physical model approach Suzuki et al. originally developed to describe simultaneous chemical equilibria and mass transfer of basic and acidic solutes through lipoidal barriers [14]. We assume that

drug transport is controlled by diffusional resistance arising from a hydrodynamically controlled or "stagnant" diffusion layer on each side of the aqueous-organic interface, and use the steady diffusion across a thin film approximation to predict the total flux of drug across the two diffusion layers in series. Model assumptions are as follows.

1. The diffusion coefficient in each medium is not concentration dependent and aqueous diffusion coefficients of ionized and non-ionized drug are equal.
2. Aqueous and organic media behave as ideal solutions.
3. Drug transport via convection is minimal and can be neglected.
4. An initial bolus of drug in solution is injected into the aqueous medium and net flux of drug occurs in one direction across each diffusion layer from the well-mixed, bulk aqueous medium to the well-mixed, bulk organic medium.
5. The instantaneous concentration profile within each diffusion layer resembles a steady state (pseudo-steady-state approximation).
6. Drug concentrations at the aqueous and organic sides of the interface are in equilibrium.
7. Drug transfer across the aqueous-organic interface is instantaneous.
8. Mass transfer from the aqueous to the organic medium occurs only through the interface.
9. Concentration of dissolved drug in either phase is not affected by processes such as chemical reaction, degradation, precipitation, etc.
10. The thickness of each diffusion layer is constant with time.

Figure 2.2 is a schematic diagram of a two-phase system tipped on its side, to which a monoprotic weak acid has been added to the aqueous buffer. The first transport step is the diffusion of ionized and non-ionized drug across the aqueous diffusion layer of thickness h_a. According to Fick's First Law and using assumptions 1-5, the flux across the aqueous diffusion layer, j_a, is given in **Equation 2.1**, where RH are R^- are the concentrations of non-ionized and

ionized species, respectively, and D_a is the aqueous diffusion coefficient for both species.

(2.1) $j_a = -D_a \dfrac{d\left(RH\right)}{dx} - D_a \dfrac{d\left(R^-\right)}{dx}$

Upon integration from x equal to $-h_a$ to zero (the thickness of the diffusion layer) the flux across the aqueous diffusion layer is given as a function of the concentration of drug species in the bulk, $R_{a,b}$, $RH_{a,b}$, and the concentration of drug species on the aqueous side of the interface, $R_{a,i}$, and $RH_{a,i}$, as shown in **Equation 2.2**.

(2.2) $j_a = \dfrac{D_a}{h_a}\left[\left(R_{a,b} + RH_{a,b}\right) - \left(R_{a,i} + RH_{a,i}\right)\right]$

Using the same assumptions as above, the flux of drug from the organic side of the interface to the bulk organic phase can be defined in an analogous manner as **Equation 2.1**. We do not assume that only non-ionized drug partitions into the organic medium, allowing for cases when ionized drug may form complexes with counterions and partition into the organic medium, for example (and the model does not change whether or not this assumption is made)[15]. Upon integration from x equals 0 to h_o (the thickness of the organic diffusion layer), the flux of drug across the organic interface, j_o, is given by **Equation 2.3**, where $R_{o,i}$ and $RH_{o,i}$, are the concentrations of ionized and non-ionized drug on the organic side of the interface respectively, and $R_{o,b}$ and $RH_{o,b}$ are the concentrations of ionized and non-ionized drug in the bulk organic phase, respectively. D_o, is the drug diffusion coefficient in the organic phase.

(2.3) $j_o = \dfrac{D_o}{h_o}\left[\left(R_{o,i} + RH_{o,i}\right) - \left(R_{o,b} + RH_{o,b}\right)\right]$

The concentration of drug on the organic side of the interface can be related to the concentration of drug on the aqueous side of the interface (assumption 6) using the apparent partition coefficient at the interface defined by **Equation 2.4**. If aqueous buffer capacity is high enough to maintain a constant bulk pH during the experiment, then aqueous surface pH is constant and is equal to bulk pH, and K_{ap} surface is equal to K_{ap} bulk.

(2.4) $\quad K_{ap} = \dfrac{RH_{o,i} + R_{o,i}}{RH_{a,i} + R_{a,i}}$

Using the pseudo-steady-state approximation (assumption 5) and assuming instantaneous transfer across the interface (assumption 7) the fluxes across the aqueous and organic diffusion layers can be set equal. Setting **Equation 2.2** equal to **Equation 2.3**, eliminating $R_{o,i}$ and $RH_{o,i}$ using **Equation 2.4**, and letting C_a equal the total aqueous bulk drug concentration, $RH_{a,b} + R_{a,b}$, and C_o equal the total organic bulk drug concentration, $RH_{o,b} + R_{o,b}$, gives the pseudo-steady-state flux of drug as a function of the bulk aqueous and the bulk organic phase concentrations, shown in **Equation 2.5**.

(2.5) $\quad j = \dfrac{D_o D_a K_{ap}}{\left[D_a h_o + D_o h_a K_{ap} \right]} \left[C_a - \dfrac{C_o}{K_{ap}} \right]$

The interface permeation rate, P_I, across the aqueous and organic diffusion layers (barriers in series) defined by **Equation 2.6** allows for further simplification of the total flux from the bulk aqueous to the bulk organic phase as shown in **Equation 2.7**. P_I can also be described in terms of the mass transfer coefficient across the organic diffusion layer, k_o, and the mass transfer coefficient across the aqueous diffusion layer, k_a, according to **Equation 2.8**, where $k_{org} = D_o/h_o$ and $k_{aq} = D_a/h_a$.

$$\text{(2.6)} \quad \frac{1}{P_I} = \frac{h_o}{D_o K_{ap}} + \frac{h_a}{D_a}$$

$$\text{(2.7)} \quad j = P_I \left[C_a - \frac{C_o}{K_{ap}} \right]$$

$$\text{(2.8)} \quad \frac{1}{P_I} = \frac{1}{k_{org} K_{ap}} + \frac{1}{k_{aq}}$$

Equation 2.6 can be further simplified by relating D_o to D_a through the viscosities of the aqueous and organic media. According to the Hayduk and Laudie (HL) and Othmer and Thakar (OT) methods of estimating diffusion coefficient[16], [17], the diffusion coefficient is a function of the molal volume of the drug and the liquid viscosity. Using the HL method, D_o can be related to D_a according to **Equation 2.9.** When 1-octanol is used as the organic medium, assuming the viscosity of the aqueous buffer is 0.6915 cP (viscosity of water) and the viscosity of 1-octanol is 4.84 cP at 37 degrees Celsius[18], [19], then D_o is about equal to $0.11D_a$[1].

$$\text{(2.9)} \quad \frac{D_o}{D_a} \approx \left(\frac{\mu_a}{\mu_o} \right)^{1.14}$$

If it is assumed that h_a and h_o are equal, then the equation for P_I simplifies to **Equation 2.10**. h_a and h_o depend on factors such as liquid viscosity, stirring rate, agitator length and design, and vessel geometry. In reality, h_o is probably somewhat larger than h_a due to the higher viscosity of the organic medium (assuming similar rotational speeds and impeller geometries). However, the value of these simplifying assumptions is evident from **Equation 2.10**. When K_{ap}

---

[1] D_o is equal to ~$0.12D_a$ according to the OT method. The Wilke-Chang method gives diffusion coefficient as a function of an association parameter and liquid molecular weight in addition to liquid temperature and viscosity, and would estimate that D_o is equal to ~$0.54D_a$.

is greater than about ten, P_I is primarily determined by the aqueous diffusion layer permeability (or mass transfer coefficient, k_{aq}) since the organic phase is effectively functioning as a sink for the partitioning drug.

(2.10) $P_I \approx \dfrac{D_a}{h_a} \left(\dfrac{K_{ap}}{9.1 + K_{ap}} \right)$

The time-dependent concentration of drug in the aqueous medium can be expressed according to **Equation 2.11** since mass transfer only occurs through the interface and drug is not generated or destroyed in the system (assumptions 8 and 9). A_I is the surface area of the aqueous-organic interface, and V_a is the volume of aqueous medium. **Equation 2.7** can be substituted into **Equation 2.11** to give **Equation 2.12**. The aqueous and organic concentrations and K_{ap} are given the subscript, t, to indicate their time dependence. As stated previously, if the buffer capacity is high enough, then K_{ap} is not time dependent.

(2.11) $\dfrac{dC_a}{dt} = -\dfrac{A_I}{V_a} j$

(2.12) $\dfrac{dC_a}{dt} = -\dfrac{A_I}{V_a} P_I \left[C_{a,t} - \dfrac{C_{o,t}}{K_{ap,t}} \right]$

Before integrating **Equation 2.12**, $C_{o,t}$ must be related to $C_{a,t}$ using mass balance. Using assumptions 4 and 9 we can write **Equation 2.13**, where M_T is the total amount of drug in the system and V_o is the volume of organic medium.

(2.13) $M_T = C_{a,t} V_a + C_{o,t} V_o$

Since, experimentally, the initial bolus of drug is injected into the aqueous phase at time equals 0, $C_{a,t=0}$ is equal to M_T. Integrating **Equation 2.12** using this initial condition gives an expression for $C_{a,t}$ as a function of time, as shown in

Equations 2.14-2.15. Using the mass balance in **Equation 2.13** allows determination of the concentration of drug in the organic phase as a function of time, which is given in **Equation 2.16**. **Equations 2.17 and 2.18** give the fraction of drug in the aqueous and organic phases as a function of time, respectively.

$$\textbf{(2.14)} \quad C_{a,t} = \frac{M_T}{V_a(1+\beta)}\left[e^{-\frac{A_I}{V_a}P_I(1+\beta)t} + \beta\right]$$

$$\textbf{(2.15)} \quad \beta = \frac{V_a}{K_{ap}V_o}$$

$$\textbf{(2.16)} \quad C_{o,t} = \frac{M_T}{V_o(1+\beta)}\left[1 - e^{-\frac{A_I}{V_a}P_I(1+\beta)t}\right]$$

$$\textbf{(2.17)} \quad F_{a,t} = \frac{1}{(1+\beta)}\left[e^{-\frac{A_I}{V_a}P_I(1+\beta)t} + \beta\right]$$

$$\textbf{(2.18)} \quad F_{o,t} = \frac{1}{(1+\beta)}\left[1 - e^{-\frac{A_I}{V_a}P_I(1+\beta)t}\right]$$

The value of β (defined in **Equation 2.15**) is the volume ratio of aqueous to organic media normalized by the apparent partition coefficient, K_{ap}, and it impacts the rate of partitioning into the organic medium and the fraction of drug in each phase at equilibrium. As the normalized organic volume ($K_{ap}*V_o$) increases, such as for drugs with high partition coefficients, the value of β decreases towards zero. The rate of partitioning is reflected in the decay constant, which is equal to $(1+\beta)*(A_I/V_a)*P_I$. The fraction of the dose in the organic medium at equilibrium, $F_{o,\infty}$, is equal to $1/(1+\beta)$. When β is less than about 0.1, **Equations 2.14 and 2.16-2.18** can be simplified to **Equations 2.19-2.22**, since the predicted concentration or fraction of drug in each phase at any given time is within ten percent of the value predicted using the full equations.

The exponential decay **Equations 2.19-2.20** are the integrated solutions to first-order ordinary differential equations with respect to concentration or fraction in the aqueous phase, respectively. **Equations 2.21-2.22** are analogous to first-order absorption equations prevalent in pharmacokinetic modeling. The decay constant, k_p, which is equal to $(A_l/V_a)*P_l$, can be directly compared to the pharmacokinetic first-order "absorption rate coefficient, k_a", since the equations are analogous.

(2.19) $$C_{a,t} = \frac{M_t}{V_a} e^{-\frac{A_l}{V_a}P_l t} = \frac{M_t}{V_a} e^{-k_p t}$$

(2.20) $$F_{a,t} = e^{-\frac{A_l}{V_a}P_l t} = e^{-k_p t}$$

(2.21) $$C_{o,t} = \frac{M_T}{V_o}\left[1 - e^{-\frac{A_l}{V_a}P_l t}\right] = \frac{M_T}{V_o}\left[1 - e^{-k_p t}\right]$$

(2.22) $$F_{o,t} = 1 - e^{-\frac{A_l}{V_a}P_l t} = 1 - e^{-k_p t}$$

Materials

Ibuprofen (Albermarle Lot No. 2050-0032F for experiments 1-4, and Sigma Aldrich, Cat No. I4883-10G for experiments 5-10), Nimesulide (Sigma Aldrich, Cat No. 1016-25G), and Piroxicam (Sigma Aldrich, Cat No. P0847-10G) powder, as well as 1-octanol (99% purity) and HPLC-grade methanol, were purchased commercially. Relevant material properties are included in **Table 2.1**.

Apparent partition coefficient

The K_{ap} of Piroxicam at 37°C in pH 7.4 buffer was determined. Ten mg of drug was added to a glass vial containing 7 mL of 50 mM pH 7.4 sodium phosphate buffer and 7 mL of 1-octanol. The glass vial was placed in an incubator shaker at 37°C and 150 rpm and allowed to shake for two days, after

which two samples were removed from each phase and prepared for concentration analysis using UV. Absorbance was measured at 340 nm for the 1-octanol phase and 356 nm for the aqueous phase.

The K_{ap} of Ibuprofen at 37°C in pH 7.5 was measured. Either 50 ml or 100 ml (preparation 1 or 2, respectively) of a 511 mcg/ml solution of Ibuprofen in 1-octanol saturated with 50 mM sodium phosphate buffer (pH 7.5) was added to either 75 ml or 150 ml (preparation 1 or 2, respectively) of 50 mM sodium phosphate buffer (pH 7.5) saturated with 1-octanol, and the mixture was stirred vigorously overnight at 37°C.

The media were allowed to separate for half a day and two samples were removed from both phases and prepared for concentration analysis via UV. Absorbance was measured at 274 nm for the 1-octanol samples and 221 nm for the aqueous samples.

The K_{ap} of Ibuprofen at 37°C in pH 1.2 buffer was measured. Seventy-five ml of a solution of 1-octanol containing 15.6 mg/ml ibuprofen saturated with 65 mM HCl and 50 ml of 65 mM HCl saturated with 1-octanol were added to a 37°C vessel and stirred vigorously overnight (two preparations were made). The media were allowed to separate for half a day and two samples were removed from both phases and prepared for concentration analysis via UV. The second derivative of the absorbance was measured at 284 nm for the 1-octanol samples and 237 nm for the aqueous samples.

For each analysis K_{ap} was determined by calculating the ratio of the concentration of drug in the 1-octanol to the concentration of drug in the aqueous medium at equilibrium.

In vitro partitioning experiments

In vitro partitioning experiments were performed to test the validity of the model. Experiments were conducted using BCS II model compounds Ibuprofen, Nimesulide, and Piroxicam in three different types of two-phase dissolution apparatuses, in two different laboratories, by three different researchers. As all three model compounds are at least partially ionized within the physiological pH,

experiments were conducted across a pH range to test the effect of apparent partition coefficient on the model. 1-octanol was used as the organic medium in all cases. Different volumes of buffer (150, 250 ml), different volumes of 1-octanol (150, 200, 250 ml), different impeller rotational speeds (40, 50, 75, 77 rpm), different pHs, and different doses (2.5, 3.75, 4, 5, 6.25, 12.5, 15.0 mg) were used for the experiments. Details for each experiment are given in **Table 2.2**. Apparatus 1 was a 9-cm diameter jacketed glass vessel with a flat bottom. This apparatus utilized a dual paddle, which consisted of two identical 5 cm diameter paddles, which were centered vertically in each phase.

Apparatus 2 consisted of a USP 2 vessel with a diameter of 9.8 cm, and the paddle was mounted such that the bottom of the compendial paddle was approximately 2.5 cm from the bottom of the vessel and the additional paddle was centered vertically in the 1-octanol. Apparatus 3 was a USP 2 apparatus (1000 ml with a hemispherical bottom), which utilized a dual paddle consisting of an additional paddle (5 cm diameter) mounted on the regular compendial paddle, with a vessel diameter of 10.1 cm. The compendial paddle was mounted such that the bottom of the paddle was approximately 2 mm from the bottom of the vessel, and the additional paddle was mounted such that it was centered vertically in the 1-octanol.

For all experiments the buffer solution was made up and mixed overnight with 1-octanol in a 1:1 ratio at 37 °C. The solutions were separated using a separatory funnel and stored at 37 °C before and between partitioning runs. The pH of the buffer saturated with 1-octanol was measured using a calibrated pH meter. The pH was adjusted using concentrated HCl or NaOH solution as necessary to bring it to the desired pH. The appropriate volumes of buffer saturated with 1-octanol and 1-octanol saturated with buffer were then measured using a graduated cylinder and added to the dissolution vessel, which was heated to 37 ± 0.2 °C using a water bath. The phases were stirred at the desired rotational speed for at least 20 minutes prior to the beginning of the run. Prior to starting the run, the temperature was measured with an external thermometer. At the start of the experiment, drug in solution was injected into the aqueous buffer.

The concentration in each phase was measured as a function of time until a plateau was reached in each phase (in most cases). In all cases, calibrated, UV Fiber Optic Probes (StellarNet Inc. Black Comet, Tampa, Florida for Apparatus 1 and 3, or Pion Rainbow, Billerca, MA for Apparatus 2) were mounted such that one collected absorbance data in the aqueous medium and/or one collected absorbance data in the 1-octanol as a function of time. For Ibuprofen in Apparatus 1 and 3, the difference between the absorbance at 222 nm and 375 nm was correlated to concentration in either the aqueous or organic medium using standard solutions. For Apparatus 2, absorbance of Ibuprofen at 222 nm (aqueous and 1-octanol for all pHs), Piroxicam at 336 or 356 nm (aqueous at pH 1.2 or 7.5), and Nimesulide at 300 or 390 nm (aqueous at pH 1.2 or aqueous and 1-octanol at pH 7.5) were correlated to concentration using standard solutions. Experiments were run in duplicate or triplicate for each condition.

Data analysis

The fraction of the dose in the aqueous buffer and/or 1-octanol was plotted as a function of time. The full model (**Equation 2.17**) for fraction of drug in the buffer was fit to the buffer data and the full model (**Equation 2.18**) for fraction of drug in the organic phase was fit to the 1-octanol data for each experiment using non-linear least squares regression with the Nelder-Mead simplex algorithm as the optimization method using Python^{TM}, Software (Python Foundation, Wolfeboro Falls, NH). P_l was the only adjustable parameter in the analysis. The value of β was calculated using a measured value of K_{ap} when available, but was otherwise calculated using an estimated value of K_{ap}, which was calculated assuming only non-ionized drug partitions into 1-octanol. Fitted values and 95% confidence intervals for P_l for each experimental condition were reported. If both buffer and 1-octanol data for a single condition were available, a single, best-fit P_l was determined. The average h_a for each experiment was estimated using **Equation 2.10**.

The model was also fit to experimental two-phase partitioning data generated by Grassi et al [12]. Numerical values for fraction of the dose in the

aqueous phase as a function of time were determined by carefully extracting the average concentration at each time point from concentration-time plots using the ruler tool in Adobe® Photoshop® CS3 (Adobe, San Jose, CA) and dividing by the dose.

Results

Apparent partition coefficient

The measured apparent partition coefficients for Ibuprofen at pH 1.2 and pH 7.5 were 6670.5 (7.9% Relative Standard Deviation (RSD)), and 8.7 (3.7% RSD), respectively. The measured apparent partition coefficient for Piroxicam at pH 7.4 was 0.49 (2.0% RSD).

In vitro experiments

Plots of experimental fraction of drug in aqueous buffer and/or 1-octanol as a function of time along with model fits using the best fit P_l value are included in **Figures 2.3-2.6**. The best fit P_l and h_a values for each experimental condition are included in **Table 2.3**.

Discussion

Comparison of mechanistic analysis to kinetic models

A few researchers have introduced kinetic models to describe aqueous-to-organic phase partitioning[13] [20]. In 2002 Grassi, Coceani, and Magarotto published a comprehensive mathematical model describing the partitioning kinetics of a solute from an aqueous to an organic medium[12]. They proposed a steady-state differential rate equation for aqueous drug concentration as a function of rate constants for transfer from the aqueous to the organic (k_{wo}) and from the organic to aqueous (k_{ow}) phases. Their solution for aqueous concentration, C_w, as a function of time is shown in **Equation 2.23**, where M_o is the total mass of dissolved drug in the system, V_w and V_o are the volumes of the

aqueous and organic phases, respectively, and A is the surface area of the interface. Upon inspection, one can see that **Equation 2.23** is analogous to **Equation 2.14** of our mechanistic model if one sets k_{ow} equal to P_I/K_{ap} and k_{wo} equal to P_I.

$$(2.23) \quad C_w = \frac{k_{ow}M_o}{k_{wo}V_o + k_{ow}V_w} - \left(\frac{k_{ow}M_o}{k_{wo}V_o + k_{ow}V_w} - C_{wi} \right) e^{-\left(A\frac{k_{wo}V_o + k_{ow}V_w}{V_oV_w} \right)}$$

Grassi et al. state that **Equation 2.23** cannot be applied to partitioning of "sparingly soluble drugs in one or both phases" and propose an empirical modification resulting in four different equations for C_w as a function of time. They select the proper equation based upon the values of defined model parameters that are a function of both experimental and fitted parameters (k_{ow} and k_{wo}), which, according to their analysis cannot be determined a priori. When "Case 3" of their model is satisfied (a = 0), their model simplifies to their original model (**Equation 2.23**). Setting k_{ow} equal to P_I/K_{ap}, and k_{wo} equal to P_I reveals that this occurs for cases when C_{so}/C_{sw} is close to or equal to K_{ap}, where C_{sw} is the equilibrium solubility of drug in the aqueous phase, and C_{so} is the equilibrium concentration of drug in the organic phase. For the majority of small molecular compounds, $K_{ap} \sim C_{so}/C_{sw}$, assuming the effect of organic/aqueous mutual saturation on the K_{ap} is small, and phenomenon such as micellization or self-association are not occurring[21]˙[22]. If C_{so} and C_{sw} are measured in mutually-saturated organic medium and aqueous medium respectively, then K_{ap} should be equal to C_{so}/C_s, and **Equation 2.23** of the Grassi model (which is equivalent to **Equation 2.14** our model) should be adequate in describing the partitioning kinetics of the majority of drugs of pharmaceutical interest.

An advantage of our model over existing kinetic models is that all model parameters are defined by the experimental set up, can be measured or calculated, or can be estimated a priori. The values of M_T, V_a, V_o, and A_I are defined by the experimental set up. K_{ap} can be measured using established methods or can be estimated using molecular descriptors [15]˙[23]˙[24]. P_I is a

function of K_{ap}, D_a, D_o, h_a, and h_o. As D_a and D_o can be estimated, the only unknown parameters are h_a and h_o [16], and when K_{ap} is sufficiently large, P_l is simply a function of D_a and h_a, which simplifies estimation of P_l. Alternatively, P_l can be easily determined experimentally in the two-phase system as has been done for other systems such as Caco-2 [25].

Apparent partition coefficient

The partition coefficient of Ibuprofen at pH 1.2 (drug is 100% unionized) of 6670.5 (Log P of 3.82) is in close agreement with the calculated Log P value of 3.84 [26]. The measured apparent partition coefficient of Ibuprofen of 8.7 at pH 7.5 is about 40% higher than the estimated value of 5.2, which was calculated assuming only non-ionized drug partitions into the 1-octanol (using a pK_a of 4.4 and the measured partition coefficient of the non-ionized drug at pH 1.2). The apparent partition coefficient of Piroxicam of 0.49 at pH 7.4 is relatively close to the value of 0.8 at pH 7.5 determined by Yazdanian et al., which was also determined at 37 °C [27].

In vitro **partitioning experiments**

The model fit the data quite well in all cases. Deviations from the model are likely due to errors in the analytical method and/or suboptimal estimates for K_{ap}. As demonstrated in Figures 3-6, the fraction of dose versus time curves for each run deviated slightly. These deviations are not surprising, as analytical error was noted when taking absorbance readings of mutually saturated solvents at elevated temperatures. In addition, using measured rather than calculated values for K_{ap} for Ibuprofen at pH 4.3, 4.4, 4.5, 6.3, and 6.8, and using a measured value for Piroxicam at pH 7.5 rather than pH 7.4 may have given better estimates for P_l in these experiments.

Based on the mass transport analysis, when β is less than about 0.1 the organic diffusion layer should cause negligible diffusional resistance, and the value of P_l should be primarily a function of D_a and h_a. Therefore, experiments 3-6 conducted with Ibuprofen in Apparatus 1 are predicted to have similar P_l values

(β was less than or equal to 0.01 for all conditions). While P_l values were similar between pH 4.3 and 6.3, P_l was somewhat smaller at pH 1.5. The best-fit P_l value for all conditions was 3.0×10^{-3} (range of $2.2 - 4.8 \times 10^{-3}$) cm/s. Since the contribution of the organic diffusion layer is expected to be small, h_a values calculated from these experiments should be reasonably accurate. The best-fit value across all conditions was 25 (range of 16 to 34) mcm, which is in the range of 10 to 50 mcm that was hypothesized a priori to be a practical range. Ibuprofen partitioning in Apparatus 2 (Exp. 7) and 3 (Exp. 13) at pH values low enough to assume negligible organic diffusional resistance was also measured. Estimated h_a values were 39 (37-41) mcm and 26 (23-29) mcm, respectively in these systems. As with Apparatus 1, the values fall within the expected range. Comparisons between h_a in the different apparatuses cannot easily be made due to the different geometries and rotational speeds. When β is not less than 0.1, P_l should increase with increasing K_{ap}. The expected trend was observed for Ibuprofen in Apparatus 2 (Compare experiments 10 and 12 and experiments 9 and 11), Piroxicam in Apparatus 2 (Compare experiments 15 and 18 and experiments 16 and 19), Piroxicam in Grassi et al.'s work (Compare experiments 21 and 22), and Nimesulide in Grassi et al.'s work (Compare experiments 23 and 24).

Since an increase in impeller rotational speed should act to decrease the thickness of the aqueous and organic diffusion layers, P_l should increase with increasing rotational speed. This trend was observed in all experiments in which it was tested. For Ibuprofen in Apparatus 2, a two-fold increase in impeller rotational speed led to a two-and-a-half-fold increase in P_l at both pH 6.8 (compare experiments 9 and 10) and pH 7.5 (compare experiments 11 and 12). For Piroxicam in Apparatus 2, a two-fold increase in rotational speed led to about a six-and-a-half fold increase in P_l (compare experiments 17 and 18). This result may be occurring due to the smaller K_{ap} of Piroxicam at pH 7.5 (~0.49) compared to Ibuprofen at pH 6.8 (~25.0) or pH 7.5 (8.7). When K_{ap} is large, although an increase in rotational speed decreases both h_a and h_o, the contribution of h_o to P_l is minimal. However, when K_{ap} is small, the values of both h_a and h_o have an

effect on the value of P_I. For instance, assuming h_a and h_o are equal, and $D_o = 0.11 D_a$ (valid for a system of buffer and 1-octanol at 37 °C), when K_{ap} is between 10 and 20, the contributions of h_a and h_o on P_I are about equal. However, when K_{ap} is 0.5, the contribution of h_o is about 20 times that of h_a.

The value of M_T/V_a is not expected to have an effect on P_I. A small difference (~7%) between P_I values was observed for Ibuprofen at pH 6.8 in Apparatus 2 (compare experiments 8 and 9). More significant differences were observed for Piroxicam in Apparatus 2 at pH 1.2 (compare experiments 14, 15, and 16), for which P_I values differed by anywhere between about 14 and 64%, and Piroxicam in Apparatus 2 at pH 7.5 (compare experiments 18 and 19), for which values differed by about 73 and 275%. M_T/V_a and P_I. Since there was no trend between an increase in M_T/V_a and P_I, and because the concentration of drug in the aqueous medium was far from saturation for all experiments (≤0.3% for Ibuprofen at pH 6.8, ≤24% for Piroxicam at pH 1.2, and ≤3% for Piroxicam at pH 7.5.[2]) the unexpected impact of M_T/V_a on P_I may be due to experimental error. As can be observed by examining Figures 3-6, replicate runs at each condition varied in some cases, and the shapes of the experimental curves sometimes deviated slightly from the predicted curves.

Scaling parameters for ensuring physiological relevance

To maintain the physiological relevance of the two-phase system, $C_{a,t}$ *in vitro* should be maintained close to $C_{a,t}$ *in vivo*. Maintaining a physiological $C_{a,t}$ is important for drugs with high dose numbers since C_a can be very close to C_s, and can thus have a large impact on both the dissolution and partitioning rates in these cases[3]. As A_I, V_a, P_I, and M_T all influence $C_{a,t}$ in the two-phase system, they are important parameters to consider.

The partitioning rate coefficient, k_p, (equal to $(A_I/V_a)*P_I$) reflects the rate at which drug partitions into the organic medium. Therefore, one approach to

---

[2] The saturation solubility of Ibuprofen at pH 6.8 was estimated using the intrinsic solubility and pK_a values given in Table 1. The saturation solubilities of Piroxicam at pH 1.2 and pH 7.5 were taken from reference 12.

establish physiological relevance is to keep the *in vitro* k_p equal to the expected absorption rate coefficient, k_a, *in vivo*. This approach assumes first-order absorption kinetics and a relatively high fraction absorbed *in vivo* (F_a). Using a known or estimated k_a and after measuring or estimating P_I, we can adjust A_I/V_a such that k_p and k_a are similar according to **Equation 2.24**.

(2.24) $$k_p = \left(\frac{A_I}{V_a} P_I\right)_{\text{in vitro}} = k_a \left(\frac{A}{V} P_{\text{eff}}\right)_{\text{in vivo}}$$

While ideally V_a *in vitro* would be set equal to the intestinal liquid volume, V, *in vivo*, it is not necessary to do so for dissolution studies as long as M_T/V_a and dose/V are similar. The average total fasted intestinal volume *in vivo* is about 100 ml in humans, which may be contained within a number of liquid pockets [28]. Neglecting gastric emptying rate and assuming a bolus of dissolved drug in the intestine *in vivo*, M_T is equal to the dose. For more slowly releasing dosage forms, M_T is equal to the amount of dissolved drug, which depends on a number of factors. Thus, the simplest way to ensure physiological relevance of the *in vitro* dissolution test is to set M_T/V_a *in vitro* equal to dose/V (dose/100 ml in fasted humans).

Although k_a is not typically known *a priori* (especially for drugs early in development) it may be estimated. Several models exist for estimating *in vivo* k_a in humans for passively absorbed drugs [29]. The value of k_a can also be estimated using estimates of A/V and P_{eff}. P_{eff} in humans for passively absorbed drugs can be estimated using models that use molecular descriptors as input parameters [29] [30], and it can also be estimated based on Caco-2 or rat perfusion studies [29]. While P_{eff} must be estimated for each drug, we propose using an average *in vivo* A/V to estimate k_a. Assuming the small intestine to be a perfect cylinder, Amidon et al. estimated A/V to be equal to 2/r, where r is the radius of the small intestine [3]. Assuming a radius of 2 cm [5], this relationship would suggest an A/V of 1.0. However, as the human small intestine is a convoluted tube, it is likely that a compressed rather than a perfect cylindrical

geometry would allow for a more accurate calculation of the geometrical surface area and A_l/V_a. Assuming a radius of 2 cm, a volume of 100 ml, and a constant perimeter, we calculated A_l/V_a based on percent compression, as shown in **Table 2.4**. While there is evidence that the liquid in the small intestine is not continuous, but instead is contained in multiple liquid pockets, for simplicity, our calculation method assumes that the compressed cylinder is completely full of liquid. Assuming the liquid contained in the liquid pockets assumes the shape of the intestine, our calculation method should be valid for discrete or continuous liquid since the surface area of each pocket would be additive. Literature values of total small intestinal length give an average of about 300 cm [5]. As shown in **Table 2.4**, zero percent compression (perfect cylinder) shows that 100 ml of liquid would fill 8 out of the 300 centimeters (assuming the liquid takes the shape of the intestine), while the 100 ml would reside in 19 out of the 300 centimeters if the intestine were 70% compressed.

Rather than using geometrical considerations, Sugano used an equation relating human jejunal effective permeation rate to F_a to estimate A_l/V_a in humans *in vivo* to be about 2.3 cm^{-1} [31][3]. We estimated A_l/V_a in humans to be about 1.9 +/- 1.4 cm^{-1} by dividing average k_a values from the literature by their estimated human jejunal permeation rate, P_{eff}, for drugs dosed as oral solutions to humans that were at least 90% absorbed. Values for P_{eff} were estimated using molecular descriptors using model 1b from Winiwarter et al., 1998 [32]. Use of these k_a values to determine A_l/V_a is only valid if the drug solutions were completely permeation rate limited (e.g. appearance in plasma was independent of gastric emptying rate or any other process other than intestinal absorption). If appearance in plasma was indeed determined in all or in part by gastric emptying rate, k_a values determined using plasma deconvolution methods could be artificially low. A_l/V_a values in the range of 1.9 to 2.3 suggest percent

---

[3] In Sugano's analysis A_l/V_a is represented by A/V for a perfect cylinder times the Degree of Flatness (DF), such that A_l/V_a in our analysis = 2/r X DF in Sugano's analysis. They take r to be 1.5 cm in humans and DF to be 1.7. This analysis also assumes gastric emptying rate >> absorption rate.

compressions in the range of 60 to 70, which seem plausible anatomically. While it is convenient to assume an average human A_l/V_a, it is likely that this ratio varies based on differences in the volume of liquid and how it is distributed throughout the small intestine, and perhaps on the drug itself depending on the site of absorption.

Since the *in vitro* A_l/V_a is dictated by the diameter and geometry of the vessel, options for this parameter are limited if standard, hemispherical vessels are used. **Table 2.5** shows the minimum and maximum A_l/V_a that can be achieved in a 1000-ml USP II vessel and a 100-ml vessel of similar proportions. These estimates are based on practical constraints such as maintaining a minimum aqueous volume to achieve a practical liquid height.

While P_l is dependent upon properties of the drug substance and aqueous buffer, the diffusion layer thicknesses can be modified to some extent through the stirring rate, agitator length and design, and vessel geometry. A balance must be maintained between keeping the dosage form adequately suspended (if necessary), maintaining a level aqueous-organic interface with a well-defined surface area, and maintaining physiological hydrodynamics (if desired). Given these constraints, P_l is more of a defined rather than an adjustable parameter.

Given the somewhat limited range of *in vitro* A_l/V_a and the inability to fully control P_l, the desired k_p won't be achievable in all cases. **Table 2.6** gives the estimated ranges for k_a and k_p for BCS II compounds. Since the range of k_p (0.01 to 50 X 10^4 cm/s) values envelops the range of estimated k_a values when A/V is assumed to be 2, there is a good chance that k_p may be obtained as desired in many cases. However, the ability to do so depends on the relationship between P_{eff} and P_l, which cannot be easily predicted.

In addition to maintaining the correct k_p and M_T/V_a values, ideally a two-phase experiment should be designed such that $F_{o,\infty}$ is similar to F_a *in vivo*. F_a can be estimated using **Equation 2.25**, where t_{res} is the residence time in the small intestine. An average value for t_{res} in the fasted human small intestine is about 3.5 h[5]. Once F_a has been estimated, the value of β required to achieve a $F_{o,\infty}$ similar to F_a can be determined using **Equation 2.26**. As K_{ap} increases, the

required V_o relative to V_a needed to achieve a given $F_{o,\infty}$ decreases. An upper limit of a V_o that is three times V_a ($V_a/V_o \geq 0.33$) seems to be a practical cutoff for determining when the required V_o becomes impractical. When the Log K_{ap} of a compound at the desired pH is at least ~0.5 and V_a/V_o is at least 0.33, then $F_{o,\infty}$ is at least 0.90 ($\beta \leq$ ~0.11).The importance of K_{ap} can be demonstrated by examining the required *in vitro* V_a/V_o for Metoprolol, which is used as a reference compound to designate drug substances as having low or high permeability according to the BCS[33]. Greater than 90% of an oral dose of Metoprolol is known to be absorbed in the small intestine. Metoprolol has a log P of 2.2 (neutral species), but a log K_{ap} of about -0.8 at pH 6.5[34], which is often taken to be the average fasted state pH in the upper small intestine. Because of its low K_{ap} in the intestinal pH range, six liters of 1-octanol would be required to achieve a $F_{o,\infty}$ of 0.9 (similar to its F_a), making Metoprolol a less than ideal candidate for the two-phase system despite its high extent of *in vivo* absorption. However, for Ibuprofen, which is > 99% absorbed in humans and has a calculated Log K_{ap} of 1.7 at pH 6.5, only 200 ml of 1-octanol would be needed to achieve a $F_{o,\infty}$ of 0.99 (V_a/V_o of 0.5) [35].

(2.25) $F_a = 1 - e^{-k_a t_{res}}$

(2.26) $\beta = \dfrac{V_a}{K_{ap} V_o} = \dfrac{1 - F_a}{F_a}$

We present a few case studies to demonstrate how a two-phase system would be set up to mimic *in vivo* absorption rate for a few compounds for which *in vivo* k_a values have already been determined in humans. We took the k_a values of four compounds dosed as oral solutions (Ibuprofen, Valproic acid, Felodipine, and Ondansetron) from the publication by Linnankoski et al. [36] that were said to be passively absorbed and demonstrate completely permeation rate-limited absorption, had F_a values of one, and had calculated Log D values at pH 6.5

(average fasted human intestinal pH [5]) greater than one [4]. We then used our proposed scaling factors, A_l/V_a, M_T/V_a, and $V_a/(K_{ap} V_o)$ to estimate the vessel size, aqueous volume, organic volume, and dose that would be required to achieve a "physiological two-phase set-up" for these compounds when performing two-phase dissolution experiments, as outlined below.

1. Determine dissolution vessel size and *in vitro* V_a using A_l/V_a.
2. Estimate k_a *in vivo*.
3. Estimate P_l using **Equation 2.10** with the following values.
4. Estimate D_a using Hayduk-Laudie method.
5. Assume h_a equals 30 µm.
6. $K_{ap} = 10^{cLogD\ 6.5}$
7. Estimate desired A_l/V_a using **Equation 2.24**.
8. Determine which dissolution vessel size can achieve similar A_l/V_a (with the preference being a 1000-ml USP 2 vessel using the standard set-up for stirrer position) and which value of V_a must be used to achieve that value.
9. Determine M_T (dose *in vitro*) using M_T/V_a.
10. Estimate *in vivo* dose/V (dose/100 ml in fasted humans).
11. M_T *in vitro* = *in vivo* dose/V * V_a
12. Determine V_o *in vitro* using $\beta = V_a/(K_{ap} V_o)$.
13. Determine F_a *in vivo* using **Equation 2.25**.
14. Determine ideal β *in vitro* using **Equation 2.26**.
15. $V_o = V_a/(10^{cLogD\ 6.5} * \beta)$. Select V_o such that $F_{o,\infty}$ is within 10% of F_a.

Results are tabulated in **Table 2.7**. Valproic acid requires a high A_l/V_a of 0.52, which is at the top of the achievable range. An A_l/V_a as high as about 0.47 can be achieved with a standard 100-ml vessel and minimum height of 1 cm below the impeller. Ibuprofen and Ondansetron require A_l/V_a values of 0.29 and

---

[4] While not investigated by Linnankoski and coworkers, if appearances of these compounds in plasma were determined in all or part by gastric emptying, the k_a values given may be artificially low.

0.31, respectively. Values in this range can be achieved with any vessel in the range of 100 to 1000-ml. Felodipine requires an A_l/V_a of 0.62, which cannot be conveniently achieved in the two-phase system. **Figure 2.7** compares the average *in vivo* absorption profiles using the given k_a values with the predicted *in vitro* partitioning profiles using the k_p values from **Table 2.7** for Ibuprofen, Valproic Acid, and Ondansetron. Despite the differences between k_a and k_p due to the constraints of the vessels, the *in vitro* and *in vivo* curves match up quite well, demonstrating similarities between *in vivo* absorption and predicted *in vitro* two-phase partitioning profiles of drugs in solution that result when the apparatus is scaled using the parameters A_l/V_a, M_T/V_a, and $V_a/(K_{ap} V_o)$.

The purpose of these case studies is to demonstrate how a two-phase system can be set-up to be physiologically relevant when conducting an experiment using a solid dosage form. When these scaling parameters are maintained at physiological values as described above, and a physiological aqueous buffer is used, the saturation conditions in the aqueous medium of the two-phase system are expected to be similar to saturation conditions *in vivo*, and the *in vitro* partitioning rate is expected to be similar to the *in vivo* absorption rate, facilitating potential IVIVCs for some drug candidates as described in the next section.

Potential drug candidates

Two-phase dissolution apparatuses can be useful tools to scientists developing solid oral drug formulations. As no one dissolution apparatus currently captures the range of physiological conditions affecting dissolution and absorption, it is important that the chosen apparatus encompasses the most important factors for the particular drug product of interest. If the key physiological scaling parameters (A_l/V_a, M_T/V_a, and $V_a/(K_{ap} V_o)$) for the two-phase system described above are properly designed, and a physiological aqueous buffer is used, it is reasonable to expect similar saturation conditions between the *in vitro* aqueous medium and the intestinal lumen and to expect an *in vitro* partitioning rate that is similar to the *in vivo* absorption rate of a drug substance.

However, an IVIVC has the potential to be developed only for drug substances for which the F_a is similar to the fraction bioavailable. Thus, for a drug substance to be a candidate for the two-phase system it should have a relatively high F_a *in vivo*, should be relatively hydrophobic (i.e. Log K_{ap} at pH 6.5 should be greater than about ~0.5-1 so a practical volume of organic medium can be used to achieve an extent of *in vitro* partitioning that is similar to the F_a), and its F_a should be similar to its fraction bioavailable (i.e. low first-pass metabolism and gut metabolism/degradation).

The feasibility of using the two-phase system to predict *in vivo* performance should be verified by properly scaling the apparatus as discussed above and performing experiments using solid dosage forms of drugs with different physicochemical properties (e.g. acid-base character, particle size, pH-solubility profile, human jejunal effective permeation rate, dose), using relevant aqueous media types (e.g. surfactant level, buffer species, constant or variable pH). In each case, solubility and dissolution rate of drug in the chosen buffer should be compared with solubility and dissolution rate of drug in the chosen buffer saturated with organic medium. Unpublished data from our laboratory shows no difference between dissolution rates of Ibuprofen particles in sodium acetate buffer (50 mM, pH 4.5, isotonic) and sodium acetate buffer saturated with 1-octanol. However, the presence of organic medium in buffer containing surfactant could have greater effects on solubility and dissolution rate as well as on rate and extent of partitioning into the organic medium [37]. Research has shown that long-chain alcohols like 1-octanol can form mixed micelles with ionic surfactants [38]. Depending on the relative concentrations of the long-chain alcohol and surfactant, the alcohol can decrease the critical micelle concentration (CMC) of surfactant, increase the ionization of micelles, and change the micellar size and structure [38], [39].

In addition to the possible impact of surfactants on dosage form performance in the two-phase apparatus, integrity of the aqueous-organic interface should also be considered. Shi et al. successfully performed two-phase experiments at polysorbate 80 concentrations as high as 0.23 mM [11]. We have

demonstrated the formation of a clear, distinct aqueous-organic interface using Fasted State Simulated Intestinal Fluid and Fed State Simulated Intestinal Fluid (Phares FaSSIF and FeSSIF, Muttenz, Switzerland), and 0.7 mM Sodium Dodecyl Sulfate (SDS) in a USP II apparatus as 25, 50, and 75 rpm (unpublished data). The interface was somewhat obscured at 100 rpm. However, we recommend running USP II two-phase experiments at speeds lower than 75 rpm to minimize formation of a vortex.

Since the two-phase system adds a level of complexity compared to single-phase systems it's also important to outline for which drug substances and drug products a two-phase system may lead to improved IVIVCs over a single-phase system that employs a large aqueous volume (e.g. 900 ml). A two-phase system will likely be more useful when dissolution is limited by solubility (i.e. dose number is high), which often occurs when solubility is low and dose is moderate-to-high. In this situation the drug saturation profile in the aqueous medium will likely be different in a two-phase system with 100 ml of aqueous buffer and a sufficient volume of organic medium to achieve physiologically relevant extent and rate of partitioning than it would be in a single-phase system with 900 ml of medium. Another case when a two-phase system may provide an improved IVIVC over a single-phase system is when the rate of appearance of drug in the organic medium is limited at least in part by permeation rate, which can occur for drugs with low to moderate average intestinal permeation rates.

In general, a two-phase test may be most useful for some BCS II compounds (which often have solubility limitations), but may presumably also be useful for some BCS IV compounds (which often have solubility and permeation rate limitations). As each class contains drugs with a range of properties, it will be important to assess the potential applicability of two-phase systems based on key drug physicochemical properties such as acid-base character, particle size, pH-solubility profile, human jejunal effective permeation rate, and dose.

Conclusions

Two-phase dissolution apparatuses simultaneously capture the processes of drug dissolution and partitioning, thereby simulating absorption while maintaining a physiological volume of buffer. They have the potential to provide meaningful predictions of *in vivo* performance for some drug products, and can therefore be useful tools to industrial and academic scientists for designing and developing drug product formulations.

While researchers have been exploring the utility of two-phase systems for simple and novel oral dosage forms since the 1960s, and have shown improved predictive capabilities over conventional methods, no one has elucidated the mechanism by which two-phase dissolution apparatuses may facilitate improved IVIVCs over conventional single-phase systems, or determined for which drugs and dosage forms these apparatuses could be most useful. We performed a mechanistic, drug-transport analysis of the partitioning of solutes in solution in an in vitro two-phase dissolution apparatus, and demonstrated the ability of our model to successfully describe the in vitro partitioning profiles of three BCS II weak acids in four different experimental set-ups. In contrast to previous kinetically derived mathematical models, our model uses physical input parameters that are known or can be estimated a priori. To establish the physiological relevance of the test for the drug product of interest, we have proposed scaling factors (A_l/V_a, M_T/V_a, and $V_a/(K_{ap} V_o)$), the values of which can be determined based on molecular descriptors. When these scaling parameters are maintained at physiologically relevant values and a physiological aqueous buffer is used, the saturation conditions in the aqueous medium of the two-phase system are expected to be similar to saturation conditions in vivo, and the in vitro partitioning rate is expected to be similar to the in vivo absorption rate. Potential IVIVCs between the in vitro partitioning and in vivo absorption profiles may result for some drug products that have relatively high fraction absorbed values and low extents of hepatic first-pass metabolism and gut degradation/metabolism. While this manuscript focuses on an analysis of drugs in solution, these scaling factors

can be applied to dissolution of solid dosage forms in two-phase dissolution apparatuses, which will be the focus of future work.

The two-phase system may be a more physiologically relevant tool than a conventional single-phase system for some BCS II, and possibly some BCS IV drugs. Although the dissolution-partitioning behavior of a drug dosage form is complex and dependent upon drug physicochemical properties, dose, permeation rate, dosage form type, and formulation composition, it's probable that two-phase systems may be particularly useful for drug products that experience solubility-limited dissolution and/or a permeation rate limitation *in vivo*, or include functional excipients that may affect dissolution and/or absorption at physiological concentrations. To help determine the general applicability of the two-phase system and provide recommendations for determining for which drugs and dosage forms a two-phase dissolution apparatus may be most useful, our mass transport analysis could be extended to include simultaneous dissolution and partitioning of drug substances from dosage forms, and tested in a two-phase system using solid dosage forms of drugs with different physicochemical properties (such as acid-base character, particle size, pH-solubility profile, human jejunal effective permeation rate, and dose) using relevant aqueous media types. The *in vivo* relevance could be ascertained by performing studies in dogs or humans (or by using existing in vivo data from the literature) and comparing the deconvoluted *in vivo* absorption profiles with the *in vitro* organic phase partitioning profiles.

Tables and Figures
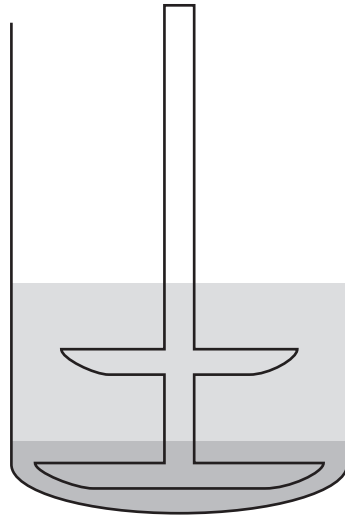
Figure 2.1. Schematic diagram of a two-phase dissolution apparatus
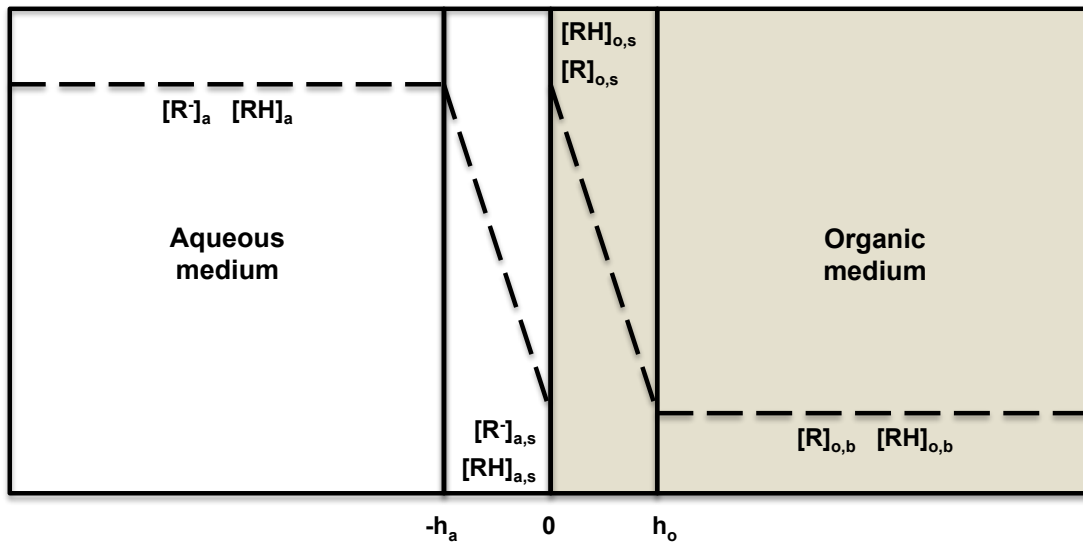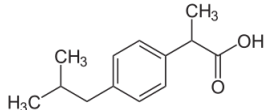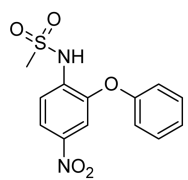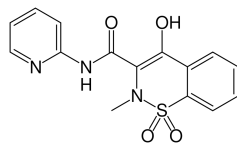
Figure 2.2. Schematic diagram of physical model with key parameters

Table 2.1. Properties of the model drugs

Drug	Ibuprofen	Nimesulide	Piroxicam
BCS Class	II	II	II
Structure			
Molecular weight (g/mol)	206.3	308.3	331.3
pK$_a$ at 37°C	4.4 (acidic)[a]	6.8 (acidic)[b]	2.3 (basic)[c]
			5.3 (acidic)[c]
cLog P	3.84[d]	1.79[d]	0.60[d]
Log D	pH 4.5 – 3.4 [e]	pH 1.2: 1.92[f]	pH 1.2: 0.92[f]
	pH 5.0 – 3.1 [e]	pH 7.5: -0.10[e]	pH 7.5: 0.8[g]
	pH 6.5 – 1.7 [e]		
	pH 6.8 – 1.4 [e]		
	pH 7.5 – 0.7 [e]		
Intrinsic solubility at 37°C (M)	3.3 X 10^{-4} [a]	3.8 X 10^{-5} [f]	6.6 X 10^{-5} [f]

[a] Measured value from reference [40]

[b] Calculated value from reference [30]

[c] Measured value from reference [41]

[d] Calculated value from reference [26]

[e] Calculated using a pK$_a$ of 4.4 and a Log P of 3.8, assuming only non-ionized drug partitions into 1-octanol.

[f] Measured value from Reference [12]

Table 2.2. Experimental details for *in vitro* partitioning experiments
(Continued on next page)

Exp./Fig No.	Apparatus	Drug	pH	Buffer Species[a]	Buffer Conc. mM	Rotational speed rpm	V_a ml	V_o ml	M_T mg	A_l[b] cm^2	β	M_T/V_a mcg/ml	A_l/V_a cm^{-1}	No. rep.[c]
3/3(a)	1	Ibuprofen	1.5	HCl	10	77	150	150	2.5	63.6	1.58×10^{-4}	16.7	0.42	2
4/3(b)	1	Ibuprofen	4.3	Sodium Acetate	50	77	150	150	2.5	63.6	3.17×10^{-4}	16.7	0.42	2
5/3(c)	1	Ibuprofen	4.4	Sodium Acetate	50	77	150	150	2.5	63.6	2.84×10^{-4}	16.7	0.42	2
6/3(d)	1	Ibuprofen	6.3	Sodium Phosphate	43	77	150	150	2.5	63.6	1.28×10^{-2}	16.7	0.42	2
7/4(a)	2	Ibuprofen	5	Sodium acetate	50	75	250	200	6.25	75.4	9.87×10^{-4}	25	0.3	3
8/4(b)	2	Ibuprofen	6.8	Sodium phosphate	50	75	250	200	12.5	75.4	5.00×10^{-2}	50	0.3	3
9/4(c)	2	Ibuprofen	6.8	Sodium phosphate	50	75	250	200	6.25	75.4	5.00×10^{-2}	25	0.3	3
10/4(d)	2	Ibuprofen	6.8	Sodium phosphate	50	40	250	200	6.25	75.4	5.00×10^{-2}	25	0.3	3
11/4(e)	2	Ibuprofen	7.5	Sodium phosphate	50	75	250	200	6.25	75.4	0.144	25	0.3	3
12/4(f)	2	Ibuprofen	7.5	Sodium phosphate	50	40	250	200	6.25	75.4	0.144	25	0.3	3
13/4(g)	3	Ibuprofen	4.5	Sodium Acetate	50	50	250	250	4	80.1	3.58×10^{-4}	16	0.32	3

[a] Buffers used in experiments 3-13 were made isotonic with bodily fluids.

[b] A_l in experiments conducted at 75 rpm in Apparatus 2 may have been as much as 4% higher than reported due to a slight vortex observed during mixing.

[c] Number of replicates performed per experimental condition.

Table 2.2. (Cont'd)

Exp./Fig No.	Apparatus	Drug	pH	Buffer Species[a]	Buffer Conc. mM	Rotational speed rpm	V_a ml	V_o ml	M_T mg	A_l[b] cm^2	β	M_T/V_a mcg/ml	A_l/V_a cm^{-1}	No. rep.[c]
14/5(a)	2	Piroxicam	1.2	HCl	0.06	75	250	200	15	75.4	0.149	60	0.3	3
15/5(b)	2	Piroxicam	1.2	HCl	0.06	75	250	200	5	75.4	0.149	20	0.3	3
16/5(c)	2	Piroxicam	1.2	HCl	0.06	75	250	200	3.75	75.4	0.149	15	0.3	3
17/5(d)	2	Piroxicam	7.5	Sodium phosphate	50	40	250	200	5	75.4	2.53	20	0.3	3
18/5(e)	2	Piroxicam	7.5	Sodium phosphate	50	75	250	200	5	75.4	2.53	20	0.3	3
19/5(f)	2	Piroxicam	7.5	Sodium phosphate	50	75	250	200	15	75.4	2.53	60	0.3	3
20/5(g)	2	Nimesulide	7.5	Sodium phosphate	50	75	250	200	12.25	75.4	8.99×10^{-2}	49	0.3	3

[a] Buffers used in experiments 3-13 were made isotonic with bodily fluids.

[b] A_l in experiments conducted at 75 rpm in Apparatus 2 may have been as much as 4% higher than reported due to a slight vortex observed during mixing.

[c] Number of replicates performed per experimental condition.
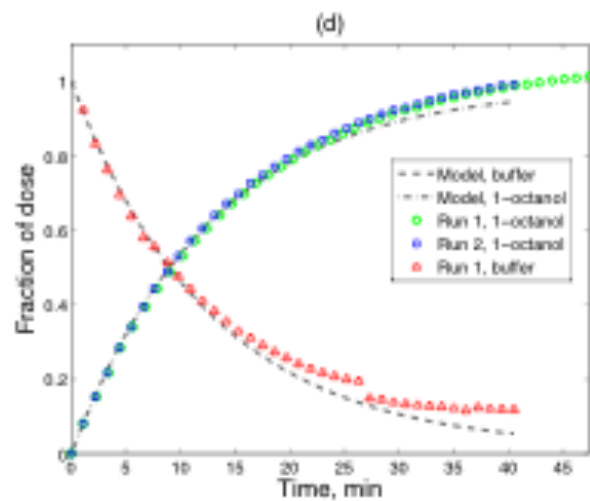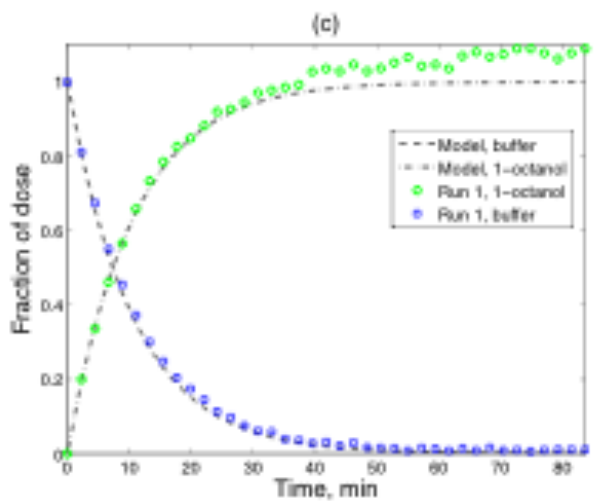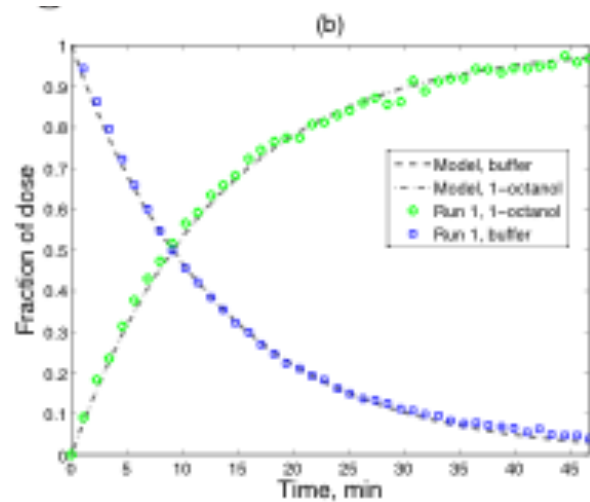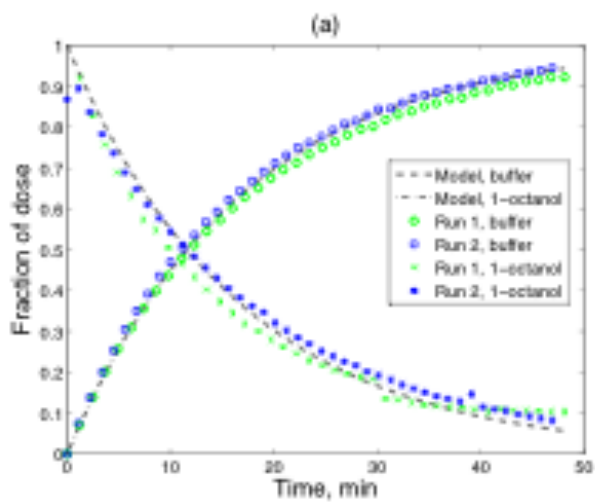
Figure 2.3. *In vitro* **fraction of dose as a function of time for Ibuprofen in Apparatus 1 (experiments 3-6 in plots (a)-(d), respectively, see also Table 2.3.**
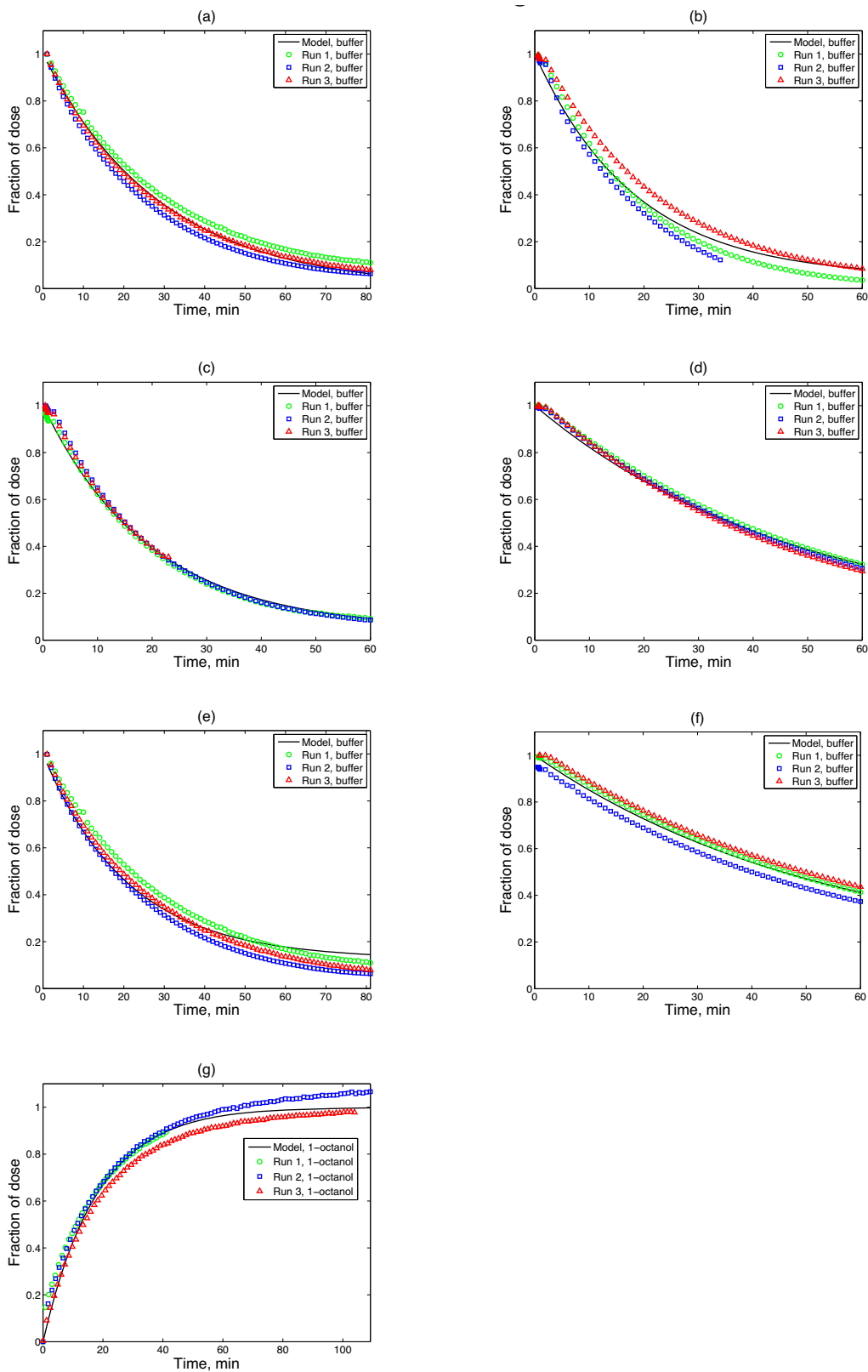
Figure 2.4. In vitro fraction of dose as a function of time for Ibuprofen in Apparatus 2 and 3 (experiments 7-13 in plots (a)-(g), respectively, see also Table 2.3.
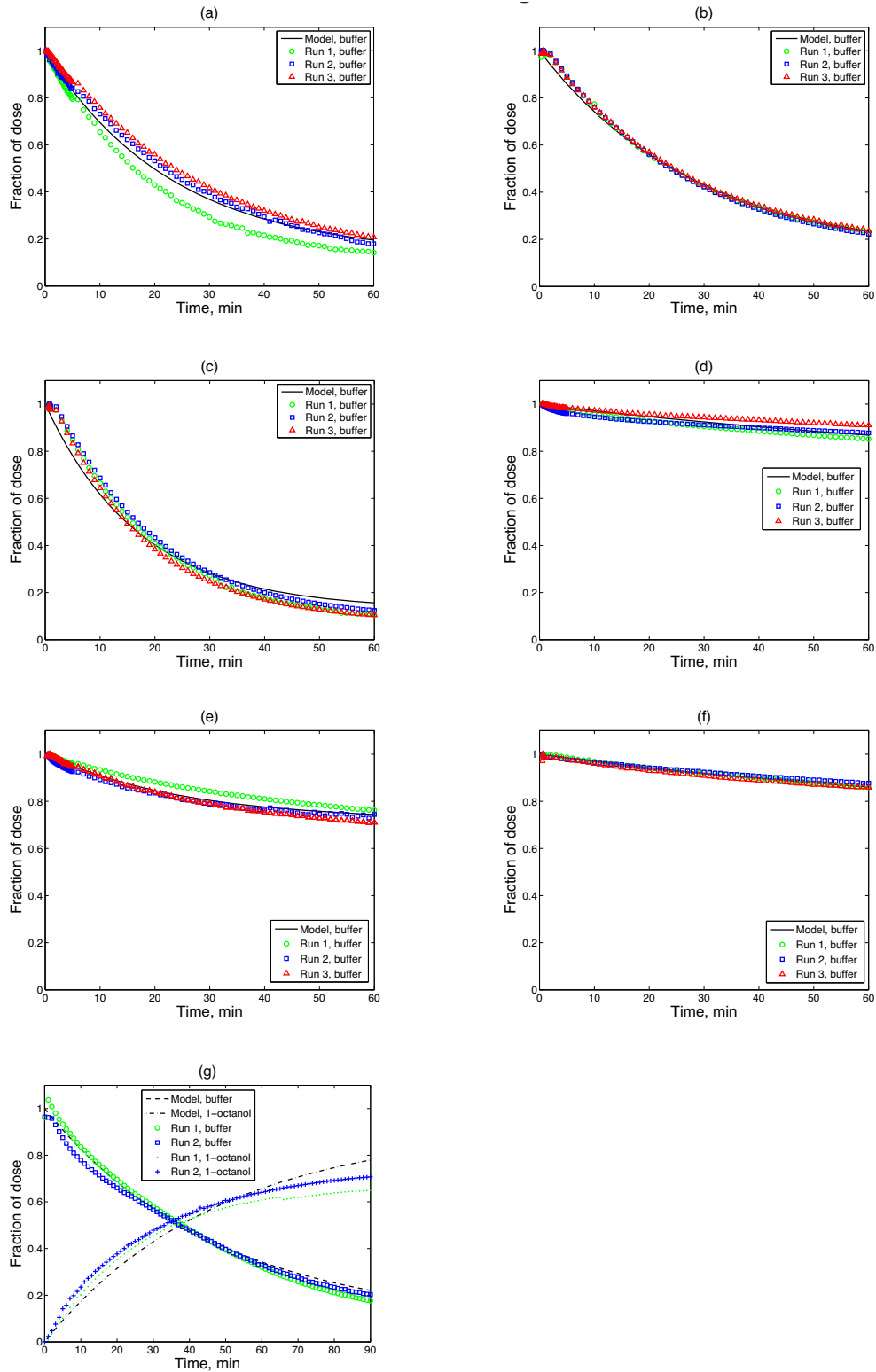
Figure 2.5. *In vitro* **fraction of dose as a function of time for Piroxicam and Nimesulide in Apparatus 2 (experiments 14-20 in plots (a)-(g), respectively, see also Table 2.3.**
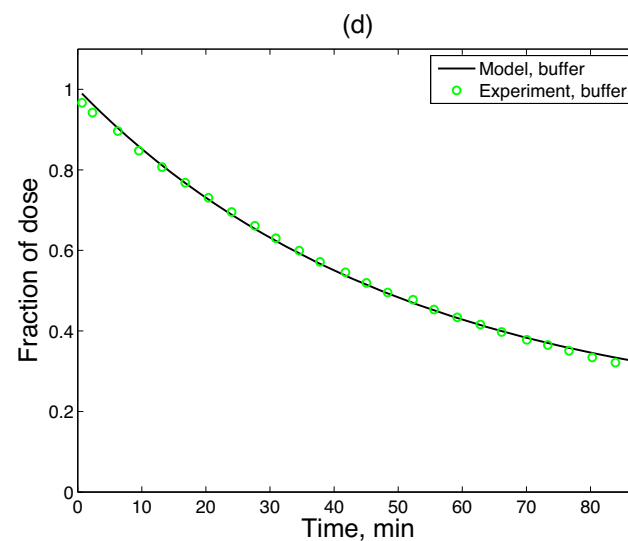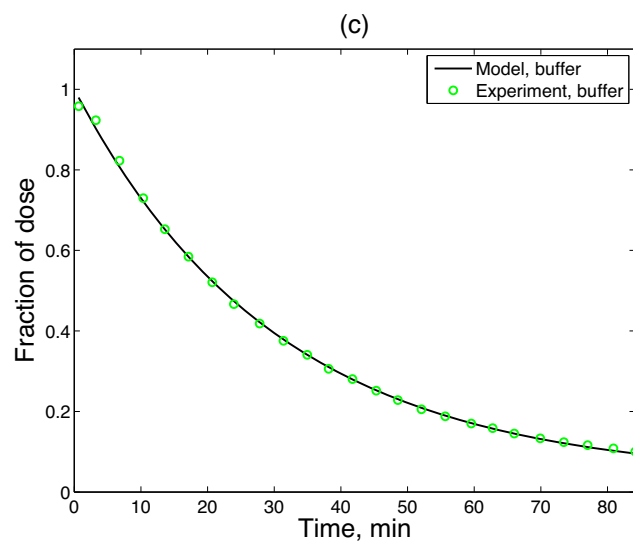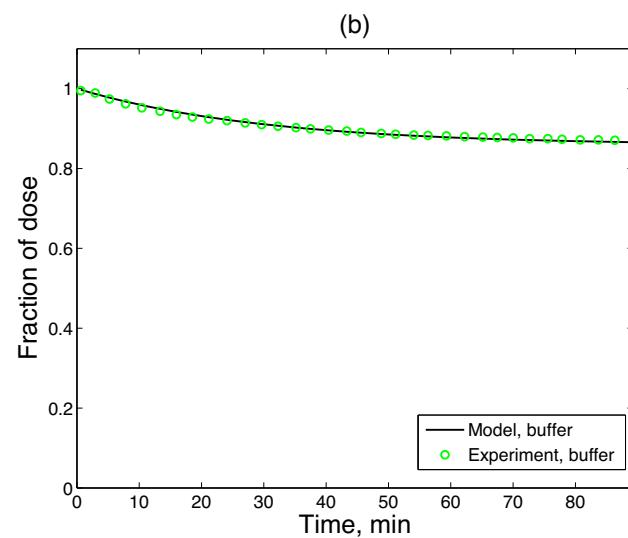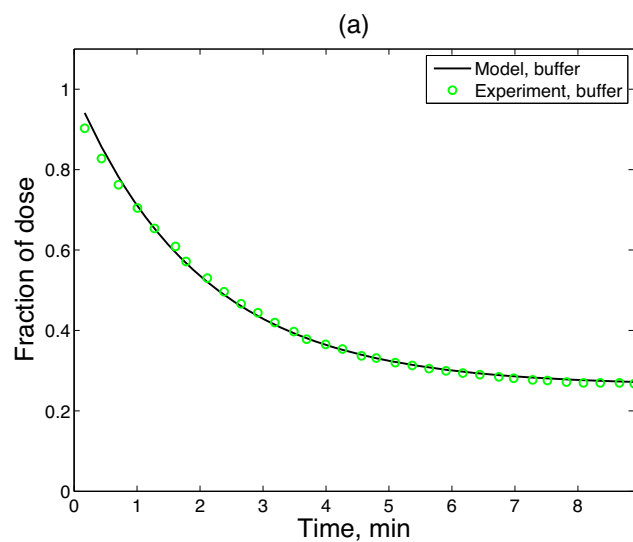
Figure 2.6. *In vitro* **fraction of dose as a function of time for Piroxicam and Nimesulide in Grassi et al's experiments (experiments 21-24 in plots (a)-(d), respectively, see also Table 2.3)**

Table 2.3. Best fit P_l and estimated h_a values from *in vitro* partitioning experiments

Exp./Fig No.	Drug	Apparatus	pH	Rotational speed	A/V_a	β	M_T/V_a	$F_{o, inf}$	$K_{ap}/(9.2+K_{ap})$	$P_l \times 10^4$	(95% CI)	h_a, full	(95% CI)
				rpm	cm^{-1}		mcg/ml			cm/s X 10^4		mcm	
3/3(a)	Ibuprofen	1	1.5	77	0.42	1.58×10^{-4}	16.7	1.00	1.00	23.71	(22.16 - 25.41)	32	(29 - 34)
4/3(b)	Ibuprofen	1	4.3	77	0.42	2.84×10^{-4}	16.7	1.00	1.00	30.06	(29.45 - 30.68)	25	(24 - 25)
5/3(c)	Ibuprofen	1	4.4	77	0.42	3.17×10^{-4}	16.7	1.00	1.00	37.52	(30.30 - 47.73)	20	(16 - 25)
6/3(d)	Ibuprofen	1	6.3	77	0.42	1.28×10^{-2}	16.7	0.99	0.89	30.81	(28.79 - 33.03)	22	(20 - 23)
7/4(a)	Ibuprofen	2	5.0	75	0.30	9.87×10^{-4}	25.0	1.00	0.99	19.08	(18.13 - 20.10)	39	(37 - 41)
8/4(b)	Ibuprofen	2	6.8	75	0.30	5.00×10^{-2}	50.0	0.95	0.73	28.73	(24.64 - 33.73)	19	(16 - 22)
9/4(c)	Ibuprofen	2	6.8	75	0.30	5.0×10^{-2}	25.0	0.95	0.73	26.85	(26.09 - 27.63)	20	(20 - 21)
10/4(d)	Ibuprofen	2	6.8	40	0.30	5.00×10^{-2}	25.0	0.95	0.73	10.92	(10.69 - 11.17)	50	(49 - 51)
11/4(e)	Ibuprofen	2	7.5	75	0.30	1.44×10^{-1}	25.0	0.87	0.49	23.01	(20.07 - 26.59)	16	(14 - 18)
12/4(f)	Ibuprofen	2	7.5	40	0.30	1.44×10^{-1}	25.0	0.87	0.49	9.03	(8.38 - 9.70)	40	(38 - 43)
13/4(g)	Ibuprofen	3	4.5	50	0.32	3.58×10^{-4}	16.0	1.00	1.00	28.72	(25.45 - 32.65)	26	(23 - 29)
14/5(a)	Piroxicam	2	1.2	75	0.30	1.49×10^{-1}	15.0	0.87	0.48	20.85	(16.47 - 26.73)	15	(12 - 19)
15/5(b)	Piroxicam	2	1.2	75	0.30	1.49×10^{-1}	20.0	0.87	0.48	17.06	(16.77 - 17.36)	19	(18 - 19)
16/5(c)	Piroxicam	2	1.2	75	0.30	1.49×10^{-1}	60.0	0.87	0.48	28.04	(24.65 - 32.12)	11	(10 - 13)
17/5(d)	Piroxicam	2	7.5	40	0.30	2.53	20.0	0.28	0.05	1.64	(1.48 - 1.80)	21	(19 - 23)
18/5(e)	Piroxicam	2	7.5	75	0.30	2.53	20.0	0.28	0.05	6.15	(5.87 – 6.44)	6	(5 - 6)
19/5(f)	Piroxicam	2	7.5	75	0.30	2.53	60.0	0.28	0.05	1.78	(1.75 - 1.81)	19	(19 - 20)
20/5(g)	Nimesulide	2	7.5	75	0.30	8.99×10^{-2}	49.0	0.92	0.60	10.71	(9.80 - 11.71)	39	(36 - 43)
21/6(a)	Piroxicam	Grassi	1.2	unknown	0.23	0.357	15.2	0.74	0.48	265.4	(257.7 - 273.5)	12	(12 - 12)
22/6(b)	Piroxicam	Grassi	7.5	unknown	0.23	6.07	21.8	0.14	0.05	3.41	(3.35 - 3.46)	10	(10 - 10)
23/6(c)	Nimesulide	Grassi	1.2	unknown	0.23	3.59×10^{-2}	8.5	0.97	0.90	22.98	(22.71 - 23.25)	27	(27 - 28)
24/6(d)	Nimesulide	Grassi	7.5	unknown	0.23	2.16×10^{-1}	45.0	0.82	0.60	11.80	(11.60 - 12.01)	36	(35 - 36)

Table 2.4. Calculated length, surface area, and surface-area-to-volume ratio, A_l/V_a, of a cylinder as a function of percent compression assuming a constant perimeter

% compression	a^a (cm)	b^b (cm)	Length^c (cm)	Surface area^d (cm^2)	A_l/V_a^e (cm^{-1})
95	0.1	2.8	112.6	1415.1	14.15
90	0.2	2.8	56.4	708.9	7.09
70	0.6	2.8	19.2	241.2	2.41
60	0.8	2.7	14.7	184.3	1.84
50	1.0	2.6	12.0	151.2	1.51
30	1.4	2.5	9.3	116.3	1.16
0	2.0	2.0	8.0	100.0	1.00

^{a} Equal to average radius, r (equal to 2 cm), times (100% - % compression)/100%

^{b} Equal to sqrt(r^2/0.5 - a^2). Uses approximate formula for the perimeter of an ellipse and sets it equal to the perimeter of a circle with a radius of 2 (2pi*r = p = 2pi*(a^2+b^2)/2)

^{c} Equal to 100 cm^3/a/b.

^{d} Equal to 2*pi*r*length.

^{e} Equal to surface area/100 cm3.

Table 2.5. Minimum and maximum A_l/V_a values for 100 and 1000 ml hemispherical *in vitro* dissolution vessels

Capacity	Diameter	Minimum aqueous volume^a	Maximum aqueous volume^b	Minimum A_l/V_a^c	Maximum A_l/V_a^c
ml	cm	ml	ml	cm^{-1}	cm^{-1}
100	4	27	50	0.25	0.47
1000 (USP II)	10	288	500	0.16	0.26

^{a} Value gives minimum volume needed to achieve an aqueous liquid height high enough to allow for 1 cm below the bottom of the impeller for the 100 ml vessel (impeller is 0.8 cm tall) and 2.5 cm below the bottom of the 2 cm high impeller for the 1000 ml vessel (impeller is 2 cm tall) as well as 1 cm above the impeller for both vessels. Values calculated assuming a perfect hemispherical bottom.

^{b} Value is half of the nominal capacity of the vessel, which assumes a 1:1 ratio of aqueous to organic medium.

^{c} Minimum A_l/V_a is the aqueous-organic surface area divided by the maximum aqueous volume and maximum A_l/V_a is the aqueous-organic surface area divided by the minimum aqueous volume.

Table 2.6. Estimated ranges of the average absorption rate coefficient *in vivo* (k_a) and the average partitioning rate coefficient *in vitro* (k_p) for BCS II compounds

Values based on ranges for surface area to volume ratio *in vivo* (A/V) and *in vitro* (A_l/V_a), and average permeation rate *in vivo* (P_{eff}) and *in vitro* (P_l).

A/V[a]	$P_{eff} \times 10^{4}$ [b]	$k_a \times 10^{4}$ [c]	A_l/V_a [d]	$P_l \times 10_4$ [e]	$k_p \times 10^{4}$ [f]
cm^{-1}	cm/s	s^{-1}	cm^{-1}	cm/s	s^{-1}
2	1 to 14	2 to 28	0.16 to 0.47	0.01 to 100	0.01 to 50
(1 to 7)		*(1 to 100)*			

[a]Estimated based on an A/V of 2 and plausible percent compression based on Table 2.2

[b]Approximate range for measured human jejunal effective permeation rate for BCS II compounds from reference [32]

[c]Calculated – equal to A/V * $P_{eff} \times 10^{4}$

[d]Range from Table 1 assuming standard USP guidelines for impeller positioning.

[e]Estimated using equation 28 assuming h_a from 10 to 50 mcm and D_a from 10^{-5} to 10^{-7}.

[f][c]Calculated – equal to A_l/V_a* $P_l \times 10^{4}$

Table 2.7. Desired and achievable *in vitro* two-phase parameters to make dissolution test physiological for Valproic acid, Ondansetron, Ibuprofen, and Felodipine based on *in vivo* properties and performance
Continued on next page.

Drug name	*in vivo* properties/performance					*in vitro* drug properties		
	F_A[1]	k_a[1] X 10^4	Dose[2]	V[3]	Dose/V	clogD 6.5[4]	D_a[5] X 10^6	P_l[6] X 10^4
	actual	decon.	theo.	est.	est.	calc.	est.	est.
		s^{-1}	mg	ml	mg/ml	-	cm^2/s	cm/s
Valproic acid (BCS II)	1	11.0	250	100	2.5	1.43	8.87	22.0
Ondansetron (BCS I or III)	1	5.25	8	100	0.08	1.65	6.63	18.4
Ibuprofen (BCS II)	1	7.42	200	100	2.00	2.19	7.50	23.6
Felodipine (BCS II)	1	12.5	5	100	0.05	3.41	6.10	20.3

[1] From reference [36]
[2] Arbitrarily chose one of the marketed oral unit doses
[3] Average human fasted intestinal volume.
[4] Determined using reference [26]
[5] Estimated using Hayduk-Laudie (H-L) method.
[6] Estimated using Equation 10 assuming $h_a = h_o = 30$ mcm.

Table 2.7 (Cont'd)

Drug name	desired *in vitro* parameters				achievable *in vitro* parameters							
	k_p[7] X 10^4	A_l/V_a [8]	$F_{o, inf}$[9]	M_T/V_a[10]	Vessel capacity	depth below impeller[11]	Vessel A_l/V_a[12]	V_a[13]	k_p[14] X 10^4	V_o[15]	$V_a/(K_{ap} V_o)$	Dose[16]
	based on k_a	est.		based on dose/V		based on USP standard		req.	est.	req.		req.
	s^{-1}	cm^{-1}	-	mg/ml	ml	cm	cm^{-1}	ml	s^{-1}	ml	-	mg
Valproic acid (BCS II)	10.0	0.52	0.974	2.5	100	1	0.47	27	10.2	70	0.027	125
Ondansetron (BCS I)	5.25	0.29	0.985	0.08	1000	2.5	0.26	301	4.77	449	0.015	24
Ibuprofen (BCS II)	7.42	0.31	0.985	2.00	1000	2.5	0.26	301	6.14	130	0.015	602
Felodipine (BCS II)	12.5	0.62	0.985	0.05	*impossible unless depth below impeller decreased & smaller vessel used*							

[7] Equal to k_a
[8] Calculated using Equation 24
[9] Value should ideally be equal or close to FA *in vivo*. 0.97 chosen for Valproic acid based on height constraints of the standard 100-ml vessel. 0.99 chosen for other compounds since it was easily achievable, but a smaller value would require less 1-octanol.
[10] Equal to Dose/V
[11] The standard set-up for distance from bottom of vessel to bottom of impeller is 2.5 cm for the 1000-ml USP 2 vessel. 1 cm chosen for 100-ml vessel, which should accommodate a tablet or capsule..
[12] From Table 2.1. Value set by apparatus geometry and minimum or maximum pratical volume of media.
[13] Volume required to achieve A_l/V_a.
[14] Equal to estimated P_l times the actual A_l/V_a.
[15] Volume required to achieve desired $F_{o,inf}$ based on cLogD 6.5 and V_a.
[16] Equal to M_T/V_a * V_a.since it was easily achievable, although a smaller value would require less 1-octanol and may be desirable.
[10] Equal to Dose/V
[11] The standard set-up for distance from bottom of vessel to bottom of impeller is 2.5 cm for the 1000-ml USP 2 vessel. 1 cm chosen for 100-ml vessel, which should accommodate a tablet or capsule.
[12] From Table 2.1. Value set by apparatus geometry and minimum or maximum practical volume of medium.
[13] Volume required to achieve A_l/V_a.
[14] Equal to estimated P_l times the actual A_l/V_a.
[15] Volume required to achieve desired $F_{o,inf}$ based on cLogD 6.5 and V_a.
[16] Equal to M_T/V_a * V_a.
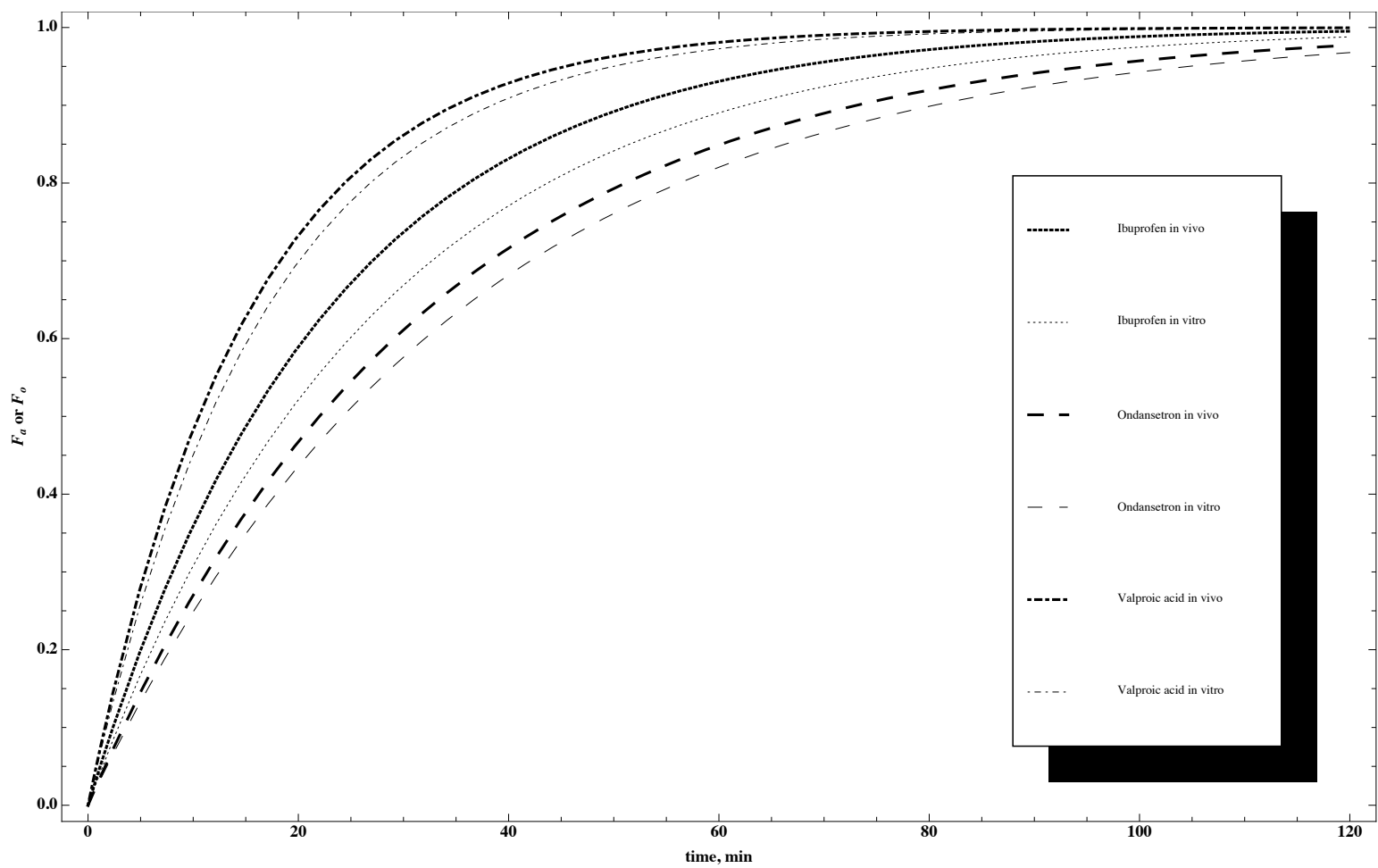
Figure 2.7. Comparison of fraction absorbed in vivo (in humans) and estimated fraction partitioned in 1-octanol in vitro in a 1000-ml USP 2 vessel for Ibuprofen, Ondansetron, and Valproic acid using the simplified model

93

References

1. Abdou HM. Effect of the physicochemical properties of the drug on dissolution rate. *Dissolution, bioavailability and bioequivalence*. Easton, PA: Mack Publishing, 1989:56-72.
2. Sheng J. Toward an In Vitro Bioequivalence Test. Ann Arbor: University of Michigan; 2007.
3. Amidon GL, Lennernas H, Shah VP, Crison JR. A theoretical basis for a biopharmaceutic drug classification: The correlation of in vitro drug product dissolution and in vivo bioavailability. *Pharm Res* 1995; 12: 413-20. DOI: 10.1023/A:1016212804288
4. FDA. Guidance for industry. Waiver of the In Vivo Bioavailability and Bioequivalence Studies for Immediate-Release Solid Oral Dosage Forms Based on a Biopharmaceutics Classification System. Washington, DC: U.S. Department of Health and Human, Food and Drug Administration (FDA), Center for Drug Evaluation and Research 2000.
5. Mudie DM, Amidon GL, Amidon GE. Physiological Parameters for Oral Delivery and in Vitro Testing. *Mol Pharmaceut* 2010; 7: 1388-405. DOI: 10.1021/Mp100149j
6. Pillay V, Fassihi R. A new method for dissolution studies of lipid-filled capsules employing nifedipine as a model drug. *Pharm Res* 1999; 16: 333-7. DOI: 10.1023/A:1011959914706
7. Hoa NT, Kinget R. Design and evaluation of two-phase partition-dissolution method and its use in evaluating artemisinin tablets. *J Pharm Sci* 1996; 85: 1060-3. DOI: 10.1021/js960115u
8. Gabriels M, Plaizier-Vercammen J. Design of a dissolution system for the evaluation of the release rate characteristics of artemether and dihydroartemisinin from tablets. *Int J Pharm* 2004; 274: 245-60. DOI: 10.1016/j.ijpharm.2004.01.022
9. Grundy JS, Anderson KE, Rogers JA, Foster RT. Studies on dissolution testing of the nifedipine gastrointestinal therapeutic system .2. Improved in vitro in vivo correlation using a two-phase dissolution test. *J Control Release* 1997; 48: 9-17. DOI: 10.1016/S0168-3659(97)01638-6
10. Heigoldt U, Sommer F, Daniels R, Wagner KG. Predicting in vivo absorption behavior of oral modified release dosage forms containing pH-

dependent poorly soluble drugs using a novel pH-adjusted biphasic in vitro dissolution test. *Eur J Pharm Biopharm* 2010; 76: 105-11. DOI: 10.1016/J.Ejpb.2010.05.006

11.   Shi Y, Gao P, Gong YC, Ping HL. Application of a Biphasic Test for Characterization of In Vitro Drug Release of Immediate Release Formulations of Celecoxib and Its Relevance to In Vivo Absorption. *Mol Pharmaceut* 2010; 7: 1458-65. DOI: 10.1021/Mp100114a

12.   Grassi M, Coceani N, Magarotto L. Modelling partitioning of sparingly soluble drugs in a two-phase liquid system. *Int J Pharm* 2007; 239: 157-69. DOI: 10.1016/S0378-5173(02)00101-1

13.   Takayama K, Nambu N, Nagai T. Analysis of Interfacial Transfer of Indomethacin Following Dissolution of Indomethacin-Polyvinylpyrrolidone Coprecipitates. *Chem Pharm Bull* 1981; 29: 2718-21.

14.   Suzuki A, Higuchi WI, Ho NFH. Theoretical Model Studies of Drug Absorption and Transport in Gastrointestinal Tract .1. *J Pharm Sci* 1970; 59: 644-51. DOI: 10.1002/jps.2600590514

15.   Ingram T, Richter U, Mehling T, Smirnova I. Modelling of pH dependent n-octanol/water partition coefficients of ionizable pharmaceuticals. *Fluid Phase Equilibr* 2011; 305: 197-203. DOI: 10.1016/J.Fluid.2011.04.006

16.   Hayduk W, Laudie H. Prediction of Diffusion-Coefficients for Nonelectrolytes in Dilute Aqueous-Solutions. Aiche J 1974; 20: 611-5. DOI: 10.1002/aic.690200329

17.   Othmer DF, Thakar MS. Correlating Diffusion Coefficients in Liquids. *Ind Eng Chem* 1953; 45: 589-93. DOI: 10.1021/ie50519a036

18.   Korson L, Drosthan.W, Millero FJ. Viscosity of Water at Various Temperatures. *J Phys Chem-Us* 1969; 73: 34-&. DOI: 10.1021/j100721a006

19.   Seki T, Mochida J, Okamoto M et al. Measurement of diffusion coefficients of parabens and steroids in water and 1-octanol. *Chem Pharm Bull* 2003; 51: 734-6.

20.   Vandewaterbeemd JTM, Vanboekel CCA, Desevaux RLF et al. Transport in Qsar-IV - the Interfacial Drug Transfer Model - Relationships between Partition-Coefficients and Rate Constants of Drug Partitioning. *Pharm Weekblad* 1981; 3: 224-5.

21.   Yalkowsky SH, Valvani SC, Roseman TJ. Solubility and Partitioning .6. Octanol Solubility and Octanol-Water Partition-Coefficients. *J Pharm Sci* 1983; 72: 866-70.

22.   Pinsuwan S, Li A, Yalkowsky SH. Correlation of Octanol Water Solubility Ratios and Partition-Coefficients. *J Chem Eng Data* 1995; 40: 623-6. DOI: 10.1021/je00019a019

23. Sangster J. Octanol-Water Partition Coefficients: Fundamentals and Physical Chemistry: John Wiley & Sons Ltd. 1997.

24. Mannhold R, Poda GI, Ostermann C, Tetko IV. Calculation of Molecular Lipophilicity: State-of-the-Art and Comparison of Log P Methods on More Than 96,000 Compounds. *J Pharm Sci* 2009; 98: 861-93. DOI: 10.1002/Jps.21494

25. Hidalgo IJ, Hillgren KM, Grass GM, Borchardt RT. Characterization of the Unstirred Water Layer in Caco-2 Cell Monolayers Using a Novel Diffusion Apparatus. *Pharm Res* 1991; 8: 222-7. DOI: 10.1023/A:1015848205447

26. ChemAxon L. MarvinSketch 5.6.0.1. MarvinSketch 5.6.0.1 ed 2011.

27. Yazdanian M, Glynn SL, Wright JL, Hawi A. Correlating partitioning and Caco-2 cell permeability of structurally diverse small molecular weight compounds. *Pharm Res* 1998; 15: 1490-4. DOI: 10.1023/A:1011930411574

28. Schiller C, Frohlich C, Giessmann T et al. Intestinal fluid volumes and transit of dosage forms as assessed by magnetic resonance imaging. *Aliment Pharmacol Ther* 2005; 22: 971-9. DOI: 10.1111/j.1365-2036.2005.02683.x

29. Linnankoski J, Ranta VP, Yliperttula M, Urtti A. Passive oral drug absorption can be predicted more reliably by experimental than computational models - Fact or myth. *Eur J Pharm Sci* 2008; 34: 129-39. DOI: 10.1016/J.Ejps.2008.03.001

30. Simulations Plus Admet Predictor version 5.5. 2011.

31. Sugano K. Theoretical investigation of passive intestinal membrane permeability using Monte Carlo method to generate drug-like molecule population. *Int J Pharm* 2009; 373: 55-61. DOI: 10.1016/J.Ijpharm.2009.02.002

32. Winiwarter S, Ax F, Lennernas H et al. Hydrogen bonding descriptors in the prediction of human in vivo intestinal permeability. *J Mol Graph Model* 2003; 21: 273-87. DOI: 10.1016/S1093-3263(02)00163-8

33. Takagi T, Ramachandran C, Bermejo M et al. A provisional biopharmaceutical classification of the top 200 oral drug products in the United States, Great Britain, Spain, and Japan. *Mol Pharmaceut* 2006; 3: 631-43. DOI: 10.1021/Mp0600182

34. Dahan A, Miller JM, Hilfinger JM et al. High-Permeability Criterion for BCS Classification: Segmental/pH Dependent Permeability Considerations. *Mol Pharmaceut* 2010; 7: 1827-34. DOI: 10.1021/Mp100175a

35. Potthast H, Dressman JB, Junginger HE et al. Biowaiver monographs for immediate release solid oral dosage forms: Ibuprofen. *J Pharm Sci* 2005; 94: 2121-31. DOI: 10.1002/Jps.20444

36. Linnankoski J, Makela JM, Ranta VP et al. Computational prediction of oral drug absorption based on absorption rate constants in humans. *J Med Chem* 2006; 49: 3674-81. DOI: 10.1021/Jm051231p

37. Sugano K. Computational Oral Absorption Simulation for Low-Solubility Compounds. *Chem Biodivers* 2009; 6: 2014-29.

38. Moya SE, Schulz PC. The aggregation of the sodium dodecyl sulfate n-octanol water system at low concentration. *Colloid Polym Sci* 1999; 277: 735-42.

39. Dubey N. Micellar Properties and Related Thermodynamic Parameters of Aqueous Anionic Surfactants in the Presence of Monohydric Alcohols. *J Chem Eng Data* 2011; 56: 3291-300. DOI: 10.1021/Je101358p

40. Levis KA, Lane ME, Corrigan OI. Effect of buffer media composition on the solubility and effective permeability coefficient of ibuprofen. *Int J Pharm* 2003; 253: 49-59. DOI: 10.1016/S0378-5173(02)00645-2

41. Avdeef A, Voloboy D, Foreman A. Dissolution and Solubility. Amsterdam: Elsevier 2007.

Chapter 3

Dissolution of spherical particles of ionizable weak acids into low buffer capacity buffers

Abstract

In vitro and *in silico* methods for predicting *in vivo* dissolution rates are often carried out under high buffer capacity and low drug saturation conditions. However, a review of the literature suggests low buffer capacities in the fasted human and canine gastrointestinal fluids. Depending upon properties such as the administered dose and intestinal permeation rate, concentration of an ionizable, acidic drug in a low buffer capacity fluid may be high enough to decrease fluid pH, which in turn can decrease dissolution rate. A mechanistic transport model was developed to understand the rate and extent of dissolution of spherical particles of a weak acid dissolving in low buffer capacity buffers under moderate-to-high drug saturation conditions, taking into account changes in pH at the particle surface and in the bulk dissolution medium. Convective diffusion with instantaneous chemical reaction was assumed to occur radially across a hydrodynamic boundary layer adjacent to the particle surface.

Experiments in a USP 2 apparatus were conducted using two different particle sizes and three different doses of the BCS 2 weak acid, Ibuprofen, under a physiological range of pH and buffer concentration. The transport model successfully predicted percent of dose dissolved and change in bulk pH as a function of time for all conditions tested, using both the Hintz and Johnson approach (with a critical particle radius of twenty micrometers) and a fluid dynamics theory approach of estimating the relationship between effective boundary layer thickness and particle radius. Dissolution rate of Ibuprofen was

98

influenced by both drug properties (particle size and dose) as well as fluid properties (pH and buffer concentration), underscoring the importance of evaluating dissolution of a weak acid using physiological buffer systems.

Success of the mechanistic transport model in predicting dissolution rate of Ibuprofen in a USP 2 apparatus *in vitro* lends credibility to its use in predicting dissolution rate of a number of different weak acids with a range of drug properties (e.g. intrinsic solubility, pK_a, particle size and dose), dissolving in a range of different physiological buffer conditions (e.g. concentration, pH and species) in physiological dissolution apparatuses. Factors such as deviation of particle shape from sphericity, and the relationship between effective boundary layer thickness and particle radius under different hydrodynamic conditions should be investigated.

Introduction

Numerous approaches describing dissolution rate of solid particles exist in the literature, many of which are derived from the Nernst-Brunner model, which assumes a hydrodynamic boundary layer adjacent to the surface of the drug particle across which the dissolved drug must diffuse before reaching the bulk solution. These models differ in terms of assumptions, including those regarding the effective boundary layer thickness relative to the radius of the dissolving particle, and whether or not they are applicable for dissolution in buffered versus non-buffered medium [1], [2].

Stella and coworkers derived a model describing dissolution of an ionizable weak acid into a high buffer capacity buffer under low percent drug saturation conditions in a rotating disk apparatus (planar surface) [3]. Later, Ozturk and coworkers refined this approach by converting the equations to spherical coordinates and modifying the boundary conditions to allow for an analytical solution of the differential equations governing the underlying processes of diffusion and chemical reaction [4]. However, both transport analyses assume that the buffer capacity is high enough such that the pH values

and relative concentrations of buffer species at the surface of the particle and in the bulk solution are constant as a function of time. This approach is sufficient for calculating dissolution rates using high buffer capacities under so called "sink-conditions", for which concentration of drug in solution at the surface of the particle is much larger than the concentration of drug dissolved in the bulk solution. However, this approach is not accurate in cases where a large dose of an acidic drug is dissolving into a buffer with a low buffer capacity. In these cases, as the drug dissolves and diffuses into the bulk solution, the pH in the bulk and at the particle surface decrease, decreasing the driving-force for dissolution to a greater extent than would be predicted if bulk and surface pH were assumed to be constant with time.

The current analysis presents a method for calculating the dissolution rate and extent of dissolution of polydisperse spherical drug particles of a weak acid dissolving into a low capacity buffer, using physical parameters that are defined by the experimental set-up or can be measured or estimated *a priori*. The effectiveness of the method to predict results *in vitro* is shown experimentally in a USP 2 apparatus using the BCS 2 model compound Ibuprofen under a range of buffer concentrations, pH values and doses. With careful consideration, this method can be used to predict the rate and extent of dissolution in a number of *in vitro* dissolution apparatuses and can be extended to predictions of dissolution rate in the gastrointestinal tract *in vivo*, for which buffer capacity is expected to be low.

Materials and Methods

Mechanistic transport model

The kinetics of dissolution of solid drug particles into buffered medium is described using the theory of mass transfer with chemical reaction. For ionizable drugs in buffered solutions, pH at the drug particle is not necessarily equal to the bulk pH. The pH at the particle surface is a function of the relative concentrations and pK_a values of the drug and buffer species at the surface of the particle. Stella

and coworkers derived a method to estimate pH at the surface of a dissolving solid ionizable drug in a buffered solution in a rotating disk apparatus (planar surface) [3]. In the present analysis the method of Ozturk and coworkers was used to determine the pH and flux of drug at the surface of spherical drug particles [4]. Simplifying assumptions include the following.

1. Particles approximate spheres
2. Net flux of drug occurs in the radial direction across a hydrodynamically controlled boundary layer around each solid particle
3. Chemical reactions are instantaneous and reversible
4. Instantaneous concentration profile across each boundary layer resembles a steady state (pseudo-steady-state approximation)
5. Bulk aqueous medium behaves as ideal solution, and is well mixed with no concentration gradients
6. Solid/liquid interface at particle surface is open only to non-ionized drug
7. Relatively little water infiltration into the solid drug occurs
8. Diffusion coefficients in the aqueous medium are not concentration dependent

Flux of non-ionized drug from the solid spherical particle surface, J_{HA}, is given in **Equation 3.1**, where D_{HA} is the diffusion coefficient of non-ionized drug, h_{eff} is the effective boundary layer thickness around the solid particle, and r is the radius of the solid drug particle. The "dynamic total concentration of drug," at the particle surface, $[HA]_{T,s}$, and in the bulk, $[HA]_{T,b}$, are defined in **Equations 3.2 and 3.3**, respectively, where γ_{HA} is equal to D_A/D_{HA} [4]. In the present analysis D_{A-} and D_{HA} are assumed to be equal, so $[HA]_T$ is simply the sum of the concentrations of non-ionized and ionized drug species. For this analysis, $[HA]_{T,s}$ will be referred to as C_s, and $[HA]_{T,b}$ will be referred to as C_b. **Equation 3.4** describes the dissolution flux in terms of the mass transfer coefficient, k_d, where $k_d = D_{HA}/h (1 + h_{eff}/r)$ and assumes γ_{HA} is equal to one.

(3.1) $\quad J_{HA} = D_{HA}/h_{eff} (1 + h_{eff}/r) ([HA]_{T,s} - [HA]_{T,b})$

(3.2) $[HA]_{T,s} = [HA]_s + \gamma_{HA}[A^-]_s$

(3.3) $[HA]_{T,b} = [HA]_b + \gamma_{HA}[A^-]_b$

(3.4) $J_{HA} = k_d (C_b - C_s)$

The dissolution rate, dM_d/dt, is a product of the dissolution flux and the surface area, A, of the drug particles, and is given in **Equations 3.5-3.10**, where M_T is the dose, ρ_p is the true particle density, N is the total number of drug particles, and $V_{p,o}$ is the initial volume of a single drug particle, $M_{p,t}$ is the mass of a single particle, and $M_{u,t}$ is the total mass of non-dissolved drug [1]. As designated by the subscript "t", the values of many of the variables can change with time as the particles dissolve, including the surface area between the solid drug particles and the buffered medium, A_t, the effective boundary layer thickness, $h_{eff,t}$, the particle radius, r_t, and the concentrations of drug in solution at the particle surface and in the bulk medium, $C_{s,t}$ and $C_{b,t}$, respectively.

(3.5) $dM_{d,t}/dt = A_t J_{HA,t} = 4\pi\, r_{,t}^{\,2}\, N\, D_{HA}/\, h_{eff,t}\, (1 + h_{eff,t}\,/r_{,t}\,)\, (C_{s,t} - C_{b,t})$

(3.6) $A_{,t} = 4\pi\, r_{,t}^{\,2}\, N$

(3.7) $N = M_T / (V_{p,o}\, \rho_p)$

(3.8) $V_{p,o} = 4/3\, \pi\, r_{,o}^{\,3}$

(3.9) $M_{p,t} = M_{u,t}/N$

(3.10) $r_{,t} = (3\, M_{p,t} / (\rho_p\, 4\, \pi)\,)^{1/3}$

Ozturk and coworkers give an equation for calculating the pH at the surface of a drug particle dissolving in a diprotic buffer. The equation is a function of the diffusion coefficients of drug and buffer species in solution (D_{HA}, D_A, D_{HB}, D_B, D_{OH}, D_H), concentrations of drug and buffer species in solution, and ionization rate constants (K_A, $K_{A,B}$, K_w) (not reproduced here)[1]. This equation is used in the current analysis to determine particle surface pH, pH_s. In the analyses by Ozturk and coworkers and Mooney and coworkers pH_s and therefore C_s is assumed to be constant as a function of time. This assumption holds in their analyses because the buffer capacity of the buffer is assumed to be high enough to maintain a constant bulk pH, pH_b, and C_b is assumed to be a lot lower than C_s, such that so called "sink conditions" hold, and C_b is assumed to be equal to zero. Therefore, the relative concentrations of buffer species in the bulk and at the surface of the particle are constant as the particle dissolves. An improvement of the current analysis over those of Ozturk and coworkers or Mooney and coworkers is that pH_s, pH_b, $C_{s,t}$ and $C_{b,t}$ are not assumed to be constant as a function of time. Instead, proton balance equations are written to determine the relative concentrations of drug and buffer species, and corresponding pH values in the bulk and at the surface as a function of time as the drug dissolves and diffuses into the bulk solution [5].

The approach of Hintz and Johnson was used to determine the value of h_{eff} as a function of time [6]. With this method it is assumed that $h_{eff,t}$ is equal to the critical particle radius, h_c, when particle radius, $r_{,t}$, is greater than or equal to h_c, but equal to $r_{,t}$ when $r_{,t}$ is less than h_c, as written out in **Equation 3.11**. Another method for determining $h_{eff,t}$ based on Fluid Dynamics (FD) Theory is discussed later and compared with the Hintz and Johnson approach.

(3.11) $h_{eff,t} = h_c$ when $r_{,t} \geq h_c$ & $h_{eff,t} = r_{,t}$ when $r_{,t} < h_c$

---

[1] Omission of a negative sign in the equation for θ (used in surface pH calculation) was noted and corrected. The correct equation is $\theta = \cos^{-1}(R/\sqrt{-Q^3})$

The dissolution rate and change in the variables discussed above can be calculated using an iterative process, which can be expedited by writing a script in a program such as MATLAB®. The following steps can be conducted and quantities can be determined over small time increments (such as 1 s).

For time = 0 s (before drug begins dissolving)
1. Let $r_{,t} = r_o$ and calculate $h_{eff,t}$ (**Equation 3.11**)
2. Calculate N based on M_T and r_o (**Equation 3.7**)
3. Calculate pH_b and concentrations of buffer species in the bulk solution (before drug is added) using proton balance equations

For time > 0s
4. Calculate pH_s and $C_{s,t}$ at the surface of the drug particles
5. Calculate mass dissolved (**Equation 3.5)** and $\Delta t = 1s$ (Let $C_{b,t}$ equal 0 for the first iteration)
6. Calculate the new particle mass, $M_{p,t}$, and radius, $r_{,t}$ (**Equations 3.9 and 3.10**)
7. Calculate the new value of $h_{eff,t}$ using $r_{,t}$ and h_c
8. Calculate bulk pH and bulk concentrations of buffer species using proton balance equations
9. Repeat steps 4 through 8 until $(C_{s,t} - C_{b,t}) = 0$ or $r_{,t} = 0$

Drug and buffer properties

Ibuprofen was chosen as the model compound for this study. It is a non-steroidal anti-inflammatory drug (NSAID) widely used for the treatment of mild to moderate pain. It is characterized as a Biopharmaceutics Classification System (BCS) 2 weak acid [7]. Shaw and coworkers as well as Levis and coworkers reported an intrinsic solubility of about 0.067 mg/ml and apparent pK_a of about 4.4 at 37 °C. Ibuprofen is mostly unionized and thus has a low solubility at low pH, but is 98-99.9% ionized under typical fasted intestinal (pH range of about 6-7.5) with an expected 50-1,000-fold increase in solubility. Additional Ibuprofen properties of aqueous diffusion coefficient and true density were calculated using

established methods or taken from the results of measurements reported in the literature and are included in **Table 3.1**.

Sodium phosphate was chosen as the buffer for the *in vitro* experiments. Within the pH range tested, phosphate buffer can be considered monoprotic, and the ionization reaction between dihydrogen phosphate and hydrogen phosphate can be considered instantaneous, which is an assumption used in the current transport analysis. Phosphate buffer is used extensively in dissolution testing because of its ease of preparation, lack of appreciable absorption in the UV spectrum making UV analysis of the drug substance straightforward, and because it has a pK_a within the physiological range, giving it a potentially high buffer capacity at reasonable buffer concentrations (e.g. 50 mM). Buffer properties relevant to the dissolution analysis include the aqueous diffusion coefficients of the hydrogen phosphate ion, dihydrogen phosphate ion, hydroxide ion and hydronium ion, as well as the pK_a of the dissociation of dihydrogen phosphate to hydrogen phosphate. These values were taken from the literature and included in **Table 3.1** [8]. The initial buffer capacity (in absence of drug species) for each experiment was calculated using **Equation 3.12.**

(3.12) $\beta = 2.3\ ([BH]+[B])\ (K_{a,b}\ [H_3O^+])/(K_{a,b} + [H_3O^+])^2$

Materials

The free acid form of Ibuprofen drug powder was purchased commercially. All additional chemicals were of analytical grade or purer and were purchased commercially.

Preparation of sieve cuts & particle size analysis

To obtain the desired particle size of Ibuprofen, bulk Ibuprofen was blended with 0.5% colloidal silicon dioxide in a V-blender to facilitate flowability of Ibuprofen through and recovery from the mesh screens. 10 g of the blend was added to the top of a stack of 3-inch diameter screens with a range of mesh sizes that were then placed in an ATM Sonic Sifter and pulsed for at least 5-minute

increments at a pulse amplitude of 8. The percentage of drug on each screen was determined after each pulsing increment and the sieves were again placed in the sonic sifter and pulsed for again until the percentage change of mass of drug recovered on each sieve was no more than 5%. The sieve cuts from the 63-75 and 212-250 mesh screens were selected for use in the dissolution experiments.

The particle size distributions of the 63-75 and 212-250 mesh sieve cuts of Ibuprofen were determined using microscopy. Particles were visualized using a Nikon OPTI-PHOT – POL optical microscope with SPOT Insight color camera model 3.2.0 and SPOT 5.1 Advanced Imaging software (SPOT Imaging Solutions, Sterling Heights, MI). The widths, lengths and thicknesses of about 10-15 particles from each sieve cut were determined and a mean thickness-to-width ratio was calculated for each sieve cut. The maximum lengths and widths of about 300 randomly selected particles from each sieve cut were then determined. The mean thickness-to-width ratio determined using the 10-15 particles was used to estimate the thicknesses of the ~300 particles for which width and length values were determined. The volume of each particle, V_p, was calculated by calculating the product of the length, width and thickness. The equivalent spherical diameter, ESD, of each particle was calculated using **Equation 3.13**. The mass of each particle was determined by multiplying the true density (1.1 g/cm^3 [9]) by V_p. The D50 (median) and D90 ESD by mass were determined by finding the ESD of the particles with a mass at the 50th and 90th percentiles, respectively, of the total mass of the ~300 particles. The value of D90/D50 for each sieve cut was calculated as a means of assessing the breadth of the size distributions.

(3.13) $\mathrm{ESD} = (3/2\ V_p\ \pi)^{\frac{1}{3}}$

In Vitro dissolution experiments

In vitro dissolution experiments were performed to test the validity of the model. All experiments were performed in a 1-L USP jacketed dissolution vessel

with a hemispherical bottom (10.1 cm diameter) using a standard USP 2 paddle (7.5 cm diameter). The bottom of the paddle was positioned approximately 2 mm from the bottom of the vessel. All experiments were conducted in 200 ml of buffer stirred at 50 rpm and heated to 37.0 ± 0.2 °C using an external water bath. Phosphate buffers of the appropriate pH and concentration were prepared using appropriate amounts of sodium phosphate monobasic monohydrate and sodium hydroxide. The required amount of sodium chloride was added to each buffer to reach a calculated ionic strength of 0.154 ± 0.005 M. Final pH at 37 °C as measured using an Accumet Research™ AR60 pH meter and pH probe (ThermoFisher Scientific, Inc., Waltham, MA) was adjusted to the desired value with 1 N HCl or 2 N NaOH. The buffer solution was then deaerated under vacuum for 30-60 minutes. The experimental conditions of initial buffer pH, buffer concentration, initial buffer capacity, Ibuprofen particle size and dose are specified in **Table 3.2**. Buffer pH chosen was in the range of typical values in the upper small intestine of humans and dogs in the fasted state (Chapter 1 and 4), and buffer concentration was chosen in the range of values documented in the fasted state (10 mM) to those typically used in conventional dissolution studies (50 mM) (Chapter 1). Each condition was performed in duplicate.

For each experiment 200 ml of buffer was added to the dissolution vessel and stirred for 20-30 minutes. Actual buffer temperature was measured with a thermometer to ensure the buffer had reached 37.0 ± 0.2 °C. Next, the desired mass of drug particles was added directly to the dissolution vessel. Ultraviolet (UV) absorbance of Ibuprofen in solution was measured using a StellarNet BLACK-Comet concave grating spectrometer with SL5 light source and 300-micron transmission dip probe with a 10-mm pathlength tip (StellarNet Inc., Tampa, FL) at a wavelength of 272 nm at regular time intervals. Absorbance values were correlated to concentration of Ibuprofen in solution using a standard curve developed using solutions with known Ibuprofen concentrations. The bulk pH of the solution was also recorded at regular intervals. Each experiment was concluded once one hundred percent of the dose had dissolved.

Data analysis

Predictions of percent of the dose dissolved versus time as well as bulk pH versus time for each experimental condition were made using the theoretical dissolution analysis using the parameters specified in **Table 3.1**, along with values for initial median particle radius, dose, bulk pH and total buffer concentration provided in **Table 3.2**. Each parameter remained fixed expect for h_c. Theoretical percent of dose dissolved versus time and bulk pH versus time were compared with experimental results for each condition. The value of h_c that appeared to describe the experimental data best for all of the combined experimental conditions was selected as the best fit value describing the hydrodynamic conditions in the *in vitro* dissolution vessel.

Results

Particle size distributions

The particle size distributions of the two different particle size sieve cuts of Ibuprofen are shown in **Figure 3.1** and particle characteristics of the two sieve cuts are shown in **Table 3.3.** The median particle diameters of the small and large particle size sieve cuts were 87 μm, and 330 μm, respectively. Particles were lath shaped, and particle size distributions were very narrow as suggested by the D90/D50 values of 1.2 for both sieve cuts.

In vitro experiments and transport model predictions

Results of the *in vitro* experiments together with predictions from the transport analysis are shown in **Figures 3.2-3.5**. The value of h_c that best described the change in effective boundary layer thickness for all of the experiments was 20 μm. Experimental values for average time to reach twenty-five percent dissolved, $t_{25\%}$, fifty percent dissolved, $t_{50\%}$ and seventy-five percent dissolved, $t_{75\%}$, for each experimental condition are included in **Table 3.4**. Theoretical values for change in pH at the particle surface, change in pH in the bulk medium, percent drug saturation in the bulk medium and initial dissolution

rate are included in **Table 3.5**. Buffer component concentrations and properties are included in **Table 3.6**.

Discussion

In vitro experiments and transport model predictions

The transport model described the experimental data well, particularly for the first 75-90% of the dose dissolved. For the experiment conducted with 100 mg of the 87-µm median diameter particles dissolving in pH 6, 20 mM phosphate, dissolution rate was over-predicted by the model for about the last 25% of the dose. However, for all other experiments, dissolution rate was predicted well for at least the first 90% of the dose dissolved. Deviation from experimental values near the end of the dissolution process could be explained by possible particle agglomeration, leading to a decreased total surface area for dissolution. Evaluating the transport model assuming a polydisperse particle size distribution, with each sieve cut described using five particle size bins, had a negligible effect on the predictions, and did not explain the slower dissolution rate of particles toward the end of the experiments. Deviations of predictions from experimental values could also be due to the non-spherical shape of Ibuprofen, which is the assumed geometry in the analysis. The median diameter chosen for determining the predicted dissolution rate was the ESD, based on the volume of an equivalent sphere. In actuality, Ibuprofen particles are lath-shaped, with a surface-area-to-volume ratio of 1.2 cm^{-1}. The equivalent spherical diameter based on the surface area, rather than the volume, of an equivalent sphere is 104.4 µm. Use of this diameter may be more appropriate for calculation of the total surface area available for dissolution as a function of time, which, holding all other parameters constant, should have the effect of increasing the predicted dissolution rate. Since the predicted rates using the ESD based on volume were adequate for this analysis, the transport model was not modified to include a factor to correct for deviation from spherical geometry.

109

Results of the *in vitro* dissolution experiments demonstrated the influence of particle size, buffer concentration, dose and pH on dissolution rate of Ibuprofen particles dissolving into 200 ml of aqueous buffer. Influence of particle size on dissolution rate is shown in **Figure 3.2** (dissolution into pH 7 10 mM buffer) and **Figure 3.3** (dissolution into pH 6 50 mM buffer) and in **Table 3.4**. Under both conditions, the particles with the smaller diameter dissolve faster than the particles of the larger diameter, due to the increase in the number of particles at a given mass, and therefore the increase in surface area for dissolution. For Ibuprofen dissolving in pH 6 50 mM buffer there is roughly a four-fold increase in $t_{25\%}$, $t_{50\%}$ and $t_{75\%}$ for the larger compared to the smaller particles. For Ibuprofen dissolving in pH 7, 10 mM buffer there is roughly a five-fold increase in $t_{25\%}$, but a six-fold increase in $t_{50\%}$ and $t_{75\%}$ for the larger compared to the smaller particles. If the same two sets of experiments had been conducted in a large enough volume of medium to maintain sink conditions, then a consistent five-fold increase in $t_{25\%}$, $t_{50\%}$ and $t_{75\%}$ for the larger compared to the smaller particles would have theoretically occurred in both cases. A five-fold increase is the expected increase based on the ratio of the theoretical initial dissolution rates shown in **Table 3.5**, and represents the theoretical change in dissolution rate based on particle size alone. For the experiments discussed above, dissolution rate was also a function of the difference between C_s and C_b, which changed as the particle dissolved.

The effect of buffer concentration on dissolution rate was demonstrated experimentally by comparing dissolution rates of the smaller particles dissolving in pH 6, 50 mM buffer as shown in **Figure 3.3,** and pH 6, 20 mM buffer as shown in **Figure 3.4** (experiments 1 and 3 in **Tables 3.4 and 3.5**). The particles dissolved faster in the 50 mM buffer compared to the 20 mM buffer, with roughly a 2-fold increase in $t_{25\%}$, $t_{50\%}$ and $t_{75\%}$ for the particles dissolving in the 20 mM versus the 50 mM buffer. The decrease in dissolution rate of the particles dissolving in the buffer with lower buffer concentration is due to the lower pH at the particle surface for those particles. The lower buffer concentration in the bulk leads to lower buffer concentration at the particle surface resulting in a lower

buffer capacity at the surface. Therefore, as drug dissolves the pH at the particle surface is lowered to a greater extent in the lower buffer capacity buffer. As a result, the drug solubility at the surface is lower and therefore the concentration at the surface, C_s, is lower as well. The theoretical initial particle surface pH is 5.7 for the 50 mM buffer, but only 5.5 for the 20 mM buffer, resulting in an initial C_s of 1.4 mg/ml, versus an initial C_s of 0.9 mg/ml, respectively. Tsume and coworkers also demonstrated the effect of buffer concentration on dissolution performance of commercial Ibuprofen tablets [10]. They noted a decrease in dissolution rate at a pH of 6.8 in 10 compared to 50 mM phosphate buffer, and a decrease in both the rate and the extent of dissolution at a pH of 6.0 in 10 compared to a 50 mM phosphate buffer.

The effect of dose is evident by comparing 100 mg of the smaller particles dissolving in pH 6 20 mM buffer, as shown in **Figure 3.3** versus 50 mg of the smaller particles dissolving in the same buffer, as shown in **Figure 3.4** (experiments 3 and 4 in **Tables 3.4 and 3.5**). The values of $t_{25\%}$ and $t_{50\%}$ are equal between the two experiments, whereas there is a 1.2-fold increase in $t_{75\%}$ for the higher compared to the lower dose. Due to the same buffer conditions and initial particle size, fluxes are initially equal. However, as the particles dissolve the value of C_b increases to a higher extent for the higher dose, leading to a smaller value of $C_s - C_b$ and therefore a smaller flux as a function of time.

While no two sets of experiments differed by pH alone, the affect of initial pH on dissolution rate can be explained in terms of its affect on the pH at the particle surface. For Ibuprofen a higher pH in the bulk medium would lead to a higher pH at the particle surface, and thus a higher drug saturation solubility at the surface. The higher saturation solubility would increase the value of C_s and therefore the flux of drug. Tsume and coworkers also demonstrated a decrease in rate and extent of dissolution when conducting experiments in a pH 6.0 compared to a pH 6.8 phosphate buffer at two different buffer concentrations (10 mM and 50 mM) [10].

Effective boundary layer thickness estimation

The value of h_c used in the transport model that best describes the experimental results for all conditions tested is 20 µm. This value of h_c also described the experimental data well for a low dose (4 mg) of three different particle size sieve cuts of Ibuprofen (median diameters ranging from 87 – 330 µm) dissolving in 200 ml of 50 mM pH 5.8 sodium phosphate buffer [11]. It should be noted that the value of h_{eff} remains equal to 20 µm for the first 90% of the dissolved dose for the 87-µm particles and for 99.8% of the dissolved dose for the 330-µm particles, since r does not drop below h_c until that amount of the dose has dissolved. Therefore, for median particle diameters greater than about 87 µm, choosing a constant value of h_{eff} in the transport model gives virtually analogous results to the more complicated method of calculating h_{eff} based on the relationship between r and h_c. A value for h_c of 20 µm is in line with experiments conducted by other researchers. A value for h_c of 30 µm was initially suggested by Hintz and Johnson based on experiments in a rotating disk apparatus, and was later estimated to be about 14-18 µm based on ~ 50-µm diameter hydrocortisone particles dissolving in 900 ml of buffer in a USP 2 apparatus at 75 rpm, assuming spherical particles [12].

Another means of estimating h_{eff}, which is a more complex, but perhaps more realistic approach, is based upon Fluid Dynamics (FD) theory. The value of h_{eff} can be calculated according to **Equations 3.14-3.17**, where d_p is particle diameter, Sh is Sherwood number, Rep is particle Reynold's number, Sc is Schmidt number, $V_{rel,tot}$ is total relative velocity of the particle, and v is kinematic viscosity [13]. Different relationships between Sh, Re_p and Sc have been suggested in the literature. **Equation 3.15** is a semi-empirical approximation developed by Ranz and Marshall, which is often used for spherical particles.

(3.14) $h_{eff} = d_p / Sh$

(3.15) $Sh = 2 + 0.6 \, Re_p^{1/2} \, Sc^{1/3}$

(3.16) $Re_p = d_p V_{rel,tot} / v$

(3.17) $Sc = v / D_{HA}$

All parameters in **Equations 3.14-3.17** are relatively well defined, with the exception of $V_{rel,tot}$. Sugano suggests calculating $V_{rel,tot}$ using **Equation 3.18**, where v_t is the terminal (sedimentation) slip velocity, and v_{me} is the relative effective velocity between particles and microeddies. The value of v_t can be calculated using **Equation 3.19** when Re_p is less than 0.3, or **Equations 3.20-3.21** when Re_p is greater than 0.3, where g is the gravitational constant, μ is the dynamic viscosity of the fluid. For spherical particles under $0.3 < Re_p < 100$, A=20.5, B=0.310 and m=2.07, based on fitting to experimental data [14]. The value of v_{me} can be calculated using **Equation 3.22**, where ε is the power input per unit mass. An expression for ε is shown in **Equation 3.23**, where PN is the power number specific to the paddle shape, N_{paddle} is rotational speed, D_{paddle} is paddle diameter, and V_{fluid} is fluid volume. The value of ε was shown to be 0.004 m^2/s^3 for 1 L of fluid stirred at 50 rpm [15]. To account for different fluid volumes, this value could be multiplied by the quotient of 1000 cm^3 times the relevant volume in cm^3.

(3.18) $v_{rel,tot} = \sqrt{(v_t^2 + v_{me}^2)}$

(3.19) $v_t = (\rho_p - \rho_f) d_p^2 g/ (18\mu)$ for $Re_p < 0.3$

(3.20) $v_t = v/d_p (\sqrt{((1/4) (A/B)^{2/m} + (4/3 d_{p*}^3/B)^{1/m})} - \frac{1}{2}(A/B)^{1/m})^m$ for $Re_p > 0.3$

(3.21) $d_{p*} = ((\rho_p/\rho_f - 1) g(1/v)^2)^{1/3} d_p$

(3.22) $v_{me} = 0.195 d_p^{1.1} \varepsilon^{0.525} \mu^{-0.575}$

(3.23) $\varepsilon = PN \rho_f N_{paddle}^3 D_{paddle}^5 / V_{fluid}$

The theoretical values of h_{eff} as a function of r calculated according to the current approach (Hintz and Johnson), where h_c = 20 μm, is compared with the values determined using FD theory in **Figure 3.6**. Values of the constants used for the FD theory calculations are shown in **Table 3.7**. Values of h_{eff} for the two approaches are approximately equal up to a radius of 5 μm, whereas h_{eff} values for a given radius are smaller using FD theory compared to the Hintz and Johnson approach when r is greater than about 5 μm. The FD theory approach leads to a maximum value of h_{eff} of 19 μm for the largest particles. For values of r ranging from 0 to 165 μm, the values for $v_{rel,tot}$ and Re_p range from 0 to 1.5 cm/s and from 0 to 7, respectively. These calculated velocities for the particles themselves fall within plausible values for the fluid in the USP 2 apparatus at 50 rpm, based on recent estimates by Bai and coworkers, who determined velocity profiles in the USP 2 apparatus at different impeller rotational speeds using both Laser Doppler Velocimetry (LDV) and Computational Fluid Dynamics (CFD), results from which were in good agreement [16]. Experiments/simulations were conducted using 1 L of deionized water at 25 °C with the impeller blade at the typical height from the bottom recommended for USP 2 experiments, namely 5 cm. With the exception of directly next to the impeller blade, for which velocities approached those of the impeller tip speed (20 cm/s at 50 rpm), the majority of values for velocity magnitude ranged from 0 to about 12 cm/s, with the majority of values appearing to be in the range of about 5-8 cm/s.

Inputting equations based on FD theory into the transport model to determine h_{eff} leads to very similar predictions for the *in vitro* results. For example, for all experimental conditions, predictions for $t_{50\%}$ the 87-μm particles are within less than one minute of predictions using the Hintz and Johnson approach, with an h_c of 20 μm, with the FD theory approach leading to slightly faster dissolution rates. For the 330-μm particles, predictions based on both methods of predicting h_{eff} are nearly identical. Assuming $v_{rel,tot}$ to be independent of particle size, and instead using values for fluid velocity determined by Bai and coworkers lead to either significant under-prediction of dissolution rate for the larger particle size sieve cut or significant over-prediction of dissolution rate for

the smaller particle size sieve cut. The "best fit" velocity for the smaller size was about 0.08 cm/s, but 1.3 cm/s for the larger size (data not shown).

Another important consideration is that, while selection of an h_c of 20 µm (or use of FD theory with the suggested parameters) seems to be appropriate under the conditions tested, it may not be appropriate using different volumes of buffer, different depths of the USP 2 paddle, or different rotational speeds. An advantage of the FD theory over the Hintz and Johnson method is that it allows for *a priori* calculation of $h_{eff,t}$ for different experimental conditions. However, the accuracy of the resulting predictions for particle dissolution rate under these differing hydrodynamic conditions should be explored.

Prediction of drug dissolution in physiological *in vitro* dissolution apparatuses and the *in vivo* gastrointestinal tract

The ability of the transport model to predict the *in vitro* results lends credibility to use of the analysis to predict the rate and extent of dissolution of Ibuprofen particles using different combinations of properties such as median particle size, buffer pH and concentration, and dose under sink and non-sink conditions. The mechanistic model has also been successful in describing dissolution rate for Ibuprofen particle suspensions (data not shown) as well as rapidly-disintegrating tablets ([11]. While not tested as part of this analysis, predictions could be extended to additional monoprotic acidic drugs, simply by using the appropriate pK_a and solubility in the transport model. Effects of different particle shapes (e.g. non-spherical or non-lathe shaped) should be considered and incorporated into the analysis (e.g. addition of a shape factor). The analysis could also be extended to different monoprotic buffer systems, by changing the pK_a of the buffer in the transport model, as long as the assumption of instantaneous chemical reaction was still appropriate. Extension of the model to the physiological bicarbonate buffer could also be performed, by taking the kinetics of CO_2 hydration into account.

While the current analysis has been presented in the context of drug particles dissolving into a single buffer, of great interest is prediction of drug transport in *in vitro* physiological dissolution apparatuses, such as the two-phase

or two-compartment (e.g. ASD) system. Extension of the transport model for both systems can be fairly simply achieved by considering the major transport steps involved. Chapter 2 of this thesis described transport of drugs in solution from an aqueous to an organic medium. By considering the processes of drug particle dissolution and solute partitioning occurring simultaneously, transport of drug in a two-phase apparatus could be described. In addition, transport of drug in a two-compartment system could be described simply by considering drug particles emptying in a first-order manner into the bulk dissolution medium with the onset of dissolution occurring once the particles have reached the vessel. In Chapter 4, transport of Ibuprofen in a two-phase dissolution apparatus as well as a two-compartment dissolution apparatus is described using these two approaches.

To apply this analysis to prediction of drug dissolution *in vivo*, one must have an understanding of the range of important physiological properties affecting dissolution rate of ionizable weak acids *in vivo*, including buffer species and concentration, pH, ionic strength, aqueous volume and hydrodynamics. Chapter 1 presents average values and ranges for gastrointestinal properties in fasted humans, and Chapter 4 extends this analysis to the fasted canine gastrointestinal tract. The only variables not discussed in these chapters and potentially the least well-defined properties relevant to dissolution in the gastrointestinal tract are those impacting the values of $v_{rel,tot}$. The value of $v_{rel,tot}$ is affected by the value of the resistance coefficient from the fluid, C_D (imbedded in **Equation 3.19**) when Re_p is less than 0.1, which can change the magnitude of v_t by a factor of $C_D^{-0.5}$. When Re_p is greater than 0.3 it is shown to be dependent upon Re_p range and particle shape. The value of $v_{rel,tot}$ is also affected by the value of v_{me}, which is directly proportional to, $\varepsilon^{0.525}$, described in **Equation 3.23** for USP paddle methods. If agitation *in vivo* were comparable to a USP paddle rotational speed of 20-75 rpm, as suggested by Katori and coworkers, as well as Scholz and coworkers, ε would range from 0.0003 to 0.014 m^2/s^3 [17] [18] [13]. A plot of h_{eff} versus r for ε of 0.0003 and 0.014 m^2/s^3, together with h_{eff} versus r for the value of ε selected for the *in vitro* experiments conducted in this study is shown in **Figure 3.7**. Values of h_{eff} for the three different values of ε are nearly

116

identical up to a radius of about 5 μm, and at a radius of 12.5 μm the maximum variation in h_{eff} is only 2 μm. The maximum variation in h_{eff}, which occurs at large particle sizes is about 7 μm. It should be noted that a further decrease in ε, which might be expected to represent potentially less vigorous mixing *in vivo* does not lead to an appreciable increase in the value of h_{eff}. **Figure 3.8** shows the impact of the aforementioned range of ε on dissolution rate. A pH of 6.0 and a buffer concentration of 10 mM were chosen since those conditions would be most discriminating within a pH range of 6-7 and a buffer concentration range of 10-20 mM. Percent of dose dissolved versus time for 100 mg of three different particle sizes (r = 25, 87 and 330 μm) of Ibuprofen in 200 ml of buffer at ε values of 0.0003 and 0.014 m^2/s^3 are included. Values for $t_{50\%}$ for the 25, 87 and 330 μm sizes different by only 0, 2 and 10 min, respectively. These results suggest that for small initial particle size distributions, the value of h_{eff} within the expected range for ε has a negligible effect on dissolution rate, whereas for larger particle sizes the value of ε has a small to moderate effect.

Assuming a value of ε of 0.0003 m^2/s^3 or less to be the most indicative of *in vivo* conditions, it was desired to determine the impact of using the Hintz and Johnson approach with values of h_c ranging from 25-30 μm, as opposed to FD theory on dissolution rate prediction. Using the same conditions as above (100 mg of Ibuprofen in 200 ml pH 6 10 mM phosphate) for the same three initial particle diameters (25, 87 and 330 μm) of Ibuprofen, it was determined that when r_o = 25 μm the three curves were indistinguishable, and when r_o = 87 μm $t_{50\%}$ was 1 min greater when h_c = 25 μm and 2 min greater when h_c = 30 μm compared to FD theory. When r_o = 330 μm, there was a 2 min decrease for h_c of 25 compared to FD theory, and a 5 minute increase for h_c of 30 μm (curves not shown).

Conclusions

A review of the literature suggests low buffer concentrations and corresponding low buffer capacities of fluids in the gastrointestinal tract. Depending on the administered dose as well as the relative rates of major *in vivo*

transport processes for weak acids in the gastrointestinal tract, including emptying from the stomach, dissolution in the intestinal tract and absorption into the intestinal membrane, concentration of dissolved drug in the gastrointestinal fluid may be high enough to decrease pH of the low buffer capacity fluid, which in turn can decrease dissolution rate of a weak acid.

A mechanistic transport model was developed to understand rate and extent of dissolution of spherical particles of a weak acid dissolving in low buffer capacity buffers under moderate drug saturation conditions. Each transport parameter has a physical basis and can be measured or estimated *a priori*. Experiments in a USP 2 apparatus were conducted using two different particle sizes of the BCS 2 weak acid, Ibuprofen, under a range of pH values, buffer concentrations and doses to test the ability of the model to predict *in vitro* dissolution rates. The transport model successfully predicted percent of dose dissolved and change in bulk pH as a function of time for all conditions tested. Dissolution rate of Ibuprofen was influenced by particle size and dose, as well as buffer concentration and initial buffer pH, underscoring the importance of investigating dissolution rate using physiologically relevant fluid properties. While both the Hintz and Johnson and fluid dynamics theory approaches to calculating the relationship between effective boundary layer thickness and particle size lead to similar predictions for dissolution rate, the fluid dynamics theory approach has the advantage of allowing for *a priori* predictions for a range of hydrodynamic conditions.

Success of the mechanistic transport model in predicting dissolution rate of Ibuprofen in a USP 2 apparatus *in vitro* lends credibility to use of the model in predicting dissolution rate of a number of different weak acids dissolving in a range of different buffer conditions (e.g. concentration, pH and species), for a range of drug properties (e.g. intrinsic solubility, pK_a, particle size and dose). However, since deviations from model predictions could occur due to non-spherical particle shapes or non well-defined hydrodynamic conditions, the transport model should also be tested using weak acids with different particle shapes in different aqueous volumes, rotational speeds and or vessel types.

While the model was tested using drug powder it is also applicable to drug particle suspensions as well as rapidly disintegrating tablets and capsules.

In addition to application of this transport model to predict rate and extent of dissolution in single buffer systems, it can also be extended to the physiological two-phase dissolution apparatus and two-compartment (e.g. ASD) apparatus, by incorporating the additional transport steps of partitioning of drug in solution in an organic medium, or first-order emptying of drug particles into the buffer, respectively. Extension of this transport analysis to dissolution in the intestinal tract *in vivo* is also possible, but the same considerations must be made understanding the effects of physiological properties, including the effects of fluid hydrodynamics, on dissolution rate.

Tables and Figures

Table 3.1. Ibuprofen and phosphate buffer physicochemical properties

Ibuprofen property	Value
Molecular mass	206.3 g/mol
Diffusion coefficient in water at 37 °C	7.5×10^{-6} (unionized)[a] 7.6×10^{-6} cm^2/s (ionized)[a]
Intrinsic solubility at 37 °C	0.066 mg/ml[b], 0.068 mg/ml[c]
Apparent pK_a at 37 °C	4.4[b, c] (not corrected for ionic strength)
True density	1.1 g/cm^3 [d]

Buffer property	Value
D_(H_2PO_4)$^-$	11.5×10^{-6} cm^2/s[e]
D_(HPO_4)$^{2-}$	11.5×10^{-6} cm^2/s[e]
D_H_3O^+	104.9×10^{-6} cm^2/s[e]
D_OH$^-$	63×10^{-6} cm^2/s[e]
Apparent pK_a at 37 °C: $H_2PO_4^- \longleftrightarrow HPO_4^{2-} + H_3O^+$	6.8 (pH 7 10 mM), 6.6 (pH 6, 20 & 50 mM)[f]
K_w at 37 °C	2.57×10^{-14} [g]

[a] Calculated using the method of Hayduk and Laudie [19].
[b] Shaw and coworkers based on best-fit curve to pH-solubility profile [20].
[c] Levis and coworkers based on best-fit curve to pH-solubility profile (ionic strength values of buffers ranged from 0.15 to 0.37 M) [21].
[d] Reference [9].
[e] Reference [8]
[f] Based on experiments conducted in our lab (data not shown).
[g] Reference [5]

Table 3.2. Experimental conditions for Ibuprofen particle dissolution experiments. All experiments performed in 200 ml of buffer at 50 rpm and 37 °C

No.	Median particle Diameter (r_o)	Dose (M_T)	Initial bulk pH ($pH_b)_{t=0}$	Total buffer Concentration	Initial buffer capacity[a]
-	μm	mg	-	mM	mM
1	87	200	7	10	5.5
2	330	200	7	10	5.5
3	87	100	6	50	18.5
4	330	100	6	50	18.5
5	87	50	6	20	7.4
6	87	100	6	20	7.4
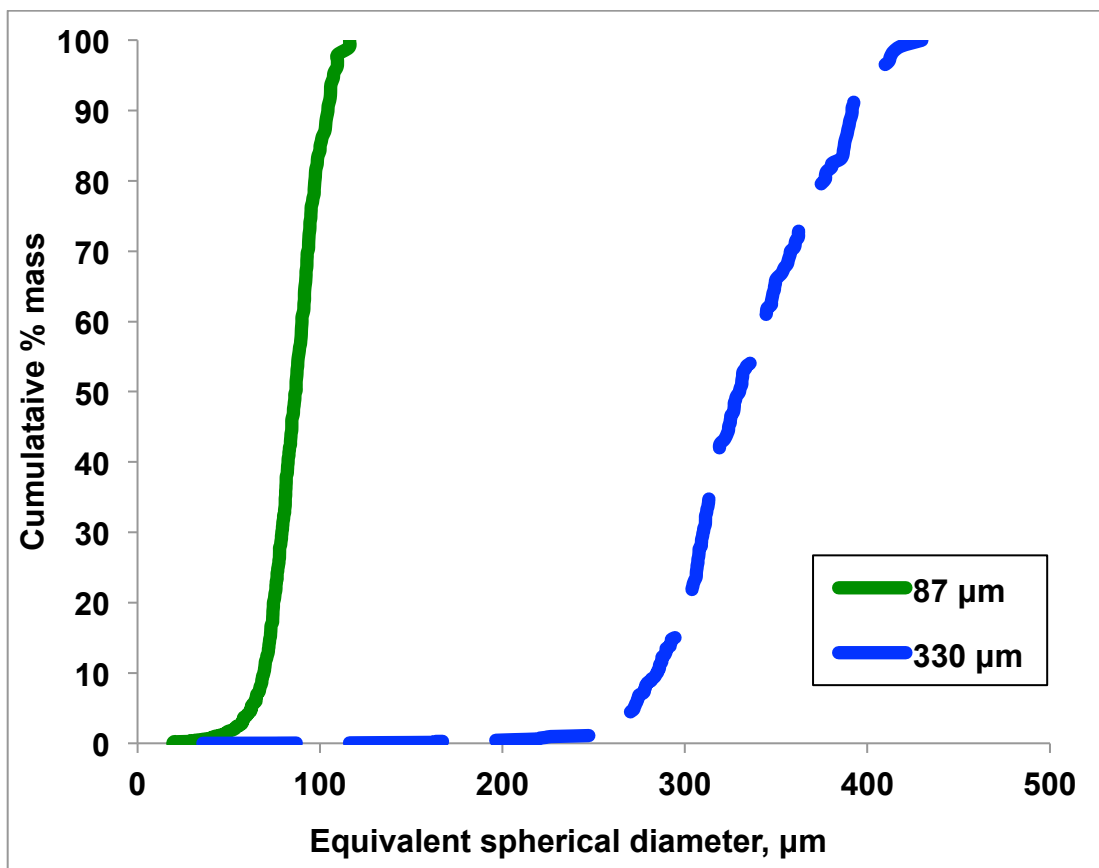
Figure 3.1. Particle size distributions by mass for the 80 and 310 µm median diameter sieve cuts of Ibuprofen determined using microscopy

Table 3.3. Particle characteristics of 87 and 330 µm median diameter sieve cuts of Ibuprofen

Median equivalent spherical diameter by mass	Median L X W X T by mass	Mean Surface-area-to-volume ratio	D90/D50	Mean aspect ratio	Mean thickness-to-width ratio	No. of particles measured
µm	*µm*	*cm⁻¹*	-	-	-	*no.*
87	116 X 73 X 41	1.2	1.2	0.50	0.56	307
330	479 X 294 X 134	1.2	1.2	0.41	0.45	300
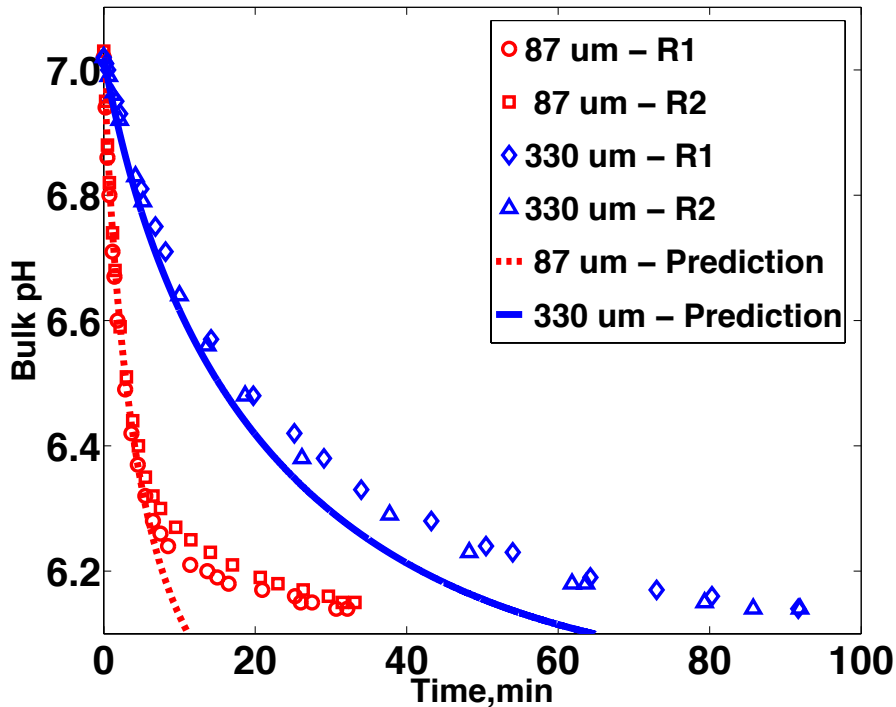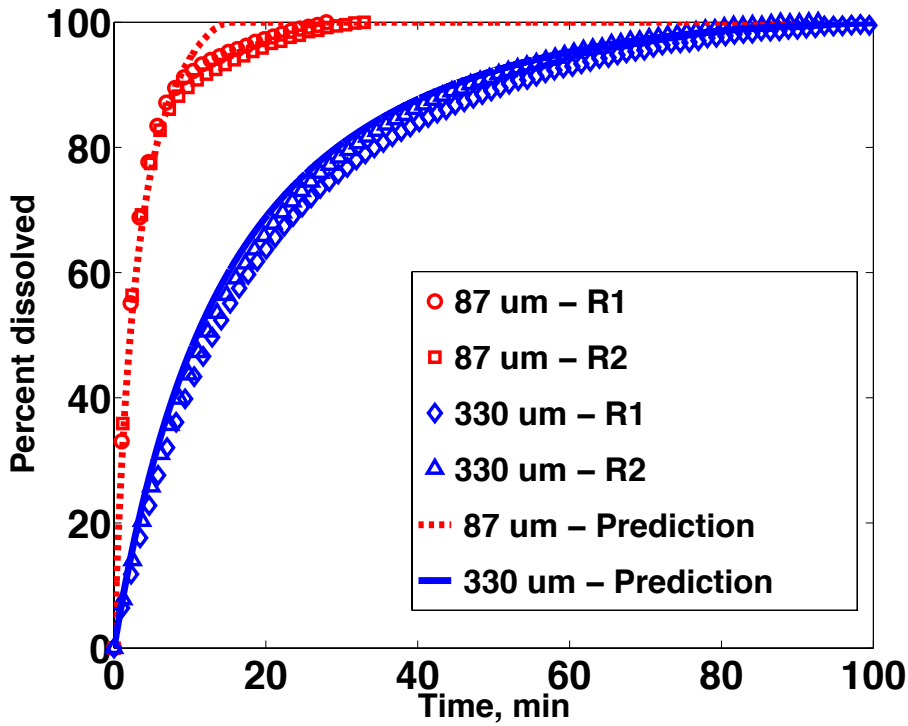
Figure 3.2: Percent of dose dissolved versus time (top) and bulk pH versus time (bottom) for 200 mg of Ibuprofen dissolving in pH 7, 10 mM buffer for the small and large median diameter particles

Data points represent results from run 1 (R1) and run 2 (R2) and lines represent transport model predictions. Percent dissolved normalized to percent of the final amount dissolved in buffer.
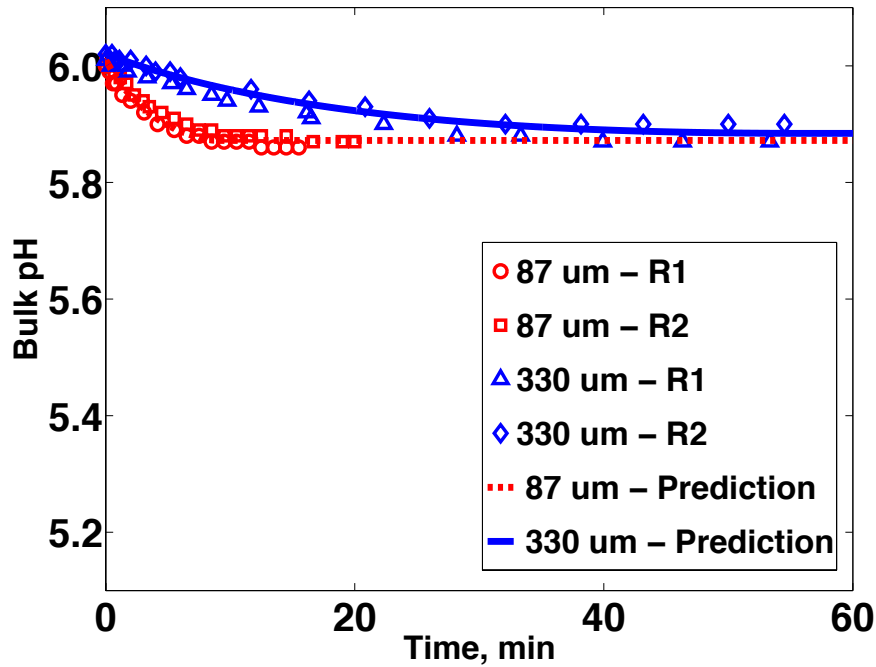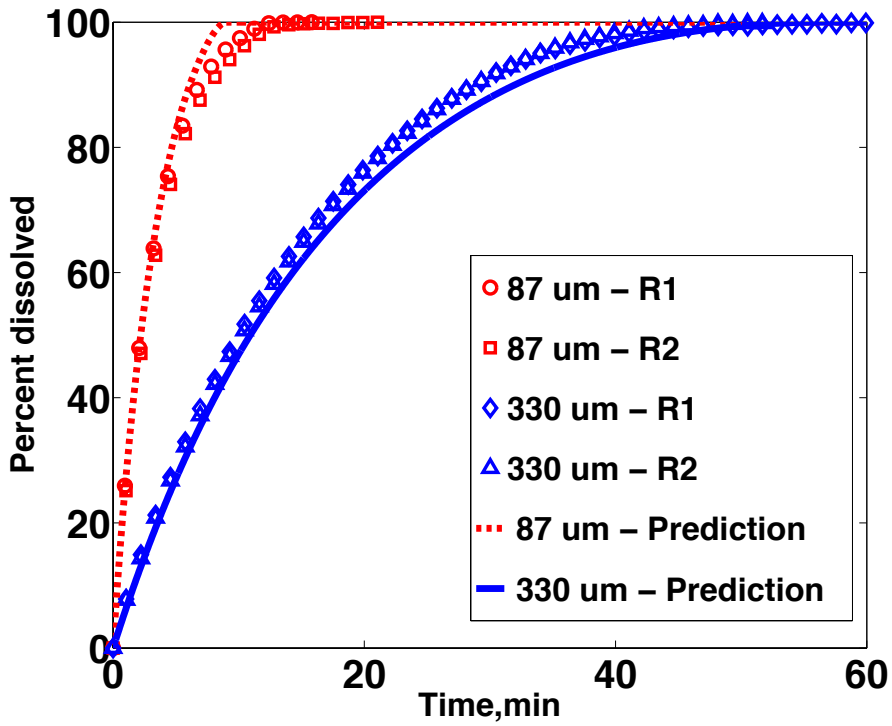
Figure 3.3: Percent of dose dissolved versus time (top) and bulk pH versus time (bottom) for 100 mg of Ibuprofen dissolving in pH 6, 50 mM buffer for the small and large median diameter particles

Data points represent results from run 1 (R1) and run 2 (R2) and lines represent transport model predictions. Percent dissolved normalized to percent of the final amount dissolved in buffer.
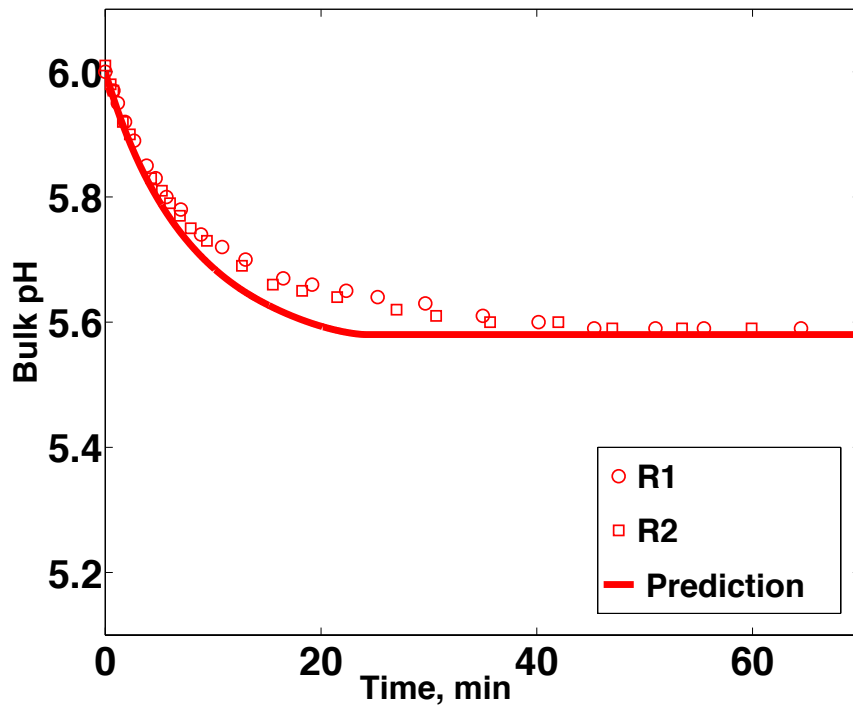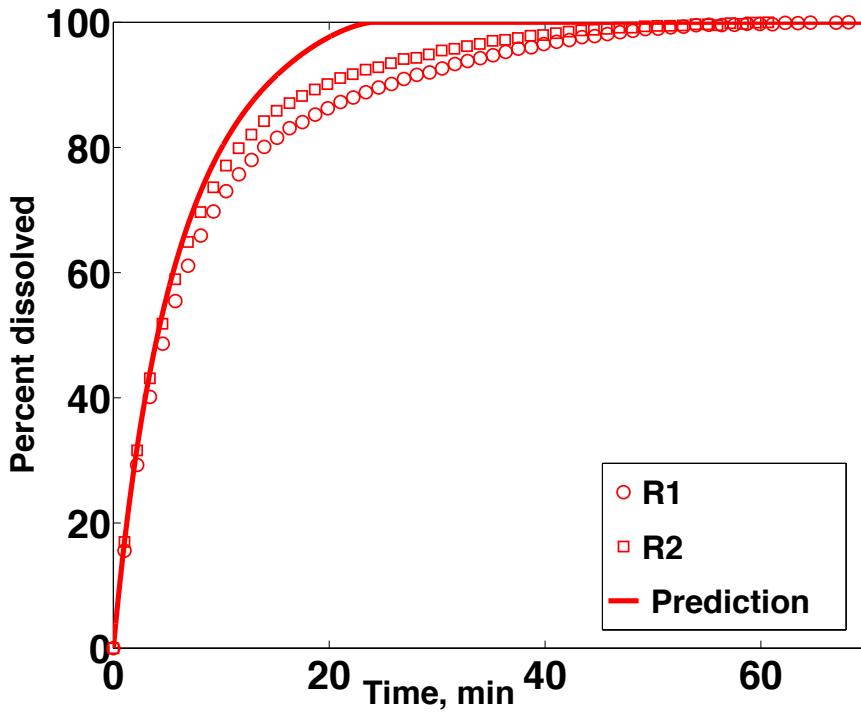
Figure 3.4: Percent of dose dissolved versus time (top) and bulk pH versus time (bottom) for 100 mg of Ibuprofen dissolving in pH 6, 20 mM buffer for the small median diameter particles

Data points represent results from run 1 (R1) and run 2 (R2) and lines represent transport model predictions. Percent dissolved normalized to percent of the final amount dissolved in buffer.
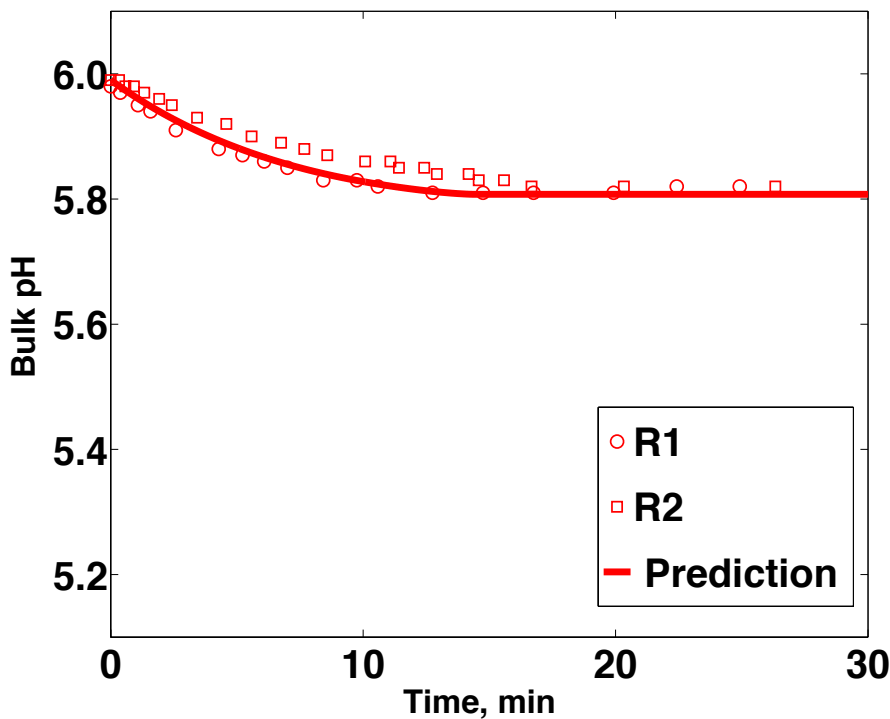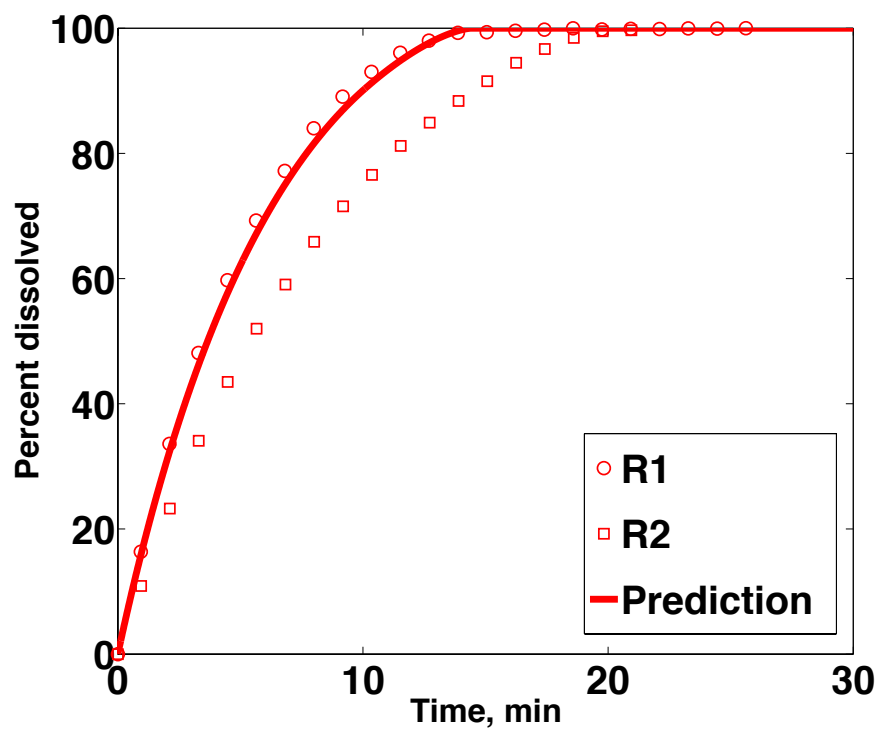
Figure 3.5: Percent of dose dissolved versus time (top) and bulk pH versus time (bottom) for 50 mg of Ibuprofen dissolving in pH 6, 20 mM buffer for the small median diameter particles

Data points represent results from run 1 (R1) and run 2 (R2) and lines represent transport model predictions. Percent dissolved normalized to percent of the final amount dissolved in buffer

Table 3.4. Experimental values for average time to reach twenty-five percent dissolved, $t_{25\%}$, fifty percent dissolved, $t_{50\%}$ and seventy-five percent dissolved, $t_{75\%}$, for each experimental condition

No.	Initial median particle diameter	Dose	Initial bulk pH	Buffer concentration	Exp. $t_{25\%}$ [a]	Exp. $t_{50\%}$ [a]	Exp. $t_{75\%}$ [a]
	μm	mg	-	mM	min	min	min
1	87	100	6	50	1 (0.9)	2.5 (2.2)	4.5 (4.2)
2	330	100	6	50	4 (4.7)	10 (11.4)	19 (22.0)
3	87	100	6	20	2 (1.6)	4.5 (4.1)	10.5 (8.6)
4	87	50	6	20	2 (1.5)	4.5 (3.6)	8.5 (6.7)
5	87	200	7	10	1 (0.8)	2 (2.2)	4.5 (4.8)
6	330	200	7	10	5 (4.2)	12.5 (11.2)	28 (25.3)

[a] Average time to dissolve 25, 50 or 75% of the dose for both experimental runs, rounded to the nearest 0.5 minutes.

Table 3.5. Theoretical values for change in pH at the particle surface, change in pH in the bulk medium, percent drug saturation in the bulk medium and initial dissolution rate

No.	Initial median particle diameter	Dose	Initial bulk pH	Buffer conc.	Theo. change in surface pH [a]	Theo. change in bulk pH [a]	Theo. final % saturated in the bulk [a]	Theo. initial dissolution rate [b]
	μm	mg	-	mM	-	-	%	$mg/s / h^{-1}$
1	87	100	6	50	5.7 – 5.7	6.0-5.9	24	0.50 / 17.8
2	330	100	6	50	5.7 – 5.7	6.0-5.9	24	0.10 / 3.6
3	87	100	6	20	5.5-5.4	6.0-5.6	41	0.32 / 11.6
4	87	50	6	20	5.5-5.4	6.0-5.8	14	0.16 / 11.6
5	87	200	7	10	5.8-5.7	7.0-6.1	30	1.24 / 22.2
6	330	200	7	10	5.8-5.7	7.0-6.1	30	0.25 / 4.5

[a] Values calculated using the transport model with an h_c of 20 µm.
[b] Calculated using **Equations 5-10** assuming $C_{b,t} = 0$ and $r_{,t} = r_o$.

Table 3.6. Buffer component concentrations and properties

Component	Millimoles added to 1 L of solution		
$NaH_2PO_4\ H_2O$	10	20	50
NaOH	7	4.2	10.6
NaCl	130	125.8	86.4
HCl	0.8	0	0
Properties at 37 °C		Value	
Initial pH[a]	7.0	6.0	6.0
Apparent pK_a [b]	6.78	6.58	6.58
Ionic strength [c]	0.153	0.154	0.158

[a] Measured using a standardized pH meter
[b] Calculated using a proton balance equation
[c] Calculated using $IS = \frac{1}{2}\sum_{i=1}^{n} c_i z_i^2$, where c_i = concentration of species i in solution in M and z_i = valence of species i in solution.
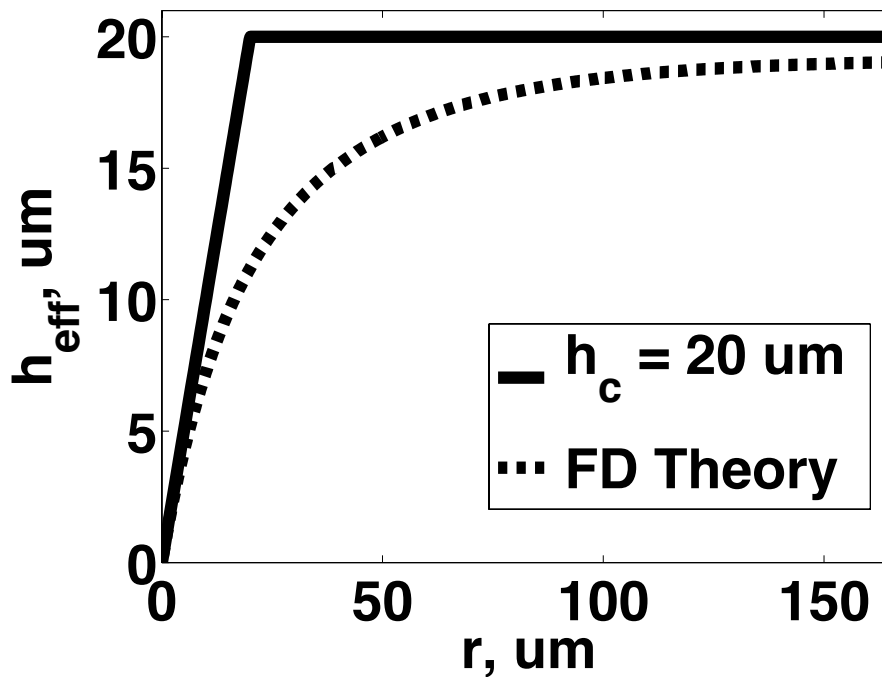
Figure 3.6. Theoretical h_{eff} as a function of particle radius calculated using FD theory and the Hintz and Johnson method (h_c = 20 μm)

Table 3.7. Parameters used to calculate h_{eff} based on FD Theory

Parameter	Value	Units
ρ_p	1.1 [a]	g/cm^3
D_{HA}	7.6×10^{-6} [a]	cm^2/s
ρ_{fluid} at 37 °C	0.99 [b]	g/cm^3
v at 37 °C	0.007 [c]	cm^2/s
g	981	cm/s^2
μ at 37 °C	0.007 [c]	$g/cm/s$
ε	200 [d], 3 [e,f], 40 [g] or 140 [h]	cm^2/s^3
m, A, B	2.07, 20.5, 0.310 [f]	-

[a] Refer to **Table 3.1** for references
[b] Reference [22]
[c] Experiments conducted in our laboratory (data not shown)
[d] Equal to 40 cm^2/s^3 (taken from Reference [13]) * 1000 cm^3 / 200 cm^3, to account for the difference in fluid volume between the value from which the original estimate was based (40 cm^2/s^3) and the current experiments.
[e] Based on 1000 ml of fluid in USP 2 apparatus at 20 rpm
[f] Reference [13]
[g] Based on 1000 ml of fluid in USP 2 apparatus at 50 rpm
[h] Based on 1000 ml of fluid in USP 2 apparatus at 75 rpm
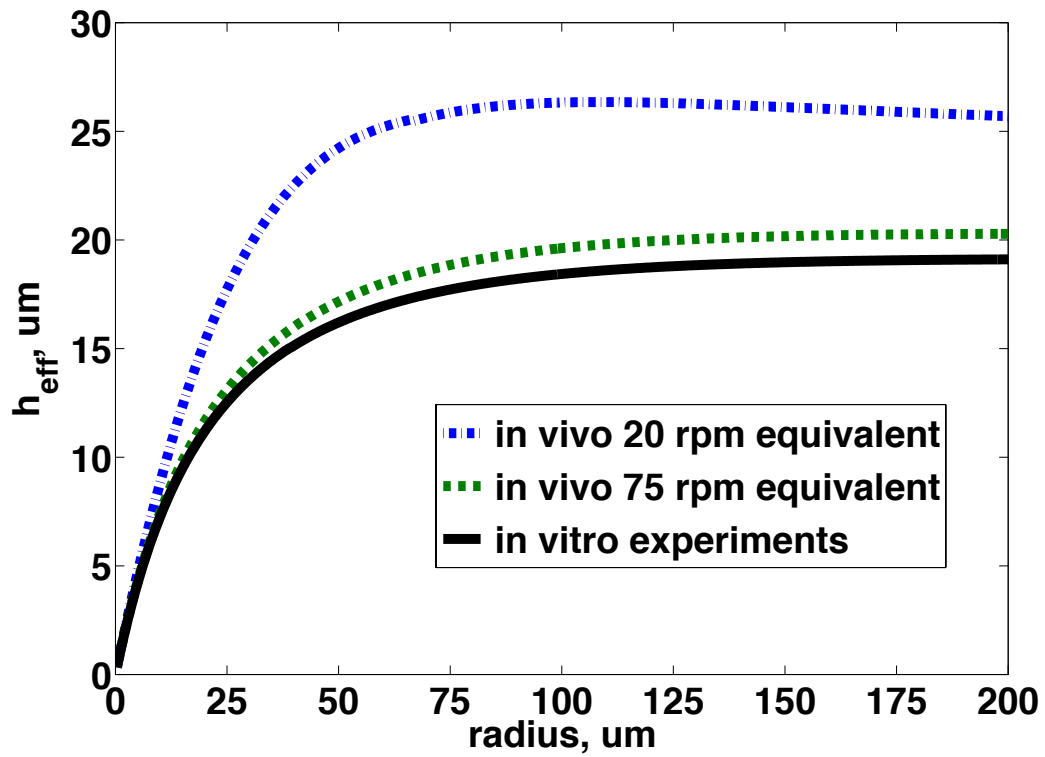
Figure 3.7. h_{eff} versus r for particle velocities calculated using ε = 0.0003 and 0.014 m^2/s^3 (representing *in vivo* 20 rpm and 75 rpm equivalent, respectively), together with h_{eff} versus r for ε = 0.02 m^2/s^3 (current *in vitro* experiments)
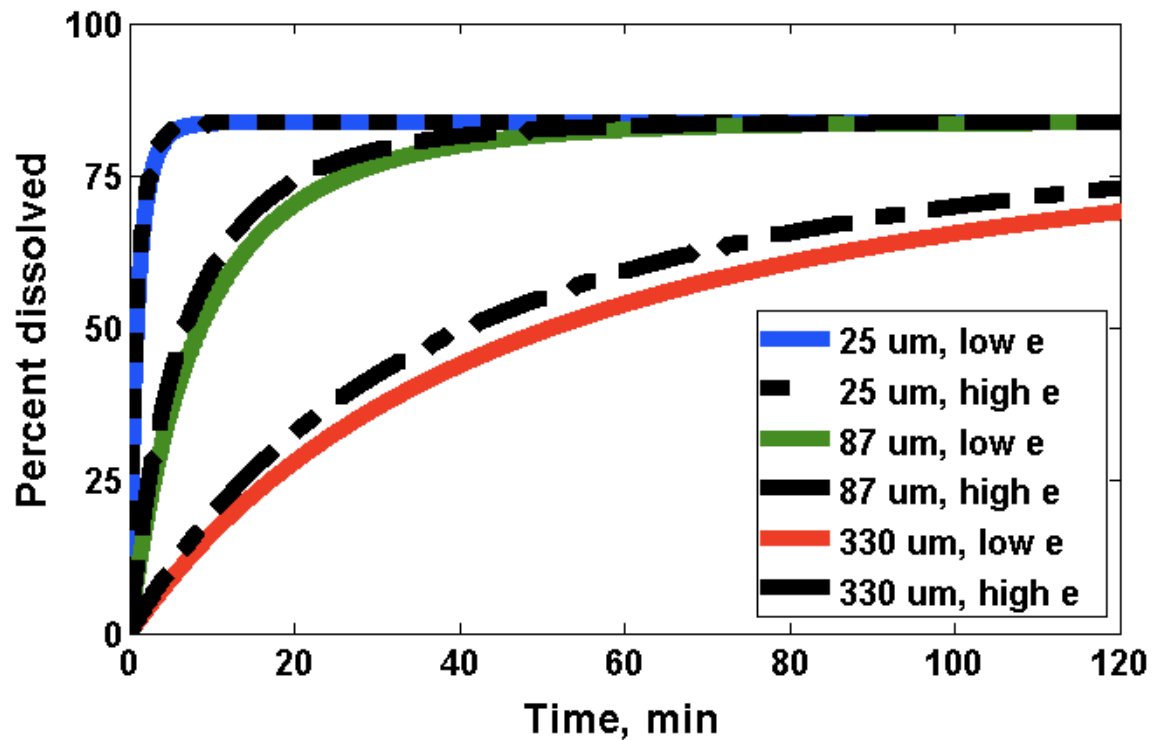
Figure 3.8. Percent of dose dissolved versus time using ε = 0.0003 and 0.014 m^2/s^3 (representing *in vivo* 20 rpm and 75 rpm equivalent, respectively), for 25 μm (fastest dissolving), 87 μm (moderately fast dissolving) and 330 μm (slowest dissolving) initial median diameter Ibuprofen particles

Conditions are 100 mg of Ibuprofen dissolving into pH 6.0, 10 mM sodium phosphate buffer.

References

1. Higuchi WI, Hiestand EN. Dissolution Rates of Finely Divided Drug Powders .1. Effect of a Distribution of Particle Sizes in a Diffusion-Controlled Process. Journal of pharmaceutical sciences 1963; **52**: 67-&. Doi 10.1002/Jps.2600520114

2. Wang JZ, Flanagan DR. General solution for diffusion controlled dissolution of spherical particles. 1. Theory. Journal of pharmaceutical sciences 1999; **88**: 731-8. Doi 10.1021/Js980236p

3. Mooney KG, Mintun MA, Himmelstein KJ, Stella VJ. Dissolution Kinetics of Carboxylic-Acids .2. Effect of Buffers. Journal of pharmaceutical sciences 1981; **70**: 22-32.

4. Ozturk SS, Palsson BO, Dressman JB. Dissolution of ionizable drugs in buffered and unbuffered solutions. Pharm Res 1988; **5**: 272.

5. Sinko P. Martin's Physical Pharmacy and Pharmaceutical Sciences. 5th ed. Baltimore, MD. Philadelphia, PA.: Lippincott Williams & Wilkins 2006.

6. Hintz RJ, Johnson KC. The Effect of Particle-Size Distribution on Dissolution Rate and Oral Absorption. International journal of pharmaceutics 1989; **51**: 9-17. Doi 10.1016/0378-5173(89)90069-0

7. Potthast H, Dressman JB, Junginger HE et al. Biowaiver monographs for immediate release solid oral dosage forms: Ibuprofen. J Pharm Sci-Us 2005; **94**: 2121-31. Doi 10.1002/Jps.20444

8. Sheng JJ, McNanara DP, Amidon GL. Toward an In Vivo Dissolution Methodology: A Comparison of Phosphate and Bicarbonate Buffers. 2009; **6**: 29-39. 10.1021/mp800148u

9. Burger A, Koller KT, Schiermeier WM. RS-ibuprofen and S-ibuprofen (dexibuprofen) - Binary system and unusual solubility behaviour. Eur J Pharm Biopharm 1996; **42**: 142-7.

10. Tsume Y, Langguth P, Garcia-Arieta A, Amidon GL. In silico prediction of drug dissolution and absorption with variation in intestinal pH for BCS class II weak acid drugs: ibuprofen and ketoprofen. Biopharm Drug Dispos 2012; **33**: 366-77. Doi 10.1002/Bdd.1800

11. Mudie DM, Amidon GL, Amidon GE. Mechanistic analysis of simultaneous drug dissolution and partitioning in an in vitro physiological two-phase

dissolution apparatus. 2013 AAPS Annual Meeting and Exposition; 2012; San Antonio, TX; 2012.

12. Lu ATK, Frisella ME, Johnson KC. Dissolution Modeling - Factors Affecting the Dissolution Rates of Polydisperse Powders. Pharmaceut Res 1993; **10**: 1308-14. Doi 10.1023/A:1018917729477

13. Sugano K. Theoretical comparison of hydrodynamic diffusion layer models used for dissolution simulation in drug discovery and development. Int J Pharmaceut 2008; **363**: 73-7. Doi 10.1016/J.Ijpharm.2008.07.002

14. Kelbaliyev G, Ceylan K. Development of new empirical equations for estimation of drag coefficient, shape deformation, and rising velocity of gas bubbles or liquid drops. Chem Eng Commun 2007; **194**: 1623-37. Doi 10.1080/00986440701446128

15. Crail DJ, Tunis A, Dansereau R. Is the use of a 200 ml vessel suitable for dissolution of low dose drug products? International journal of pharmaceutics 2004; **269**: 203-9. Doi 10.1016/J.Ijpharm.2003.09.007

16. Bai G, Wang YM, Armenante PM. Velocity profiles and shear strain rate variability in the USP Dissolution Testing Apparatus 2 at different impeller agitation speeds. Int J Pharmaceut 2011; **403**: 1-14. Doi 10.1016/J.Ijpharm.2010.09.022

17. Katori N, Aoyagi N, Terao T. Estimation of Agitation Intensity in the Gi Tract in Humans and Dogs Based on in-Vitro in-Vivo Correlation. Pharmaceut Res 1995; **12**: 237-43. Doi 10.1023/A:1016231010301

18. Scholz A, Kostewicz E, Abrahamsson B, Dressman JB. Can the USP paddle method be used to represent in-vivo hydrodynamics? J Pharm Pharmacol 2003; **55**: 443-51. Doi 10.1211/002235702946

19. Hayduk W, Laudie H. Prediction of Diffusion-Coefficients for Nonelectrolytes in Dilute Aqueous-Solutions. Aiche J 1974; **20**: 611-5. DOI: 10.1002/aic.690200329

20. Shaw LR, Irwin WJ, Grattan TJ, Conway BR. The effect of selected water-soluble excipients on the dissolution of paracetamol and ibuprofen. Drug Dev Ind Pharm 2005; **31**: 515-25. Doi 10.1080/03639040500215784

21. Levis KA, Lane ME, Corrigan OI. Effect of buffer media composition on the solubility and effective permeability coefficient of ibuprofen. International journal of pharmaceutics 2003; **253**: 49-59. DOI: 10.1016/S0378-5173(02)00645-2

22. CRC Handbook of Chemistry and Physics. 85 ed: CRC Press 2004.

Chapter 4

Mechanistic Oral Absorption Analysis of Ibuprofen in Dogs and Implications for IVIVC

Abstract

The purpose of this study was to determine *in vivo* performance of the BCS II model compound ibuprofen in dogs under well-controlled conditions and identify potential bioperformance dissolution methodologies that could be used to design and develop robust drug product formulations. Four Ibuprofen formulations were administered to dogs including an IV formulation to determine the pharmacokinetic disposition model, an oral solution to determine the rate of input into plasma due to gastric emptying and intestinal absorption processes alone, and two solid oral tablet formulations containing Ibuprofen particles of relatively small and relatively large particle size distributions to ascertain plasma input rate in the presence of a relatively fast versus a relatively slow dissolution step. A simple, mechanistic transport analysis was developed to describe average gastric emptying, dissolution and absorption rates of a BCS II weak acid in fasted dogs. Relevant canine physiological variables and Ibuprofen physicochemical properties were determined based on a review of the literature. Using this analysis, possible ranges for the relative rates of gastric emptying, dissolution, and absorption were predicted in the absence of *a priori in vivo* data.

The expected trend for rate of input into plasma (solution > small particle size tablet > large particle size tablet) was observed qualitatively over the first hour after dosing. However, there was no statistical difference in T_{max} between

the small and large particle size tablets. This lack of difference could be attributed to possible enterohepatic recirculation or another physiological phenomenon, as unexpected multiple peaks were observed in the concentration-time profiles for all four dosage forms.

Several scenarios were successful in describing average *in vivo* input rates into plasma for the oral solution and tablet formulations using common transport parameters. Two different types of practical *in vitro* bioperformance dissolution methodologies were proposed depending on the relative rates of gastric emptying and intestinal absorption. Both methodologies were predicted to be adequate in describing the average *in vivo* plasma profiles, and could likely be generalized for use with additional BCS II weak acids. Selection of the more superior methodology would require independent measures of gastric emptying rate and effective intestinal permeation rate in dogs. A conventional single-phase (e.g. USP) methodology was predicted to underestimate the time to reach seventy-five percent of the dose into plasma.

While in actuality *in vivo* drug transport displays significant complexity and heterogeneity, the aim of the current analysis was to describe average transport rates in a manner that would allow for selection of simple and practical *in vitro* biopredictive methodologies. More sophisticated techniques such as Monte Carlo simulation would be useful in explicitly describing the *in vivo* heterogeneity arising from the highly variable physiological and drug physicochemical properties.

Introduction

Prior assessment of drug product performance *in vivo* is a critical step needed to facilitate successful clinical human and animal studies. Once the chemical and physical properties of the drug substance and drug product have been characterized, predictions of the transport of the drug substance in the gastrointestinal tract *in vivo* can be made using *in silico* or *in vitro* methods. In this work a simple, mechanistic transport analysis describing gastric emptying

136

rate, dissolution rate, and absorption rate of the BCS II weak acid Ibuprofen in fasted dogs was developed. The relevant physiological variables as well as Ibuprofen physicochemical properties required for the transport analysis were determined based on a review of the literature. Using this analysis, possible ranges for the relative rates of gastric emptying, dissolution, and absorption were predicted in the absence of *a priori in vivo* data.

It was desired to determine the relevance of the transport analysis to *in vivo* data in dogs. Two studies in the literature investigated Ibuprofen bioavailability in dogs as a function of particle size [1] [2]. However, an IV solution was not dosed in either of these studies, so proper disposition models could not be determined with which to perform deconvolution to obtain curves for drug input into plasma. In addition, details of particle size and distribution were not well described in either study. Because dogs were not pretreated to control stomach pH, precipitation of the oral solution dosage form and/or dissolution of the solid oral dosage form in the stomach could have occurred. Therefore, it was determined that use of published data to support *in vitro – in vivo* comparisons directly would be difficult.

Four well controlled *in vivo* studies using Ibuprofen were designed and conducted in fasted dogs including 1) An intravenous (IV) study to determine the pharmacokinetic disposition model, 2) An oral solution study to determine the rate of input due to the gastric empting process and absorption into the intestinal membrane alone, 3) A solid oral tablet study containing Ibuprofen particles of a relatively small particle size distribution (87 µm median diameter) to ascertain the rate of input of dissolved drug into plasma in the presence of a relatively fast dissolution step, and 4) A solid oral tablet study containing Ibuprofen particles of a relatively large particle size distribution (330 µm median diameter) to ascertain the rate of input of dissolved drug into plasma in the presence of a relatively slow dissolution step.

Non-compartmental pharmacokinetic analysis of the plasma concentration time profiles from the four studies was conducted to determine pharmacokinetic parameters, such as time to peak plasma concentration (T_{max}) and peak plasma

concentration (C_{max}). A two-compartment disposition model was fit to the IV concentration time profile and used to perform numerical deconvolution of the oral solution and solid oral tablet concentration time profiles to extract the input rate of dissolved drug into plasma. Using the transport analysis (and within the constraints of the range of relevant physiological and drug physicochemical properties determined from the literature *a priori*), the average parameters for gastric emptying rate, dissolution rate, and absorption rate into the intestinal membrane that explained the average *in vivo* input rate into plasma from the oral dosage forms were determined.

Finally, based on the simple transport analysis and outcome of the *in vivo* studies, two types of bioperformance dissolution methodologies that would likely be successful in describing the *in vivo* data and developing potential IVIVCs for the solid oral dosage forms were suggested. Selection of the more superior methodology requires further knowledge not collected in the present *in vivo* studies, such as independent measures of the gastric emptying rate of Ibuprofen and the effective permeation rate of Ibuprofen in the dog intestine.

Materials and Methods

Materials

The free acid form of Ibuprofen drug powder (Albermarle Lot 11550-0005) and Ibuprofen for injection Caldolor^{TM} 800 mg/8 ml vials (Cumberland Pharmaceuticals, lot 5401 JX3) were purchased commercially. All additional chemicals were of analytical grade or purer and were purchased commercially.

Study design

The following four studies were conducted in six fasted dogs using a crossover design and a washout period of 7 days using a dose of 80 mg. All four studies were completed within a four-week timeframe.

Study 1 – IV formulation

Study 2 – Oral solution

Study 3 – Small particle size rapidly disintegrating immediate release tablets

Study 4 – Large particle size rapidly disintegrating immediate release tablets

The purpose of administering an IV formulation in study 1 was to determine the pharmacokinetic drug disposition model for use in deconvolution analysis of the oral dosage form plasma concentration-time profiles. Study 2 using an oral solution was conducted to determine the gastric emptying and absorption profiles of Ibuprofen in dogs in the absence of disintegration and dissolution steps. To help keep pH high and minimize possible precipitation of Ibuprofen from the oral solution formulation in the dog stomach, dogs were pretreated with a pH 7 BIS-TRIS buffer 10-15 minutes prior to dosing. The purpose of administering small and large particle size solid dosage forms in studies 3 and 4 was to determine the difference in absorption rates between small and large particle size formulations of Ibuprofen taking dissolution rate into account. For these studies a pH 2 HCl-KCl buffer was administered 10-15 minutes prior to dosing to help keep stomach pH low and minimize dissolution of Ibuprofen in the stomach.

Preparation of Ibuprofen tablets

To obtain the desired particle size of Ibuprofen, bulk Ibuprofen was blended with 0.5% colloidal silicon dioxide in a V-blender to facilitate flowability of Ibuprofen through and recovery from the mesh screens. 10 g of the blend was added to the top of a stack of 3-inch diameter screens with a range of mesh sizes that were then placed in an ATM Sonic Sifter and pulsed for at least 5-minute increments at a pulse amplitude of 8. The percentage of drug on each screen was determined after each pulsing increment and the sieves were again placed in the sonic sifter and pulsed for again until the percentage change of mass of drug recovered on each sieve was no more than 5%.

Direct compression blends of Ibuprofen were prepared by blending each Ibuprofen sieve cut with spray-dried lactose, microcrystalline cellulose ph 102 and crospovidone by hand in a glass jar for 3 minutes. Each direct compression

blend was compressed into tablets using a manual hydraulic press. Eighty milligrams of drug was compressed at 96.5-103.5 MPa and the pressure was maintained for one minute followed by slow decompression over thirty seconds. Weight and dimensions of each tablet were measured and the solid fraction of each tablet was calculated according to **Equation 4.1**. True density of the blend was calculated using a weighted average taking into account the true density of each component and its relative proportion in the blended formulation. Refer to **Table 4.1** for tablet composition.

(4.1) $Solid\ fraction = \dfrac{Mass}{\pi \cdot radius^2 \cdot thickness} \cdot \dfrac{1}{true\ density}$

Microscopy for particle size analysis

The particle size distributions of the two sieve cuts of Ibuprofen were determined using microscopy. Particles were visualized using a Nikon OPTI-PHOT – POL optical microscope with SPOT Insight color camera model 3.2.0 and SPOT 5.1 Advanced Imaging software (SPOT Imaging Solutions, Sterling Heights, MI). The widths, lengths and thicknesses of about 10-15 particles from each sieve cut were determined and a mean thickness-to-width ratio was calculated for each sieve cut. The maximum lengths and widths of about 300 randomly selected particles from each sieve cut were then determined. The mean thickness-to-width ratio determined using the 10-15 particles was used to estimate the thicknesses of the ~300 particles for which width and length values were determined. The volume of each particle, V_p, was calculated by calculating the product of the length, width and thickness. The equivalent spherical diameter, ESD, of each particle was calculated using **Equation 4.2**. The mass of each particle was determined by multiplying the true density (1.1 g/cm^3 [3]) by V_p. The D50 (median) and D90 ESD by mass were determined by finding the ESD of the particles with a mass at the 50th and 90th percentiles, respectively, of the total mass of the ~300 particles. The value of D90/D50 for each sieve cut was calculated as a means of assessing the breadth of the size distributions.

140

(4.2) $ESD = \left(\frac{3}{2}V_p\pi\right)^{1/3}$

Animals

  The same three male and three female beagle dogs (weights ranged from 8-12 kg) were fasted for 24 hours before administration of all dosage forms for each study. Dogs had free access to water at all times. Blood samples (1 ml each) were collected from the jugular vein at 10, 20, 30, 45, 60, 90, 120, 150, 180, 210, 240, 300, 360, 480 and 600 minutes after dosing. The study was conducted in accordance with the animal welfare requirements specified in IACUC Protocol 1104B00384.

Study protocol

Study 1 – IV formulation

0.8 ml of Caldolor® (800mg/8ml) was administered quickly to each dog as a bolus by injection into the cephalic vein.

Study 2 – Oral solution

Dogs were given 19 ml of an isotonic 0.5 M pH 7 BIS-TRIS buffer using an orogastric tube. Ten to fifteen minutes later 6 ml of an isotonic pH 7 13.34 mg/ml Ibuprofen solution (80 mg dose) was administered via an orogastric tube. Refer to **Table 4.2** for oral solution pretreatment and Ibuprofen solution compositions.

Studies 3 and 4 – Small particle size & large particle size tablets

Dogs were given 24 ml of an isotonic pH 2 HCl-KCl buffer buffer using an orogastric tube. Ten to fifteen minutes later a single 80 mg tablet of small particle size Ibuprofen (Study 3) or large particle size Ibuprofen (Study 4) was administered using an orogastric tube. Refer to **Table 4.3** for tablet pretreatment solution composition.

Assay

Whole blood samples were collected into tubes containing EDTA. Plasma was harvested after centrifugation for 10 minutes at 4000 rpm in a refrigerated (4 °C) centrifuge (Eppindorf model 5810R), and transferred to 96 well titer plates and sealed with plate mats. Plasma samples were stored at -20 °C prior to analysis. After thawing at room temperature, all samples were diluted at a ratio of 1:5 (sample:blank) with blank dog plasma. Analytical plasma aliquots (25 uL) were precipitated with 250 uL of acetonitrile (ACN). The protein was pelletized by centrifugation, and a 50 uL aliquot of supernatant was taken and diluted in 100 uL of 0.1% formic acid in water before a 10 uL aliquot was injected for analysis by high performance liquid chromatography with mass spectrometric detection (HPLC-MS).

The mobile phase was isocratic (25:75 ACN:10 mM ammonium acetate) operating at a flow rate of 0.8 mL/min. Separation was accomplished using a 50x3 mm column packed with 5 um particle size Betasil Cyano stationary phase (Thermo Scientific) with a 1.7 minute run time. The detector was an AB Sciex API-5500 mass spectrometer operating under turbo-ion spray conditions in negative ion mode.

Pharmacokinetic analysis

The plasma concentration time profiles were analyzed using Phoenix^{TM} WinNonLin® software (version 6.3.0.395; Pharsight, a Certara^{TM} company). Noncompartmental analysis was performed on the individual concentration time profiles from zero to eight hours for each of the six dogs for all four dosage forms using uniform weighting. The terminal slope, λ_z, was calculated using the linear trapezoidal rule, and the terminal half-life was determined by dividing $\ln(2)$ by λ_z. Maximum plasma concentration, C_{max}, and time to maximum plasma concentration, Tmax, were determined by inspection of the data. The area under the plasma concentration profile from the initial time point to the last non-zero plasma concentration, AUClast, was calculated using the linear trapezoidal rule. The observed AUC from dosing extrapolated in infinity AUCInf_obs was

calculated as AUClast + Clast/λ_z. Absolute bioavailability, F, was calculated for the oral dosage forms by dividing AUCInf_obs for the oral dosage form by AUCInf_obs for the IV dosage form. Total body clearance, CL_obs was calculated by dividing the F*dose by AUCInf_obs. The volume of distribution based on the terminal phase, Vz_obs, was calculated by dividing the F*dose by λ_z * AUCInf_obs. Differences between T_{max}, C_{max}, and AUCInf_obs between dosage forms was assessed using a student's t-test with a 0.05 level of significance.

Compartmental modeling was performed on the individual IV concentration time profiles from zero to eight hours after dosing. A two-compartmental model (WinNonLin® Model 8 - bolus input and first-order output, macro-constants as primary parameters using Gauss-Newton (Levenberg and Hartly) minimization) with uniform weighting was found to adequately describe the data. The concentration-time profile was described using **Equations 4.3-4.5**, where -α and –β (α > β) are the roots of the quadratic equation r*r + (k_{12}+k_{21}+k_{10})*r + k_{21}*k_{10} = 0. Secondary parameters of AUC (AUC = A/α + B/β), volume of the central compartment (V1), clearance from the first compartment (CL), volume at steady-state (V_{ss}), volume of the peripheral compartment (V2), and clearance from the peripheral compartment (CLD2), were also determined.

(4.3) $\quad C(t) = Ae^{-\alpha \cdot t} + Be^{-\beta \cdot t}$

(4.4) $\quad A = \left(\dfrac{D}{V}\right)\dfrac{(\alpha - k_{21})}{(\alpha - \beta)}$

(4.5) $\quad B = \left(\dfrac{D}{V}\right)\dfrac{(\beta - k_{21})}{(\alpha - \beta)}$

Numerical deconvolution analysis of the oral dosage form concentration profiles was also performed using Phoenix[TM] WinNonLin® software to estimate the apparent systemic availability of drug as a function of time. WinNonLin® uses the basic principle of deconvolution through convolution (DTC). The process is

143

iterative, whereby the software deconvolves the convolution integral to extract the input function (the rate of drug entry into plasma) imbedded in the convolution integral. The convolution integral can be represented as in **Equations 4.6-4.8**, where C(t) is the drug level response (plasma concentration profile), f(t) is the drug input rate into plasma, and $c_\delta(t)$ is the unit impulse response or disposition function. The variable $c_\delta(t)$ is a function of g(t), the probability that a molecule entering point A at t = 0 is present in the sampling space at time t, divided by V_s, is the volume of that sample space. The symbol "*" denotes the convolution operation. A full description of the Phoenix^{TM} WinNonLin® deconvolution methodology can be found in reference [4]. The analysis was performed using the two compartment unit disposition parameters determined for each individual subject from the IV data as the unit impulse response, $c_\delta(t)$. Automatic smoothing was selected, whereby the software finds the optimal value for the dispersion parameter.

(4.6) $\quad C(t) = \int_0^t f(t-u) \, c_\delta(u) du$

(4.7) $\quad C(t) = f(t) * c_\delta(t)$

(4.8) $\quad c_\delta(t) = \frac{g(t)}{V_s}$

Mechanistic *in vivo* transport analysis

  The major transport steps for Ibuprofen from oral administration to appearance in the bloodstream include 1) emptying of the dosage form (solution or disintegrated tablet) from the stomach into the small intestine, 2) dissolution of the oral dosage form (if applicable) in the small intestinal lumen, and 3) absorption through the intestinal membrane. Analyses of each of these steps are outlined below.

Gastric emptying

In this analysis, gastric emptying was assumed to approximate either first-order or zero-order kinetics, with the entire dose emptied in a continuous manner. **Equation 4.9** describes the first order emptying, where $dM_{e,t}/dt$ is the rate of mass transport from the stomach into the small intestine, $M_{e,t}$ is the mass emptied, k_{ge} is the first order emptying rate coefficient, and $M_{s,t}$ is the mass remaining in the stomach. The fraction of drug emptied as a function of time, $dF_{e,t}/dt$, can be described by dividing both sides of **Equation 4.9** by the dose (**Equation 4.10**). The time to empty fifty percent of the dose, t_{50}, is defined in **Equation 4.11**. **Equations 4.12** and **4.13** describe the mass and the fraction emptied as a function of time, respectively, assuming zero order kinetics. These equations were used for both the *in vivo* and *in vitro* simulations.

(4.9) $\quad \dfrac{dM_{e,t}}{dt} = k_{ge} M_{s,t}$

(4.10) $\dfrac{dF_{e,t}}{dt} = \dfrac{dM_{e,t}}{dt} \cdot \dfrac{1}{Dose}$

(4.11) $\quad t_{50} = \dfrac{0.693}{k_{ge}}$

(4.12) $\dfrac{dM_{e,t}}{dt} = k_{ge}$

(4.13) $\dfrac{dF_{e,t}}{dt} = \dfrac{k_{ge}}{Dose}$

Dissolution

Predictions of dissolution rate *in vivo* and *in vitro* were carried out using the analysis presented in Chapter 3. The Hintz and Johnson method was used to determine $h_{eff,t}$.

<u>Absorption</u>

Several researchers have given expressions for passive transport of drugs from the intestinal lumen to the intestinal membrane [5] [6]. As shown in **Equation 4.24**, drug flux across the intestinal wall, J_w, depends upon effective intestinal wall permeation rate, P_{eff}, and drug concentration at the surface of the intestinal wall, C_w, which are both dependent upon time and position along the membrane. **Equation 4.24** is written based on the assumption that the concentration of drug in the epithelial cell to essentially equal to zero.

(4.24) $J_w = P_{eff} C_w$

Assuming no luminal reactions, absorption rate of drug into the intestinal membrane is given by **Equation 4.25**, where A is the surface area of membrane in contact with dissolved drug and m is mass of drug in solution.

(4.25) $\frac{dM}{dt} = \iint_A P_{eff} C_w \, dA$

In this analysis it is assumed that P_{eff} is uniform along the intestinal wall (not position dependent), which is a reasonable assumption given that Ibuprofen absorption is relatively fast and likely happens in the upper small intestine. It is also assumed that there is no radial change of drug concentration in the intestinal lumen, so C_w is equal to the concentration of drug in the bulk intestinal lumen fluid, $C_{a,t}$. V is the volume of liquid in the intestinal lumen, and A/V is the surface-area-to-volume ratio of the liquid in contact with the intestinal membrane, which is also assumed to be time and position independent in the current analysis. The product of A/V and P_{eff} can be represented by the net absorption rate coefficient, k_a. **Equation 4.26** describes the mass of drug absorbed as a function of time, $M_{ab,t}$, which depends on k_a and the mass of drug in solution, $M_{a,t}$ at time t. The fraction of the dose absorbed into the membrane as a function of time, $F_{ab,t}$ is

146

given by **Equation 4.27**. Values for P_{eff} and A/V relevant to the current analysis are described in later sections.

(4.26) $\dfrac{dM_{ab,t}}{dt} = \dfrac{A}{V} P_{eff} C_{a,t} V = k_a M_{a,t}$

(4.27) $\dfrac{dF_{ab,t}}{dt} = \dfrac{dM_{ab,t}}{dt} \cdot \dfrac{1}{Dose}$

In an *in vitro* system, transport of drug can be described using a mechanistic transport analysis previously developed for partitioning of solutes from aqueous to organic medium (Chapter 2 and reference [7]). It describes transport of dissolved drug across two hydrodynamically controlled 'stagnant' diffusion layers on each side of an aqueous-organic interface under circumstances for which buffer capacity is high enough to maintain a constant bulk pH throughout the experiment. The flux of non-ionized drug from bulk aqueous to bulk organic medium is given by **Equations 4.28 and 4.29**, where P_l is the permeation rate of drug across the aqueous and organic diffusion layers. P_l depends on the thicknesses of the aqueous and organic diffusion layers, h_a, and h_o, the diffusion coefficients across the aqueous and organic diffusion layers, D_a, and D_o, and the apparent partition coefficient at the aqueous-organic surface, K. For drugs with high values of K (> ~10) the rate-limiting step is diffusion across the aqueous diffusion layer. The driving force for transport across this layer is the difference in total drug concentration in the bulk and on the aqueous side of the aqueous-organic interface. When K is high and/or concentration in the organic medium is low, the magnitude of the driving force simplifies to the value of the concentration of total drug in the bulk aqueous medium, as described in **Equation 4.30**. V_a is the volume of aqueous buffer in which the drug is dissolved, and A_l is the surface area of the aqueous-organic interface. The product of A_l/V_a and D_a/h_a can be represented by the net partitioning rate coefficient, k_p. The rate of transport of drug into the organic medium is described by **Equation 4.31**, where $M_{o,t}$ is the mass partitioned into the organic medium.

(4.28) $J_{HA} = P_I \left(C_A - \frac{C_o}{K} \right)$

(4.29) $\frac{1}{P_I} = \frac{h_o}{D_o K} + \frac{h_a}{D_a}$

(4.30) $J_{HA} = \frac{D_a}{h_a} C_a$

(4.31) $\frac{dM_{o,t}}{dt} = \frac{A_I}{V_a} J_{HA} \cdot V_a = \frac{A_I}{V_a} \frac{D_a}{h_a} C_{a,t} V_a = k_p M_{a,t}$

Physiological and drug related transport parameters

To determine the transport rate of Ibuprofen in dogs using the above analysis a number of physiological and drug product related parameters had to be determined. As discussed in Chapter 1 as they relate to humans, physiological parameters are highly complex with large variability both within and between individuals [8]. Drug product parameters are defined by the intrinsic properties of the drug substance itself and also depend on the properties of the physiological environment. Physiological and drug product parameters required for the current analysis are described below.

Ratio of small intestinal surface-area-to-volume (A/V)

As the mass transport rate of Ibuprofen into the intestinal membrane is directly proportional to A/V, an estimate for this parameter in dogs was required to perform the calculations. An estimated range for A/V in humans was determined in a prior publication [7]. A similar approach was used in the present analysis. Assuming the dog small intestine to approximate a compressed cylinder, a range in geometrical surface area was calculated using known dimensions of the dog small intestinal tract from the literature. Assuming a radius of 0.5 cm and a constant perimeter, A/V was calculated as a function of percent compression of the cylinder (**Refer to Table 4.4**) [9]. This method assumes that

148

the liquid takes the shape of the intestine and is thus in direct contact with the intestinal wall. The total length of the dog small intestine is estimated to be about 400 cm [10]. As shown in **Table 4.4** a percent compression of 89 would give a compressed cylinder a total length of just over 400 cm. This percent compression was chosen as the maximum, with a corresponding surface area of 1290 cm^2 and a maximum A/V of 26 cm^{-1}. A zero percent compression was chosen as the minimum with a corresponding surface area of 200 cm^2 and a minimum A/V of 4 cm^{-1}. Such a cylinder would have a length of 64 cm. A total length much shorter than the length of the small intestine is plausible since it is probable that the liquid in the small intestine is not continuous, but is separated into smaller pockets [11]. Literature values for small intestinal geometric surface area range from 990 – 1400 cm^2, which for the compressed cylinder calculations would represent percent compression values ranging from 85-90 [10] [12]. In this analysis A/V was assumed to be time and position independent, so A/V as defined here should be considered as and average value over the absorption region.

Volume

Gupta & Robinson reported that the mean resting liquid volume in the stomach in the fasted state was about 25 ml [13]. However, values for volume of liquid in the small intestine in the fasted dog could not be found in the literature. Given the lack of measurements in dogs, and the relative abundance of measurements in humans, canine small intestinal volume was estimated by comparing canine and human physiology. Using MRI Mudie and coworkers measured a human fasted small intestinal liquid volume of 43±14 ml (5-159 ml) [14]. The volume of liquid in the small intestine rose to as high as 93±24 ml on average (15-264 ml) 12 minutes after ingestion of 240 ml of water, and measured 77±14 ml (15-172 ml) 45 minutes when complete emptying had occurred. Other reports measured average values ranging from 81-165 ml of liquid in fasted humans after no ingestion of water immediately prior to testing [15] [11] [16]. The capacity for liquid is about ten times higher in humans than in dogs, based on

149

calculations using cylindrical geometry[1] [17]. However, a comparison of secretion and water absorption rates in the GI tract for both species suggests that basal small intestinal liquid volumes may be similar or only slightly lower in dogs than in humans (Refer to **Table 4.5**). It is therefore likely that average values for small intestinal liquid volume in the fasted dog before and after about 30 ml of liquid (as in the current study) range from about 30-100 ml. For this study an average value of 50 ml was assumed.

Gastric emptying rate

A cyclical phenomenon called the migrating motor complex (MMC) exists in the fasted state in dogs (and humans) and is characteristic of three distinct phases of contractions varying in frequency and amplitude followed by a fourth, short transitional phase [18]. The majority of contractions originate in the stomach and help move liquid and solids through the gastrointestinal tract. The third phase of the MMC consists of frequent, high-amplitude contractions that begin in the stomach and propagate throughout the intestine. The pylorus remains open during phase three, allowing particles and solids to move through it. Durations of each phase in dogs have been recorded as 40-65 min for phase I, 15-20 min for phase II, 10-15 minutes for phase III, and 6-16 min for phase IV [13]. A range of gastric emptying times for liquids has been documented in the literature. It is generally agreed upon that large volumes of liquids (> 100-150 ml) empty relatively fast and in a continuous fashion (due to regulation of gastric function caused by distension), whereas emptying patterns of smaller volumes are more dependent on the phase of MMC during which the liquid was administered [13]. As the current study involves movement of small volumes of liquids (~30 ml) and liquids containing solid particles less than about 500 μm from the stomach and into the small intestine, determining emptying patterns of small volumes of liquid is of interest. Gupta and Robinson studied emptying of liquids ranging from 25 to 500 ml in fasted dogs, with liquid administration

---

[1] The canine small intestinal tract has a radius of about 0.5 cm and a length of up to about 400 cm, whereas the human small intestinal tract has a radius of about 2 cm and a length of about 282 cm.

consistently occurring during phase I of the MMC [13]. They found that following administration of 25-100 ml of water only a very small amount of liquid was emptied within the first 20-30 min followed by a continuous flow of liquid around the time phase II activity was expected. Half of the administered volume was emptied between 35 and 40 minutes and the total amount was emptied after about 55-65 minutes.

Gruber and coworkers administered non-digestible solid particles with diameters of 0.5-6.4 mm in a capsule immediately prior to 50 ml of saline at the onset of phase activity [19]. They found that gastric emptying closely followed phasic activity, with little or zero discharge of liquid during phase I. Instead, emptying occurred during phase II with variable kinetics with total emptying lasting about 30-55 minutes. They found that particles of all sizes remained in the stomach until the onset of phase III activity, and emptied as a bolus after the liquid. Gupta and coworkers also found that small non-digestible particles empty as a bolus during phase III when given with small volumes (less than 100 ml) liquids of low viscosity [20].

Based on these results onset of emptying of the Ibuprofen oral solution (administered 10-15 minutes after orally administering a buffer solution of about 30 ml during an unknown phase of the MMC) should begin within zero to 116 minutes after administration (corresponding to one complete MMC cycle). Half of the dose should appear in the small intestine within 35-40 minutes and the entire dose should empty into the small intestine within 55-60 minutes. For simplicity it is desired to approximate the emptying pattern of the oral solution using a mathematical expression. Assuming zero order kinetics and a k_{ge} of 0.84 fraction of dose/h, half of the dose would empty in 35 minutes and the entire dose would empty in 70 minutes. Assuming first order emptying and a k_{ge} of 1.2 h^{-1}, half of the dose would empty in 35 minutes, but only 75% of the dose would empty in 70 minutes, with the entire dose emptying in about 4 hours. Assuming first order emptying and a k_{ge} of 4.6 h^{-1}, half of the dose would empty in 9 minutes and the entire dose would empty in 70 minutes. For small particles, onset of emptying should occur between 0 and 116 minutes after administration and complete

emptying should occur within less than 15-30 minutes after the first few particles are emptied into the small intestine (Zero order k_{ge} from about 2.1 to 3.9 fraction of dose/h).

Intestinal transit time

The average small intestinal residence time in fasted dogs is about 2 hours. Youngberg and coworkers reported a small intestinal transit time of 111±17 min (range of 15-206 min) for a Heidelberg capsule [21]. Miyabayashi and coworkers measured a transit time of 73 +/-16.4 min (range of 30-120) for a barium sulfate solution [22].

Buffer species, concentration, and pH

The liquid in the small intestine is complex and dynamic and comprises substances emptied from the stomach as well as secretions from the liver, pancreas, and small intestinal wall [8]. For the current analysis the physiological variables of interest are those affecting drug solubility and dissolution rate. For a weak acid such as Ibuprofen that is ionizable in the physiological range, import factors driving solubility and dissolution rate include buffer species, buffer concentration, pH, ionic strength, and surfactant concentration.

The pH is the upper small intestine (duodenum and jejunum) of the fasted dog has been shown by many researchers to range from about 6.0 to 7.3 [10] [23]. However, some researchers have found slightly higher pH values. Gupta & Robinson studied the pH in the duodenum after administration of different volumes of water to a fasted dog [13]. They found mean pH to be 7.7 before administration of water, and a pH between 7 and 8 after administration of water volumes up to 100 ml. Lui et al. found a maximum pH of 7.7 20 min after gastric emptying, which gradually declined to 7.2 180 min after emptying [24]. They found an overall mean intestinal pH of 7.3 +/- 0.09.

The predominant buffer species in the canine small intestine is bicarbonate, with average concentrations recorded as 17 mM (range of 14-22 mM) in the duodenum, and 22 mM (range of 5-30 mM) in the jejunum in one

study [25], and 20 ± 3.8 mM in the jejunum in another study [26]. These two studies also recorded phosphate buffer concentrations of 1.6 mM (range of 0.6-4.0) and 44.5 ± 5.5 mM, respectively.

For the current analysis it was desired to describe diffusion and reaction of Ibuprofen in a 20 mM bicarbonate buffer. However, as described above, the transport equations describing dissolution assume instantaneous chemical reactions, and it is likely that the reaction between water and carbon dioxide to form carbonic acid, followed by bicarbonate in the intestinal lumen itself is not instantaneous [27]. In many parts of the body the enzyme carbonic anhydrase catalyzes the reaction between carbon dioxide and water, making the reaction instantaneous. Carbonic anhydrase XIV is present on the apical side of the intestinal membrane and likely resides within the mucus layer to protect epithelial cells from acid-related damage [28]. While carbonic anhydrase VI is secreted in saliva and likely remains active as it travels through the stomach and intestine [29], the concentrations of this enzyme in the intestinal lumen are unknown. If they exist in high enough concentrations, they may catalyze the reaction between carbon dioxide and water, speeding up the reaction so that it occurs at a higher rate.

Krieg et al. reported that experimental dissolution rates of Ibuprofen in bicarbonate buffer were very similar to the predicted and experimental dissolution rates of Ibuprofen in phosphate buffer of the same concentration in the range of ~3-8 mM in the rotating disk apparatus [27]. At buffer concentrations higher than 8 mM, dissolution rates tended to plateau in bicarbonate buffer, but steadily increase in phosphate buffer. While the current transport analysis was not derived for bicarbonate buffer specifically, results by Krieg and coworkers suggest that a 10.5 mM phosphate buffer might be an adequate substitute for a 20 mM bicarbonate buffer. The reaction between hydrogen phosphate and dihydrogen phosphate can be assumed to be instantaneous, and can thus be described using the current transport equations. For the current analysis a buffer concentration of 10.5 mM and an apparent pK_a value of 6.8 was used in the analysis to calculate dissolution of Ibuprofen in the intestinal lumen.

153

Bile acids

Keane et al. found mean bile acid output for phase I, II, III, IV of the MMC to be 0.01, 1.42, 0.43 and 0.16 mmol/h, respectively [30]. Kalantzi et al. administered 250 mL of water containing 10 mg/mL of PEG 4000 to fasted dogs and recovered contents from a jejunal fistula in 22 ml aliquots, and analyzed bile salt and phospholipid content of pooled samples [31]. They found the bile salt content to be 2.41 and 2.94 mM for samples containing the first 20% and 40% of recovered PEG, respectively. Phospholipid content was below the limit of quantification in both samples. Given the range of MMC phase durations and the average bile output values above, the total amount of bile delivered to the small intestine during a complete phase would range from 0.45 to 0.63 mmol. Assuming a small intestinal volume of 100 ml, the concentration of bile salts would range from about 4.5-6.3 mM, and assuming a small intestinal volume of 50 ml, it would range from 9.0-12.7 mM. Given these reports it is likely that bile acid content in the fasted dog ranges from about 3-13 mM, but likely toward the lower end of the range. The critical micelle concentration (CMC) of taurocholate, which has been reported as the major bile acid in the fasted dog stomach, is approximately 8 mM [32] [33]. Bile acid concentrations exceeding 8 mM could thus lead to changes in solubility and apparent permeability of Ibuprofen *in vivo*. Bile micelle solubilization of Ibuprofen was not taken into account in this analysis.

Ibuprofen properties

Ibuprofen is a non-steroidal anti-inflammatory drug (NSAID) widely used for the treatment of mild to moderate pain. It is characterized as a BCS II weak acid [34]. Several Ibuprofen properties of interest are described below and summarized in **Table 4.6**.

Solubility

One important parameter required for the present analysis is the solubility of Ibuprofen in canine intestinal fluids. Shaw and coworkers as well as Levis and

coworkers reported an intrinsic solubility of about 0.067 mg/ml and apparent pK_a of about 4.4 at 37 C [35], [36]. Ibuprofen is mostly unionized and thus has a low solubility at low pH, but is 98-99.9% ionized under typical conditions in the fasted dog intestine (pH range of about 6-7.5) with an expected 50-1,000-fold increase in solubility. As discussed above the bile salt concentration in the fasted dog intestinal is low, and is likely below the CMC of taurocholate, which has been reported as the most prevalent bile acid in the fasted dog intestine. In cases where bile acids are present in concentrations just above their CMC, the solubility increase due to ionization would likely be significantly higher than the expected solubility enhancement due to bile micelle solubilization at pH values above 6 when Ibuprofen is 98-99.9% ionized. Levis and coworkers report a 3.5-fold increase in solubility of Ibuprofen above the expected solubility based on a pH-solubility profile at a pH of 5.0 (80% ionized) and a taurocholate concentration of 15 mM [36]. Jinno and coworkers and Sheng and coworkers demonstrated buffer species and pH effects to be more important than surfactant effects in the case of BCS II acids piroxicam and ketoprofen, respectively [37], [38].

Effective intestinal permeation rate, P_{eff}, and absorption rate coefficient, k_a

A direct measurement of P_{eff} in the small intestine in dogs could not be found in the literature. However, measurements for P_{eff} of Ibuprofen in the rat jejunum and in caco-2 monolayers have been reported. Lane and coworkers measured P_{app} in rats using intestinal perfusion in a number of different buffers at pH values from 5.0 to 8.2 (98-99.9% ionized with the exception of FeSSIF) [39]. They found the normalized P_{app} (zero water flux) to be 1.1 X 10^{-4} cm/s. In rats they suggest absorption rate to be aqueous boundary layer (ABL) controlled due to the high value of P_{app}. Assuming P_{app} is ABL controlled the thickness h_{ABL} can be calculated by dividing the diffusion coefficient by P_{app}. Assuming D_{HA} to range from 7.6 to 8.0 X 10^{-6} cm^2/s based on the Hayduk-Laudie and Wilke-Chang estimation methods for ionized Ibuprofen in water at 37 C, the calculated apparent h_{ABL} in rats would be about 700 μm.

Heikkinen and coworkers measured the permeation rate of Ibuprofen

across caco-2 cell monolayers, and suggested that ABL resistance was likely the rate-limiting step to Ibuprofen permeation [40]. They reported ABL thicknesses to range from about 100 to 700 um depending on method (transwell or side-by-side preparation of cells) and stirring speed (previous publication) (which would make P_{app} equal to 0.95 X 10^{-4} cm/s to 3.5 X 10^{-4} cm/s). Apparent transcellular + paracellular permeation rates at pH 6.5 and 7.0, were 3.1 X 10^{-4} and 2.2 X 10^{-4}, respectively. These values reflect mostly transcellular permeation, as paracellular permeation was found to be insignificant in the caco2 membrane. However, in dogs paracellular permeation rate is likely to contribute to membrane permeation, as the dog intestinal membrane tends to have a larger pore radius than the caco-2 membrane [6]. Yee found P_{app} of Ibuprofen to be 0.53 X 10^{-4} cm/s in a radiolabeled Caco-2 transwell plate study at a pH of 6.5, which did not separate contributions from the apical ABL, cell monolayers, or basolateral ABL. It's likely that the P_{app} value reflects permeation across the apical ABL, which is dependent upon rotational speed (not given).

Observations that Ibuprofen permeation in the rat intestine and in caco-2 cell monolayers is controlled by the ABL are in line with Sugano, who stated that ABL permeation is the rate-limiting step for the majority of lipophilic compounds [41] [6]. Given this assumption, P_{app} in dogs could be estimated using the thickness of the ABL in dogs *in vivo*. Levitt et al. determined the "resistance to absorption resulting from poor stirring of luminal contents, R_{LUM}" in the jejunum of conscious beagle dogs by measuring absorption of glucose and [^{14}C] warfarin and found average values to range from about 33-57 μm for the two compounds depending on perfusion rate [42]. The corresponding estimates for ABL limited permeation rate (D_{HA}/h_{ABL}) of Ibuprofen in the canine small intestine would be 23.6 X 10^{-4}, and 13.7 X 10^{-4}, respectively (Assuming D_{HA} = 7.8 X 10^{-6} cm^2/s). However, it is unlikely that Ibuprofen permeation rate is as high as that of glucose, and is in part limited by transcelluar or paracellular permeation as well. Entrapment of Ibuprofen in bile micelles could slow down diffusion of Ibuprofen across the ABL due to the smaller diffusion coefficient of micelles and also decrease the amount of free drug available at the surface of the membrane for

absorption. However, it is unlikely that bile micelle solubilization is a critical factor due to the low concentrations of bile salts that are likely in the fasted dog intestine [6]. It is likely that the above estimate of 13.7×10^{-4} to 23.6×10^{-4} would be at the very upper limit of the estimate.

Levitt and coworkers also measured R_{LUM} in rats and found it to be about 100 μm [42]. With the estimate for P_{eff} in rats mentioned above, the relative values of R_{LUM} in rats and in dogs can be used to estimate dog P_{eff}. Assuming $P_{eff, species} = SEF_{species} \times D/h_{species}$, where SEF is the "surface area enhancement factor" built in to the P_{eff} measurement and likely different from each species, $P_{eff, rat}/ P_{eff, dog} = SEF_{rat}/SEF_{dog} \times h_{dog}/ h_{rat}$, so $P_{eff, rat}/ P_{eff, dog} = 0.5$. Assuming a value of about 1.1×10^{-4} cm/s in rat, $P_{eff,dog}$ would be 2.2×10^{-4} cm/s.

Another method of estimating P_{eff} in dogs is using existing correlations from the literature. While no direct correlation between rat and dog intestinal permeation rates could be found several correlations between rat and human permeation rates exist. Using the correlation generated by Fagerholm and coworkers the estimated permeation rate in humans assuming passive diffusion is 4.0×10^{-4} cm/s. An estimate of human permeation rate using a correlation developed by Sun and coworkers is 3.8×10^{-4} cm/s (correlation without Verapamil). The software GastroPlus^{TM} (Simulations Plus, Inc., Lancaster, CA) has a built in correlation for estimating dog intestinal permeation rate based on human permeation rate. Using the estimated human permeation rates of 4.0×10^{-4} cm/s the estimated dog permeation rates using GastroPlus^{TM} is 9.7×10^{-4} cm/s. The larger P_{eff} in dogs compared to humans for Ibuprofen using this correlation is in line with a statement by Sugano that P_{eff} in dogs may generally be larger than for humans for paracellular permeation [6].

Finally, P_{eff} of Ibuprofen in dogs can be estimated by comparing permeation in caco-2 monolayer experiments to those of propranol, for which permeation rate in dogs has been measured. Lipka et al. found propranolol permeability in dogs to be 4.2×10^{-4} cm/s. Ibuprofen and propranol have been found to have similar caco-2 permeation rates in two studies [43]. At pH 7.0 Heikkinen found propranolol (0.29% unionized) had an apparent permeability of

157

4.3 X 10^{-4} cm/s, which is similar to Ibuprofen (0.28% ionized) at that pH. Yee et al found P-app of ibuprofen and propranolol to be 0.53 X 10^{-4} and 0.28 X 10^{-4} cm/s, respectively [44]. Thus, it is possible that *in vivo* in dogs Ibuprofen has a similar P_{eff} as propranolol.

Taking the above analyses into account it is likely that P_{eff} for Ibuprofen in dogs ranges from about 2 X 10^{-4} cm/s to 25 X 10^{-4} cm/s. With the estimated range of A/V of 4-26 cm^{-1}, the potential range of k_a (equal to A/V X P_{eff}) is 2.9 – 234 h^{-1}.

Dimensionless numbers

Amidon and coworkers outlined the dimensionless numbers, dose number (Do), dissolution number (Dn) and absorption number (An) used extensively in estimating dissolution and absorption behavior of small molecules *in vivo* [45]. Do for Ibuprofen as defined by Amidon using the highest marketed dose in 250 ml of buffer at the minimum solubility is relatively high at 47.7. For the purposes of this analysis, Do was defined in terms of dose given to dogs (80 mg) divided by the estimated dog intestinal volume (50 ml) divided by the calculated saturation solubility in the pH range of 6.2 to 7.2. Using this definition, Do ranges from 0.04-0.37. Given this low range of values, dissolution of Ibuprofen in dogs is not expected to be solubility rate determined. Dn was determined at two different median particle diameters (87 and 330 µm) and two different bulk pH values (6.2 and 7.2), assuming a small intestinal residence time of 3 hours. Dn ranged from 14-41 for the 87 µm median diameter particles, and 1-3 for the 330 µm median diameter particles. Since Dn is greater than or equal to 1 in all cases, a residence time of 3 hours should likely be sufficient to allow for complete or near-complete dissolution in all cases. Finally, An was calculated by defining two different values for A/V (4 and 26 cm^{-1}), P_{eff} ranging from 2 X 10^{-4} to 25 X 10^{-4} cm/s, and a small intestinal residence time of 3 hours. Under these conditions An ranges from 9-702, suggesting enough time for complete absorption of Ibuprofen in the dog small intestine. Refer to **Table 4.6**.

Additional physicochemical properties

       Additional Ibuprofen properties of aqueous diffusion coefficient, true density and apparent partition coefficient were calculated using established methods or taken from the results of measurements reported in the literature and are included in **Table 4.6**.

<u>Analysis of *in vivo* oral solution absorption profile</u>

       A schematic of the transport process of Ibuprofen in solution from ingestion to appearance in the bloodstream is included in **Figure 4.1**. The potential rate-determining steps are emptying from the stomach into the intestinal lumen and absorption from the intestinal lumen into the intestinal membrane. Precipitation of drug in the bulk solution was not considered due to the estimated low values of Do in the intestinal pH range. It is assumed that once drug appears in the intestinal membrane, appearance of drug in the blood stream happens instantaneously as described in **Equation 4.32**, where $M_{b,t}$ is mass of drug in the bloodstream.

(4.32) $\dfrac{dM_{ab,t}}{dt} \approx \dfrac{dM_{b,t}}{dt}$

       Based on an analysis of dog physiology, three possible scenarios exist to describe the potential rate determining transport steps. In the first case, emptying from the stomach is fast compared to absorption into the intestinal membrane ($dF_{e,t}/dt \gg dF_{ab,t}/dt$), so absorption into the intestinal membrane is the rate-limiting step to appearance in the blood stream. In case 2 ($dF_{e,t}/dt \approx dF_{ab,t}/dt$), both processes affect the rate of appearance of drug in the bloodstream. In case 3 ($dF_{e,t}/dt \ll dF_{ab,t}/dt$), emptying from the stomach into the intestinal lumen is the rate-limiting step to appearance of drug in the bloodstream. Based on the estimated range of k_{ge} (1.2 to 4.6 h^{-1} (first order) or 2.1-3.9 fraction of the dose/h (zero order)) and corresponding estimates for $dF_{e,t}/dt$, as well as for k_a (2.9 h^{-1} to 234 h^{-1}) and corresponding estimates for $dF_{ab,t}/dt$ (Refer to **Table 4.7**), it is likely

that the *in vivo* oral absorption process will fall under case 2 ($dF_{e,t}/dt \approx dF_{ab,t}/dt$) or case 3 ($dF_{e,t}/dt << dF_{ab,t}/dt$).

A MATLAB® script was written using the equations described for gastric emptying and absorption outlined in previous sections to determine the transport parameters of k_{ge} and k_a that describe the *in vivo* data for the Ibuprofen oral solution. It was assumed that the entire dose was emptied and absorbed in a continuous manner through zero-order or first-order gastric emptying and first-order intestinal absorption processes. Equations were solved iteratively every 0.5 seconds. The system was closed with respect to all other species besides dissolved drug. For example, emptying of stomach fluid into the intestinal lumen, secretion of fluid from the intestinal wall, pancreas and liver into the intestinal lumen, absorption of fluid from the intestinal lumen into the intestinal membrane, and passage of fluid from the small intestine into the large intestine were not considered. **Table 4.8** includes the values of the transport parameters used in the analysis. All parameters except for k_a and k_{ge} were fixed. The approach taken was to set k_a to the minimum value and vary k_{ge} until it reached a value that explained the *in vivo* data (*in vivo* and simulated input into plasma versus time curves overlapped). The value of k_a was then set to the maximum value and k_{ge} was varied until it reached a value that explained the *in vivo* data.

Analysis of *in vivo* solid oral tablet absorption profiles

For the solid oral tablets, the major transport steps were considered to be emptying of solid drug particles from the stomach, dissolution of solid drug particles in the intestinal lumen and absorption of dissolved drug from the intestinal lumen into the intestinal membrane. A schematic of the process is included in **Figure 4.2**. Disintegration of tablets was assumed to occur in the stomach instantaneously since they were formulated to be rapidly disintegrating and observed to disintegrate within seconds *in vitro* (data not shown). Dissolution of solid drug particles in the stomach was assumed to be minimal since the drug was given with a low pH buffer and Ibuprofen has a very low solubility at low pH.

160

Precipitation of drug in solution was assumed not to occur due to the low values of estimated Do *in vivo*.

Assuming the drug concentration in the intestinal fluid is far from saturation, the initial fraction of dose dissolved as a function of time, $dF_{d,o}/dt$, is described by **Equation 4.33**, where r_o is the initial particle radius, $h_{eff,o}$ is the initial effective boundary layer thickness adjacent to the particle surface and $C_{s,o}$ is the initial drug concentration at the particle surface. As the particles dissolve this value becomes smaller. An estimate of $dF_{d,o}/dt$ for both particle sizes was calculated at bulk pH values of 6.2 and 7.2. Assuming a bulk small intestinal pH of 6.2 (and a particle surface pH of 5.6) $dF_{d,o}/dt$ is 12.4 and 2.4 h^{-1} for the 87 and 330 µm particle diameters, respectively. Assuming a bulk small intestinal pH of 7.2 (and a particle surface pH of 6.1) this value is equal to 37.6 and 7.2 h^{-1} for the 87 and 330 µm particle diameters, respectively. Given these estimates it is likely that dissolution will be one of the rate-determining steps to absorption into the bloodstream. Relative rates of stomach emptying, dissolution, and absorption normalized with respect to dose are included in **Table 4.7**.

$$(4.33) \quad \frac{dF_{d,o}}{dt} = 4\pi r_o^2 \cdot N \cdot \frac{D_{HA}}{h_{eff,o}} \left(1 + \frac{h_{eff,o}}{r_o} \right) \frac{C_{s,o}}{Dose}$$

A MATLAB® script was written to demonstrate drug transport from spherical particles and describe the *in vivo* data generated in dogs. The script takes into account stomach emptying, dissolution and absorption into the intestinal membrane. A monodisperse particle size distribution was assumed due to the very narrow particle size distributions of the sieve cuts and to simplify the MATLAB® script. The system was closed with respect to all species except for drug (as described above in the oral solution sections). The first step was to determine the initial pH and concentrations of buffer in the bulk intestinal fluid, initial pH and concentrations of buffer and drug species at the particle surface, and initial pH and concentrations of buffer at the intestinal wall. An iterative

approach was used to solve for the following unknown values by evaluating equations every 0.5 seconds[2]:

1.   Mass of drug emptied from the stomach
2.   Mass of drug dissolved in the small intestinal fluid
3.   Mass of drug absorbed into the intestinal membrane
4.   pH and concentrations of buffer and drug species in the bulk intestinal fluid
5.   pH and concentrations of buffer and drug species at the particle surface
6.   pH and concentrations of buffer and drug species at the intestinal wall

Table 4.8 includes the values of the transport parameters used in the analysis. Values for k_{ge} and k_a determined using the oral solution dosage form were fixed in the analysis of the solid drug particle data. A range in bulk intestinal pH values (6.2 to 7.2) was investigated in the analysis. Predicted and actual profiles were compared.

Results

Particle size distributions

The particle size distributions of the two different particle size sieve cuts of Ibuprofen are shown in **Figure 4.3** and particle characteristics of the two sieve cuts are shown in **Table 4.9**. The median particle diameters of the small and large particle size sieve cuts were 87 µm, and 330 µm, respectively. Particles were lath shaped, and particle size distributions were very narrow as suggested by the D90/D50 values of 1.2 for both sieve cuts.

Ibuprofen tablets

---

[2] The total dose of drug was divided into 16 increments (10, 20, 30, 40, 50, 55, 60, 65, 70, 75, 80, 85, 90, 95, 97 and 99 % of the dose). Calculations were performed in a stepwise manner assuming the given % of dose was emptied as a bolus over a pre-calculated time period.

Average tablet mass was 500.2 mg (range of 500.0-500.5 mg) and 500.3 mg (range of 500.0-500.6 mg) for the 87 μm and 330 μm median sieve cut, respectively. The true density of the Ibuprofen blend was calculated to be 1.44 g/cm^3. Solid fractions ranged from 0.86-0.87 for both particle size sieve cuts using compression pressures ranging from 96.5-98.0 MPa and 96.5-103.5 MPa for the 87 μm and 330 μm median sieve cut, respectively. Tablet composition can be found in **Table 4.1**. Tablets were observed to disintegrate rapidly in buffer (data not shown).

Plasma profiles and pharmacokinetic analysis

Individual plasma concentration profiles of Ibuprofen in each of the six dogs for the IV, oral solution, small particle size tablet and large particle size tablet dosage forms are included in **Figure 4.4**. The average plasma concentration profile for the IV formulation is included in **Figure 4.5**, and average plasma concentration profiles for the oral solution, small particle size tablet and large particle size tablet are shown in **Figure 4.6**. Multiple peaks in the individual and average plasma concentration profiles were observed for all four formulations. For the IV formulation, a double peak was observed around 6 hours after dosing in two of the dogs, and plateaus in the plasma profiles occurred around 6 hours in the other four dogs. For the oral solution, small particle size tablet and large particle size tablet multiple peaking occurred in virtually all of the dogs throughout with pronounced peaking on average at 2.5 h, 1.5 h and 1.5 h, respectively.

Pharmacokinetic parameters determined from the non-compartmental analysis are shown in **Table 4.10**. Average T_{max} for the oral solution, small particle size tablet and large particle size tablet was 0.45 ± 0.11, 1.17 ± 0.21 and 1.08 ± 0.20, respectively. Results of student's t-tests showed a significant difference in T_{max} between the oral solution and the solid oral dosage forms, but no difference between the two solid oral dosage forms. Average C_{max} for the oral solution, small particle size tablet, and large particle size tablet was 62.80 ± 5.51, 62.52 ± 5.26, and 42.10 ± 6.57, respectively. Results of students t-tests did not

show a significant difference in C_{max} between the oral solution and small particle size tablet dosage forms, but did suggest a significant difference in C_{max} between the oral solution and large particle size tablets, as well as between the small particle size and large particle size tablets. Fraction bioavailable for the oral solution and small particle size tablet exceeded unity, with values of 1.27 ± 0.07 and 1.36 ± 0.14, respectively. Fraction bioavailable for the large particle size tablet was 0.94 ± 0.11. A two-compartment disposition model fit the individual and average IV data well (Refer to **Figure 4.5** and **Table 4.11**). Individual and average absorption profiles for the oral solution, small particle size tablet and large particle size tablet dosage forms determined from numerical deconvolution are included in **Figure 4.7**. Multiple plateaus in the individual and average input into plasma profiles were observed for all three oral dosage forms and the cumulative mass input into plasma exceeded the administered dose of 80 mg. Average mass input into plasma for the oral solution, small particle size tablet and large particle size tablet at 8 hours after dosing was 110 mg, 118 mg and 101 mg, respectively. A time lag for the average input into plasma profiles was not evident.

In vivo transport parameters

The individual and average profiles for input of the oral solution into plasma displayed multiple plateaus, with an average of about 90 mg in plasma at the first plateau in the average profile within the first hour after dosing. A time lag was not evident. The unknown parameters of average emptying and absorption rate coefficients were determined by examining the first hour of the average input into plasma profile and normalizing the curve by dividing by 90 mg as the theoretical dose. As shown in **Figure 4.7a**, average input into plasma during the first hour resembles first-order kinetics. Assuming the minimum estimated value of k_a of 5.2 h^{-1} (as described in a previous section), gastric emptying would have had to occur extremely quickly, with either a first-order emptying coefficient of about 90 h^{-1} ($t_{0.5}$ of about 0.5 min) or greater, or a zero-order emptying coefficient of about 67.5 fraction of dose/h or greater to describe the average absorption

kinetics (Refer to **Figure 4.8a**.). This case would describe a complete absorption rate limitation. However, assuming the maximum estimated value for k_a of 234 h^{-1}, emptying of the solution in a first-order rather than a zero-order manner would have had to occur to describe the observed absorption profile, with a first-order k_{ge} of 5.2 h^{-1} ($t_{0.5}$ of 8 min, Refer to **Figure 4.8b**.). Using this value of k_{ge} the absorption curve would be equally well described using a k_a as low as about 150 h^{-1}. Given that the aforementioned k_{ge} and k_a values fall within the extremes of the estimated ranges based on the mechanistic analysis, it is possible that the actual values fall somewhere in between, leading to a mixed gastric-emptying and absorption-rate limitation (Refer to **Figure 4.8c**).

The individual and average input into plasma profiles for the small particle size tablet displayed multiple plateaus, with an average of about 65 mg input into plasma at the first plateau in the average profile within the first hour after dosing. A time lag in the average profile was not evident. The unknown parameters of emptying and absorption rate coefficients were determined by examining the first hour after dosing and normalizing the curve by dividing by 65 mg as the theoretical dose. Assuming absorption rate << gastric emptying rate, with the same values of k_a and k_{ge} used for the solution (k_a of 5.2 h^{-1} and a k_{ge} of at least 83 h^{-1}), pH values ranging from 6.4-7.2 in the intestinal lumen yield predictions that describe the *in vivo* data, with a pH of 6.7 describing the profile best (Refer to **Figure 4.9a**). Assuming gastric emptying rate << absorption rate, with the same values for k_{ge} and k_a used for the solution (k_{ge} of 5.2 h^{-1} and the maximum estimated value of k_a of 234 h^{-1}), pH values ranging from about 6.2 to 6.5 describe the *in vivo* profile, with a value of 6.2 describing the profile best (Refer to **Figure 4.9b**).

The individual and average input into plasma profiles for the large particle size tablet displayed multiple plateaus, with an average of about 75 mg absorbed at the first plateau in the average profile within the first two hours after dosing. A time lag in the average profile was not evident. The unknown parameters of emptying and absorption rate coefficients were determined by examining the first hour after dosing and normalizing the curve by dividing by 75 mg as the

theoretical dose. Assuming absorption rate << gastric emptying rate, with the same values of k_a and k_{ge} used for the solution (k_a of 5.2 h^{-1} and a k_{ge} of at least 83 h^{-1}), pH values ranging from 6.4-7.2 in the intestinal lumen yield predictions that describe the majority of the *in vivo* profile (Refer to **Figure 4.10a**). Assuming gastric emptying rate << absorption rate, with the same values for k_{ge} and k_a used for the solution (k_{ge} of 5.2 h^{-1} and the maximum estimated value of k_a of 234 h^{-1}), pH values ranging from about 6.2 to 6.5 describe the majority of the *in vivo* profile (Refer to **Figure 4.10b**).

Predictions using optimal transport parameters together with the *in vivo* profiles for all three oral dosage forms are shown in **Figure 4.11**. **Figure 4.11a** shows the scenario for absorption rate << gastric emptying rate, assuming a pH of 6.7 in the intestinal lumen. **Figure 4.11b** shows the scenario where gastric emptying rate << absorption rate, assuming a pH of 6.4.

Discussion

Plasma profiles and pharmacokinetic analysis

The multiple peaks displayed in the plasma concentration time profiles were unexpected. Numerous examples of multiple peaking phenomena with immediate release dosage forms exist in the literature with causes including discontinuous gastric emptying, enterohepatic recirculation, binding to highly-perfused organs, solubility-limited absorption, site-specific absorption, complexation, gastric secretion-enteral reabsorption and effects of surgery and anesthesia [46]. While the cause of multiple peaks in the present analysis is unknown, possible explanations include discontinuous gastric emptying, enterohepatic recirculation and binding to a highly perfused organ followed by slow release into plasma. As irregular gastric emptying profiles do not always lead to double peaks in plasma concentration profiles, it has been suggested that the time period and extent of interruption in gastric emptying as well as the relative rates of intestinal absorption and elimination from plasma for the drug of interest have an effect on the appearance of double peaks in plasma profiles.

166

Metsugi and coworkers examined the relationship between β (rate constant for elimination from central compartment for a two-compartment disposition model) and k_a and found that when $k_a \gg \beta$, the decline in the plasma concentration profile is dictated by β and double peaks are diluted. However, when $\beta \gg k_a$, the decline in plasma concentration is determined by the absorption rate making it more likely that multiple peaks in the gastric emptying curve would lead to double peaks in the plasma concentration profile [47]. Oberle and Amidon found variable gastric emptying to increase the likelihood of double peaks in the plasma concentration profiles of cimetidine in the fasted state in humans [48]. The elimination rate of cimetidine from the central compartment was stated to be 0.79 h^{-1}, with intestinal first order absorption rate coefficients ranging from 3.8 to 6.6 h^{-1} in the duodenum and jejunum. Thus k_a was only about 5-8 times greater than k_{10}, meaning that decline in plasma concentration could have been regulated by both absorption and elimination, especially during cases where there was a large interruption in gastric emptying. However, in this study β is equal to 0.19 ± 0.03 h^{-1} and average k_a ranges from about 5.2 to >150 h^{-1}, so k_a is upwards of 30 – 800 times greater than β, making it likely that the decline in the plasma concentration profile is dictated by β and double peaks due to variable and discontinuous gastric emptying would be diluted. Also, multiple peaking continued to occur later than three hours after dosing, which is much longer than a typical MMC cycle (~2 h). It is unlikely that any fraction of the drug substance would be left in the stomach longer than one MMC cycle.

Enterohepatic recirculation could be a possible explanation for the multiple peaking phenomena. This hypothesis is supported by the fact that multiple peaking occurred for the IV dosage form and because the theoretical dose of 80 mg was exceeded in all dogs for the oral solution and small particle size dosage forms, and in 6 out of 8 dogs for the large particle size tablet. Enterohepatic recirculation has been confirmed in a study in rats and has been suggested to occur in dogs in veterinary literature [49] [50]. Bischoff and Mukai state that drugs eliminated in bile such as Ibuprofen can undergo enterohepatic recirculation [51]. The multiple peaking phenomena and the fact that the theoretical dose was

exceeded may have lead to the values of oral fraction bioavailability being greater than unity.

The pretreatment protocol for the oral solution was designed to raise gastric pH to keep the drug in solution in the stomach in the event that the natural gastric pH was low. This design should, in theory, prevent precipitation and subsequent re-dissolution, leading to the fastest input into plasma compared with the solid oral dosage forms. The pretreatment protocols for the small and large particle size tablets were designed to keep gastric pH low to prevent dissolution of drug in the stomach in the event that the natural gastric pH was high. This approach should, in theory, lead to dissolution of the particles upon entry into the small intestine at a pH around 6.2-7.2, with faster dissolution of the particles with the smaller size distribution (80 μm median) compared to the particles with the larger particle size distribution (330 μm median). The corresponding expected trend for rate of input into plasma was oral solution > small particle size tablet > large particle size tablet. As shown in **Figure 4.7d**, within the first 45 minutes to one hour after dosing the average rate of input into plasma appears to follow the expected trend, although the difference may not be statistically significant, especially for the small and large particle size tablets. The expected trend for T_{max} was oral solution < small particle size tablet < large particle size tablet. While T_{max} is higher for the solid oral tablets compared with the oral solution, there is no statistical difference between the small and large particle size tablets. This lack of difference could likely be attributed to enterohepatic recirculation or another physiological phenomenon, as theoretically the dissolution rate of the smaller particles is appreciably faster than the dissolution rate of the larger particles in the pH range of 6.2-7.2. The T_{max} for the oral solution (0.45 ± 0.11 h) is in line with values reported by Ishii and coworkers (0.5 h) and Kimura and coworkers (0.35 h) [1], [2]. However, results for the solid oral dosage forms are not necessarily in line with those from these authors. Ishii and coworkers observed an increase in T_{max} of 1.25 h (from 1.25 to 2.5 h) when increasing in size from 16 to 149 μm (an increase of 133 μm). Kimura and coworkers observed an increase in T_{max} of 1 h (from 0.5 to 1.5 h) when increasing in size from < 10

168

µm to 10-200 µm (and increase of ~ 100 µm). In our study T_{max} was about 1 hour for both the 87 um and 330 um median diameter particles, despite an increase in median particle diameter of almost 250 µm. It was expected that C_{max} would decrease as a function of particle size. While C_{max} was the same for the oral solution and small particle size tablet (62.80 ± 5.51 vs. 62.52 ± 5.26 µg/ml), it did decrease for the large particle size tablet (42.10 ± 6.57 µg/ml). Ishii and coworkers saw a decrease in C_{max} as a function of particle size (~48, ~38, and ~32 µg/ml for the oral solution, small particle size tablet, and large particle size tablet, respectively). However, Kimura saw similar C_{max} values for the oral solution and small particle size tablet (~40 µg/ml) and a smaller value for the large particle size tablet (~37 µg/ml). Multiple peaks were not observed in the data published by Kimura and coworkers or Ishii and coworkers.

In vivo transport parameters

Estimation of the *in vivo* transport parameters was conducted using the average profiles for input of drug into plasma. For the oral solution the average profile appeared to follow first-order kinetics. However it does seem to deviate slightly from a first order shape suggesting that perhaps either gastric emptying rate or absorption rate may have occurred more quickly over about the first 30 minutes and then slowed down over the last 30 minutes. Inspection of the individual profiles for each dog suggests that they follow mostly a first-order rate with a lag time between about 0 and 5 minutes after dosing (**Figure 4.7a**). Evaluation of the profile with the fastest input into plasma suggested a 0-2.5 min lag time with a first order input rate of about 25-40 h^{-1}, while evaluation of the profile with slowest input into plasma suggested or a lag time of about 5 min with a first order input rate in the range of about 4 $h^{-1.}$

It is difficult to conclude whether or not gastric emptying rate into the small intestine or absorption of drug from the intestinal lumen into the intestinal membrane was the rate limiting for the oral solution or whether both processes affected the rate at which drug entered systemic circulation. When examining the average profile, it is evident that if gastric emptying were rate limiting, then the

gastric emptying process would have had to occur via a first order process with a constant k_{ge} of about 5.2 h^{-1} over the one-hour period with a k_a at least 15-20 times greater in magnitude ($k_a > 75$ h^{-1}) (**Figure 4.8a**). Given the estimated range for k_a of 2.9 to 234 h^{-1} (**Table 4.7**), this scenario is certainly possible. If absorption into the membrane were the rate-limiting step to systemic availability, then average gastric emptying would have occurred near instantaneously via either a zero or first order emptying process, with the entire dose empting within about 10 minutes after ingestion. The average k_a would have been about 5.2 h^{-1}, with a k_{ge} value at least about 15 times higher in magnitude ($k_{ge} > 75$ h^{-1}) (**Figure 4.8b**). While the literature data testing gastric emptying rates of small volumes of solution cited in this paper suggest much longer total emptying times, rapid emptying of the 6 ml of solution that the drug was dissolved in could have emptied within 10 minutes, particularly if it happened to be dosed close to phase III of the fasted motility cycle, or if the motility cycle were to have switched to a fed state pattern, perhaps due to the anticipation of a meal. **Figure 4.8c** shows the two scenarios discussed above ($k_{ge} >> k_a$ and $k_a >> k_{ge}$), together with a curve describing a process whereby both gastric emptying and absorption were rate determining, with $k_{ge} = k_a = 10.4$ h^{-1}. Comparing the three curves suggests that the mixed scenario may be more unlikely since it acts to slow down appearance into systemic circulation at the beginning of the profile and speed it up at the end of the profile, which is opposite of the observed *in vivo* profile for the average rate of input into plasma. As mentioned in a previous section, and as shown in **Table 4.8**, all three scenarios are possible, but the absorption rate has the potential to be much higher than the gastric emptying rate, which may make the scenario where absorption rate << emptying rate less probable.

Predictions for the solid oral tablets were made assuming either absorption rate << gastric emptying rate or gastric emptying rate << absorption rate. Due to the dissolution process, several additional variables were added to the transport analysis (Refer to **Table 4.7**). Namely, the pH in the small intestinal lumen is unknown, but expected to be in the range of about 6.2-7.2. Without knowing the true value of pH (and knowing the likely inter- and intra-subject

170

variability) transport parameters were selected using pH values spanning the entire range. For the scenario assuming absorption rate << gastric emptying rate, pH values in the range of 6.4-7.2 describe the data for both particle sizes (**Figure 4.9a-b**). For the scenario assuming gastric emptying rate << absorption rate, pH values within a narrower range of 6.2-6.5 describe the data (**Figure 4.10a-b**).

It was attempted to select common transport parameters that would describe input rate into plasma for all three oral dosage forms. As shown in **Figure 4.11a**, assuming absorption rate << gastric emptying rate, with k_a = 5.2 h^{-1}, k_{ge} = 83 h^{-1} and a pH of 6.7, provides reasonable predictions for the rate of input into plasma for all three dosage forms. As shown in **Figure 4.11b**, assuming absorption rate >> gastric emptying rate, with k_a = 234 h^{-1}, k_{ge}= 5.2 h^{-1} ($t_{0.5}$ of 8 min) and an average pH of 6.4 in the intestinal lumen, leads to the generation of profiles that describe the average rate of input into plasma for all three dosage forms reasonably well. While not shown for the small and large particle size tablets, mid-range values for absorption rate and gastric emptying rate would likely also explain profiles for the small and large particle size tablets.

Bioperformance dissolution methodology

In addition to using a physiological transport analysis to aid in predicting the bioperformance of a drug product, it is useful to have *in vitro* tools to help understand the effects of physical and chemical properties on kinetic processes such as dissolution rate. While computational techniques are essential in making estimates of the possible range in performance of a drug product in the highly complex GI tract, it can be challenging to accurately predict the dissolution rate of all drug products. For instance, dissolution rate of a polydisperse drug substance in a complex formulation in a buffer containing multiple components, such as bile acids and lipids, may be difficult to accurately predict. While simple USP testing methods can be useful in some cases, particularly for Quality Control (QC), they do not accurately reflect physiological conditions and thus tend not to be useful tools to predict the bioperformance of a drug substance. It is necessary to develop a bioperformance dissolution methodology based on physiological

conditions of the species of interest as well as on the physicochemical characteristics of the drug substance and drug product itself.

In general, a BCS II weak acid such as Ibuprofen should have a low extent of dissolution in the stomach if the gastric pH is low, and a rapid and high extent of dissolution in the moderate pH of the small intestine in which the drug substance is partially or fully ionized. Therefore, it should not be necessary to include a gastric compartment in the dissolution test for the purpose of studying the rate of dissolution in a low pH medium, in which little dissolution is likely to occur. Based on the transport analysis it was observed that both when absorption rate is relatively low (5.2 h^{-1}) and when it is high (> 150 h^{-1}) the concentration of Ibuprofen in the intestinal lumen is low compared to its saturation solubility. It was observed that the maximum percent drug saturation reached for all simulations was less than about 30% (data not shown). These simulations were performed assuming a net and continuous intestinal volume of 50 ml. However, it is likely that the volume of intestinal liquid could range from much lower-to-much-higher and be contained within several separate liquid pockets. This phenomenon has been observed in humans in the literature [11]. Under these conditions it is likely that percent drug saturation had little-to-no effect on dissolution rate. If so, then the *in vitro* bioperformance test could be carried out using sink conditions in the intestinal compartment to understand the dissolution component at moderate pH conditions (~6.5). Rather than adding an intestinal compartment into which drug could partition (simulating absorption into the membrane) and keeping a physiologically relevant intestinal volume (such as 50 ml) a large volume of intestinal medium could be used, such as 900 ml. However, to predict the entire absorption profile (and generate a level A IVIVC) then one would have to account for either gastric emptying rate, absorption rate into the membrane or a combination of the two, depending on which process or processes contribute to appearance into plasma. Both processes could theoretically be accounted for computationally, depending on the complexity of the drug product.

Alternatively, one could design an *in vitro* system that includes the gastric emptying component, absorption component or both. Based on the *in vivo* results for Ibuprofen, it is possible that gastric emptying rate << absorption rate into the membrane. If that is the case, then gastric emptying is likely a rate-limiting step to systemic availability. To achieve a Level A IVIVC it would be necessary to introduce drug particles into an *in vitro* intestinal compartment at a physiologically relevant rate, for instance in a first-order manner. This could be achieved by either choosing to include a gastric compartment (such as with 250 ml of a pH 2 buffer) in the test and pumping gastric fluid and non-dissolved drug particles at a relevant rate into the intestinal compartment (such as with 900 ml of pH 6.4 10.5 mM sodium phosphate buffer), or by manually introducing drug particles into the intestinal compartment at a similar rate. *In vitro* systems containing separate gastric and intestinal compartments have been discussed in the literature, and are often used to study weakly basic drug substances, and those that undergo physical form changes [52] [53]. Using the mechanistic transport analysis, simulations for such an *in vitro* test, deemed "gastric single phase" for each particle size tablet are included in **Figure 4.12** (dashed lines). Disintegrated drug particles are emptied with a k_{ge} of 5.2 h^{-1} into 900 ml of "intestinal buffer" (in this case pH 6.4 10.5 mM sodium phosphate buffer). In these simulations effects of gastric fluid on pH in the intestinal compartment were not taken into account, and values for h_c, ρ, D, C_s, pK_a, and saturation solubility are included in **Table 4.12.** While h_c was assumed to be 25 µm for the *in vivo* simulations, a value of 20 µm was deemed to be more appropriate for the *in vitro* simulations, as discussed in Chapter 3. Since it is assumed that k_a *in vivo* is very large, absorption into the membrane *in vivo* should be nearly instantaneous so the amount of drug in solution in the aqueous buffer *in vitro* could be correlated directly with input rate into plasma. Simulations for both particle sizes predict the *in vivo* results well. **Figure 4.13** shows the same curves for the gastric single-phase test, but also includes a curve showing the rate of emptying of drug from the stomach into the intestinal compartment (open circles). The curve representing the percent of dose in solution for the small particle size tablet is nearly parallel to the curve

representing percent of dose emptied into the small intestinal compartment, meaning that the rate of appearance of drug in solution is mostly determined by emptying rate, with the dissolution process simply adding a time lag or delay in appearance of drug in solution. The curve representing the percent of dose in solution for the large particle size tablet is not parallel to the curve representing percent of dose emptied into the small intestinal compartment, showing that the rate of appearance of drug in solution is determined either in all or in part by dissolution rate.

Figure 4.14 shows simulations for *in vitro* tests carried out in a gastric single phase, versus a typical USP-type dissolution test. For the small particle size tablet, the curve showing appearance of drug in solution for the test without a gastric compartment predicts very rapid and nearly linear input into plasma. However, the curve representing appearance of drug in solution for the gastric single-phase test shows a delayed appearance in solution with a different shape, again confirming the contribution of gastric emptying rate. For the large particle size tablet, the two curves representing appearance of drug in solution for an *in vitro* USP-type test and a gastric single phase test are nearly parallel, showing that the rate of appearance in solution is controlled mostly by the dissolution rate, with the gastric emptying process just adding a delay or shift in appearance of drug in solution. For both particle sizes, the USP-type dissolution test underestimates the time to reach 75% of the initial dose dissolved by about 17 minutes.

Based on the *in vivo* results for Ibuprofen, it is also possible that absorption rate into the membrane << gastric emptying rate. In this case an *in vitro* system that includes an absorption component (but no gastric emptying component) would be necessary to achieve a Level A IVIVC. Simulations in such an apparatus for each particle size tablet were performed, using the transport analysis outlined for dissolution from spherical drug particles and partitioning into an organic medium, with transport parameters shown in **Table 4.12**. These simulations assume an interfacial permeation rate (equal to D_a/h_a, see **Equation 4.31**) of 3.0 X 10^{-3} cm/s across the aqueous-organic interface, vessel diameter of

174

10.1 cm^3 (USP II apparatus), buffer volume of 165 ml (to achieve the desired A/V and partitioning rate coefficient as outlined in Chapter 2 (and reference [54]), and a dose scaled to the larger volume, equal to 65 mg * (165ml/50ml) for the small particle size tablet and to 765 mg * (165ml/50ml) for the large particle size tablet. The amount of drug in the organic medium as a function of time can be correlated directly with input into plasma *in vivo*. As shown in **Figure 4.12** the simulations for both particle sizes predict the results well. While a pH of 6.4 was chosen for these simulations, a pH of 6.7 also leads to reasonable predictions of the *in vivo* input rate into plasma for both particle sizes (data not shown). As demonstrated in **Figure 4.15**, dissolution rate appears to be the rate-limiting step to appearance of drug in solution in 1-octanol for both the small and large particle size tablet (green and red lines are parallel).

As shown in **Figure 4.12**, developing an *in vitro* test based on either scenario (emptying rate << absorption rate or absorption rate << emptying rate) should lead to reasonable predictions for input into plasma *in vivo*.

Conclusions

The purpose of this study was to determine *in vivo* dissolution and absorption rates of the model compound ibuprofen in dogs under well-controlled conditions and determine potential bioperformance dissolution methodologies that could be used to establish IVIVCs. A simple mechanistic analysis was developed to understand the influence of the major transport steps to appearance of drug in the bloodstream *in vivo* (gastric emptying, dissolution, and absorption), and also to aid in developing potential *in vitro* bioperformance dissolution methodologies.

Two different types of *in vitro* bioperformance dissolution methodologies were proposed depending on the relative rates of gastric emptying and intestinal absorption, both of which are predicted to be adequate in describing the average *in vivo* plasma profiles for the two different particle size tablets using simulations based on an *in vitro* transport analysis. For the case when gastric emptying rate

<< absorption rate, it is advised to introduce the drug particles at a physiologically relevant rate (such as in a first order manner) to a large volume of intestinal buffer. For the case when absorption rate << gastric emptying rate, it is advised to empty drug particles as a bolus into a physiological volume of intestinal buffer, but to include a separate absorption compartment into the dissolution test (such as using an organic medium such as 1-octanol). Further data, which was not collected in the present study, such as an independent measure of the gastric emptying rate and/or effective permeation rate of Ibuprofen across the dog intestine, would be required to select the most relevant methodology. Due to the absence of either a gastric emptying step or an intestinal absorption step, a conventional single-phase (e.g. USP) dissolution test was predicted to significantly underestimate time to reach seventy-five percent of the dose into plasma.

While in actuality *in vivo* drug transport displays significant complexity and heterogeneity, an advantage of the current analysis is that it can be used to describe average transport rates in a manner that allows for selection of simple and practical *in vitro* biopredictive methodologies. While the current work is specific to Ibuprofen, it could be extended to other BCS 2 weak acids, simply by modifying the drug physicochemical properties required in the mechanistic model, which can all be measured or estimated *a priori* of *in vivo* data. More sophisticated techniques such as Monte Carlo simulation would be useful in explicitly describing the *in vivo* heterogeneity arising from highly variable physiological and drug physicochemical properties.

Tables and Figures

Table 4.1. Rapidly disintegrating tablet formulation compositions

Component	Mass per tablet *mg*	% per tablet *%*
Ibuprofen	80.0	16.0
Spray-dried lactose	201.0	40.2
Microcrystalline cellulose ph 102	201.0	40.2
Crospovidone	18.0	3.6
Total	500.0	100.0

Table 4.2. Compositions of pretreatment solution and Ibuprofen oral solution

	Ibuprofen acid *M*	BIS-TRIS Base *M*	HCl *M*	NaCl *M*	Total volume *L*
Pretreatment solution	0	0.5	0.13192	0.0217	0.019
Ibuprofen oral solution	0.06466	0.5	0	0	0.006

Table 4.3. Composition of pretreatment solution to administer prior to tablet dosing

	HCl *M*	KCl *M*	NaCl *M*	Total volume *L*
Pretreatment solution	0.013	0.05	0.097	0.024

Table 4.4. Ratio of small intestinal surface-area-to-liquid volume (A/V)

% compression %	a cm	b cm	Length cm	Surface area cm^2	A/V cm^{-1}
90	0.1	0.7	451.3	1417.8	28.4
89	0.06	0.70	410.48	1289.56	25.79
85	0.1	0.7	301.8	948.2	19.0
75	0.13	0.70	182.94	574.74	11.49
50	0.25	0.66	96.25	302.37	6.05
25	0.38	0.60	70.80	222.42	4.45
0	0.50	0.50	63.66	200.00	4.00

Table 4.5. Comparison of dog and human liquid secretion and absorption in the small intestine

Parameter	Value in dogs	Value in humans
Salivary secretions (resting) (ml/min)	0.34-4.24[a]	0.25-0.35[b]
Gastric acid secretions (basal) (mM/h)	0.1[c]	0.4-5.8[d]
Intestinal secretion of HCO^{3-} (mM/h)	0.2[e]	0.38[f]
Pancreatic secretions (mEq/L)	23.9[g]	20-25[h]
Bile input rate (ml/day/kg)	19-36 [i] (190-360 ml/day assuming 10 kg dog)	2.2-22.2[j] (154-1554 ml/day assuming 70 kg human)
Water absorption rate (ml/min)	0.171 +/-0.044 (basal)[k] 1-2.4 ml/min (after 75 ml of solution with varying tonicity)[l]	4.7 (average per day)[m]

[a] Reference [14], [b] Reference [15], [c] Reference [16], [d] Reference [17], [e] Reference [18], [f] Reference [19], [g] Reference [20], [h] Reference [21], [i] Reference [22], [j] Reference [23], [k] Reference [24], [l] Reference [25] [m] Reference [26]

Table 4.6. Ibuprofen physicochemical properties and dimensionless numbers relevant to the current analysis

Property	Value
Diffusion coefficient in water at 37 °C	7.5×10^{-6} (unionized)[a]
	7.6×10^{-6} cm^2/s (ionized)[a]
Intrinsic solubility at 37 °C	0.066 mg/ml[b], 0.068 mg/ml[c]
Apparent pK_a at 37 °C	4.4[b, c] (not corrected for ionic strength)
True density	1.1 g/cm^3 [d]
Log partition coefficient (pH 1.5)	3.8 [e]
Dose number, Do	47.7 [f], 0.37 [g], 0.04 [h]
Dissolution number, Dn	14 (87 µm, bulk pH 6.2)[i], 1 (330 µm, bulk pH 6.2)[i], 41 (87 µm, bulk pH 7.2)[i], 3 (330 µm, bulk pH 7.2)[i]
Absorption number, An	9 (A/V = 4 cm^{-1}, P_{eff} = 2×10^{-4} cm/s)[j], 702 (A/V = 26 cm^{-1}, P_{eff} = 25×10^{-4} cm/s)[j]

[a] Calculated using the method of Hayduk and Laudie [48].

[b] Shaw and coworkers based on best-fit curve to pH-solubility profile [49].

[c] Levis and coworkers based on best-fit curve to pH-solubility profile (ionic strength values of buffers ranged from 0.15 to 0.37 M) [39].

[d] Reference [50].

[e] Reference [6].

[f] Do = Maximum dose/250 ml/minimum solubility. Based on maximum dose of 800 mg and minimum solubility of 0.067 mg/ml, ref [47]

[g] Do = dose given to dogs/estimated dog intestinal volume/calculated C_s in bulk medium at pH 6.2 (80 mg/50 ml/4.3 mg/ml)

[h] Do = dose given to dogs/estimated dog intestinal volume/calculated C_s in bulk at pH 7.2 (80 mg/50 ml/42.3 mg/ml)

[i] Dn = $3DC_s/\rho/r^2 \times t_{res}$, where C_s = pH at the particle surface (C_s = 5.6 for bulk pH 6.2, and C_s = 6.1 for bulk pH 7.2 for 10.5 mM phosphate) and t_{res} = 3 h, ref [47]

[j] An = A/V $P_{eff} \times t_{res}$, where t_{res} = 3 h, ref [47]

Table 4.7. Maximum estimated stomach emptying, dissolution and intestinal absorption rates for Ibuprofen

Median Particle Diameter	Stomach Emptying (First-order)[a] $dF_{e,t}/dt$	Dissolution[b] $dF_{d,o}/dt$	Absorption[c] $dF_{ab,t}/dt$
μm	*h^{-1}*	*h^{-1}*	*h^{-1}*
87		pH 6.2: 12.4	
	1.2 – 4.6	pH 7.2: 37.6	1.4 – 117
330		pH 6.2: 2.4	
		pH 7.2: 7.2	

[a] Calculated according to **Equations 4.9** and **4.10**.

[b] Calculated according to **Equation 4.33**, where $C_{s,o}$ = 5.6 for a bulk pH of 6.2, $C_{s,o}$ = 6.1 for a bulk pH of 7.2, $h_{eff,o} = h_c$ = 25 μm, and a dose of 80 mg. Additional parameter values can be found in **Table 4.6**.

[c] Calculated according to **Equations 4.26** and **4.27**, assuming the fraction of drug in solution in the intestinal lumen is never greater than 0.5.
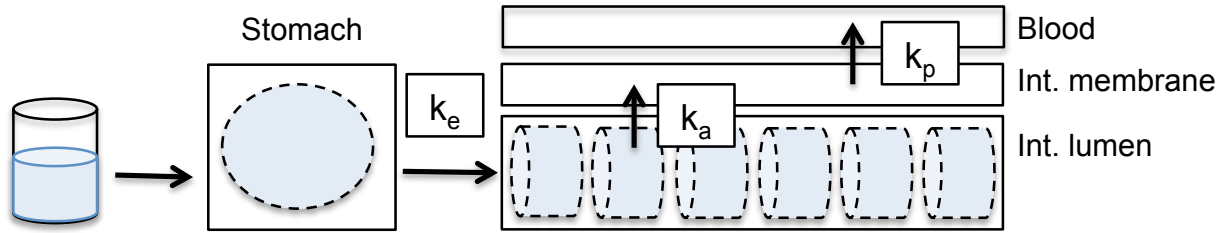
Figure 4.1. Flow diagram describing the major transport steps involved in drug absorption in dog after ingestion of the oral solution
Shaded portions outlined with dashed lines represent dissolved drug.
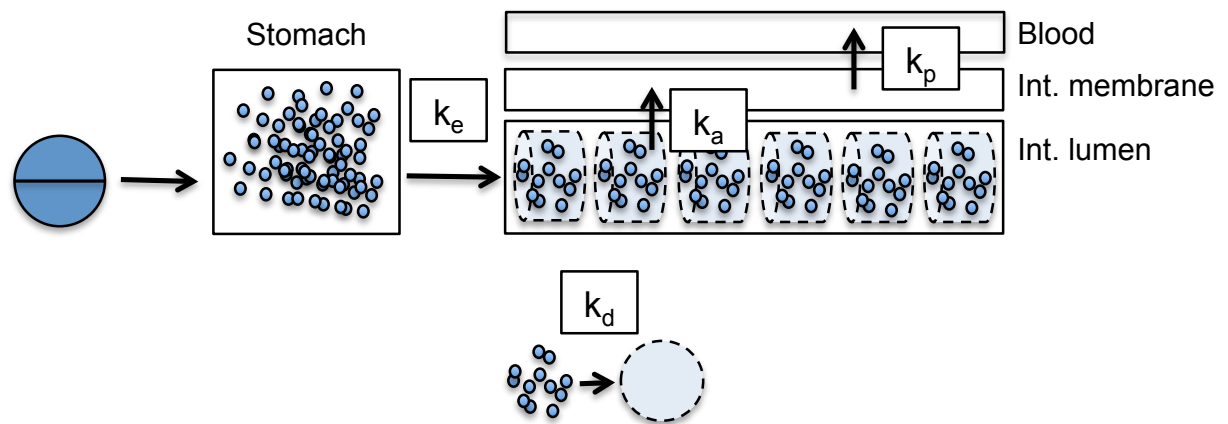
Figure 4.2. Flow diagram describing the major transport steps involved in drug absorption in dog after ingestion of tablets
Small circles represent solid drug particles and shaded portions outlined with dashed lines represent dissolved drug.

Table 4.8. Values of transport parameters used in the analysis of *in vivo* input into plasma profiles

Parameter	Oral solution	Solid tablets
A/V	Varied from 4 to 26 cm^{-1}	Varied from 4 to 26 cm^{-1}
P_{eff}	Varied from 2 X 10^{-4} cm/s to 25 X 10^{-4} cm/s	Varied from 2 X 10^{-4} cm/s to 25 X 10^{-4} cm/s
k_a (A/V* P_{eff})	2.9 – 234 h^{-1}	2.9 – 234 h^{-1}
Buffer species	Phosphate	Phosphate
Buffer pK$_a$	N/A	6.8
Buffer concentration	N/A	10.5 mM
pH	N/A	6.2 - 7.2
k_e (first-order)	1 to 90 h^{-1} ($t_{0.5}$ = 0.5-40 min)	1 - 90 h^{-1} ($t_{0.5}$ = 0.5-40 min)
k_e (zero-order)	1 to 67.5 fraction of dose/h ($t_{0.5}$ = 0.5-40 min)	
h_c	-	25 µm
ρ	-	1.1 g/cm^3
drug pK$_a$	N/A	4.4
D	N/A	7.6 X 10^{-6} cm^2/s
V_a	N/A	50 ml
Cs	N/A	0.068 mg/ml
Saturation solubility	N/A	$C_s(1+10^{pH-pKa})$
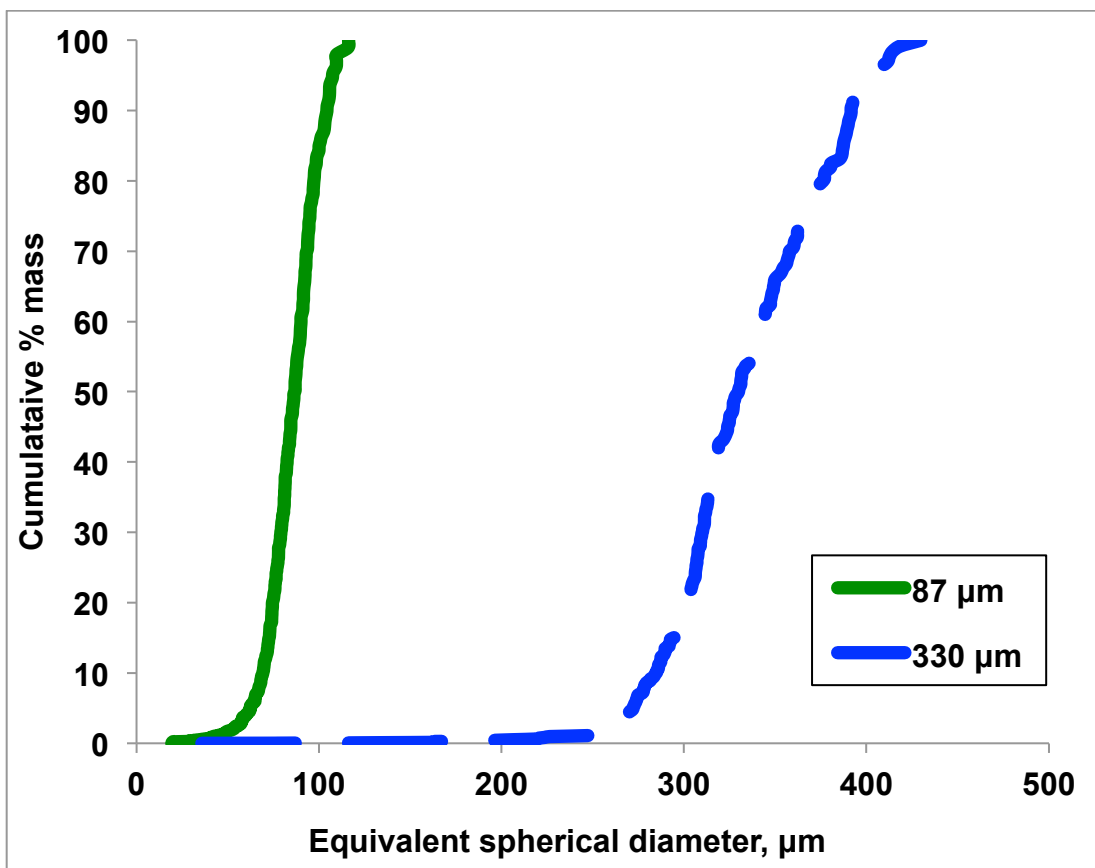
Figure 4.3. Particle size distributions by mass for the 80 and 310 µm median diameter sieve cuts of Ibuprofen determined using Microscopy

Table 4.9. Particle characteristics of 87 and 330 µm median diameter sieve cuts of Ibuprofen

Median equivalent spherical diameter by mass	Median L X W X T by mass	D90/D50	Mean thickness-to-width ratio	No. of particles measured
µm	*µm*	-	-	*no.*
87	116 X 73 X 41	1.2	0.56	307
330	479 X 294 X 134	1.2	0.45	300
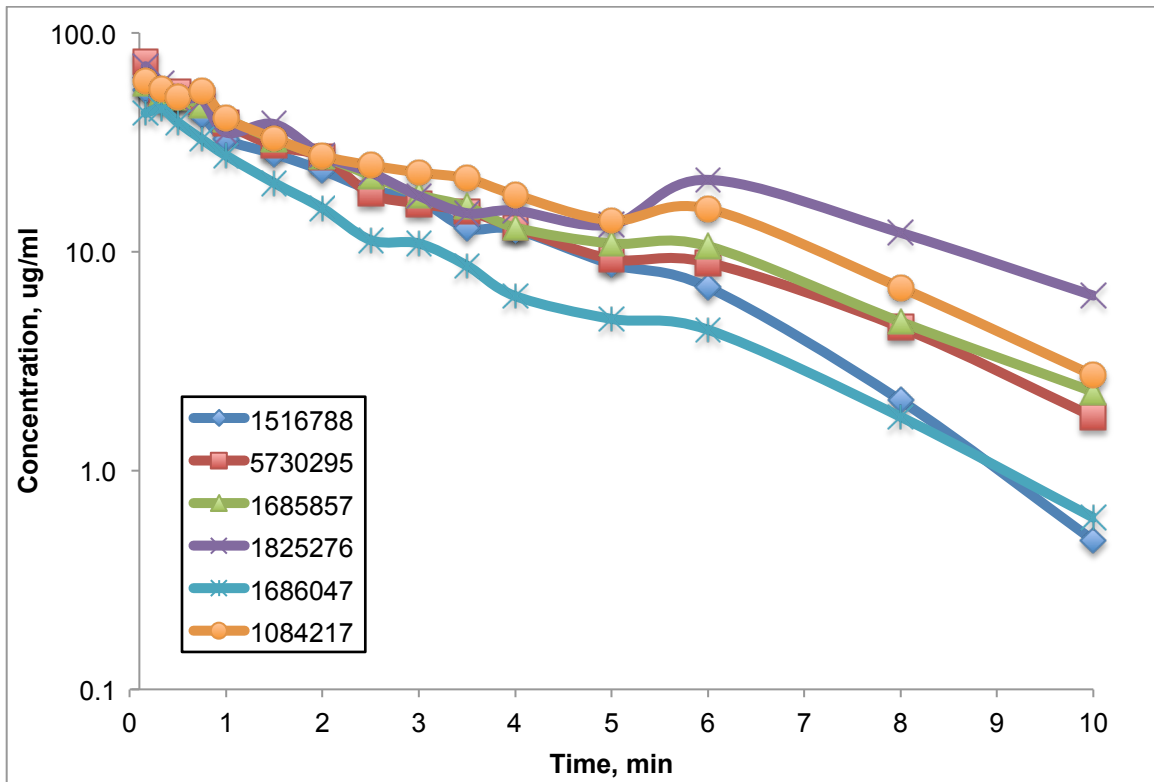
Figure 4.4a. Individual plasma concentration profiles for IV formulation
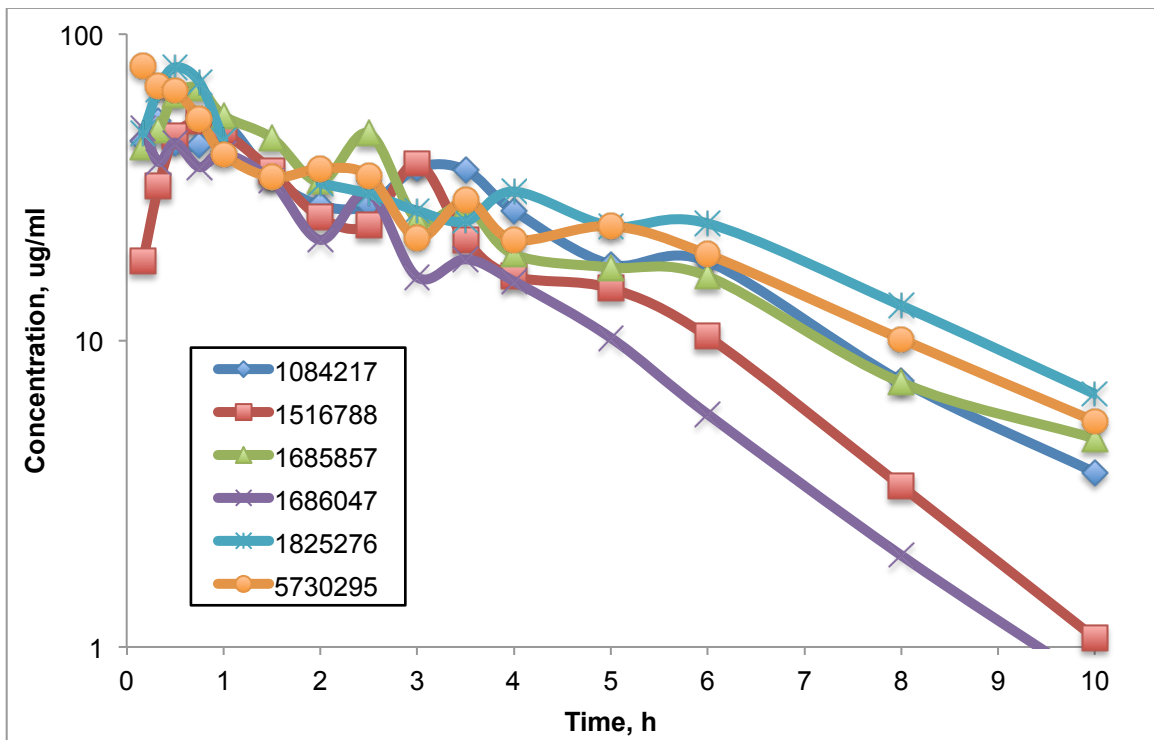
Figure 4.4b. Individual plasma concentration time profiles for the oral solution

184
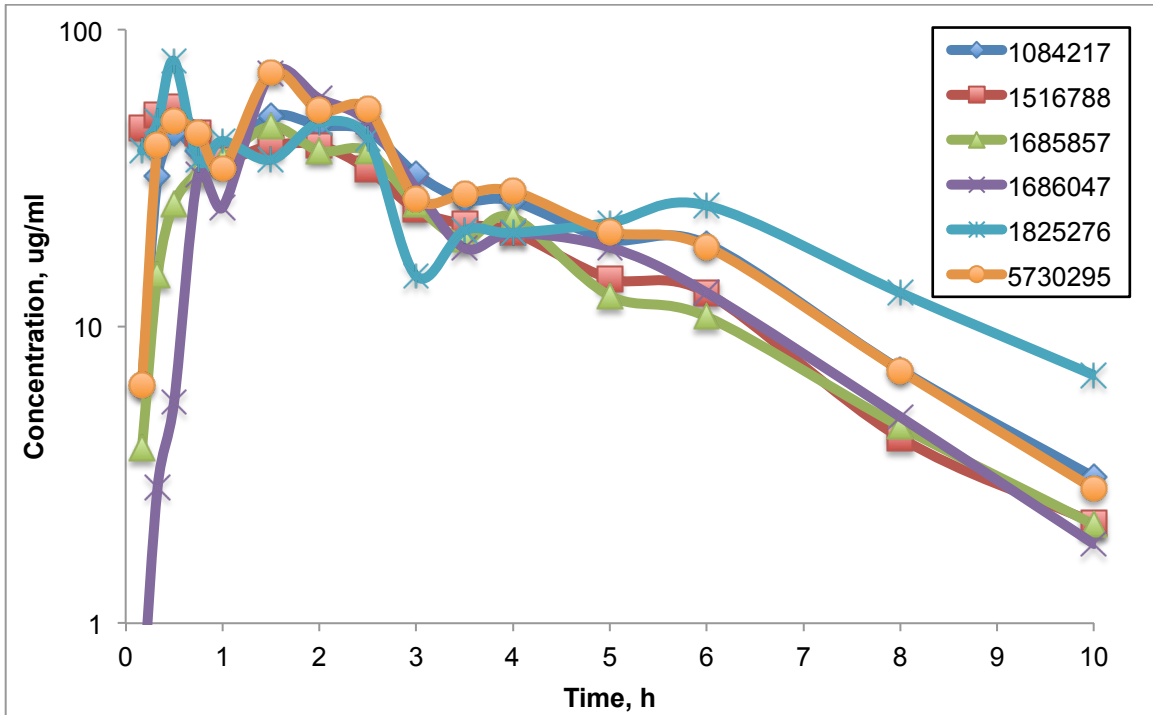
Figure 4.4c. Individual plasma concentration time profiles for the small particle size tablet
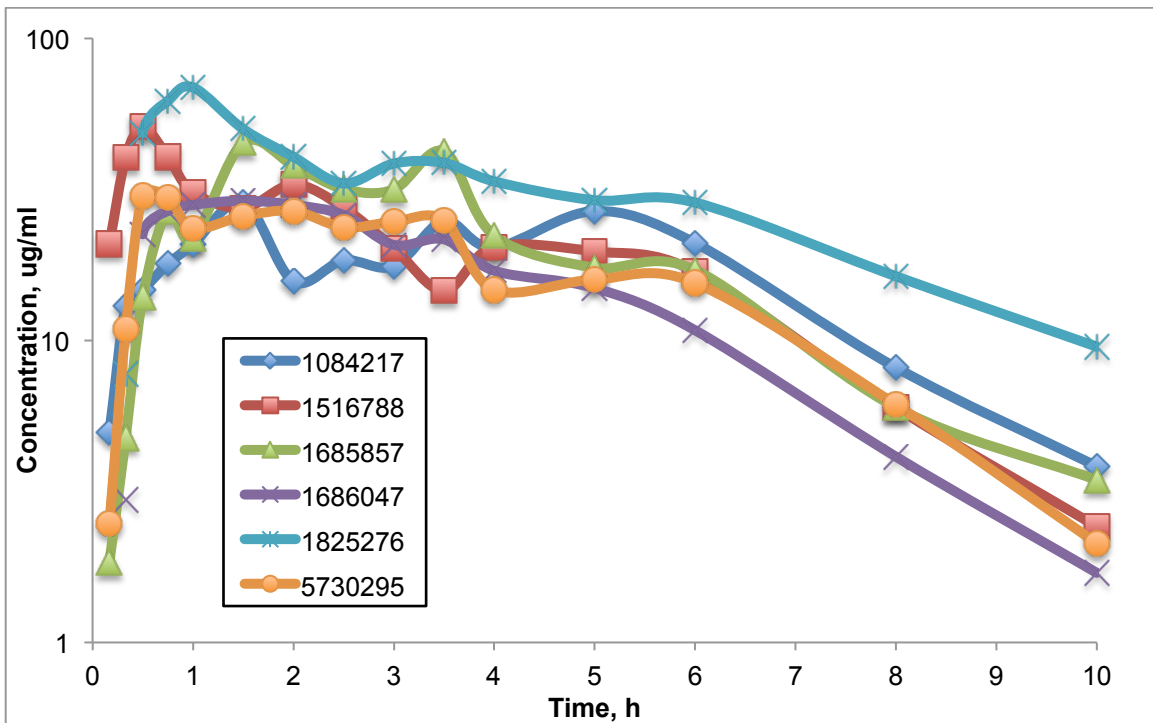
Figure 4.4d. Individual plasma concentration time profiles for the large particle size tablet
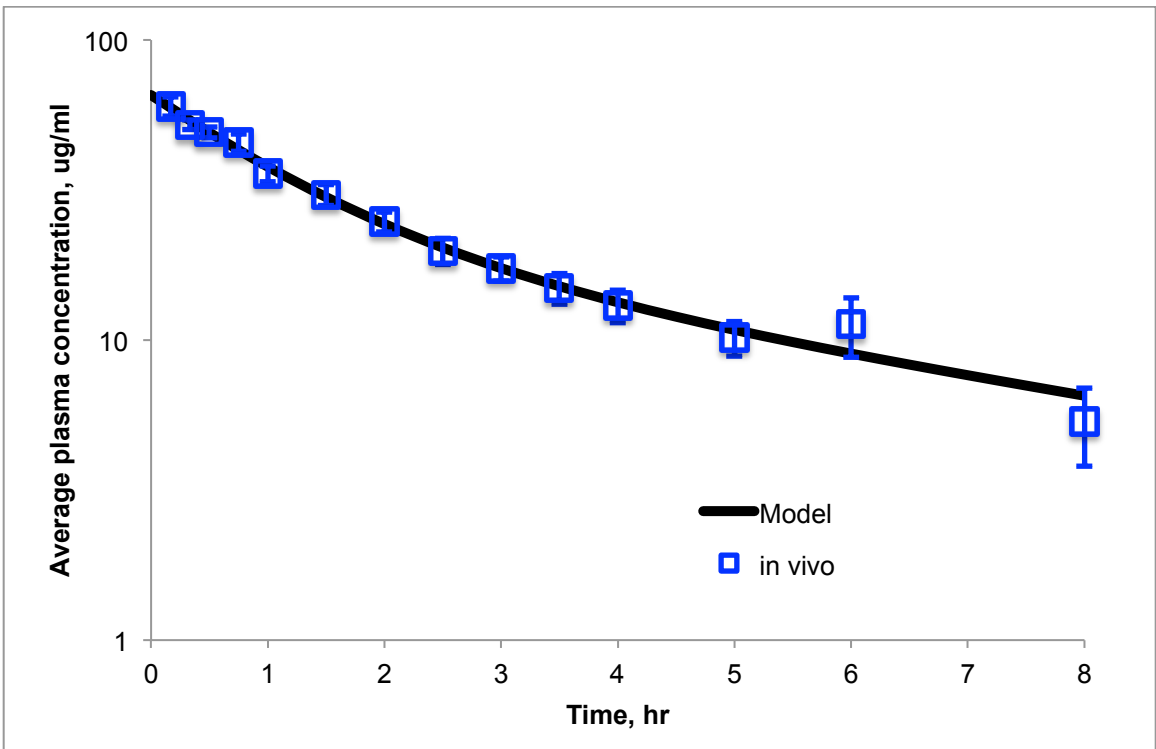
Figure 4.5. Average IV plasma concentration profile with two-compartment model
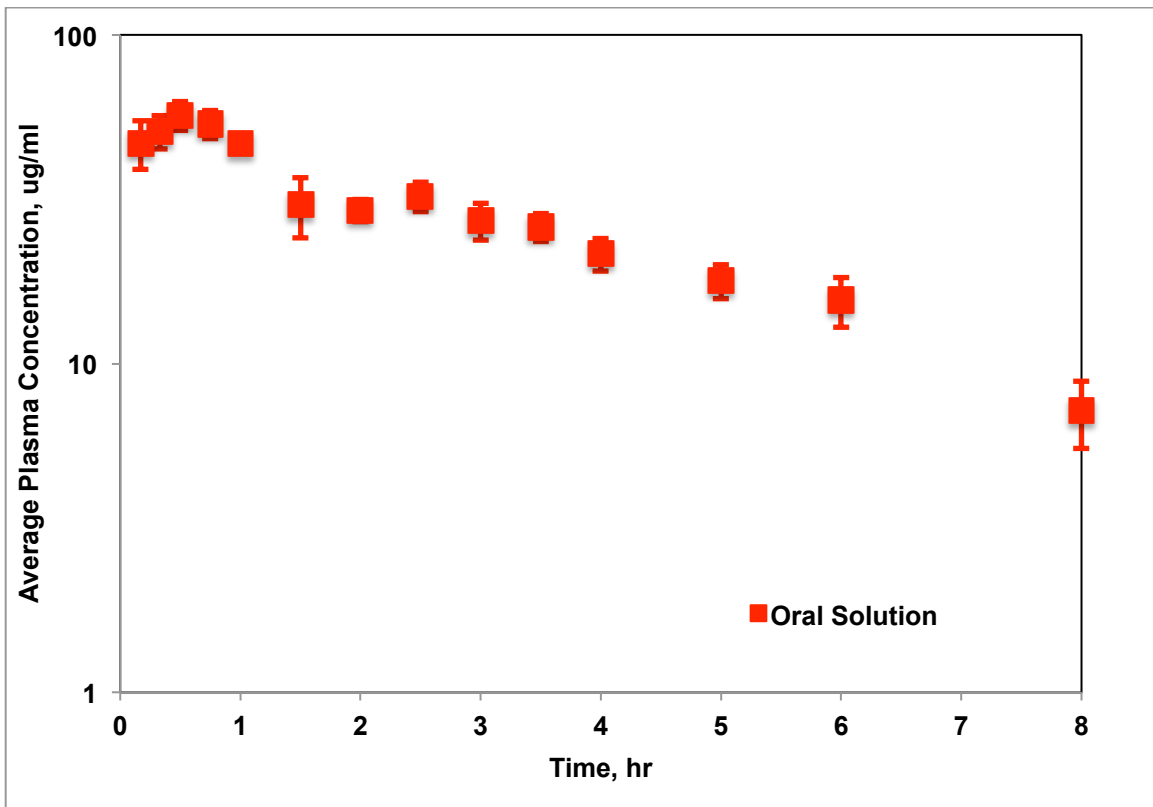
Figure 4.6a. Average plasma concentration time profile for the oral solution
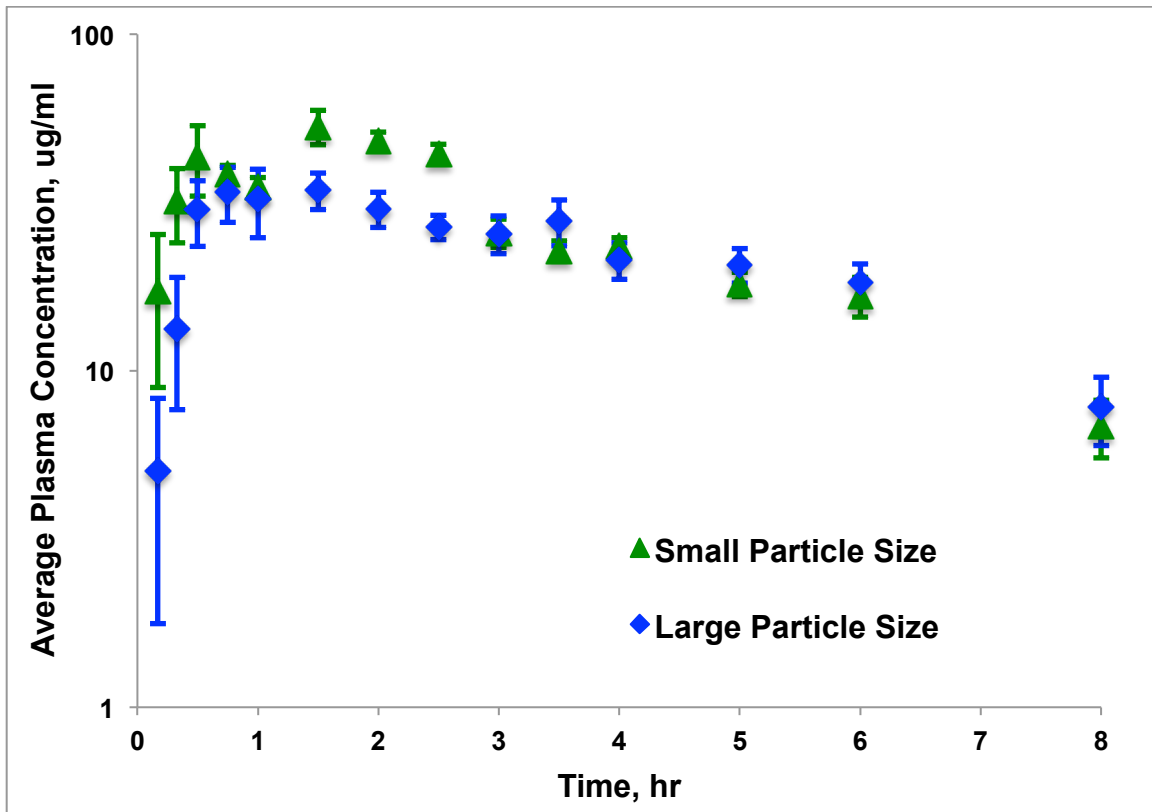
Figure 4.6b. Average plasma concentration time profiles for the small and larger particle size tablets

Table 4.10. Pharmacokinetic parameters generated from non-compartmental analysis performed on the first 8 hours after dosing.
Values are given as average of all six subjects ± SE

Parameter	IV	Oral solution	Small particle size	Large particle size
C_{max} (µg/ml)	60.38 ± 4.23	62.80 ± 5.51	62.52 ± 5.26	42.10 ± 6.57
t_{max} (h)	0.20 ± 0.03	0.45 ± 0.11	1.17 ± 0.21	1.08 ± 0.20
λ_z (h^{-1})	0.30 ± 0.03	0.39 ± 0.05	0.33 ± 0.03	0.34 ± 05
AUClast (µg/ml h)	155.72 ± 14.58	207.17 ± 16.53	204.41 ± 10.90	174.23 ± 19.71
AUCInf_obs (µg/ml h)	176.79 ± 21.38	218.76 ± 19.85	228.65 ± 17.06	204.93 ± 32.65
CL_obs (ml/h)	492.00 ± 68.24	492 ± 68.24	492 ± 68.24	384.27 ± 41.26
Vz_obs (ml)	1639.81 ± 128.83	1278.96 ± 140.80	1479.81 ± 89.44	1216.72 ± 148.80
F	-	1.27 ± 0.07	1.36 ± 0.14	0.94 ± 0.11

Table 4.11. Primary and secondary parameters from IV two-compartment disposition model

Parameter	Average	SE
A (µg/ml)	40.87	1.55
B (µg/ml)	25.77	1.55
Alpha (hr^{-1})	0.98	0.14
Beta (hr^{-1})	0.19	0.03
AUC (hr µg/ml)	202.40	33.42
k_{10} (1/hr)	0.36	0.05
k_{12} (1/hr)	0.29	0.07
k_{21} (1/hr)	0.51	0.13
C_{max} (µg/ml)	66.64	4.22
V1 (ml)	1225.65	80.62
CL (ml/hr)	451.65	73.20
Vss (ml)	2006.41	175.95
V2 (ml)	780.76	169.44
CLD2 (ml)	332.18	58.73
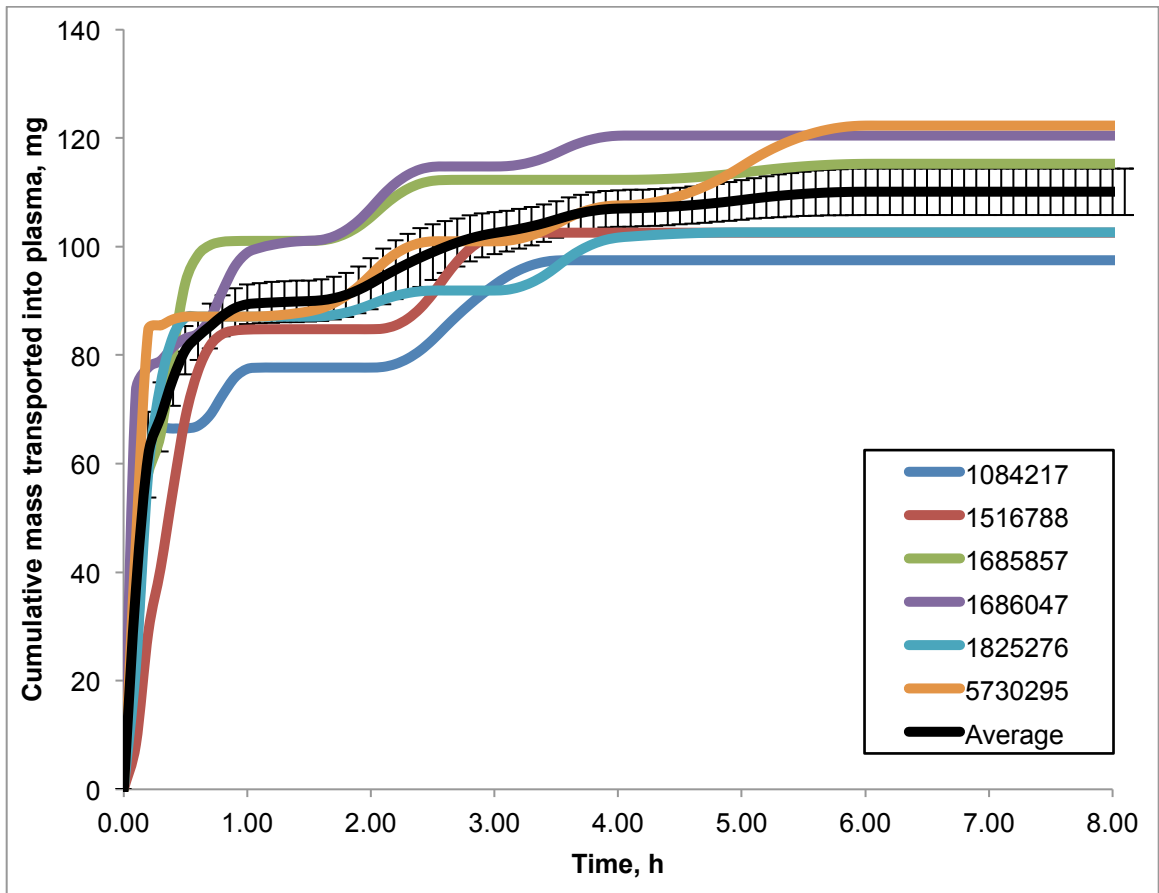
Figure 4.7a. Cumulative mass transported into plasma for the oral solution over 8 hours
Average profile is for all six subjects with error bars representing ± SE.
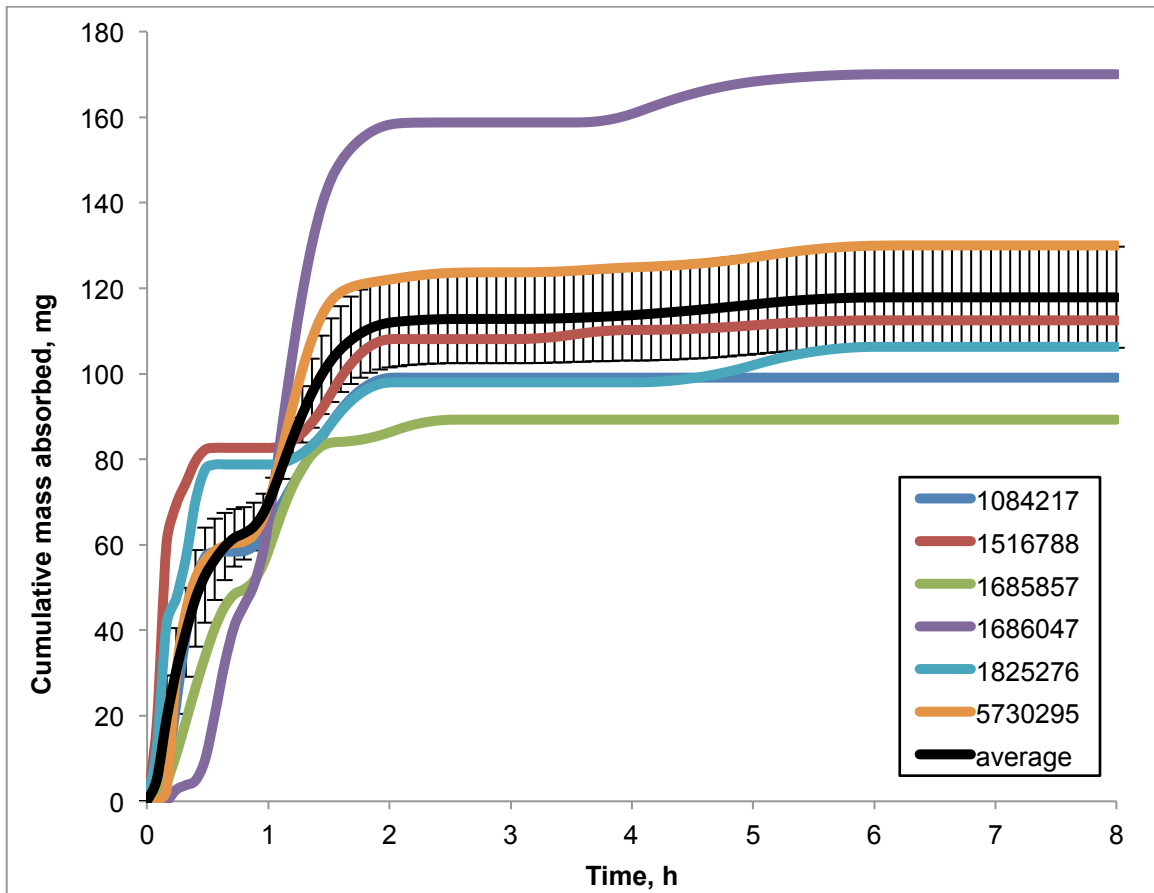
Figure 4.7b. Cumulative mass transported into plasma for the small particle size tablet over the first 8 hours
Average profile is for all six subjects with error bars representing ± SE.
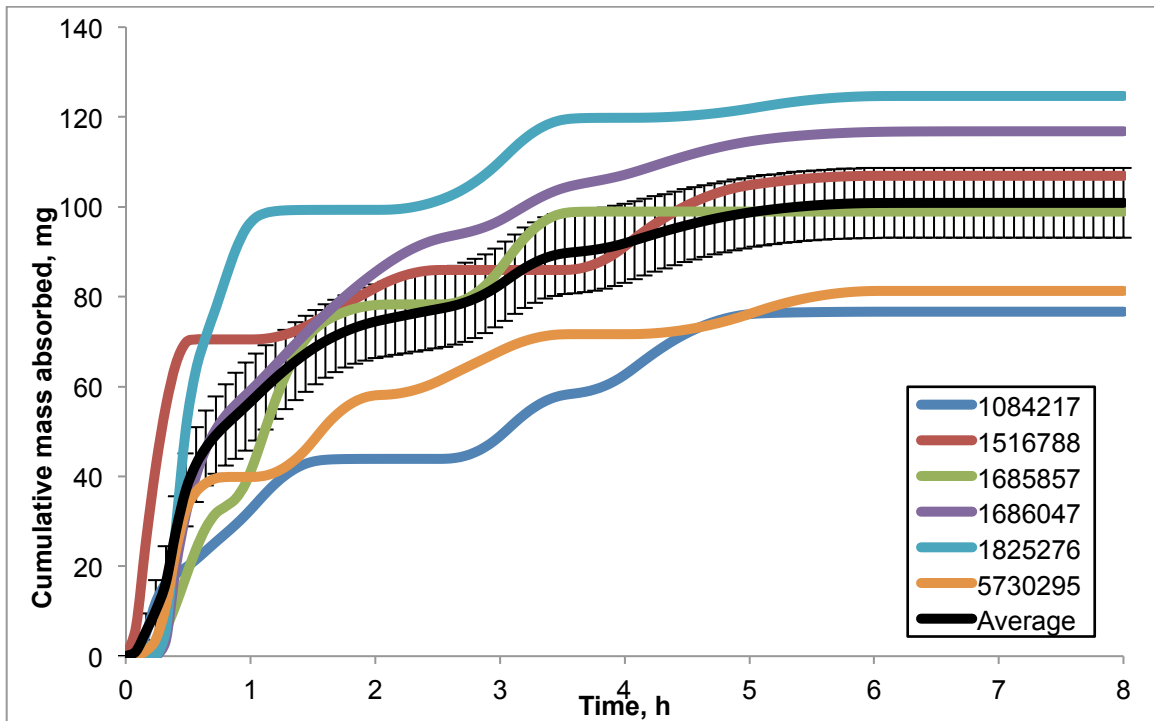
Figure 4.7c. Cumulative mass transported into plasma for the large particle size tablet over the first 8 hours
Average profile is for all six subjects with error bars representing ± SE.
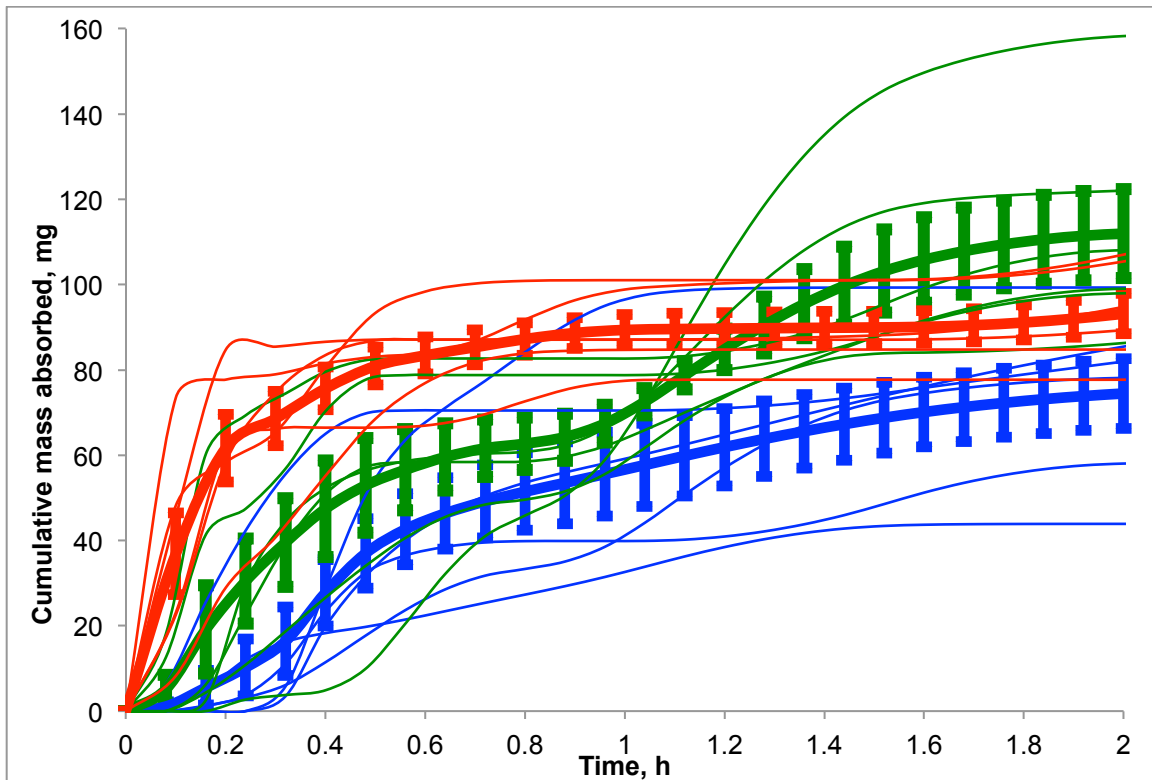
Figure 4.7d. Cumulative average and individual mass transported into plasma for the oral solution, small particle size tablet and large particle size tablet over the first 2 hours after dosing
Average profiles shown using thick lines and individual profiles shown using thin lines (oral solution in red, small particle size tablet in green and large particle size tablet in blue). Error bars represent ± SE.
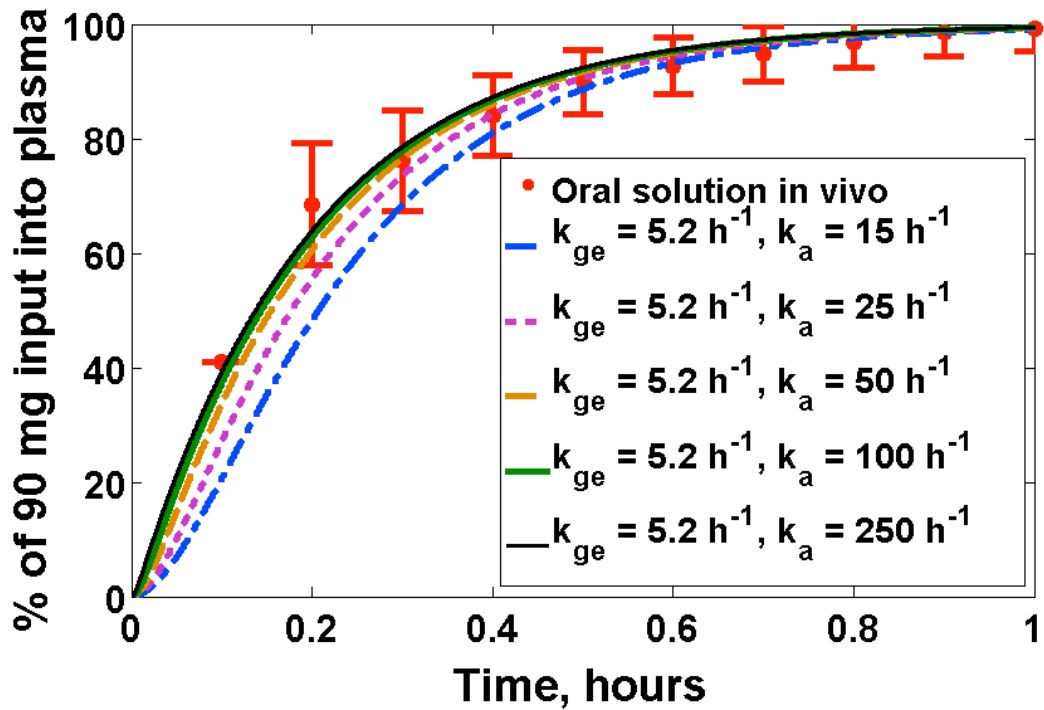
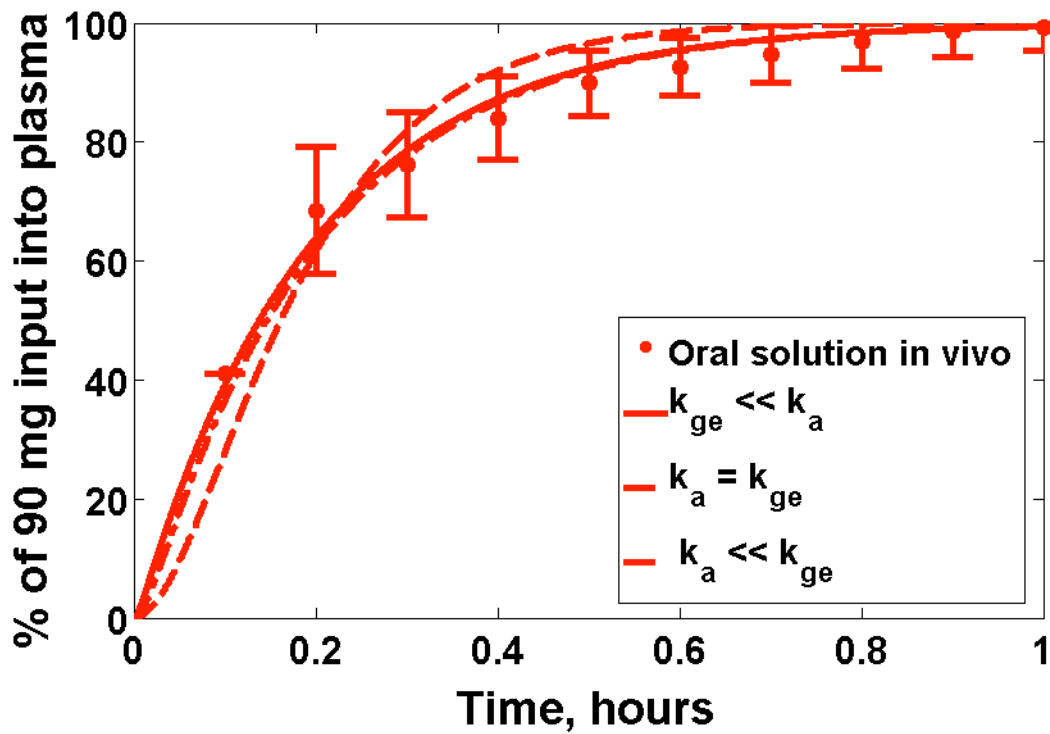**Figure 4.8a. Percent input into plasma versus time for the oral solution assuming gastric emptying rate << absorption rate**

Assumes first order k_{ge} is equal to 5.2 h^{-1} ($t_{0.5\ emptying}$ = 8 min^{-1}). Gastric emptying is the rate limiting step in this scenario when k_a is between ~100-250 h^{-1}.
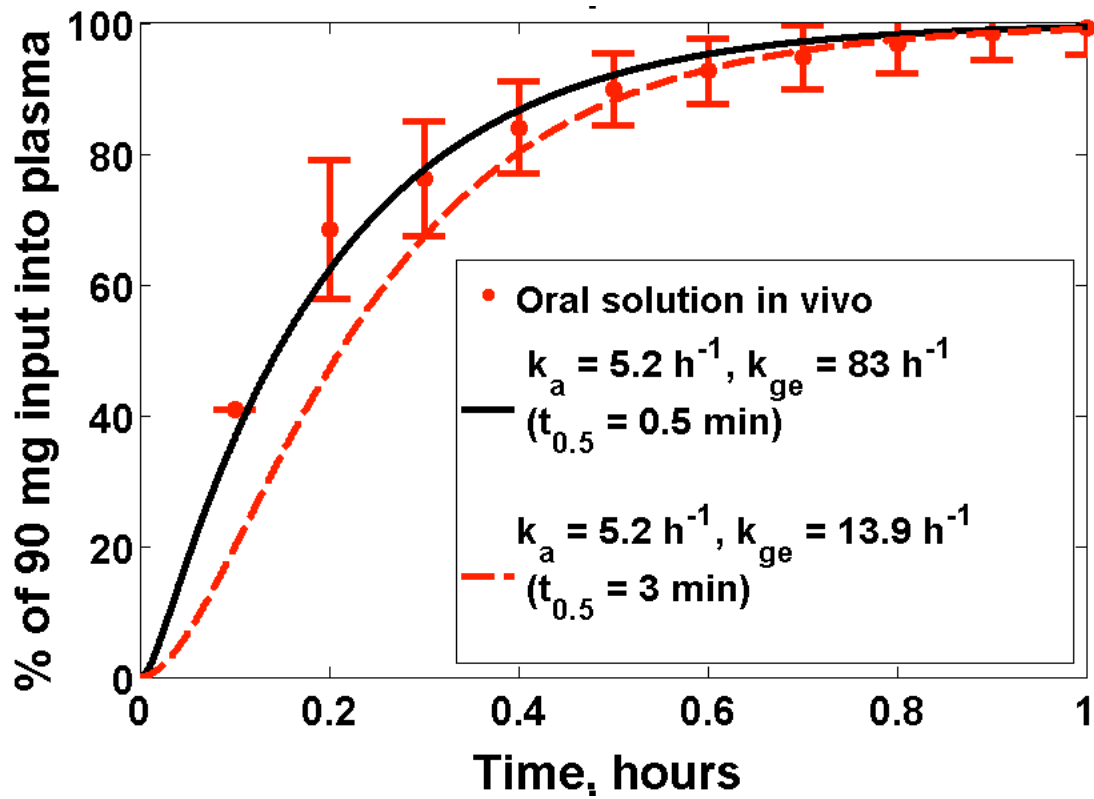
Figure 4.8b. Percent input into plasma versus time for the oral solution assuming absorption rate << gastric emptying rate
Assumes first order absorption with k_a equal to 5.2 h^{-1}. Emptying must be near instantaneous with a first order k_{ge} of at least about 83 h^{-1} to match *in vivo* profile.
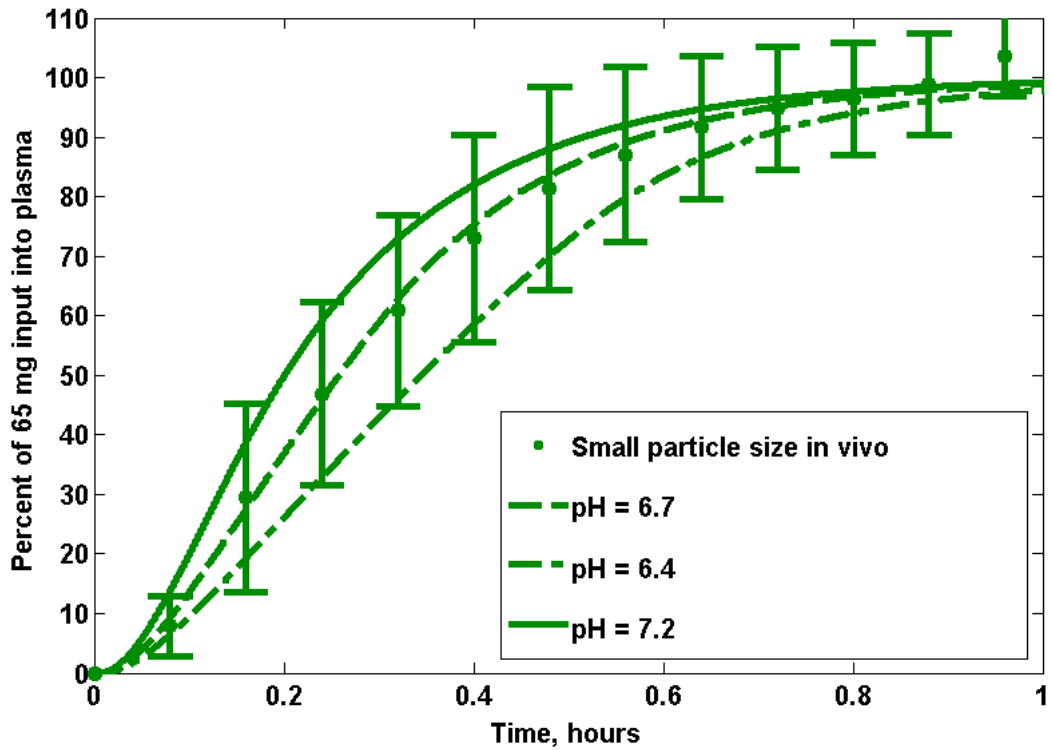
Figure 4.8c. Percent input into plasma versus time for the oral solution assuming gastric emptying rate << absorption rate (k_{ge} = 5.2 h^{-1}, k_a = 234 h^{-1}), absorption rate << gastric emptying rate (k_a = 5.2 h^{-1}, k_{ge} = 83 h^{-1} and absorption rate ≈ gastric emptying rate (k_a = k_{ge} = 10.4 h^{-1}).
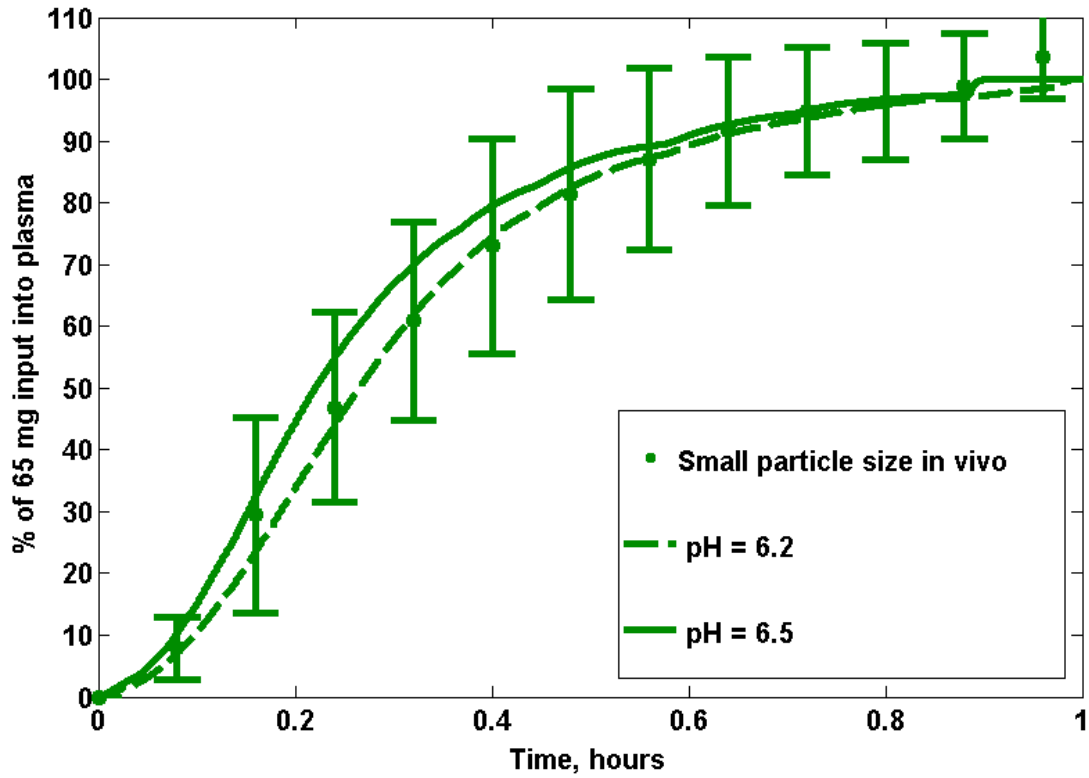
Figure 4.9a. *In vivo* profile analysis for small particle size (87 μm median) assuming absorption rate << gastric emptying rate

Profile as a function of pH for a buffer concentration of 10.5 mM. $t_{0.5}$ of 0.5 min for a k_a value of 5.2 h^{-1}, and a k_{ge} value of 83 h^{-1}.
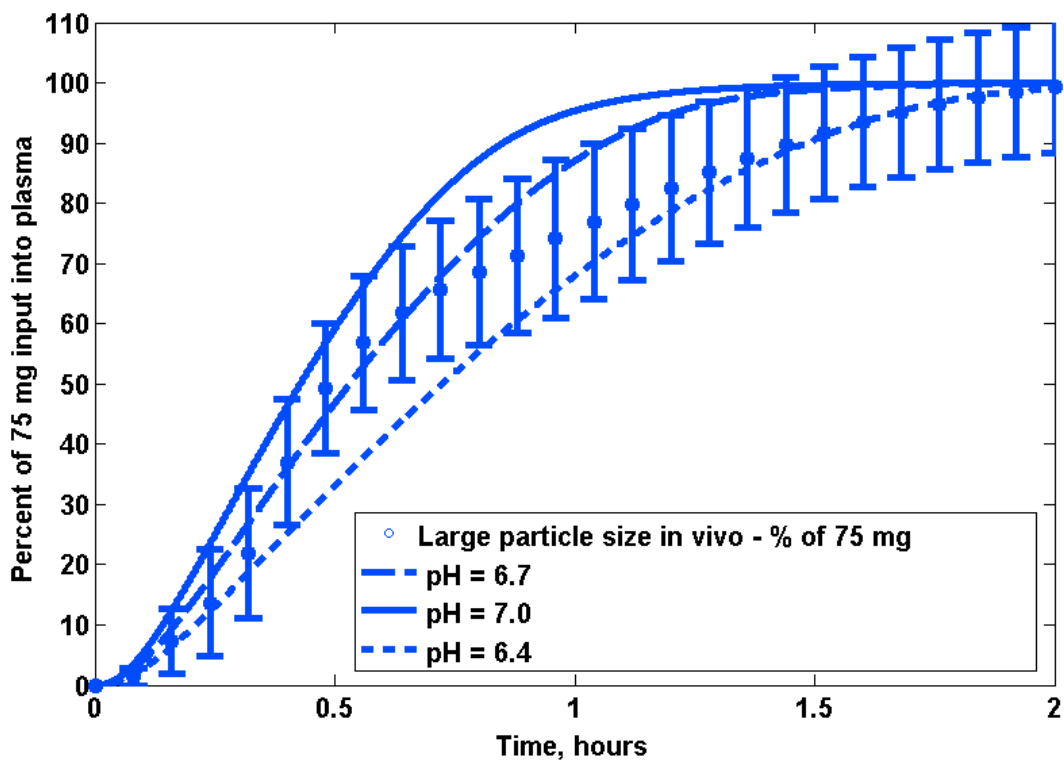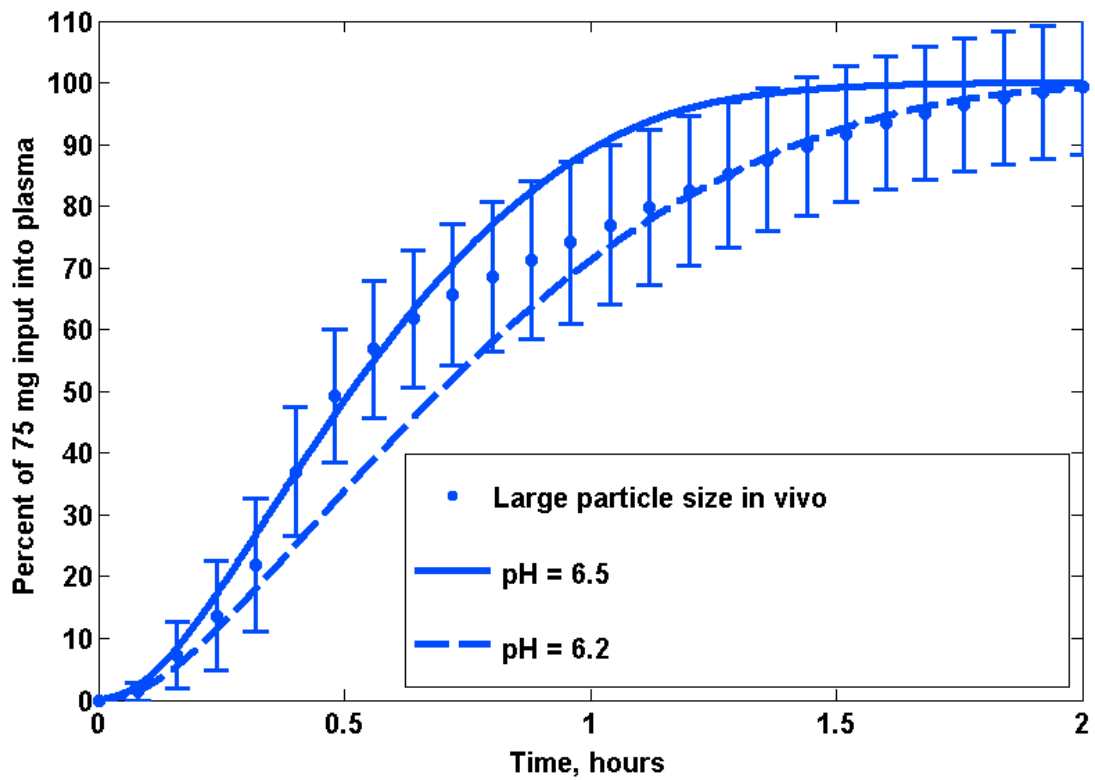
Figure 4.9b. *In vivo* **profile analysis for large particle size (330 μm median) assuming absorption rate << gastric emptying rate**

Profile as a function of pH for a buffer concentration of 10.5 mM. $t_{0.5}$ of 0.5 min for a k_a value of 5.2 h^{-1}, and a k_{ge} value of 83 h^{-1}.

**Figure 4.10a.** *In vivo* profile analysis for small particle size (87 µm median) assuming gastric emptying rate << absorption rate

Profiles at pH values ranging from 6.2-6.5 for a buffer concentration of 10.5 mM. $t_{0.5}$ of 8 min (k_{ge} value of 5.2 h^{-1}) and k_a of 234 h^{-1}.

Figure 4.10b. *In vivo* profile analysis for large particle size (330 µm median) assuming gastric emptying rate << absorption rate

Profiles at pH values ranging from 6.2-6.5 for a buffer concentration of 10.5 mM. $t_{0.5}$ of 8 min (k_{ge} value of 5.2 h^{-1}) and k_a of 234 h^{-1}.
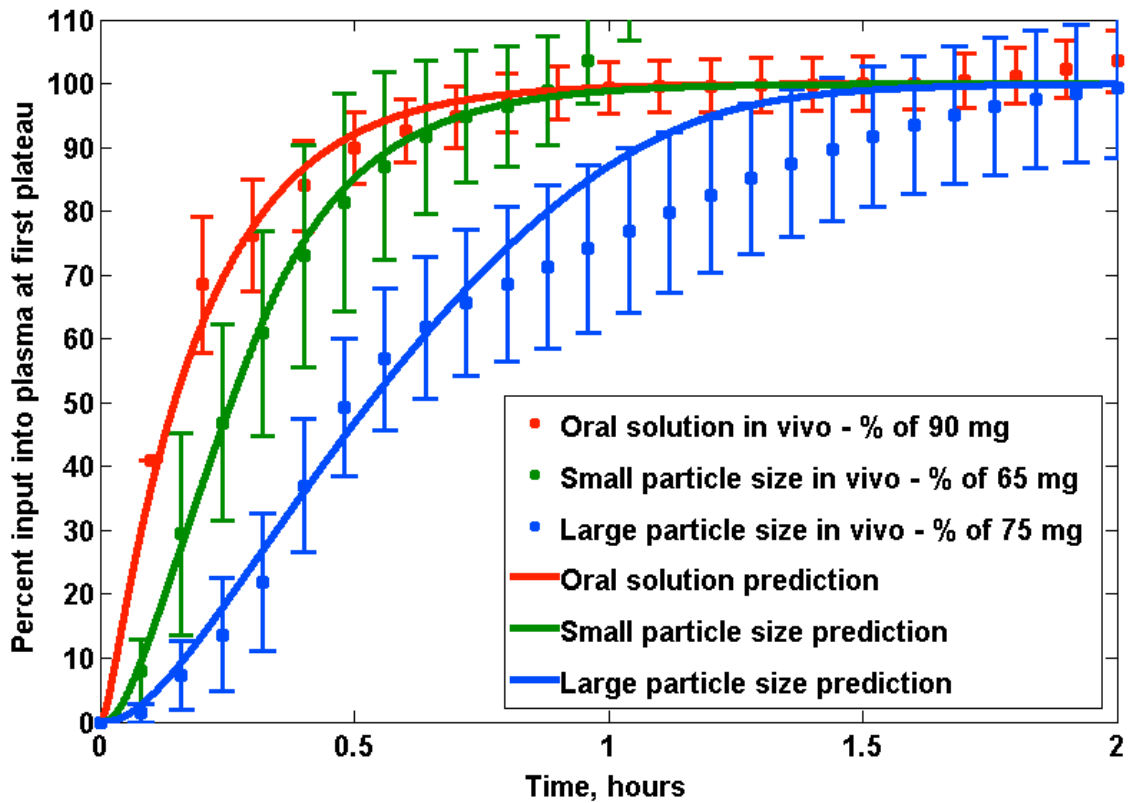
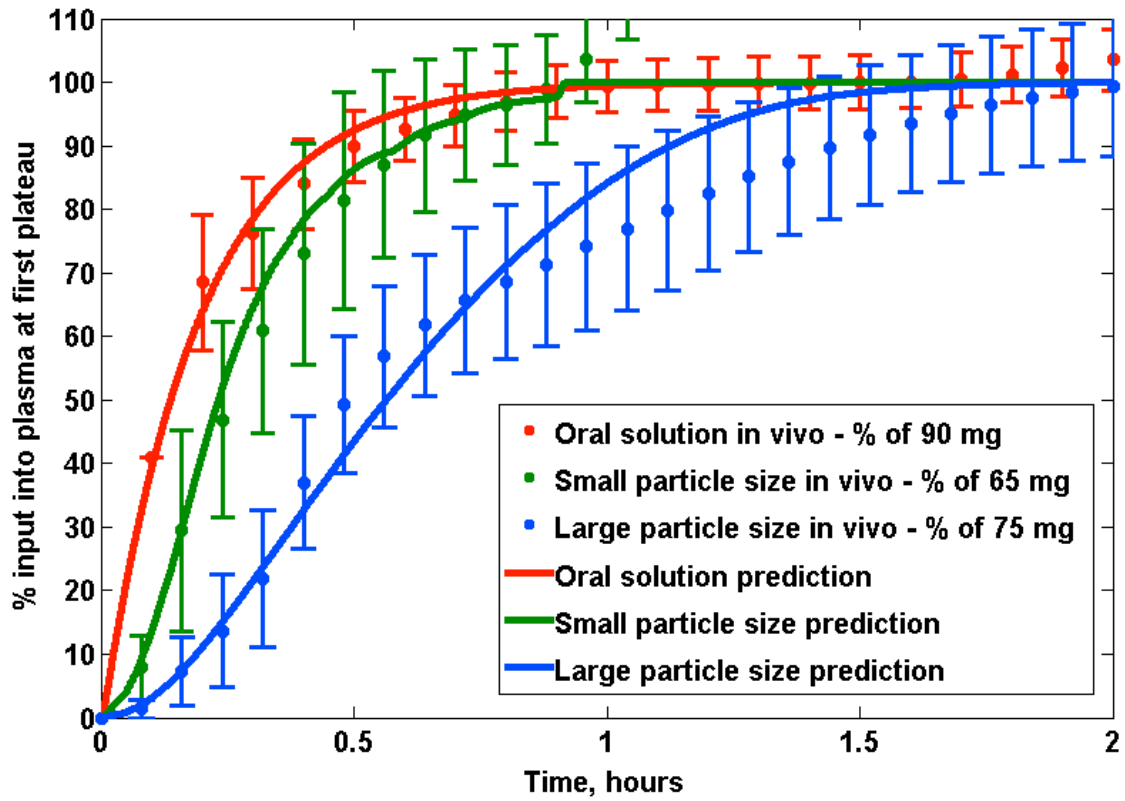**Figure 4.11a. Predictions for oral solution, small particle size tablet and large particle size tablet at a pH of 6.7 assuming absorption rate << gastric emptying rate**

$k_a = 5.2$ h^{-1} and $k_{ge} = 83$ h^{-1} ($t_{0.5} = 0.5$ min)

Figure 4.11b. Predictions for oral solution, small particle size tablet, and large particle size tablet at a pH of 6.4 assuming gastric emptying << absorption

$k_a = 234 \ h^{-1}$ and $k_{ge} = 5.2 \ h^{-1}$ ($t_{0.5} = 8$ min)

Table 4.12 Values for transport parameters used in the *in vitro* simulations

| Parameter	Gastric single phase	Two phase	USP
A/V_a	-	0.5	-
P_{eff}	-	30×10^{-4} cm/s	-
Buffer species	Phosphate	Phosphate	Phosphate
Buffer pK_a	6.8	6.8	6.8
Buffer concentration	10.5 mM	10.5 mM	10.5 mM
pH	6.4	6.4	6.4
k_{ge} (first-order)	$5.2\ h^{-1}$	-	-
h_c	20 μm	20 μm	20 μm
ρ	$1.1\ g/cm^3$	$1.1\ g/cm^3$	$1.1\ g/cm^3$
drug pK_a	4.4	4.4	4.4
D_{HA}	$7.6 \times 10^{-6}\ cm^2/s$	$7.6 \times 10^{-6}\ cm^2/s$	$7.6 \times 10^{-6}\ cm^2/s$
V_a	900 ml	165 ml	900 ml
Cs	0.068 mg/ml	0.068 mg/ml	0.068 mg/ml
Saturation solubility	$C_s(1+10^{pH-pKa})$	$C_s(1+10^{pH-pKa})$	$C_s(1+10^{pH-pKa})$
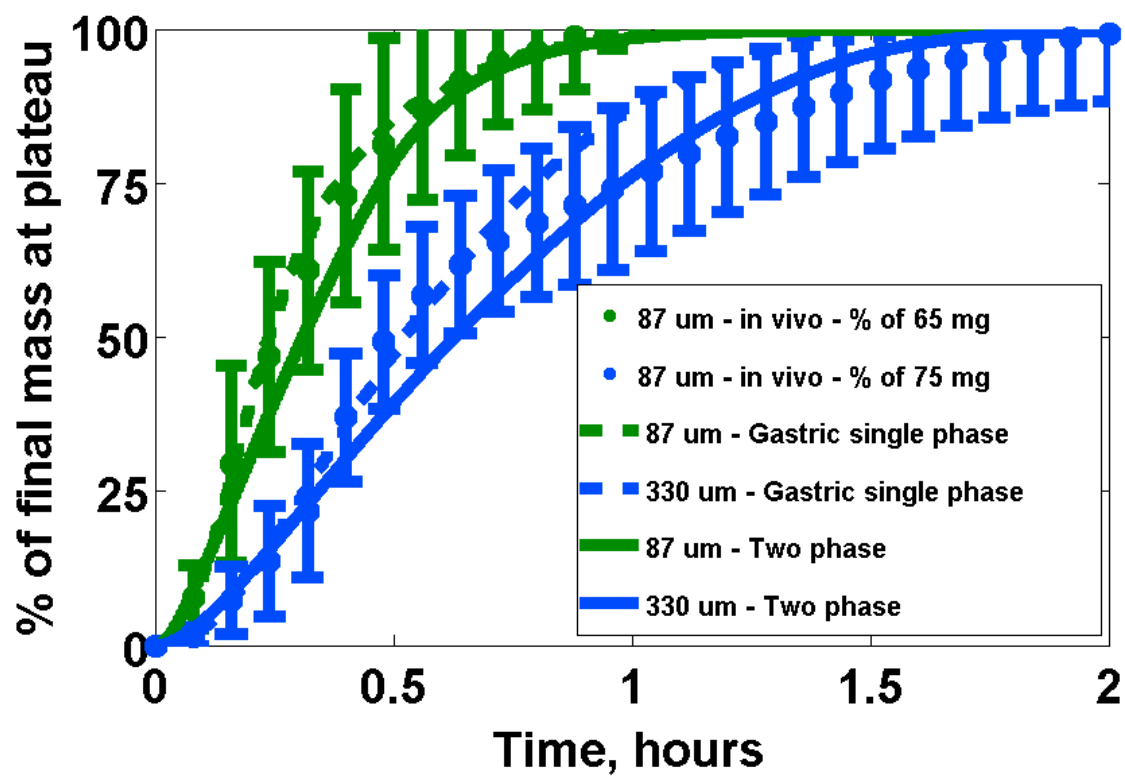
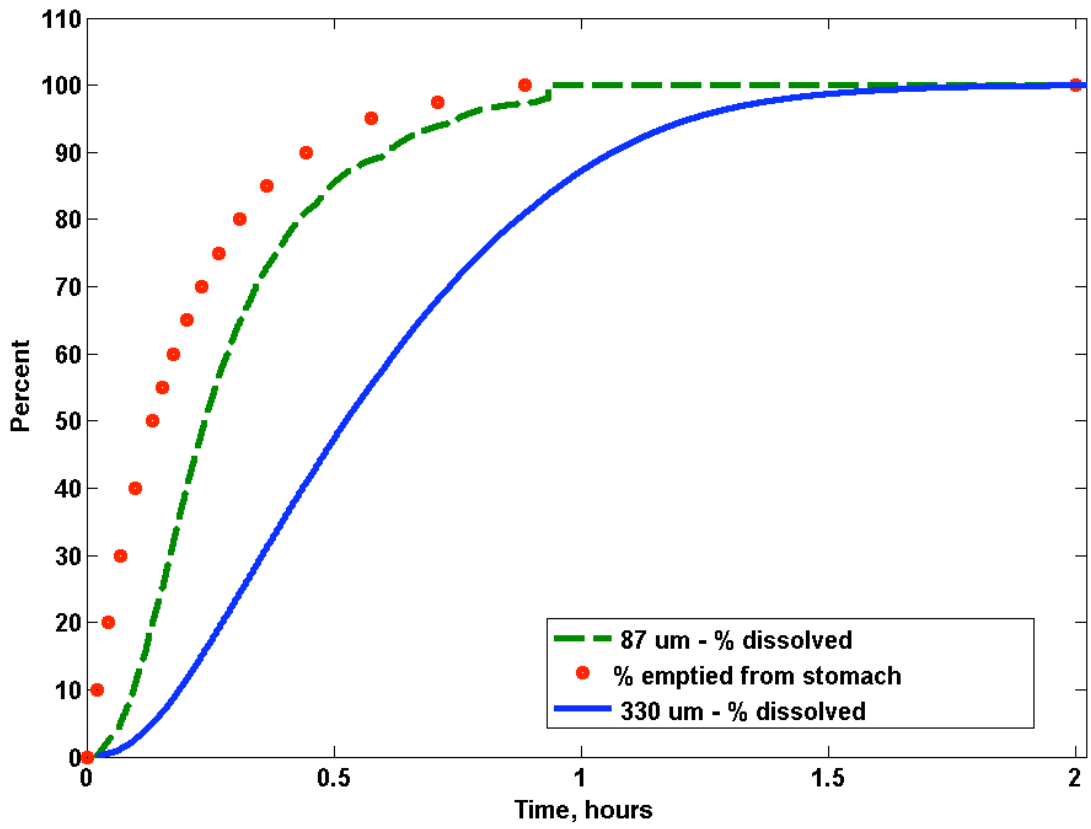**Figure 4.12. Simulations for two different types of *in vitro* dissolution methodologies compared with average *in vivo* input into plasma profiles**
Simulations performed at a pH of 6.4

Figure 4.13. Percent dissolved versus time compared with percent emptied versus time in an *in vitro* gastric single-phase apparatus for the small and large particle tablets
Simulations performed at a pH of 6.4
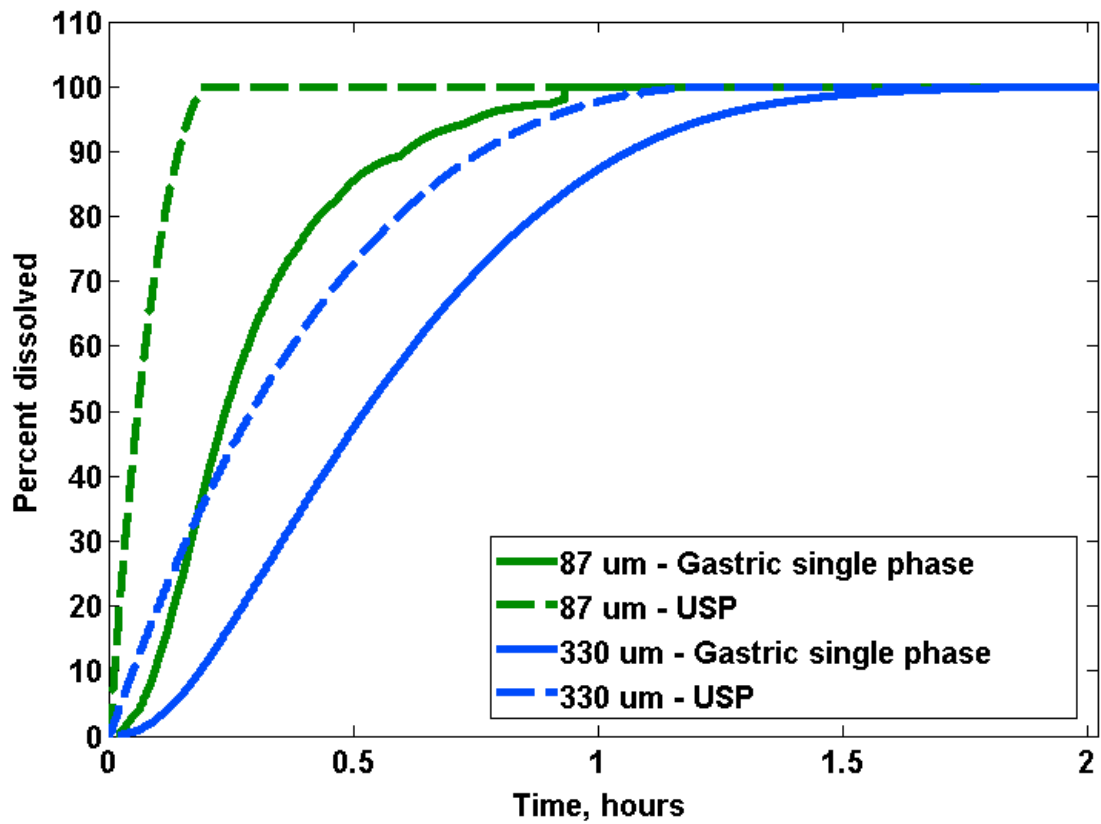
Figure 4.14. Percent dissolved versus time in an *in vitro* gastric single-phase apparatus versus an *in vitro* USP-type apparatus for the small and large particle tablets
Simulations performed at a pH of 6.4
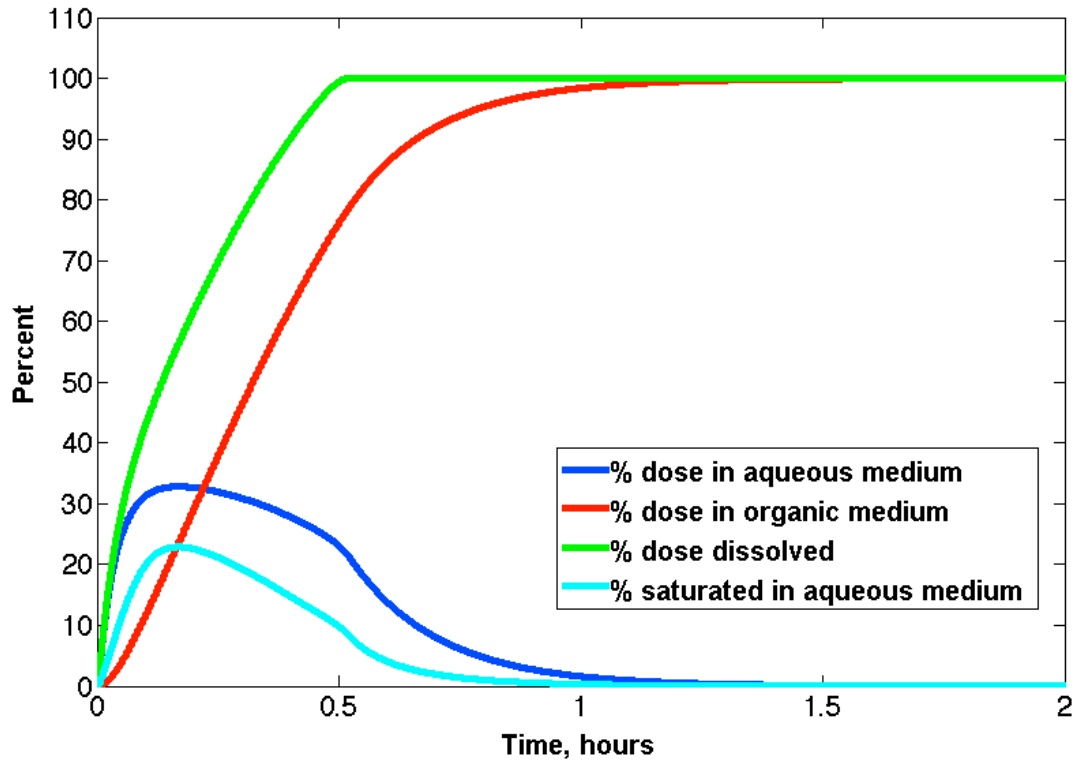
Figure 4.15a. Simulations for 87 µm median particles dissolving in 165 ml of a pH 6.4 10.5 mM sodium phosphate buffer in a two-phase dissolution apparatus

Figure 4.15b. Simulations for 330 μm median particles dissolving in 165 ml of a pH 6.4 10.5 mM sodium phosphate buffer in a two-phase dissolution apparatus

References

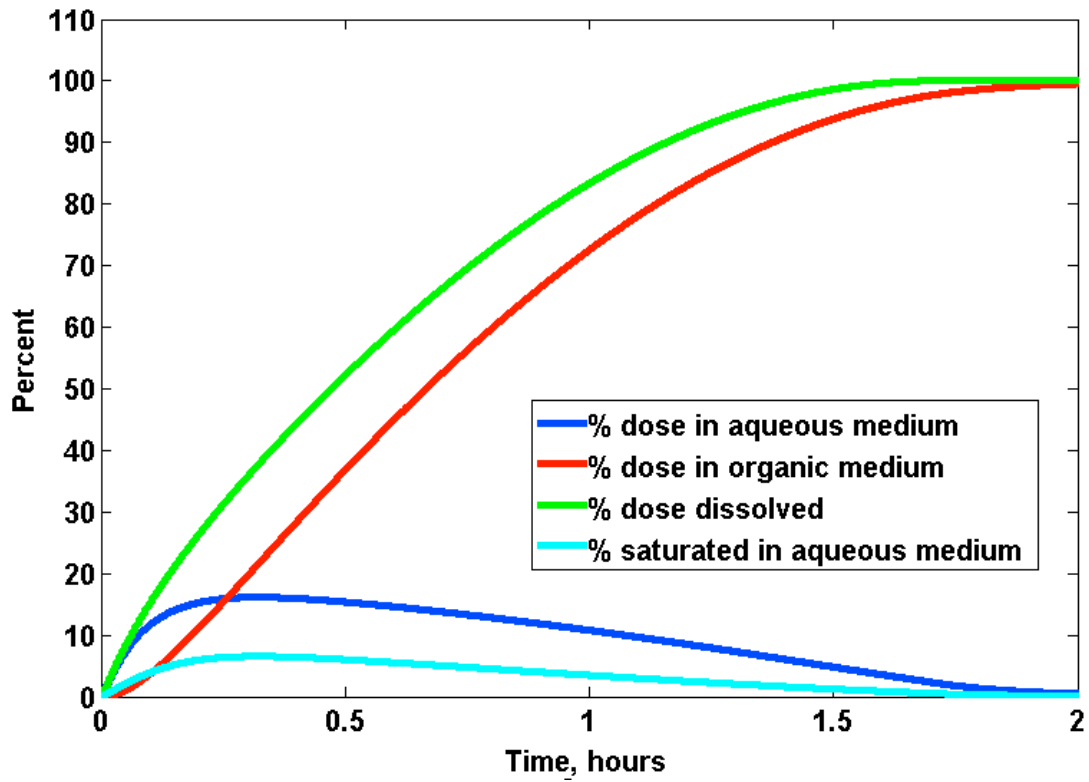1.	Ishii K, Saitou Y, Yamada R et al. Novel approach for determination of correlation between in vivo and in vitro dissolution using the optimization technique. Chem Pharm Bull 1996; **44**: 1550-5.

2.	Kimura S, Imai T, Ueno M, Otagiri M. Pharmaceutical Evaluation of Ibuprofen Fast-Absorbed Syrup Containing Low-Molecular-Weight Gelatin. Journal of pharmaceutical sciences 1992; **81**: 141-4.

3.	Burger A, Koller KT, Schiermeier WM. RS-ibuprofen and S-ibuprofen (dexibuprofen) - Binary system and unusual solubility behaviour. Eur J Pharm Biopharm 1996; **42**: 142-7.

4.	Fischbach M. Forecasting the in vivo performance of modified release (MR) dosage forms using biorelevant dissolution tests. Goettingen, Germany: Cuvillier Verlag Goettingen 2006.

5.	Amidon GL, Lennernas H, Shah VP, Crison JR. A Theoretical Basis for a Biopharmaceutic Drug Classification - the Correlation of in-Vitro Drug Product Dissolution and in-Vivo Bioavailability. Pharmaceut Res 1995; **12**: 413-20. Doi 10.1023/A:1016212804288

6.	Sugano K. Theoretical investigation of passive intestinal membrane permeability using Monte Carlo method to generate drug-like molecule population. International journal of pharmaceutics 2009; **373**: 55-61. DOI: 10.1016/J.Ijpharm.2009.02.002

7.	Mudie DM, Shi Y, Ping HL et al. Mechanistic analysis of solute transport in an in vitro physiological two-phase dissolution apparatus. Biopharm Drug Dispos 2012; **33**: 378-402. Doi 10.1002/Bdd.1803

8.	Mudie DM, Amidon GL, Amidon GE. Physiological Parameters for Oral Delivery and in Vitro Testing. Mol Pharmaceut 2010; **7**: 1388-405. DOI: 10.1021/Mp100149j

9.	Anderson AC. Beagle Dog as an Experimental Animal. Ames, IA: Iowa State University Press 1970.

10.	DeSesso JM, Williams AL. Contrasting the Gastrointestinal Tracts of Mammals: Factors that Influence Absorption. Annu Rep Med Chem 2008; **43**: 353-71. Doi 10.1016/S0065-7743(08)00021-3

11.	Schiller C, Frohlich C, Giessmann T et al. Intestinal fluid volumes and transit of dosage forms as assessed by magnetic resonance imaging.

Aliment Pharmacol Ther 2005; **22**: 971-9. DOI: 10.1111/j.1365-
2036.2005.02683.x

12.   Snipes RL, Snipes H. Quantitative investigation of the intestines in eight
       species of domestic mammals. Z Saugetierkd 1997; **62**: 359-71.

13.   Gupta PK, Robinson JR. Gastric-Emptying of Liquids in the Fasted Dog.
       International journal of pharmaceutics 1988; **43**: 45-52. Doi 10.1016/0378-
       5173(88)90057-9

14.   Mudie DM, Murray K, Pritchard SE et al. Quantification of Gastrointestinal
       Liquid Volumes Following a Glass of Water. 2013 AAPS Annual Meeting
       and Exposition; 2013; San Antonio, TX; 2013.

15.   Marciani L, Cox EF, Hoad CL et al. Postprandial changes in small bowel
       water content in healthy subjects and patients with irritable bowel
       syndrome. Gastroenterology 2010; **138**: 469-77, 77 e1.
       10.1053/j.gastro.2009.10.055

16.   Marciani L, Foley S, Hoad CL et al. Effects of Ondansetron on Small
       Bowel Water Content: A Magnetic Resonance Imaging Study. 2007.

17.   Snyder WS, Cook, M.J., Nasset, E.S., Karhausen, L.R., Howells, G.P.,
       Tipton, I.H. Anatomical Values for Reference Man. *Report of the Task
       Group on Reference Man*. New York: Pergamon Press 1975:8-46.

18.   Itoh Z, Takeuchi S, Aizawa I, Takayanagi R. Characteristic motor activity
       of the gastrointestinal tract in fasted conscious dogs measured by
       implanted force transducers. The American journal of digestive diseases
       1978; **23**: 229-38.

19.   Gruber P, Rubinstein A, Li VH et al. Gastric emptying of nondigestible
       solids in the fasted dog. Journal of pharmaceutical sciences 1987; **76**:
       117-22.

20.   Gupta PK, Robinson JR. Effect of Volume and Viscosity of
       Coadministered Fluid on Gastrointestinal Distribution of Small Particles.
       International journal of pharmaceutics 1995; **125**: 185-93. Doi
       10.1016/0378-5173(95)00111-U

21.   Youngberg CA. Radiotelemetric Determination of GI pH in Man and Dog.
       Ann Arbor: University of Michigan; 1984.

22.   Miyabayashi T, Morgan JP, Atilola MAO, Muhumuza L. Small Intestinal
       Emptying Time in Normal Beagle Dogs - a Contrast Radiographic Study.
       Vet Radiology 1986; **27**: 164-8.

23.   Banta CA, Clemens ET, Krinsky MM, Sheffy BE. Sites of Organic-Acid
       Production and Patterns of Digesta Movement in the Gastro-Intestinal
       Tract of Dogs. J Nutr 1979; **109**: 1592-600.

24.   Lui CY, Amidon GL, Berardi RR et al. Comparison of Gastrointestinal Ph
       in Dogs and Humans - Implications on the Use of the Beagle Dog as a

Model for Oral Absorption in Humans. Journal of pharmaceutical sciences 1986; **75**: 271-4. Doi 10.1002/Jps.2600750313

25. Altman PL, Katz DD, American Institute of Biological S et al. Metabolism. Bethesda, Md.: Federation of American Societies for Experimental Biology 1968.

26. Alexander F. The Concentration of Electrolytes in the Alimentary Tract of the Rabbit, Guinea Pig, Dog and Cat. Research in veterinary science 1965; **6**: 238-44.

27. Krieg BJ. Personal communication. In: Mudie DM, ed. 2013.

28. Kaunitz JD, Akiba Y. Review article: duodenal bicarbonate - mucosal protection, luminal chemosensing and acid-base balance. Aliment Pharm Therap 2006; **24**: 169-76. Doi 10.1111/J1365-2036.2006.00041.X

29. Parkkila S, Parkkila AK, Lehtola J et al. Salivary carbonic anhydrase protects gastroesophageal mucosa from acid injury. Digest Dis Sci 1997; **42**: 1013-9. Doi 10.1023/A:1018889120034

30. Keane FB, Dimagno EP, Dozois RR, Go VLW. Relationships among Canine Interdigestive Exocrine Pancreatic and Biliary Flow, Duodenal Motor-Activity, Plasma Pancreatic-Polypeptide, and Motilin. Gastroenterology 1980; **78**: 310-6.

31. Kalantzi L, Persson E, Polentarutti B et al. Canine intestinal contents vs. simulated media for the assessment of solubility of two weak bases in the human small intestinal contents. PharmRes 2006; **23**: 1373.

32. Smeets-Peeters M, Watson T, Minekus M, Havenaar R. A review of the physiology of the canine digestive tract related to the development of in vitro systems. Nutrition research reviews 1998; **11**: 45-69. 10.1079/NRR19980005

33. Poelma FGJ, Breas R, Tukker JJ. Intestinal-Absorption of Drugs .4. The Influence of Taurocholate and L-Cysteine on the Barrier Function of Mucus. International journal of pharmaceutics 1990; **64**: 161-9. Doi 10.1016/0378-5173(90)90265-6

34. Potthast H, Dressman JB, Junginger HE et al. Biowaiver monographs for immediate release solid oral dosage forms: Ibuprofen. J Pharm Sci-Us 2005; **94**: 2121-31. Doi 10.1002/Jps.20444

35. Shaw LR, Irwin WJ, Grattan TJ, Conway BR. The effect of selected water-soluble excipients on the dissolution of paracetamol and ibuprofen. Drug Dev Ind Pharm 2005; **31**: 515-25. Doi 10.1080/03639040500215784

36. Levis KA, Lane ME, Corrigan OI. Effect of buffer media composition on the solubility and effective permeability coefficient of ibuprofen. International journal of pharmaceutics 2003; **253**: 49-59. DOI: 10.1016/S0378-5173(02)00645-2

37. Jinno J, Oh DM, Crison JR, Amidon GL. Dissolution of ionizable water-insoluble drugs: The combined effect of pH and surfactant. Journal of pharmaceutical sciences 2000; **89**: 268-74. Doi 10.1002/(Sici)1520-6017(200002)89:2<268::Aid-Jps14>3.3.Co;2-6

38. Sheng JJ, Kasim NA, Chandrasekharan R, Amidon GL. Solubilization and dissolution of insoluble weak acid, ketoprofen: Effects of pH combined with surfactant. Eur J Pharm Sci 2006; **29**: 306-14. Doi 10.1016/J.Ejps.2006.06.006

39. Lane ME, Levis KA, Corrigan OI. Effect of intestinal fluid flux on ibuprofen absorption in the rat intestine. International journal of pharmaceutics 2006; **309**: 60-6. Doi 10.1016/J.Ijpharm.2005.11.016

40. Heikkinen AT, Monkkonen J, Korjamo T. Determination of permeation resistance distribution in in vitro cell monolayer permeation experiments. Eur J Pharm Sci 2010; **40**: 132-42. Doi 10.1016/J.Ejps.2010.03.012

41. Sugano K. Estimation of effective intestinal membrane permeability considering bile micelle solubilisation. International journal of pharmaceutics 2009; **368**: 116-22. Doi 10.1016/J.Ijpharm.2008.10.001

42. Levitt MD, Furne JK, Strocchi A et al. Physiological Measurements of Luminal Stirring in the Dog and Human Small-Bowel. J Clin Invest 1990; **86**: 1540-7. Doi 10.1172/Jci114873

43. Lipka E, Spahn-Langguth S, Mutschler E, Amidon GL. In vivo non-linear intestinal permeability of celiprolol and propranolol in conscious dogs: evidence for intestinal secretion. Eur J Pharm Sci 1998; **6**: 75-81. Doi 10.1016/S0928-0987(97)00070-5

44. Yee S. In vitro permeability across Caco-2 cells (colonic) can predict in vivo (small intestinal) absorption in man--fact or myth. Pharmaceutical research 1997; **14**: 763-6.

45. Amidon GL, Lennernas H, Shah VP, Crison JR. A theoretical basis for a biopharmaceutic drug classification: The correlation of in vitro drug product dissolution and in vivo bioavailability. Pharmaceutical research 1995; **12**: 413-20. DOI: 10.1023/A:1016212804288

46. Davies NM, Takemoto JK, Brocks DR, Yanez JA. Multiple Peaking Phenomena in Pharmacokinetic Disposition. Clin Pharmacokinet 2010; **49**: 351-77.

47. Metsugi Y, Miyaji Y, Ogawara KI et al. Appearance of double peaks in plasma concentration-time profile after oral administration depends on gastric emptying profile and weight function. Pharmaceutical research 2008; **25**: 886-95. Doi 10.1007/S11095-007-9469-Z

48. Oberle RL, Amidon GL. The Influence of Variable Gastric-Emptying and Intestinal Transit Rates on the Plasma-Level Curve of Cimetidine - an

Explanation for the Double Peak Phenomenon. J Pharmacokinet Biop 1987; **15**: 529-44. Doi 10.1007/Bf01061761

49. Dietzel K, Beck WS, Schneider HT et al. The Biliary Elimination and Enterohepatic Circulation of Ibuprofen in Rats. Pharmaceut Res 1990; **7**: 87-90. Doi 10.1023/A:1015847912059

50. Merck. The Merck Veterinary Manual. 2013.

51. Bischoff K, Mukai, M. Toxicology of Over-the-Counter Drugs. In: Gupta RC, ed. *Veterinary Toxicologh: Basic and Clinical Principles*. 2nd ed. London, UK: Elsevier 2012.

52. Bhattachar SN, Perkins EJ, Tan JS, Burns LJ. Effect of Gastric pH on the Pharmacokinetics of a BCS Class II Compound in Dogs: Utilization of an Artificial Stomach and Duodenum Dissolution Model and GastroPlus,(TM) Simulations to Predict Absorption. J Pharm Sci-Us 2011; **100**: 4756-65. Doi 10.1002/Jps.22669

53. Carino SR, Sperry DC, Hawley M. Relative bioavailability estimation of carbamazepine crystal forms using an artificial stomach-duodenum model. 2006; **95**: 116-25. 10.1002/jps.20495

54. Mudie DM, Amidon GL, Amidon GE. Mass Transport Analysis of an In Vitro Two Phase Dissolution Apparatus for Oral Bioperformance Prediction of Solid Oral Dosage Forms. 2011.